

# Reduction of transhorizon radio interference in satellite earth stations

**Citation for published version (APA):**

Scheeren, P. M. J. (1988). *Reduction of transhorizon radio interference in satellite earth stations*. [Phd Thesis 1 (Research TU/e / Graduation TU/e), Electrical Engineering]. Technische Universiteit Eindhoven. <https://doi.org/10.6100/IR290643>

**DOI:**

[10.6100/IR290643](https://doi.org/10.6100/IR290643)

**Document status and date:**

Published: 01/01/1988

**Document Version:**

Publisher's PDF, also known as Version of Record (includes final page, issue and volume numbers)

**Please check the document version of this publication:**

- A submitted manuscript is the version of the article upon submission and before peer-review. There can be important differences between the submitted version and the official published version of record. People interested in the research are advised to contact the author for the final version of the publication, or visit the DOI to the publisher's website.
- The final author version and the galley proof are versions of the publication after peer review.
- The final published version features the final layout of the paper including the volume, issue and page numbers.

[Link to publication](#)

**General rights**

Copyright and moral rights for the publications made accessible in the public portal are retained by the authors and/or other copyright owners and it is a condition of accessing publications that users recognise and abide by the legal requirements associated with these rights.

- Users may download and print one copy of any publication from the public portal for the purpose of private study or research.
- You may not further distribute the material or use it for any profit-making activity or commercial gain
- You may freely distribute the URL identifying the publication in the public portal.

If the publication is distributed under the terms of Article 25fa of the Dutch Copyright Act, indicated by the "Taverne" license above, please follow below link for the End User Agreement:

[www.tue.nl/taverne](http://www.tue.nl/taverne)

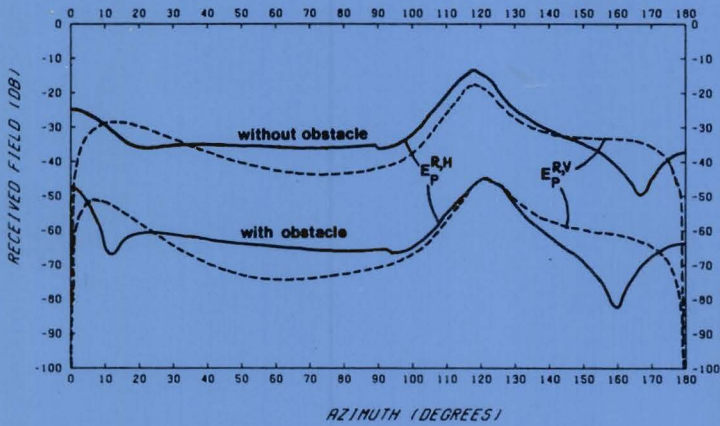
**Take down policy**

If you believe that this document breaches copyright please contact us at:

[openaccess@tue.nl](mailto:openaccess@tue.nl)

providing details and we will investigate your claim.

# REDUCTION OF TRANSHORIZON RADIO INTERFERENCE IN SATELLITE EARTH STATIONS



P.M.J. SCHEEREN

**REDUCTION OF  
TRANSHORIZON RADIO INTERFERENCE IN  
SATELLITE EARTH STATIONS**

**REDUCTION  
OF  
TRANSHORIZON RADIO INTERFERENCE  
IN  
SATELLITE EARTH STATIONS**

Proefschrift

ter verkrijging van de graad van doctor aan  
de Technische Universiteit Eindhoven, op gezag  
van de rector magnificus, prof. ir. M. Tels, voor  
een commissie aangewezen door het College van  
Dekanen in het openbaar te verdedigen op  
dinsdag 11 oktober 1988 te 16.00 uur

door

**PETER MARIA JOSEPH SCHEEREN**

geboren te Heerlen

Dit proefschrift is goedgekeurd  
door de promotoren:

**PROF. DR. J.C. ARNBAK**

en

**PROF. DR. J. BOERSMA**

## CONTENTS

<i>Abstract</i>	5
<i>List of abbreviations</i>	7
<i>List of major symbols</i>	8
<b>1. Introduction</b>	<b>11</b>
1.1. Background	11
1.2. Terminology	14
1.3. Organizations and responsibilities	15
1.4. Scope of the thesis and survey of the contents	19
1.5. References	21
<b>2. Radio-interference problems and mutual coordination</b>	<b>23</b>
2.1. Introduction	23
2.2. Review of practical interference problems	23
2.2.1. General remarks	23
2.2.2. Interference between terrestrial stations	24
2.2.3. Interference between satellite-earth links	26
2.2.4. Interference between terrestrial stations and earth stations	28
2.2.5. System studies	30
2.3. Interference from digital radio-relay stations into satellite TV receivers	32
2.4. Coordination areas	34
2.5. References	40
<b>3. Transhorizon propagation mechanisms — a review</b>	<b>43</b>
3.1. General introduction	43
3.2. Introduction to transhorizon-propagation research	43
3.2.1. Time variability	43
3.2.2. General concepts and terminology	44
3.2.3. Presentation of results	50
3.3. Review of transhorizon-propagation mechanisms	50
3.3.1. General remarks	50
3.3.2. Permanent clear-air mechanisms	52
3.3.3. Occasional clear-air mechanisms	55
3.3.4. Permanent scatter mechanisms	58
3.3.5. Occasional scatter mechanisms	58
3.4. Relative importance of the mechanisms	61
3.5. References	61
<b>4. Clear-air transhorizon propagation</b>	<b>65</b>
4.1. Introduction	65
4.2. Review of clear-air interference-prediction models	65
4.2.1. General remarks	65
4.2.2. CCIR interference-prediction model	66
4.2.3. Other clear-air interference-prediction models	68
4.3. Transhorizon-propagation experiments	70
4.3.1. Measurement programme and equipment	70
4.3.2. Experimental results obtained at EUT	72
4.3.3. Discussion of the experimental results	73

4.4.	Theoretical ducting model	79
4.4.1.	Review of tropospheric-propagation theory	79
4.4.2.	Review of mode theory	81
4.4.3.	Tropospheric ducting produced by an elevated inversion layer	87
4.4.4.	Numerical results	96
4.4.5.	Prediction model based on mode theory	100
4.5.	General transhorizon-interference prediction procedure	102
4.6.	References	105
5.	<b>Interference-reduction techniques</b>	<b>109</b>
5.1.	Introduction	109
5.2.	Review of interference-reduction techniques	110
5.2.1.	General survey	110
5.2.2.	Antenna-sidelobe suppression	115
5.2.3.	Site shielding	119
5.2.4.	Reciprocal signal processing, including (de)modulation	122
5.2.5.	Interferometric cancellation	124
5.3.	Reduction of transhorizon interference in satellite earth stations	128
5.4.	Application of interference cancellation for the protection of cable networks against radio pirates ( <i>reprint</i> )	131
5.5.	References	143
6.	<b>Obstacle diffraction</b>	<b>149</b>
6.1.	Introduction	149
6.2.	Knife-edge diffraction model	150
6.3.	Notations and symbols	152
6.4.	Knife-edge diffraction of a uniform plane wave	155
6.4.1.	Sommerfeld's solution	155
6.4.2.	Kirchhoff's approximation	155
6.4.3.	CCIR formula	158
6.4.4.	Keller's GTD	159
6.4.5.	Uniform theories of edge diffraction	160
6.5.	Knife-edge diffraction of a non-uniform plane wave	162
6.5.1.	Introduction	162
6.5.2.	Exact solution for the linear case	163
6.5.3.	Kirchhoff's approximation for the non-uniform case	164
6.5.4.	Extension of the CCIR formula to the non-uniform case	165
6.5.5.	High-frequency asymptotic solutions for the non-uniform case	166
6.6.	Comparison of knife-edge diffraction theories	169
6.7.	Modelling of a realistic site-shielding geometry	173
6.7.1.	Atmospheric influence	173
6.7.2.	Influence of the ground	174
6.7.3.	Oblique incidence	175
6.7.4.	Finite obstacles	178
6.7.5.	Thickness of the obstacle	178
6.7.6.	Surface roughness and finite conductivity of the obstacle	180
6.8.	References	181

<b>7. Site shielding for earth-station antennas – theory</b>	<b>185</b>
7.1. Introduction	185
7.2. Formulation of the site-shielding problem	185
7.3. Review of CCIR site-shielding model	187
7.3.1. Derivation of the CCIR model	187
7.3.2. Limitations of the CCIR model	190
7.4. Fundamental approach of the site-shielding problem	191
7.4.1. General description	191
7.4.2. Description of the earth-station antenna	193
7.4.3. Influence of the obstacle on the wanted radiation	197
7.5. Review of the geometrical theory of diffraction for a curved edge	200
7.5.1. Introduction	200
7.5.2. Fundamentals of the general GTD	200
7.5.3. Description of the electromagnetic fields	201
7.5.4. Description of the curved edge and the reflector surface	203
7.5.5. Auxiliary parameters	205
7.5.6. The GTD solution	208
7.5.7. The UTD solution	210
7.5.8. Limitations of the GTD/UTD solution	211
7.6. Application of GTD/UTD to the site-shielding problem	212
7.6.1. General considerations	212
7.6.2. Determination of the diffraction points	214
7.6.3. Calculation of the diffracted field	218
7.6.4. Summation of the ray-optical fields at the feed	222
7.7. References	225
<b>8. Site shielding for earth-station antennas – results</b>	<b>229</b>
8.1. Introduction	229
8.2. Numerical results obtained by GTD/UTD	229
8.2.1. Radiation pattern of the parabolic antenna	229
8.2.2. SSF as a function of elevation	237
8.2.3. SSF in relation to antenna polarization	238
8.2.4. SSF as a function of azimuth	242
8.2.5. Discussion of the numerical results	245
8.3. An engineering prediction model for site shielding	246
8.3.1. Description of the engineering model	246
8.3.2. Application of the engineering model to a specific example	249
8.4. The effect of site shielding on coordination areas	252
8.5. References	255
<b>9. Summary and conclusions</b>	<b>257</b>
Appendix A. Definitions of relevant terms by the ITU	263
Appendix B. Numerical solution of the mode equation associated with an elevated refractive-index discontinuity	269
Appendix C. Geometrical parameters of the axisymmetric parabolic reflector antenna	281
<i>Acknowledgements</i>	287
<i>Samenvatting</i>	289
<i>Verantwoording</i>	291
<i>Curriculum vitae</i>	299





## ABSTRACT

Because of the increasing demands for telecommunication services, assignment of the same radiocommunication channel to different services is inevitable. The risk of service interruption due to radio-frequency interference is inherent to the multiple use of frequency bands ("frequency sharing"). Specific interference problems are caused by unwanted transhorizon propagation of microwaves emitted by terrestrial transmitters. This propagation may severely hamper the trouble-free reception of (relatively weak) satellite signals in earth stations. Protective measures are often necessary to satisfy the operational requirements (e.g., outage-free reception during 99% of the time).

This thesis gives a survey of the mechanisms responsible for transhorizon propagation. The most important mechanism is tropospheric ducting, which is further investigated. Experimental support is obtained from a number of measurements, carried out in the framework of the European COST-210 cooperative project. These measurements suggest shortcomings of existing (semi-)empirical prediction models. A theoretical model of the ducting mechanism is described and elaborated for a specific example.

A review of the literature on interference-reduction techniques is presented. One of these techniques employs an adaptive cancellation system; this technique has been elaborated for the application in cable distribution systems, to combat failures due to ether piracy. For the protection of satellite earth stations against transhorizon interference, site shielding of the earth station turns out to be a suitable technique.

Protection by site shielding is inherently limited by the diffraction at the edge(s) of the shielding obstacle. Existing methods for the calculation of the shielding effect of an obstacle cannot generally be applied. A fundamental investigation of the site-shielding problem has been carried out by means of a model based on the geometrical theory of diffraction (GTD). The numerical results from this model agree with comparable results reported in the literature. Based on the GTD model, a simpler, practical model has been developed, the results of which agree well with the results of the GTD model.

The practical relevance of site shielding for frequency sharing is illustrated by an example. The results suggest that site shielding may be especially attractive for relatively small earth stations.



## LIST OF ABBREVIATIONS

BTRL	British Telecom Research Laboratories
CATV	cable television
CCIR	Comité Consultatif International des Radiocommunications
COST	Coopération Européenne dans le Domain de la Recherche Scientifique et Technique
DC	direct current
DNL	Dr. Neher Laboratories (research institute of the Netherlands PTT)
ECS	European Communications Satellite
EUT	Eindhoven University of Technology
FI/DBP	Forschungsinstitut der Deutsche Bundespost (research institute of the German PTT)
FM	frequency modulation
FRG	Federal Republic of Germany
GTD	geometrical theory of diffraction
HF	high frequency (3 MHz – 30 MHz)
IF	intermediate frequency
IFRB	International Frequency-Registration Board
ITU	International Telecommunication Union
MSK	minimum-shift keying
NL	Netherlands
PTT	Post, Telegraph and Telephone
QPSK	quadrature phase-shift keying
RF	radio frequency
RR	Radio Regulations
UAT	uniform asymptotic theory of diffraction
UHF	ultra high frequency (300 MHz – 3 GHz)
UK	United Kingdom
UTD	uniform geometrical theory of diffraction
VHF	very high frequency (30 MHz – 300 MHz)
VSAT	very small aperture terminal
WARC	World Administrative Radio Conference
WG	Working Group

## LIST OF MAJOR SYMBOLS

All quantities are expressed in MKSA units, unless otherwise indicated.

$a$	radius of a spherical approximation to the earth, $a=6370$ km
$a_e$	effective earth radius, eq. (3.6)
$D$	antenna diameter
$D^{i,r}$	diffraction coefficient, eq. (6.28)
$d$	distance, path length (km)
$d_a$	angular distance, fig. 3.2
dB	dB relative to a (fictitious) isotropic antenna
$\vec{E}$	electric field
$F(\cdot)$	Fresnel integral, eq. (6.10)
$F_{KP}(\cdot)$	transition function of UTD, eq. (6.32)
$f$	<i>i</i> ) frequency; <i>ii</i> ) focal distance of the parabolic antenna
$G$	antenna gain (dBi)
$G_f(\cdot)$	feed-antenna gain (dBi)
$\vec{H}$	magnetic field
$H_0^{(2)}(\cdot)$	Hankel function of zero order and second kind
$\text{Im}\{\cdot\}$	imaginary part
$k$	effective earth-radius factor, eq. (3.6)
$k_0$	wavenumber, $k_0=2\pi/\lambda$
$L_b$	basic transmission loss, path loss (dB), eqs. (3.3)–(3.4)
$L_{bf}$	free-space basic transmission loss (dB), eq. (3.3)
$L_m$	excess path attenuation (dB), eq. (3.4)
$M$	modified refractivity, eq. (3.9)
$m$	modified refractive index, eq. (3.8)

$N$	refractivity, eq. (3.5)
$n$	refractive index
$P$	electromagnetic power
$p$	time percentage
$r_M$	distance between obstacle edge and antenna aperture centre $M$ , fig. 7.1
$\text{Re}\{\cdot\}$	real part
SSF	site-shielding factor (dB), sec. 5.2.3
$U$	general field quantity
$Z_0$	intrinsic impedance of free space, $Z_0=120\pi \Omega$
$\{i \rightarrow r\}$	repeat all previous terms with superscript "r" instead of "i"
$\Gamma$	reflector edge
$\gamma$	specific attenuation (dB/km)
$\delta(\cdot)$	Dirac delta function
$\Theta(\cdot)$	unit step function
$\theta_M$	diffraction angle of the ray-optical field towards the antenna aperture centre $M$ , fig. 7.1
$\lambda$	wavelength
$\xi^{i,r}$	detour parameter
$\rho_M$	distance between antenna aperture centre and feed phase centre, eq. (7.5a)
$\rho_0$	distance between reflector edge point and feed phase centre, eq. (7.5b)
$\Sigma$	reflector surface
$\varphi_A$	azimuth
$\varphi_E$	elevation
$\psi_0$	subtended angle of the parabolic antenna, eq. (7.5c)
$\omega$	angular frequency



## 1. INTRODUCTION

### 1.1. Background

*Telecommunication* is defined as the transmission, emission or reception of any signs, signals or messages by electromagnetic systems [1, art. 1]. Useful messages contain *information* which can be exchanged by these systems between human beings or "intelligent" machines. The utilization of telecommunication has shown a rapid increase since the last century, and has become essential in modern technological society.

The electromagnetic waves which carry the information in the form of signals, may propagate either along an artificially guided path, e.g. a metal cable or an optical fibre (*guided communication*), or propagate unguided in space (wireless communication, better known as *radiocommunication*).

Guided communication offers some distinct advantages compared to radiocommunication. In particular, a guided propagation path is well protected against unwanted external influences. However, guided communication suffers from a loss which increases exponentially with distance. Thus, long-distance guided communication is only possible with the use of repeaters. Classical guided-communication systems employ metal cables, which are expensive and limited in bandwidth. Optical fibres suffer considerably less from these limitations, and are therefore especially attractive for wideband communication between fixed terminals at relatively long distances.

Radiocommunication is more flexible than guided communication, and is therefore especially attractive for some specific telecommunication purposes, e.g. broadcasting, point-to-multipoint communication and mobile communication. However, radiocommunication has some important inherent problems. Firstly, the



propagation may be strongly affected by the earth's atmosphere. The time-variability of the atmospheric conditions implies a time-variability of the propagation characteristics and thus of the received field. Any valid general description of the latter is therefore necessarily of a statistical nature. Secondly, the open nature of radiocommunication makes it much more vulnerable to natural or man-made influences from outside the system. In particular, electromagnetic radiation from other radiocommunication systems may be present, in addition to the wanted radiation. This effect, known as (*radio-frequency*) *interference*, may cause a degradation of the communication system, or even entirely prevent its proper operation.

The use of different frequency bands for each radiocommunication system seems the most obvious way of avoiding this interference problem. However, owing to the limited extent of the usable radio-frequency spectrum, this solution is seldom possible. The present need for frequency assignments exceeds by far the available spectrum. The expected increase in the use of existing radiocommunication services and the demands for new services will considerably enhance the need for frequency bands in the next decades.

Exploiting new (i.e., higher) frequency bands is one way of trying to meet the increasing demands. At present, operational radiocommunication services are employing the frequency bands up to about 15 GHz. Research on the properties of electromagnetic wave propagation in the 20 and 30 GHz bands for satellite communications is carried out with much effort, for example within the planned European programme of measurements using the "Olympus" satellite [2]. Incidentally, some experiments with millimeter waves (frequencies above 30 GHz) have also been carried out [3-5], but much research remains to be undertaken before these bands can be reliably used, because of the severe propagation losses in the atmosphere at these wavelengths.

Meanwhile, the existing frequency bands should be used as efficiently as possible, in order to allow for maximum capacity. To this end, techniques for *frequency reuse* and *frequency sharing* are essential.

Frequency reuse is the use of the same frequency several times within the *same* telecommunication system. Examples are the utilization of two orthogonal polarizations and the spatial reuse of frequencies in satellite communication systems [6, sec. 2.3.4] and in cellular (mobile) radio systems [7]. In both types of systems, the frequency reuse is based on the isolation, between links using the same frequency, afforded by polarization discrimination and by spatial isolation, respectively.

Frequency sharing is the use of the same frequency by *different* radio-communication systems. The fact that these systems are often operated by different organizations makes frequency sharing much more difficult to exploit. Complicated interference problems may arise in the planning, realization and operation of a new system in a frequency band already employed by existing systems. These problems have various legal, regulatory, operational and technical aspects. This thesis concentrates on the latter aspects, by considering questions like:

- Can the interference level be predicted at the planning stage?
- Are technical means available to avoid unwanted radiation into other systems?
- How can the reception of unwanted radiation be reduced or cancelled?

A legal problem is the question whether the operator of a system that is causing interference into another system, can be held responsible or be liable to punishment for this effect [8]. Regulations on the agreed modes of sharing the frequency bands (*frequency management*) obviously constitute another essential aspect of interference problems (sec. 1.3).

## 1.2. Terminology

The *International Telecommunication Union* (ITU) has developed a well-considered terminology, to avoid confusion due to inappropriate use of terms related to radiocommunication. The definitions of these terms are laid down in article 1 of the *Radio Regulations* (RR) [1]. In this thesis we adopt this terminology. Here, we summarize the definitions of the most important terms; the relevant terminology of the RR is more completely given in appendix A.

A *radiocommunication service*, or briefly (*radio*) *service*, involves the transmission, emission or reception of radio waves for specific telecommunication purposes. These services are usually defined in terms of the *stations* involved. A *station* is defined as one or more transmitters or receivers (or a combination thereof), including the accessory equipment, needed at one location to carry on a service. Thus, we distinguish e.g. *space stations* (located beyond the major portion of the earth's atmosphere), *earth stations* (located close to the earth's surface and intended for communication with a space station, or – in a few cases – with another earth station by means of a reflecting satellite) and *terrestrial stations* (effecting terrestrial radiocommunication). Examples of radiocommunication services are:

- the *fixed service*, a service between fixed terrestrial stations;
- the *fixed-satellite service*, a service between fixed earth stations using one or more satellites;
- the *broadcasting service*, where signals transmitted by a terrestrial broadcasting station are intended for direct reception by the general public;
- the *broadcasting-satellite service*, where such signals are transmitted by a space station;
- the *mobile service* for terrestrial communication with mobile stations;

- the *radiodetermination service*, for the determination of the position and/or velocity of moving objects, e.g. by radar.

In relation to frequency management, the ITU defines the terms *allocation*, *allotment* and *assignment*. Frequency bands are *allocated* by the ITU on a world-wide basis to the radio services. A specific frequency channel is *allotted* to a service in one or more identified countries or geographical areas. On a national level, a frequency channel is *assigned* to a specific radio station.

For frequency-sharing purposes, the ITU defines some terms related to interference. *Interference* is the effect of unwanted energy due to an emission, radiation or induction upon reception in a radiocommunication system, manifested by a performance degradation. *Permissible interference* is interference which complies with quantitative interference and sharing criteria contained in the RR. In practice, a higher interference level may occasionally be agreed upon between the organizations involved (*accepted interference*). *Harmful interference* is defined as interference that endangers or repeatedly interrupts a service operating in accordance with the RR. Clearly, such interference should be avoided as far as possible.

### 1.3. Organizations and responsibilities

The regulatory task of frequency management on a world-wide basis is performed by the ITU, a United Nations specialized agency with more than 160 member states, which are represented by national administrations (usually PTTs). The decisions of the ITU in the field of radiocommunication, in particular the frequency allocations and frequency-sharing procedures, are recorded in the RR [1], which are periodically updated. The member states of the ITU have agreed to

perform their national frequency-management procedures in accordance with the international RR.

The frequency allocations to the radio services are given in article 8 of the RR. On mainly historical grounds, the ITU has divided the earth surface into three regions. For each region, and for the entire radio-frequency spectrum (up to 400 GHz), the allocation table in article 8 lists the frequency bands with the corresponding radio services. These services are classified into three categories: *primary, permitted or secondary* services. Primary and permitted services have equal rights, except that in frequency planning the primary services have the prior choice of frequencies. Secondary services cannot claim protection from harmful interference due to stations of primary and permitted services, and are not allowed to cause harmful interference into such stations, even if the latter are established at a later date.

Frequency allocations and frequency allotments are formally adopted by a competent international conference, e.g. the *World Administrative Radio Conference* (WARC). Frequency assignments are given by national administrations to stations in the respective countries, after being approved by a special committee of the ITU, the *International Frequency-Registration Board* (IFRB). The IFRB decides whether a frequency to be assigned to a station is in accordance with the RR and will not cause harmful interference to other stations. If the outcome is favourable, the frequency assignment is registered and has thereby obtained formal approval. The IFRB may also, at the request of an administration, mediate for the settlement of a dispute between two administrations in case of harmful interference. However, such disputes are normally settled bilaterally between the administrations involved.

The technical foundations required for the RR are provided on an advisory basis by another committee of the ITU, the *Comité Consultatif International des Radiocommunications* (CCIR). The findings of the CCIR are formulated and

consolidated every four years in the "Recommendations and Reports of the CCIR" [9]. Although these documents have no legal status, they are adhered to by many organizations involved in planning and operation of radio systems. Technical input to the CCIR is provided by the members (or groups of members) of the ITU at the interim meetings of the CCIR, and may lead to updates, extensions or additions of the "Recommendations and Reports" at the Plenary Assembly of the CCIR, held every four years.

The relation between the organizations mentioned in the preceding paragraphs is illustrated in fig. 1.1.

In the context of this thesis, another international organization, independent from the ITU, is of importance: the *Coopération Européenne dans le Domaine de la Recherche Scientifique et Technique* (COST). This European organization was set up in 1971 by the European Community to coordinate and stimulate technical and scientific research in Europe (both within and outside the Community). The work of COST is organized in the form of numerous projects, each dealing with specific problems. One of these projects is *COST 210*, entitled "The influence of the atmosphere on interference between radiocommunication systems at frequencies above 1 GHz" [10]. Ten countries are participating in this project, which has been scheduled from mid-1984 until mid-1990. The main goal of this COST project is the development and testing of suitable models for prediction and control of the interference problem in modern engineering practice. The output of COST 210 may possibly be submitted to the CCIR at its interim meeting in 1992.

The work of COST 210 has been organized in three working groups (WGs):

- WG1: "Interference in clear air";
- WG2: "Interference by hydrometeor scatter";
- WG3: "Interference-reduction techniques".

The author of this thesis was the chairman of WG3 and a member of WG1 from 1984 until 1988. A major part of the research reported in this work was performed in support of COST 210.

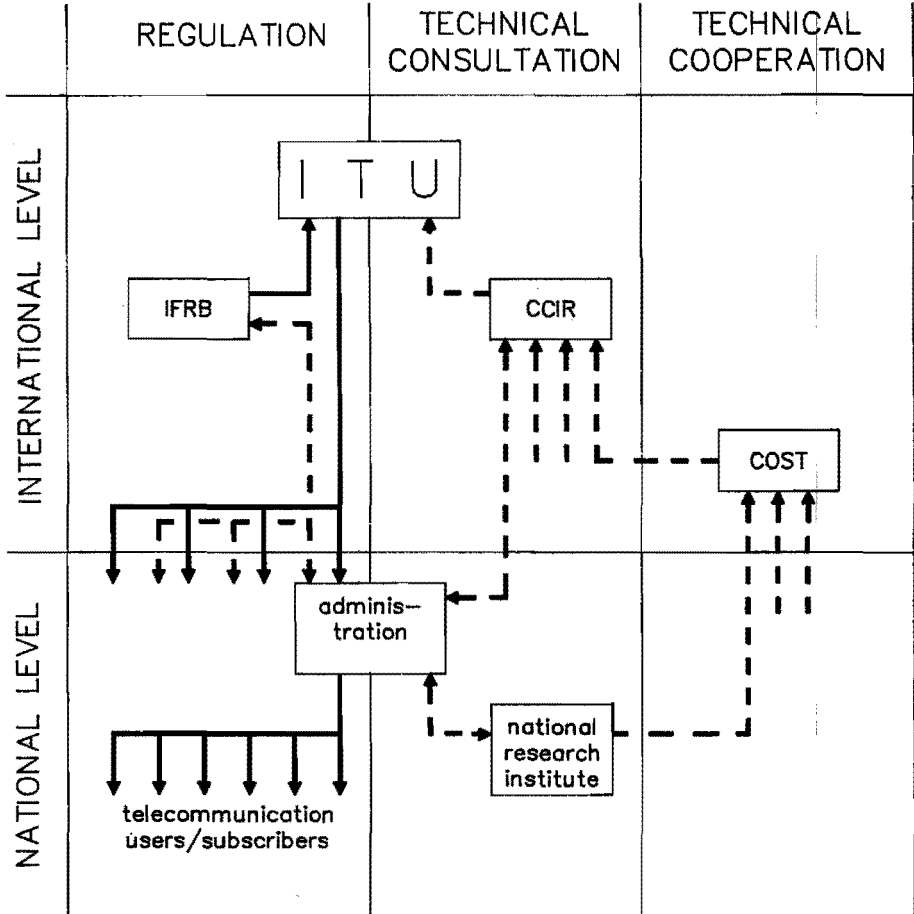


Fig. 1.1. Organizations involved in frequency regulation and technical consultation.

———— Regulatory activities;      - - - - consultative activities.

### 1.4. Scope of the thesis and survey of the contents

This thesis is intended as a contribution to the development of technical solutions to radio-interference problems. To allow better control of these complex problems, we have distinguished a number of partial problems. Various existing theories and models are reviewed and – if necessary – extended for better application to these partial problems. However, development of new theories is not the primary goal of the present investigation.

We start with a survey of the major radio-interference problems encountered in modern radio systems (chapter 2). An important class of – often international – problems arises in frequency sharing between a terrestrial service and a satellite service. Fig 1.2a illustrates a typical geometry, where a receiving earth station (intended for satellite communication) suffers from interference from a terrestrial station. This is the interference situation which is selected for further study.

In chapter 3, the propagation mechanisms responsible for the interference in this situation are surveyed. The relative importance of each mechanism is discussed. The most important mechanism (propagation in an atmospheric duct) is investigated

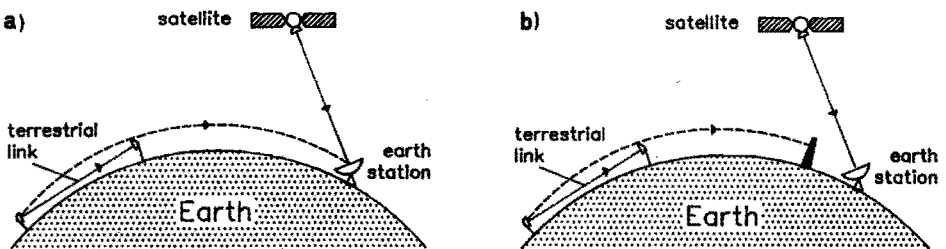


Fig. 1.2. Interference from a terrestrial station into an earth station.  
—— wanted paths;      - - - - unwanted paths.  
a) Without protection of the earth station; b) with site shielding.



quantitatively in chapter 4, both experimentally and theoretically. Prediction models for this type of interference are reviewed and compared to these investigations.

Chapter 5 contains a discussion of possible solutions to interference problems, known as interference-reduction techniques. These techniques can roughly be classified according to their place of application: at the transmit terminal, at the receive terminal or on the unwanted propagation path. Techniques for reduction of terrestrial interference in satellite earth terminals (fig. 1.2a) are compared qualitatively. An example is included of the engineering design approach to the development of a specific technique in a given interference situation (namely, interference caused by radio pirates).

The particular interference-reduction technique to be studied thoroughly in the remainder of this thesis is site shielding. Basically, this technique consists of blocking the unwanted propagation path by the erection of an obstacle between transmitter and receiver, see fig. 1.2b. The shielding effect of such an isolated obstacle is studied by theoretical means in chapter 6. However, if the obstacle is located in the vicinity of the earth-station antenna (which is often the case in practice), the shielding effect cannot be treated without respect to the antenna geometry. Therefore, chapters 7 and 8 discuss the problem of site shielding by an obstacle located in the vicinity of a specific receiving antenna. A theoretical model is developed in chapter 7, the results of which are validated in chapter 8 with the (not very extensive) results available in the literature. Based on this model, a simplified approximate method is suggested, suitable for system-engineering purposes.

Finally, in chapter 9 the main results of this thesis are summarized and conclusions drawn.

## 1.5. References

- [1] ITU, "Radio Regulations", Geneva, 1986.
- [2] G. Brussaard, "The Olympus propagation experiment OPEX: a unique example of European cooperation", *ESA bulletin*, no. 54, pp. 34-38, 1988.
- [3] W.J. Vogel, J.H. Davis and C.E. Mayer, "Line-of-sight observations at 86 GHz with a very large and small antenna", *IEEE Trans. Ant. Prop.*, vol. AP-32, no. 2, pp. 113-118, 1984.
- [4] W.W. Clarke, III, J.E. Miller and P.H. Richardson, "Sky brightness temperature measurements at 135 GHz and 215 GHz", *IEEE Trans. Ant. Prop.*, vol. AP-32, no. 9, pp. 928-933, 1984.
- [5] T. Manable, T. Ihara, J. Awaka and Y. Euruhamu, "The relationship of raindrop-size distribution to attenuations experienced at 50, 80, 140 and 240 GHz", *IEEE Trans. Ant. Prop.*, vol. AP-35, no.11, pp. 1326-1330, 1987.
- [6] CCIR, "Handbook on satellite communications", Geneva, 1985.
- [7] "Mobile-radio systems and techniques", IEE Conf. Publ., no. 238, 1984.
- [8] R. Perret, "International law in space - the regulation of satellite telecommunications", *Interavia*, vol. 30, no. 12, 1975.
- [9] CCIR, Plenary Assembly, "Recommendations and Reports of the CCIR", vols. I-XIV, Geneva, 1986.
- [10] COST 210 Management Committee, "COST 210 activities to model transhorizon cochannel interference paths in Europe", Proc. Int. Conf. Ant. Prop. (ICAP), *IEE Conf. Publ.*, no. 274, pp. 351-354, 1987.



## 2. RADIO-INTERFERENCE PROBLEMS AND MUTUAL COORDINATION

### 2.1. Introduction

In this chapter a survey is presented of the major radio-interference problems encountered in modern frequency-sharing radiocommunication systems or to be expected in future systems. Some examples are given to illustrate the particular class of interference problems which has been selected for further study in this thesis. Possible solutions to these problems by means of interference reduction techniques are not discussed here; they are reviewed in chapter 5.

### 2.2. Review of practical interference problems

#### 2.2.1. General remarks

Mutual interference between present-day or future radiocommunication systems is directly related to the ITU frequency allocations laid down (for the services provided by these systems) in article 8 of the Radio Regulations (RR) [1]. Many types of mutual interference are possible between frequency-sharing systems. To order the presentation, these interference situations are classified into three categories: interference between terrestrial stations (sec. 2.2.2), interference between satellite-earth links (sec. 2.2.3) and interference between terrestrial stations and earth stations (sec. 2.2.4). In each category the main problem areas will be identified and discussed. In principle, additional interference situations are possible as well (e.g. mutual interference between satellite stations), but these have less practical relevance. Finally, studies on the effect of interference on the system performance are reviewed in sec. 2.2.5.

### 2.2.2. Interference between terrestrial stations

The lower part of the radio frequency spectrum (up to about 100 MHz) has been allocated mainly to various terrestrial services, i.e., services that do not use any objects or radio sources in space. These services already occupy completely this part of the spectrum, thus offering little or no room for new services. Mutual interference between the different services has been limited to an acceptable level by careful frequency planning on a national (PTT) and international (ITU) level. Major interference problems normally do not arise, as long as all agreements on spectrum usage are strictly adhered to. Where this is not done, serious problems can arise, as evidenced by the phenomenon of ether piracy: unauthorized broadcast transmissions severely disturb the normal distribution of official broadcast programmes, or — more dangerously — the proper operation of aeronautical navigation services. Piracy is discussed in some detail in sec. 5.4.

At higher frequencies (i.e., above 100 MHz), where there is more room for new services, space communication services are important, especially above 1 GHz. In addition, these bands are also being occupied more and more by terrestrial radiocommunication systems, to meet the growing demand for existing and new services. At these frequencies, the fixed service (i.e., the service using terrestrial stations at fixed positions) normally applies radio-relay networks in order to overcome the limited coverage area of individual microwave transmitters. These networks employ relatively high transmit powers because of possible fading due to occasional multipath effects [2, chapter 4] and are therefore potential interferers for other services in the same frequency band. Although such "point-to-point" radio-relay links can use highly directional antennas that concentrate the radiation into the forward direction, other stations may still be affected even if located outside the

main beams. The mechanisms responsible for these unwanted couplings are discussed in chapter 3.

Radars form another important category of potential interference sources, because they may utilize pulses with high peak powers and short rise and fall times, leading to broad frequency spectra. Moreover, radars are often very mobile (e.g. mounted on aircraft or ships), and for some radars it is difficult to obtain the relevant information on the system characteristics because of military secrecy.

A broadcasting service is normally not exposed to interference from other stations, as most terrestrial broadcasting bands up to 1 GHz are not shared with other primary or permitted services. Broadcast-programme distribution in the VHF and UHF bands is usually carried out with networks of auxiliary transmitters similar to the radio-relay networks of the fixed service. The 12 GHz terrestrial-broadcasting band is shared with the broadcasting-satellite service. The latter is considered the more attractive alternative in Europe, although in Japan a local terrestrial broadcasting network at 12 GHz is successfully operating [3].

In recent years, cellular land mobile radio networks have been rapidly expanding. In Europe, the capacities of the existing 150 MHz and 400 MHz systems appear to be insufficient to satisfy the growing demands. In 1982 [1], the 900 MHz band was allocated to the mobile service on a primary basis, to be shared with the fixed service. This band will be used for a new pan-European digital land mobile communication system, mainly for telephony, which is planned for the nineties [4]. Interference is an inherent feature of such cellular systems, as their operation is based on frequency reuse in non-adjacent cells. However, this interference is caused by the system itself (intra-system interference), and is therefore under the control of the same system operator.

### 2.2.3. Interference between satellite-earth links

The first satellite-communication experiments were carried out around 1960, mainly with passive satellites (i.e., satellites without on-board repeaters, merely reflecting the incident radiation). Because of the excessively high transmit powers needed in systems with passive satellites, these systems were soon replaced by systems with active satellites. Many of the early satellite-communication systems were based on low-altitude, non-synchronous satellites operating at frequencies between 100 and 1000 MHz. These systems need "hand-over" from one satellite to another to maintain permanent connections between earth stations. Although such low-orbit systems are still in use for various important applications (e.g. the radionavigation-satellite service), the growth of satellite communications is mainly due to the possibility of utilizing geostationary-satellite systems, to which we confine the present discussion. The satellites in these systems are viewed from the earth at approximately stationary positions; this yields obvious operational advantages.

However, utilization of the geostationary orbit is limited, because interference criteria restrict the allowable minimum spacing between neighbouring frequency-sharing satellites, see fig. 2.1. Additional satellite spacing is required to take into account the small but inevitable perturbations of the satellites around their nominal orbital positions [5, sec. 1.4]. The efficient use of both spectrum and orbit is therefore an inherent problem in satellite-communication design. An excellent treatment of this topic is found in the monograph by Jansky and Jeruchim [6], which gives a survey of both the technical and the related regulatory aspects of geostationary-satellite communication.

Apart from "traditional" services like telephony and telex, satellite communication offers possibilities for many new services, e.g. domestic satellite

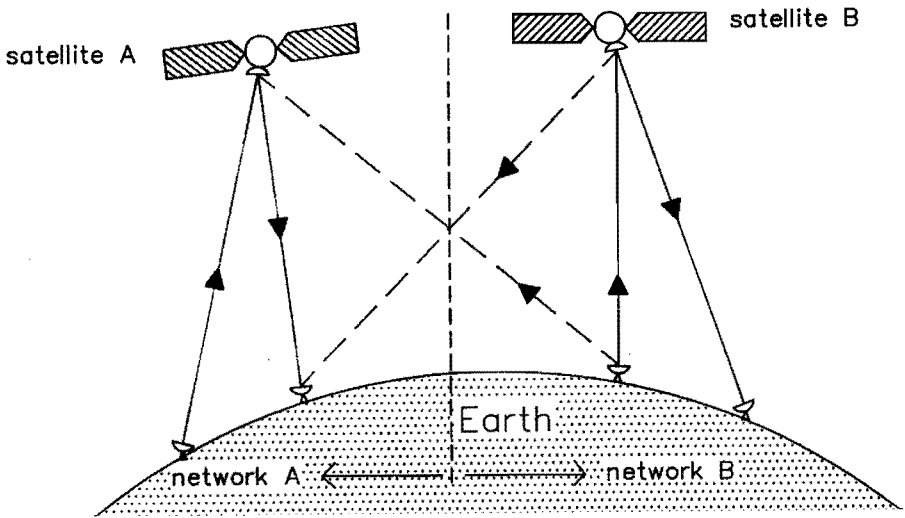


Fig. 2.1. Interference from one satellite network (B) into another (A).

———— wanted paths;      - - - - - unwanted paths.

services, broadcasting-satellite services, "business" services (e.g. video conferencing), mobile-satellite services, etc. Many of these new services are to be designed for a large number of users. This implies that the individual earth stations should be small and cheap, in turn requiring large satellite antennas and high satellite transmit powers. The latter requirements increase the risk of harmful interference into stations used for other services (either terrestrial or via satellite), especially because almost all geostationary-satellite services must share their frequency bands (which lie above 1 GHz) with other primary services.

To prevent the most serious interference problems, the ITU has prescribed in the RR [1] some general requirements to all satellite-communication systems. Thus, the maximum power-flux densities on the earth surface due to transmitting space stations, and the sidelobe levels of transmitting and receiving earth stations, have been limited. Operators of broadcasting-satellite transmitters are urged to confine the radiation to the intended coverage area, and to reduce the radiation into other



territories as much as possible (e.g. by means of multiple-beam or contoured-beam antennas [7,8]). Improved antenna systems for space stations and earth stations are the most obvious means to try to meet these (or even tighter future) requirements [5].

From the preceding discussion, it is evident that the planning of a new satellite service in a frequency band shared with another service often has to include detailed calculations of the levels of mutual interference in both systems. In appendix 29 of the RR [1] an approximate method is described to estimate the mutual interference between two frequency-sharing geostationary-satellite networks. This method models the interference as an apparent increase in the noise levels of the receiving stations of the networks. The highest value of this increase for all receiving stations is then compared with an agreed reference value. The outcome of this comparison indicates whether or not a detailed coordination procedure between the two networks is required.

#### 2.2.4. Interference between terrestrial stations and earth stations

Many satellite services above 1 GHz have to share their frequency bands with terrestrial services. The much-used 4 GHz and 6 GHz bands for the fixed-satellite service (the former band is used for the downlinks, the latter for the uplinks) have to be shared with the fixed service. The same holds for the 11 GHz and 14 GHz fixed-satellite service and the 12 GHz broadcasting-satellite service, which are both rapidly developing. The typical mutual-interference situation is shown in fig. 2.2. Because of the relatively low receive powers in satellite transmissions and the relatively high transmit powers used in the fixed (terrestrial) service, the risk of harmful interference from transmitting terrestrial stations into receiving earth stations is normally higher than that of harmful interference from transmitting earth

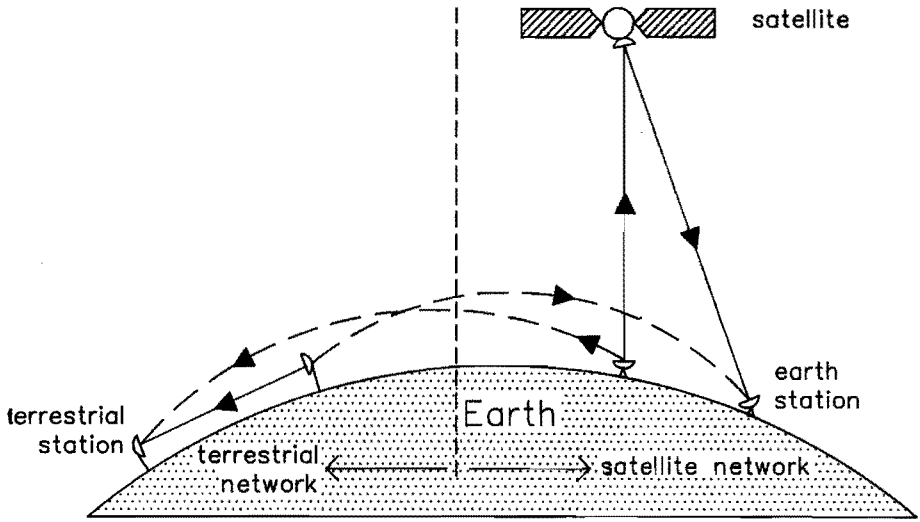


Fig. 2.2. Mutual interference between terrestrial stations and earth stations.

———— wanted paths;      - - - - unwanted paths.

stations into receiving terrestrial stations. Therefore, although the latter interference phenomenon cannot be ignored, the former phenomenon is normally more problematic, especially because typical multi-destination satellite systems involve more receiving earth stations than transmitting earth stations, e.g. for television-programme distribution. Many of these receiving earth stations are located close to or within urban areas, where the density of terrestrial stations is relatively high, too.

In addition to the general technical requirements imposed to limit the number of occurrences of harmful interference mentioned in the previous section, the ITU has restricted [1, art. 27–28] the permissible horizontally radiated power of both earth stations and radio-relay stations operating in shared frequency bands. In addition, a minimum elevation angle of  $3^\circ$  is prescribed for transmitting earth stations (except space-research earth stations). However, these limitations are far from sufficient to guarantee interference-free operation of frequency-sharing systems. The problem here is much more complicated than the problem of frequency sharing between

satellite-earth links, discussed in the previous section, where the unwanted propagation path is a satellite-earth or earth-satellite path. The influence of the atmosphere on such a path can be extra propagation losses of the unwanted signal. The corresponding reduction of the interference level is usually strongly correlated with - and of comparable magnitude to - the extra reduction of the wanted-signal level. The signal-to-interference ratio is therefore more or less constant in this case. On the other hand, the interference phenomenon studied in this section is unwanted propagation along a terrestrial path. This interference can very well be enhanced by atmospheric or terrestrial influences. Although such propagation anomalies may be relatively rare, they can nevertheless disturb the successful operation of frequency-sharing systems, because the services provided by these systems must generally be available for very high time percentages (typically 99% for broadcasting services, 99.99% for the public-telephone services).

In appendix 28 of the RR [1] a procedure is described for the calculation of the *coordination area* of an earth station, i.e., the area around the earth station outside which a frequency-sharing terrestrial station does not need any coordination with the earth station. This procedure, discussed in more detail in sec. 2.4, is based on several "worst-case" assumptions because of uncertainties in the probability of occurrence of various propagation phenomena. The study of (some of) these phenomena and the related protection of receiving earth stations against interference from transmitting terrestrial stations are the main topics of the present thesis.

#### 2.2.5. *System studies*

The effect of radio-frequency interference on the performance of a communication system depends on numerous factors. Ideally, one would like to

specify a maximum-permissible degradation in the service quality and then be able to determine the corresponding maximum-permissible radio-frequency interference level. However, it is virtually impossible to establish a general relation between the service quality and the interference level. Important system factors are the carrier-to-noise ratios and the modulation and coding parameters of the wanted and unwanted signals, their frequency separation, and the receiver filter and demodulator characteristics (including imperfections).

Detailed system studies are needed to evaluate the impact of all these parameters. Because of the numerous possible combinations of parameters involved, the subject matter is very complex. Therefore, most of the published studies have concentrated on those canonical problems that appear most relevant from a practical point of view. Representative publications up to 1980 have been collected and reprinted by Stavroulakis [9]. A more systematic approach has been presented by Jansky and Jeruchim [6, part III], who attempt to develop more or less rigorous calculation methods. In both references the subject matter is divided into two categories: interference into analogue transmission systems, and interference into digital transmission systems. The latter category is also treated in a monograph by Feher [10]. In principle, the interfering signal will also belong to either of these categories, but studies of "mixed" cases (where one of the signals involved is analogue and the other is digital) are rather rare. An example of such a mixed case is discussed in sec. 2.3.

For analogue systems the relative level of the interference in the baseband output signal can be calculated in a number of cases [6], but relating this level to the system performance (e.g. speech or picture quality) is a different matter, which generally needs subjective tests [11]. For interference into digital systems, the derivation of such relations appears to be even more complicated; however, in this

case the bit-error probability can generally be employed as an objective measure for the system performance.

### 2.3. Interference from digital radio-relay stations into satellite-TV receivers

Although direct-broadcasting satellites for the 12 GHz band are not yet fully operational in Europe, television-programme distribution by satellite has long been possible in the 11 GHz band via transponders of the European Communications Satellite (ECS). The ECS signals are received by multiple medium-sized receive-only stations, processed and then distributed via cable television (CATV) networks to the subscribers. Reception of these signals in the Netherlands is authorized only on a secondary basis, i.e., no guarantee will be given against harmful interference from a primary service in the same frequency band, notably the 11 GHz digital radio-relay network planned by the Netherlands PTT. Therefore, it is of special interest to investigate the effect of the potential interference from this network on the quality of the television pictures.

As a first step, Haagh [12] has derived a relation between the carrier-to-interference ratio at the output of the receiving antenna and the corresponding baseband-interference spectrum. Although this spectrum cannot be used directly as a measure for the picture quality (only subjective tests can give this information), it does provide a useful insight into the nature and magnitude of the degradations caused by the potential interference. Referring to [12] for the details of the calculations, we only present some illustrative measured results here.

The problem is outlined in the block diagram of fig. 2.3. The wanted radio-frequency signal is a frequency-modulated colour-television (FM-TV) signal, with peak deviation 19 MHz, carrying a stationary colour-bar picture. The measured FM-TV spectrum is shown in fig. 2.4a. An analytical parametric representation has been

determined for this spectrum; the parameters are chosen such that the analytical spectrum fits the envelope of the measured spectrum. The interfering signal is a 34 Mbit/s QPSK-modulated carrier with pulse shaping and a 3 dB bandwidth equal to 22 MHz, see fig. 2.4b. A random data signal represents the baseband signal corresponding to a multichannel trunk connection, as will be used in the 11 GHz radio-relay network for the public-telephone service. The frequency separation between the two carriers ( $\Delta f$ ) and the carrier-to-interference level (C/I) at the receiver input are taken as variable parameters.

The baseband spectrum of the received signal has been calculated and measured for several values of C/I and  $\Delta f$ . Typical measured results are shown in fig. 2.5. The main disturbances in the video spectrum appear to occur at the medium and higher baseband frequencies, although the chrominance signal with peak at 4.5 MHz, containing the colour information of the TV-picture, remains almost undisturbed. The effects on the television pictures are observed as irregular transitions between the individual colour bars and noisy disturbances inside the bars. Subjective tests have to be carried out to determine the maximum-acceptable disturbance, and the corresponding maximum-permissible C/I at the receiver input, for different  $\Delta f$ .

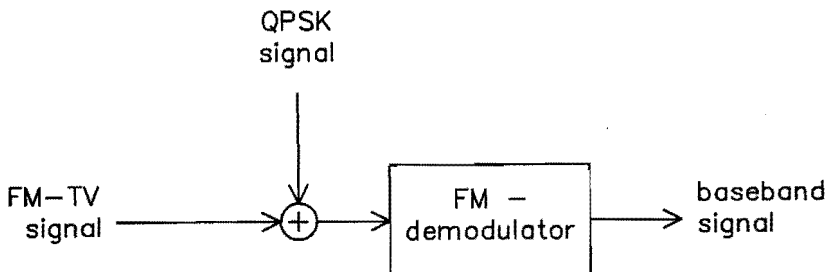


Fig. 2.3. Interference of a QPSK signal to FM-TV reception.

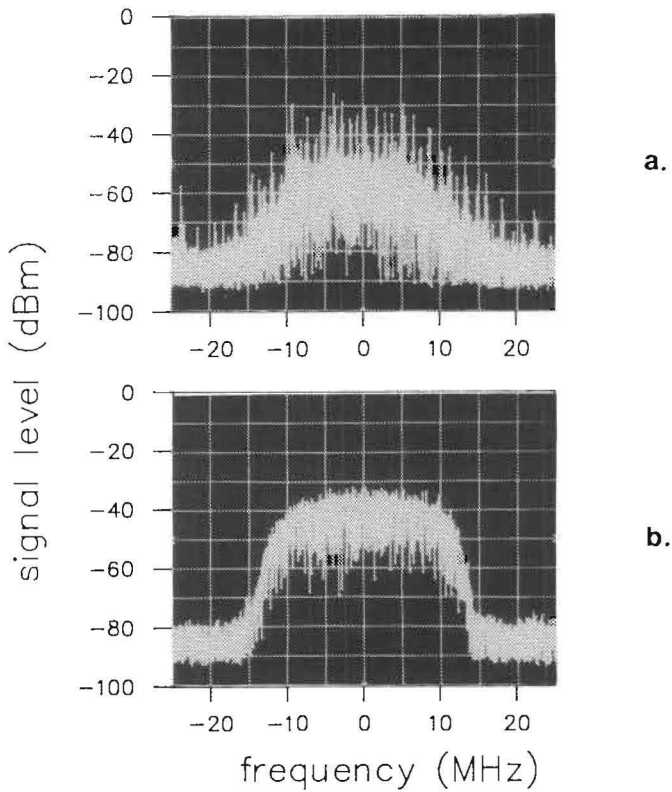


Fig. 2.4. Spectra of the RF signals.

a) Wanted FM-TV signal;

b) interfering QPSK signal.

## 2.4. Coordination areas

An important concept in frequency sharing between earth stations and terrestrial stations is the earth-station's *coordination area*. This area is defined in the RR as "the area associated with an earth station outside which a terrestrial station sharing the same frequency band neither causes nor is subject to interfering

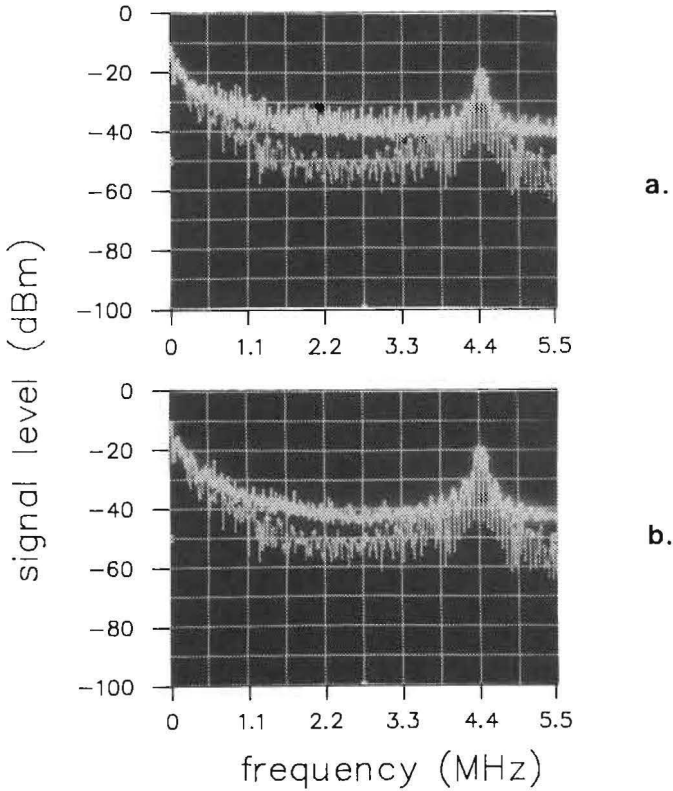


Fig. 2.5. Baseband spectrum in the presence (upper trace) and absence (lower trace) of interference.  $C/I=2.3$  dB.

a)  $\Delta f=0$ ;      b)  $\Delta f=10$  MHz.

emissions greater than a permissible level" [1, art. 1]. Such a coordination area, enclosed by a curve known as the *coordination contour*, is determined by calculating for all azimuths the *coordination distance*, i.e., the distance from the earth station beyond which a terrestrial station neither causes nor is subject to interfering emissions greater than the specified permissible level. This concept assumes that for



terrestrial stations outside the coordination area no problems of impermissible interference are to be expected, whereas for each terrestrial station inside the area detailed coordination is required. This can be an immense task, especially if the coordination area is unnecessarily large; on the other hand, it is better to be on the safe side to avoid any unforeseen problems after installation of the costly facilities.

In appendix 28 of the RR [1] a method is described for the calculation of the coordination area on the basis of several "worst-case" assumptions. The method employs the CCIR prediction models [13-15] concerning terrestrial propagation both within and (especially) beyond the horizon. These models predict the transmission loss along a given terrestrial (transhorizon) path as a function of the distance between the terminals, with time percentage as a parameter. This information is used in appendix 28 of the RR to calculate the coordination distance for a specific fixed time percentage (typically 0.01%). By repeating this calculation for all azimuths, the coordination contour can be traced on a map.

As an example, the coordination contours for the Burum-1 earth station of the Netherlands PTT, operating in the INTELSAT network using frequency-modulated carriers at 4 GHz and 6 GHz, are indicated in fig. 2.6 by the dashed and solid curves, for the transmit and receive mode, respectively [16]. It is seen that the coordination area for the receive mode is much larger than that for the transmit mode. The reason is that receiving earth stations are much more vulnerable to interference from transmitting terrestrial stations than vice versa, as explained in sec. 2.2.4. It is also clear from this figure that the coordination distances over sea are much longer than those over land, due to the higher probability of propagation anomalies above the sea (sec. 3.3.3).

In principle, all terrestrial stations inside the coordination contour require detailed coordination with the earth station. Such a coordination involves a more

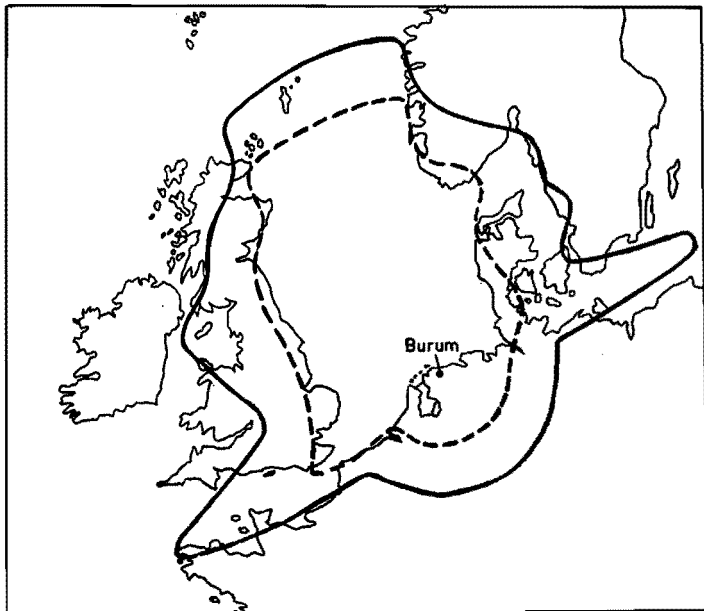


Fig. 2.6. Coordination contours for the transmitting (dashed curve) and receiving (solid curve) Burum-1 earth station, based on appendix 28 of the RR [1]. Courtesy: Netherlands PTT [16].

detailed calculation of the interference levels, based on the exact parameters of the earth station and each terrestrial station, instead of the "worst-case" parameters assumed in appendix 28 of the RR [1]. Protective measures have to be taken for each terrestrial station that causes or suffers from impermissible interference levels. If the density of terrestrial stations is high, coordination is a considerable task. As an illustration, the Dutch 4 GHz radio-relay network, located entirely within the coordination area of the receiving Burum-1 earth station, is shown in fig. 2.7 [16]. By assuming a constant sidelobe level of the earth station's radiation pattern of  $-10$  dBi, contours can be drawn around all terrestrial stations, within which the interference level would be unacceptably high for an earth station present. The result for the Dutch radio-relay network is shown in fig. 2.8 [16]. According to this

result, protection of the Burum-1 earth station is needed against interference from one radio-relay station in the Netherlands. The same procedure should be repeated for all foreign terrestrial stations within the coordination area shown in fig. 2.6.

In fact, the Netherlands PTT has recently changed the structure of its 4 GHz radio-relay network [16], in order to avoid radio interference into the Burum-1

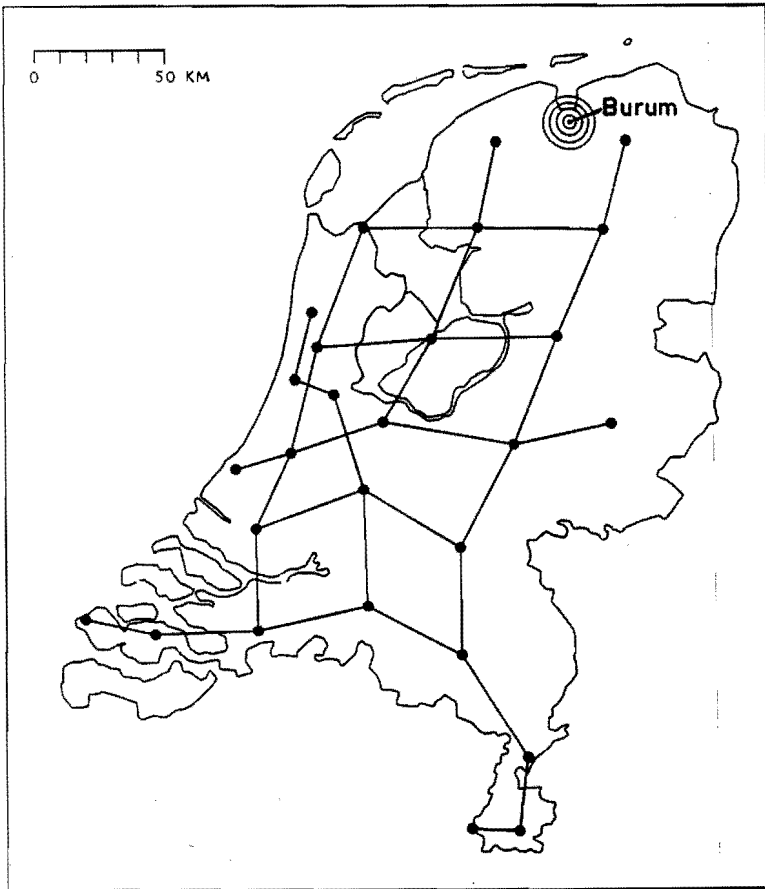


Fig. 2.7. The 4 GHz radio-relay network of the Netherlands PTT, as of February 1984.

Courtesy: Netherlands PTT [16].

earth station. The most harmful radio-relay links are now operating outside the 4 GHz band.

Better quantitative knowledge of the transhorizon-propagation phenomena may permit a considerable reduction of coordination areas. This close relationship between the transhorizon-propagation models and the size of coordination areas

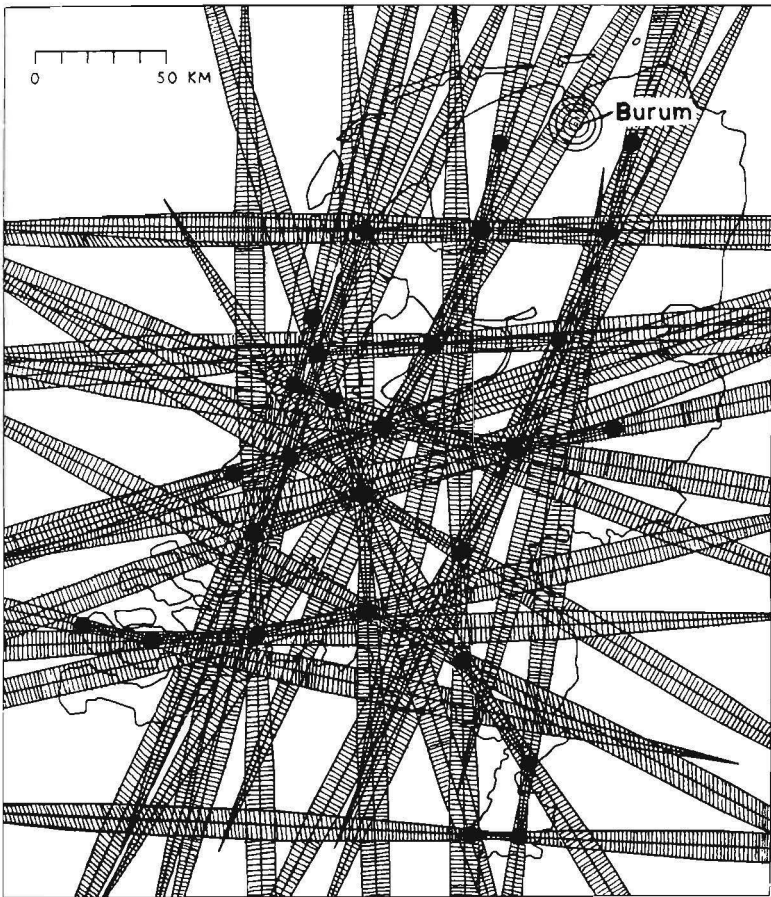


Fig. 2.8. Interference contours for the Dutch 4 GHz radio-relay stations, for coordination with the receiving Burum-1 earth station.

Courtesy: Netherlands PTT [16].

justifies a thorough investigation into the transhorizon-propagation phenomena (see chapters 3 and 4).

## 2.5. References

- [1] ITU, "*Radio Regulations*", Geneva, 1982.
- [2] M.P.M. Hall, "*Effects of the troposphere on radio communication*", Peter Peregrinus, Stevenage, 1979.
- [3] CCIR, Plenary Assembly, "Terrestrial television broadcasting in the 12 GHz band (band VI)", *Recommendations and Reports of the CCIR*, Vol. XI-1, Rep. 961-1, Geneva, 1986.
- [4] ETCO, "*Detailed analysis of second generation mobile communications*", Commission of the European Communities, Brussels, 1985.
- [5] R. Mitra, W.A. Imbriale and E.J. Maanders, ed., "*Satellite communication antenna technology*", North-Holland, Amsterdam, 1983.
- [6] D.M. Jansky and M.C. Jeruchim, "*Communication satellites in the geostationary orbit*", 2nd ed., Artech House Inc., Dedham, 1987.
- [7] A.R. Dion and L.J. Ricardi, "A variable-coverage satellite antenna system", *Proc. IEEE*, vol. 59, no. 2, pp. 252-262, 1971.
- [8] M.H.A.J. Herben, "Designing a contoured-beam antenna", *EUT-report*, no. 79-E-104, Eindhoven University of Technology, Eindhoven, 1979.
- [9] P. Stavroulakis, "*Interference analysis of communication systems*", IEEE Press, New York, 1980.
- [10] K. Feher, "*Digital modulation techniques in an interference environment*", Don White Cons. Inc., Germantown, 1977.

- [11] CCIR, Plenary Assembly, "Method for the subjective assessment of the quality of television pictures", *Recommendations and Reports of the CCIR*, Vol. XI-1, Rec. 500-3, Geneva, 1986.
- [12] J.P.N. Haagh, "RF-interference from digital radio-relays into satellite FM-TV reception", *Master's Thesis*, Eindhoven University of Technology, Eindhoven, 1985 (in Dutch).
- [13] CCIR, Plenary Assembly, "Radiometeorological data", *Recommendations and Reports of the CCIR*, Vol. V, Rep. 563-3, Geneva, 1986.
- [14] CCIR, Plenary Assembly, "The evaluation of propagation factors in interference problems between stations on the surface of the earth at frequencies above about 0.5 GHz", *Recommendations and Reports of the CCIR*, Vol. V, Rep. 569-3, Geneva, 1986.
- [15] CCIR, Plenary Assembly, "Propagation data required for the evaluation of coordination distance in the frequency range 1-40 GHz", *Recommendations and Reports of the CCIR*, Vol. V, Rep. 724-2, Geneva, 1986.
- [16] C.A.M. Geus and H.J. Nijland, PTT Dr. Neher Laboratories, private communications, 1984 and 1987.



### 3. TRANSHORIZON-PROPAGATION MECHANISMS - A REVIEW

#### 3.1. General introduction

It has been shown in the previous chapter (sec. 2.2.4) that transhorizon interference from terrestrial stations can severely hamper the successful operation of an earth station operating in the same frequency band. Various propagation mechanisms are responsible for this type of interference. These mechanisms are reviewed and described qualitatively in this chapter. In addition, we determine the relative importance of each mechanism from the point of view of transhorizon interference. The most important one is studied quantitatively in the next chapter.

In studying tropospheric propagation, geometric-optical considerations are often helpful. The use of geometrical optics is justified if the wavelength is small compared to the physical dimensions of the objects involved (and to the gradient lengths of the inhomogeneous atmosphere). At the frequencies of interest here (1 to 30 GHz), this assumption may or may not be valid, depending on the actual situation. Nevertheless, the method may be applied to obtain at least qualitative physical insights. Geometric-optical considerations are therefore used throughout this chapter to assist in modelling tropospheric-propagation phenomena.

#### 3.2. Introduction to transhorizon-propagation research

##### 3.2.1. *Time variability*

As explained in chapter 2, the frequency bands above 1 GHz are of primary interest for frequency sharing between terrestrial stations and earth stations. At these frequencies, it is mainly the lower part of the atmosphere (the *troposphere*,



extending from 0 to 10 km above the earth surface) which affects radio propagation (although geodesists and radio astronomers must also take into account the influence of the *ionosphere*, extending from 70 to 1000 km above the earth surface). The behaviour of the troposphere is highly time-variable because of seasonal, diurnal and weather influences. Statistical studies are therefore necessary to describe or predict (transhorizon) tropospheric propagation.

Availability requirements for satellite-earth stations are usually given in terms of a maximum out-of-service time in a certain period (a month or a year), or, equivalently, of a minimum in-service time [1]. Typical values of the latter are 99% of the time for broadcasting services and 99.99% of the time for public-telephone services. As a consequence, a maximum-permissible interference level is specified as a certain level not to be exceeded for more than a given time percentage  $p$ , where  $p$  is in the order of 1% or below. Occasionally, the operational requirements are less tight, in which case  $p$  is in the order of 10%.

Propagation research for interference calculations must therefore concentrate on the highest signal levels, which occur only for a small percentage of time. To obtain sufficiently reliable statistics, experiments have to be carried out continuously for several years, to cope with seasonal and year-to-year variabilities; the lowest time-percentages ( $0.001\% \leq p \leq 0.01\%$ ) correspond to less than an hour per year.

### 3.2.2. *General concepts and terminology*

In free space, radio-wave-propagation parameters are related by the classical *radio equation* [2, eq. (2.16)]

$$P_r = P_t G_t G_r (\lambda/4\pi d)^2, \quad (3.1)$$

where  $P_r$  is the received power and  $P_t$  is the transmit power;  $G_r$  and  $G_t$  denote the gains of the receive antenna and the transmit antenna, respectively;  $d$  is the distance between the two terminals and  $\lambda$  is the wavelength of the (monochromatic or narrowband) radio wave. The *free-space basic transmission loss*  $L_{bf}$  is defined as the ratio  $P_t/P_r$  when ideal loss-free isotropic antennas ( $G_t=G_r=1$ ) are assumed; thus,  $L_{bf}$  is given by

$$L_{bf} = (4\pi d/\lambda)^2, \quad (3.2)$$

or in decibels (using logarithms with base 10)

$$L_{bf} = 92.5 + 20 \log f + 20 \log d \quad (\text{dB}), \quad (3.3)$$

where  $f$  is the frequency of the radio wave in GHz and  $d$  is the distance in km. The quantity  $L_{bf}$  is useful as a reference value for a given path, to which actual transmission losses on that path may be compared. The *basic transmission loss*  $L_b$  of a propagation path (also known as the *path loss*) is the ratio of the actual  $P_t$  and  $P_r$  for that path, assuming loss-free isotropic antennas.  $L_b$  is normally higher than  $L_{bf}$ , because of the higher losses of the actual propagation mechanism(s) as compared to the free-space propagation. The difference is called the *excess path attenuation*  $L_m$ ; thus,

$$L_b = L_{bf} + L_m \quad (\text{dB}). \quad (3.4)$$

As distinct from  $L_{bf}$ , the quantity  $L_b$  (and thus  $L_m$ ) is not fixed for a certain path, but strongly time variable, due to the time variability of the actual propagation

mechanisms. For interference calculations, the lowest values of  $L_m$  are of interest, occurring for small percentages of time.

An important statistical parameter for studies of isotropic wave propagation is the *refractive index*  $n$  (at a given point) of the atmosphere. Because  $n$  is close to unity for the troposphere, it is more convenient to work with the *refractivity*  $N$ , which is defined by

$$N = (n-1) \cdot 10^6. \quad (3.5)$$

The quantity  $N$  varies both in time and in space (due to changing weather conditions). Horizontal variations in  $N$  are often much smaller than vertical variations and are usually neglected.

Under median atmospheric conditions and near the earth surface,  $N$  decreases approximately linearly with height  $h$ , by about 40 units per km. The *standard atmosphere* is defined as a fictitious inhomogeneous atmosphere in which  $dN/dh = -40 \text{ km}^{-1}$  everywhere in time and space. A geometric-optical illustration of propagation in standard atmosphere is shown in fig. 3.1a. The radius of curvature  $r$  of a ray is larger than the radius  $a$  of the spherical approximation to the earth, so the ray moves away from the earth surface.

The geometry of fig. 3.1a (a curved ray above a curved earth surface) can be simplified by a transformation, in which the distance between each point of the ray and the surface remains unchanged. Two different transformations are commonly applied [3, sec. 2.4], leading to two models in which either the curvature of the ray or the curvature of the earth surface has disappeared in the transformed coordinate system. Both transformations are based on Snell's law in the spherical geometry of fig. 3.1a, i.e., the constancy of  $n(h)(a+h)\cos\alpha(h)$ , where  $\alpha(h)$  is the angle between the tangent to the ray and the horizontal.

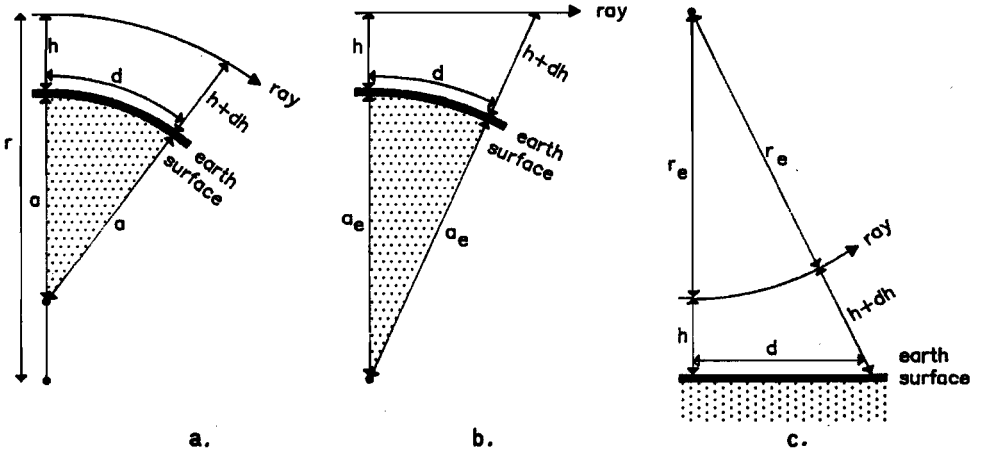


Fig. 3.1. Geometric-optical models of tropospheric refraction in the standard atmosphere, valid for  $d \ll a$  and  $h \ll a$ .

- a) Realistic situation with earth radius  $a$  and ray radius  $r$ .
- b) Straight-ray model with effective earth radius  $a_e$ .
- c) Flat-earth model with effective ray radius  $r_e$ .

i) The *straight-ray model* (fig. 3.1b) compensates the curvature of the rays by defining an *effective earth radius*  $a_e$ , and the rays are drawn as straight lines. This can be done if  $a_e$  is chosen to satisfy [3, eq. (2.23)]

$$\frac{1}{a_e} = \frac{1}{a} + \frac{dn}{dh} = (157 + \frac{dN}{dh}) \cdot 10^{-6} \quad \text{km}^{-1}, \quad (3.6)$$

where  $a=6370$  km, and  $h$  is the height above the surface measured in km. The ratio  $a_e/a$  is known as the *effective earth-radius factor*  $k$ , which is obviously also a statistical variable. Standard atmosphere corresponds to  $k=4/3$ . If  $k>4/3$ , the atmosphere is said to be *superrefractive* (see sec. 3.3.3). The straight-ray model assumes that the gradient  $dN/dh$  is constant (at least in the height interval of interest).

ii) The flat-earth model (fig. 3.1c) compensates the curvature of the earth by defining an effective radius of curvature of the ray  $r_e$ , and the earth surface is treated as flat. This is possible if  $r_e$  is chosen to satisfy [3, eq. (2.24)]

$$\frac{1}{r_e} = \frac{1}{a} + \frac{dn}{dh} = (157 + \frac{dN}{dh}) \cdot 10^{-6} \quad \text{km}^{-1}. \quad (3.7)$$

Thus,  $r_e$  is equal to  $a_e$  of the former model (i). For the latter model (ii), it is practical to define the modified refractive index  $m$  and the modified refractivity  $M$ , respectively, as

$$m = n + h/a, \quad (3.8)$$

$$M = (m-1) \cdot 10^6 = N + (h/a) \cdot 10^6. \quad (3.9)$$

In this model, standard atmosphere corresponds to  $dM/dh=117 \text{ km}^{-1}$ , super-refraction to  $dM/dh < 117 \text{ km}^{-1}$ . If  $dM/dh$  is not constant, the model can still be applied by allowing a height dependence of  $r_e$ .

Although these two models are approximate, it has been shown [4] that, for the heights and path lengths of interest (i.e.,  $h \ll a$  and  $d \ll a$ ), they may both be applied with very good accuracy.

The straight-ray model is helpful for the definition of some geometrical parameters, by means of a *path profile*. This is a cross section of the earth surface, drawn with a fixed effective earth radius  $a_e = ka$  (usually  $k=4/3$ ), in the *great-circle plane*, i.e., the plane containing the transmitter location, the receiver location and the centre of the earth. An example of a path profile is shown in fig. 3.2. This figure also illustrates some geometrical parameters which are defined now. The *radio horizon* of a terminal is defined as the point(s) on the earth surface where the radio

ray from that terminal is tangent to the surface (point P or Q in fig. 3.2). The corresponding ray is known as the *horizon ray* of the terminal. The *radio-horizon distance* ( $d_t$  or  $d_r$ ) for a terminal is defined as the distance between the terminal and its radio horizon. The *angular distance*  $d_a$  of a transhorizon path is the distance between the two radio horizons. The distances  $d_t$ ,  $d_r$ , and  $d_a$  are related to the total path length  $d$  by

$$d = d_t + d_a + d_r . \tag{3.10}$$

Note that the distances at the right-hand side of (3.10) are time variable, due to the time variability of  $k$  and thus  $a_e$ . If  $d_a$  becomes negative (e.g. during occasional superrefractive conditions), the path is in fact no longer a transhorizon path. If this condition is satisfied also for standard atmosphere, so that the influence of obstacles along the path can be neglected, the path is called a *line-of-sight path*.

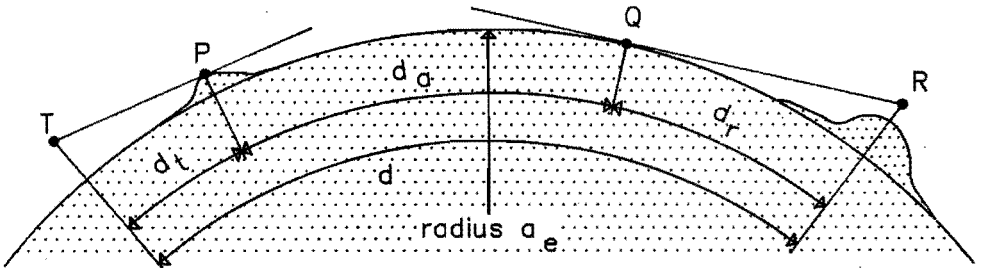


Fig. 3.2. Example of a path profile.

T: transmit terminal, R: receive terminal, P: transmitter radio horizon, Q: receiver radio horizon,  $d_t$ : transmitter radio-horizon distance,  $d_r$ : receiver radio-horizon distance,  $d_a$ : angular distance,  $d$ : path length,  $a_e$ : effective earth radius.

### 3.2.3. Presentation of results

Results of statistical transhorizon—propagation research are usually displayed by the *cumulative distribution* of  $L_m$  or  $L_b$ . The value of this function for a certain time percentage  $p$  indicates the value of  $L_m$  (or  $L_b$ ) that is not exceeded for  $p\%$  of the time. In an interference situation, a certain value of the cumulative distribution of  $L_m$  corresponds to a certain interference level exceeded for  $p\%$  of the time. The cumulative distribution of  $L_m$  is therefore important for interference calculations (see sec. 3.2.1).

For the explanation of increased signal levels in terms of atmospheric processes, *diurnal distributions* are useful as well. They are displayed for several values of the parameter  $L_m$ , and averaged over all days in a certain period.

Examples of measured cumulative and diurnal distributions are given in sec. 4.3.2.

## 3.3. Review of transhorizon—propagation mechanisms

### 3.3.1. General remarks

The influence of the troposphere on terrestrial radio propagation is quite complex. Gaseous absorption and absorption by hydrometeors (e.g. rain drops) may attenuate the received signal significantly at microwave frequencies, and especially at frequencies above about 5 GHz [3, chapter 3]. However, more important for interference calculation is the fact that various mechanisms may also enhance the received signal, thereby limiting the possibilities of successful frequency sharing between stations on the earth. The latter class of mechanisms is reviewed in this section.

A distinction is made between mechanisms operating in the great-circle plane (known as "clear-air" mechanisms), and mechanisms which can also operate outside this plane ("scatter" mechanisms). Modelling of scatter mechanisms is, in general, more difficult, because three-dimensional geometries are involved.

Another distinction can be made, namely between propagation mechanisms that are permanently present (with or without temporal fluctuations), and mechanisms that occur only occasionally. The former category is often responsible for the lower signal levels at higher percentages of the time, whereas the second category causes the occasional higher signal levels ( $p < 10\%$ ). Most of the "permanent" mechanisms are determined by topographical features along the propagation path, which hardly vary in time. The "occasional" mechanisms are mainly caused by time-variable atmospheric processes.

The mechanisms to be reviewed in the following are listed in table 3.1, in which these classifications are clearly visible. The discussion deals specifically with interference into earth stations caused by terrestrial stations. However, many of the mechanisms discussed also apply to other interference situations.

	permanent mechanisms	occasional mechanisms
clear-air mechanisms	a) line-of-sight propagation b) diffraction	d) superrefraction e) ducting f) elevated-layer reflection
scatter mechanisms	g) terrain scatter	h) hydrometeor scatter i) aircraft scatter

Table 3.1. Classification of tropospheric-propagation mechanisms which can cause interference from terrestrial stations into earth stations.



### 3.3.2. Permanent clear-air mechanisms

These mechanisms are well-known in tropospheric propagation theory, because they are exploited for wanted terrestrial communication links. From the point of view of interference, the time variability of these mechanisms is of interest, especially possible enhancements of the received signal levels caused by these mechanisms.

a) Line-of-sight propagation. If a receiving earth station is located within the radio horizon of a transmitting terrestrial station under standard atmospheric conditions, then line-of-sight propagation is possible between the two stations. The attenuation along a line-of-sight path is in the same order of magnitude as free-space attenuation (i.e.,  $L_m$  is small), hence the risk of harmful interference into the earth station is high.

On line-of-sight paths, the received signal level varies and occasionally fades owing to multipath effects [3, chapter 4]. This fading is an unwanted effect in terrestrial radio-relay links, which has been studied extensively [5]. On an interference path, on the other hand, occasional enhanced signal levels can be of concern. Enhanced line-of-sight propagation has received much less attention in the literature, because it is unimportant for the planning of radio-relay networks. The available data suggest that for most of the time, the signal enhancement is limited to a few dB [5].

Line-of-sight path lengths normally do not exceed some tens of kilometers, depending on antenna heights. On longer (i.e., transhorizon) paths, continuous signal reception is only possible by the diffraction mechanism (see *b*) or the troposcatter mechanism (*c*).

b) Diffraction. Along a path obstructed by the earth surface or by an obstacle, diffraction can be responsible for transhorizon propagation. The diffraction mechanism introduces a loss, which is strongly dependent on the radius of curvature (in the great-circle plane) of the top of the obstacle. Two extreme cases are shown in fig. 3.3: spherical-earth diffraction (fig. 3.3a) and knife-edge diffraction (fig. 3.3b). The larger the radius of curvature, the higher is the diffraction loss [6,7]. In practice, interference by diffraction at the spherical earth is therefore limited to distances only slightly beyond the radio horizon [7]. Obstacle diffraction can be an important interference mechanism on much longer paths, if the radius of curvature of the top of the obstacle is small. Repeated diffraction occurs on paths with more than one relevant obstacle. If these obstacles resemble knife-edges (e.g. sharp ridges), the received interference levels may be significant in spite of the multiple diffraction losses [8].

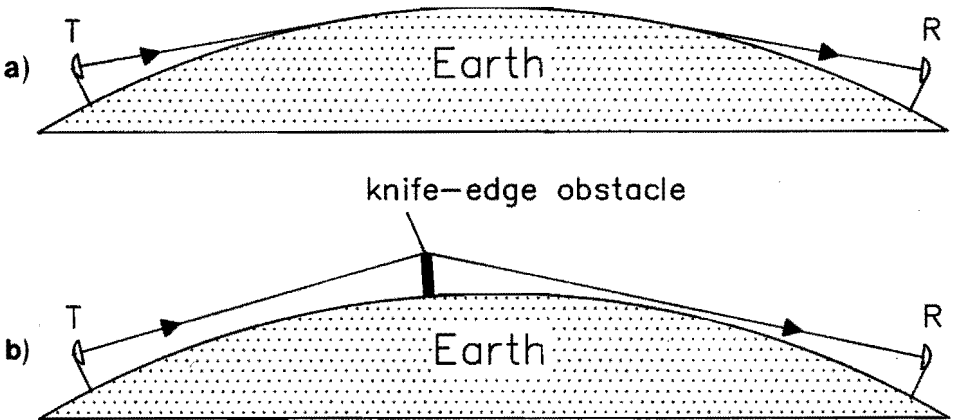


Fig. 3.3: Diffraction mechanisms:  
a) spherical-earth diffraction; b) knife-edge diffraction.  
T: transmitter, R: receiver. The straight-ray model is applied.

c) Troposcatter. Propagation by tropospheric scatter (usually known as troposcatter) is caused by local, small-scale refractive-index irregularities in the troposphere, which scatter the incident wave into various directions. These directions are not limited to the great-circle plane, so strictly speaking troposcatter belongs to the category of "scatter" mechanisms (see table 3.1). However, it has been observed that the power flux of the scattered wave is very small for directions outside the great-circle plane. In fact, the power flux is an exponentially decreasing function of the scatter angle  $\theta$ , which is defined as the angle between the directions of the incident wave and the scattered wave (see fig. 3.4). Thus, troposcatter is only relevant for very small values of  $\theta$ , and the power scattered outside the great-circle plane is usually neglected. Inside this plane, the smallest value of  $\theta$  occurs between the horizon rays of the two terminals.

Troposcatter can be utilized to establish reliable communication links over distances of some hundreds of kilometers [9, chapters 6-8]. The level of the received signal is time variable, because of the variability of the spatial distribution of the scattering irregularities. The excess path attenuation  $L_m$  is typically in the order of

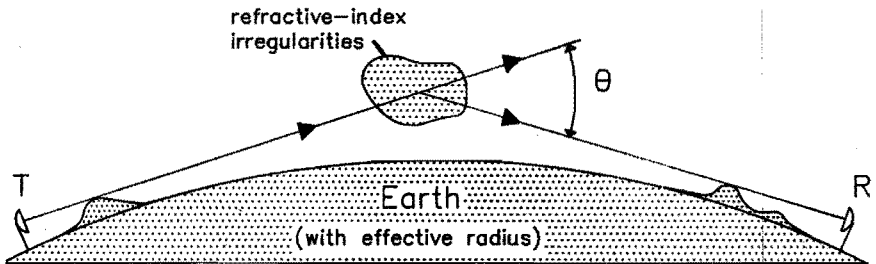


Fig. 3.4. Troposcatter propagation.  $\theta$ : scatter angle; T: transmitter; R: receiver. The straight ray model is applied.

40–50 dB and has diurnal and seasonal variations. Superimposed on these slow variations is a rapid fluctuation, which is characteristic for the troposcatter mechanism.

From an interference point of view, signal levels due to troposcatter are generally of minor concern, relative to the (much higher) interference levels due to occasional superrefraction or ducting (see sec. 3.3.3). However, when less demanding operational requirements (say 90% of the time) are imposed on a radio service, the interference levels exceeded for higher time percentages ( $p=10\%$ ) become important; these levels are often determined by troposcatter. On very rough land paths, troposcatter can be the dominant mechanism even for  $p<1\%$ , because ducting is unlikely there.

### 3.3.3. Occasional clear-air mechanisms

Occasional propagation mechanisms cannot be used to establish reliable communication links. The coverage area of a terrestrial transmitter is sometimes increased by these mechanisms, which may be considered a favourable effect for radiodetermination, broadcasting or radio amateur services. It is an unfavourable effect from an interference point of view, however.

d) Superrefraction. Certain weather conditions enhance the atmospheric refraction, so that the radio horizon distance of a terrestrial station becomes larger (see sec. 3.2.2). This effect, known as superrefraction, is well known in VHF and UHF terrestrial broadcasting: the coverage area of a radio or TV transmitter increases significantly during such weather conditions. This effect also occurs at microwave frequencies, and thus leads to increased interference levels. Several atmospheric processes contribute to this effect [2, chapter 3; 10, sec. 4.4.2].

e) Ducting. Ducting is an extreme form of superrefraction, in which the atmospheric refraction is so enhanced that radio rays are bent down towards the earth surface, see fig. 3.5a. This effect occurs for  $dN/dh < 157 \text{ km}^{-1}$ , or equivalently,  $k < 0$ . The rays bent down towards the surface can, by repeated reflection, propagate over considerable distances (in practice sometimes over 1000 km). Ducting is similar to a waveguiding effect, the upper boundary being formed by an elevated tropospheric inhomogeneity. The lower boundary is often the earth surface (in the event of ground-based ducts), but can also consist of another atmospheric layer (elevated ducts), see fig. 3.5a and fig. 3.5b, respectively. In an "ideal" duct (i.e., a duct without leakage of energy at the top and the bottom boundaries), the power flux from a source spreads cylindrically, as distinct from the spherical spreading in free space or under median atmospheric conditions. As a consequence, signal levels at large distances from the source can be very high during ducting and even exceed the free-space levels ( $L_m < 0 \text{ dB}$ ).

The atmospheric processes responsible for ducting conditions are the same as those causing "normal" superrefraction. These processes have, in general, a much higher probability of occurrence above sea than above land [10, sec. 4.4.2]. Nevertheless, for small time percentages ducting is the dominant propagation mechanism on many land paths as well.

Ducting is one of the most troublesome phenomena for the coordination of earth stations with terrestrial stations, especially in frequency bands below about 5 GHz (at higher frequencies, hydrometeor scatter — see sec. 3.3.5 — becomes the dominant mechanism). Coordination contours at frequencies below 5 GHz are most often a consequence of the ducting mechanism, as is the case in the example shown in fig. 2.6. A thorough investigation of this mechanism is therefore justified (see chapter 4).

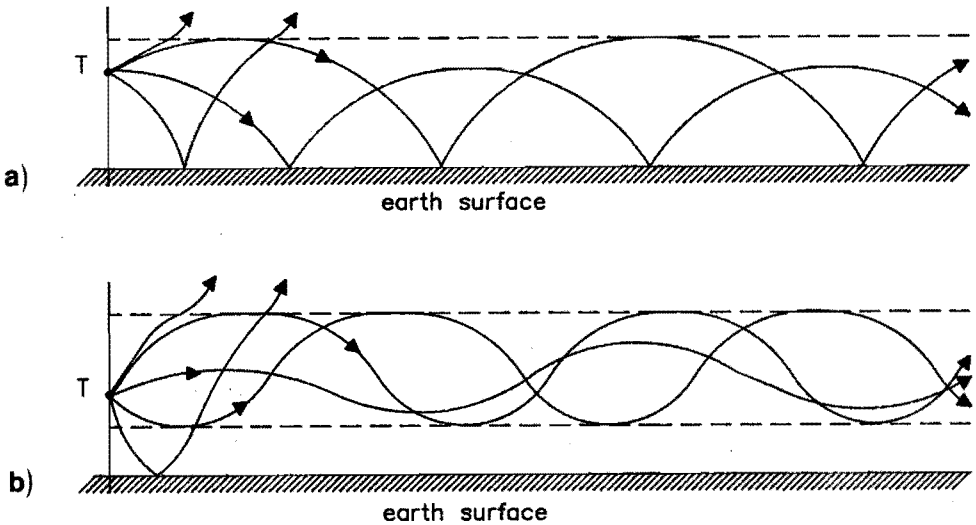


Fig. 3.5. Ducting mechanisms: a) ground-based duct; b) elevated duct.  
T: transmitter. The flat-earth model is applied.

f) Elevated-layer reflection. Reflection of HF radio waves at the *ionosphere* is a well-known effect, allowing e.g. trans-oceanic propagation. Though this effect is normally limited to frequencies of about 30 MHz, sporadic ionospheric reflection sometimes occurs at frequencies up to 100 MHz. Terrestrial radio waves with frequencies above 100 MHz are hardly influenced by the ionosphere. However, they can occasionally be reflected by an elevated *tropospheric* layer, if the corresponding refractive-index discontinuity at the layer is sufficiently large. It has been argued that this effect is limited in practice to frequencies below 1 GHz [3, sec. 2.6] because at higher frequencies such layers normally cause ducting instead of reflection. For interference calculations above 1 GHz, the atmospheric-reflection mechanism is therefore usually ignored. However, it has been suggested [11] that this mechanism may be responsible for occasional interference phenomena at microwave frequencies as well.

### 3.3.4. Permanent scatter mechanisms

As distinct from the corresponding clear-air mechanisms, permanent scatter mechanisms are seldom used to establish communication links. The latter mechanisms are therefore less known in microwave-propagation theory.

g) Terrain scatter. Radiation which is incident on terrain obstacles (hills or buildings) is scattered into various directions. This scatter mechanism can cause unwanted propagation from one station to another, thus leading to interference into the latter, see fig. 3.6. Propagation by terrain scatter is not limited to the great-circle plane of the two antennas, but it is a three-dimensional effect. Interference by this mechanism is strongest if the scattering obstacle is located in the main beams of both antennas. In that case, the received scattered signal may be stronger than the signal received from clear-air mechanisms, because the latter suffers from lower antenna gains (due to sidelobe transmission and reception). This has been demonstrated recently [12,13] for interference between two terrestrial stations.

The main beam of an earth station is most often free from obstruction by terrain, provided that the antenna elevation is not too small. Then, interference by terrain scatter is only possible via a sidelobe of the earth-station antenna (which obviously has a lower gain than the main beam). It is therefore doubtful whether terrain-scatter has any relevance in interference calculations for earth stations.

### 3.3.5. Occasional scatter mechanisms

The mechanisms to be treated in this section are similar to the terrain-scatter mechanism (sec. 3.3.4). A major difference for earth-station interference is the fact, that here the scatterer can be located in the main beams of *both* stations. The

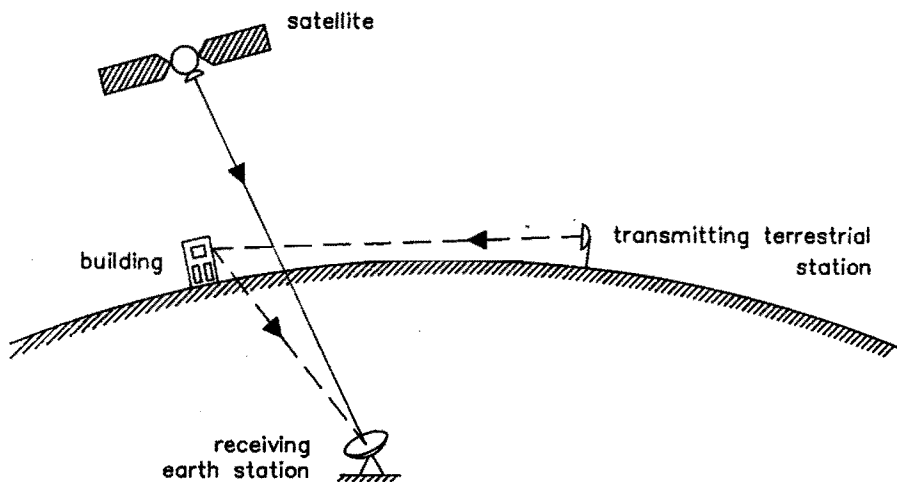


Fig. 3.6. Interference by building scatter from a terrestrial station into an earth station. ——— wanted path; - - - unwanted path.

consequence is not only a stronger received signal (compared to sidelobe reception of terrain-scatter interference), but also increased difficulties in separating the wanted and unwanted signals by means of interference-reduction techniques based on angular discrimination (see chapter 5).

*h) Hydrometeor scatter.* Interference due to unwanted scatter from hydrometeors (raindrops or ice crystals) becomes increasingly important at frequencies above 1 GHz. Above about 10 GHz, the mechanism dominates the occasional clear-air mechanisms. Hydrometeor-scatter interference is especially a matter of concern if the main beam of the earth station crosses the main beam of a terrestrial station, and becomes effective when a rain shower passes the intersection of the beams, see fig. 3.7.

Characteristic of a signal received by hydrometeor scatter are its rapid fluctuations. Such a signal has a very low spatial and temporal autocorrelation and



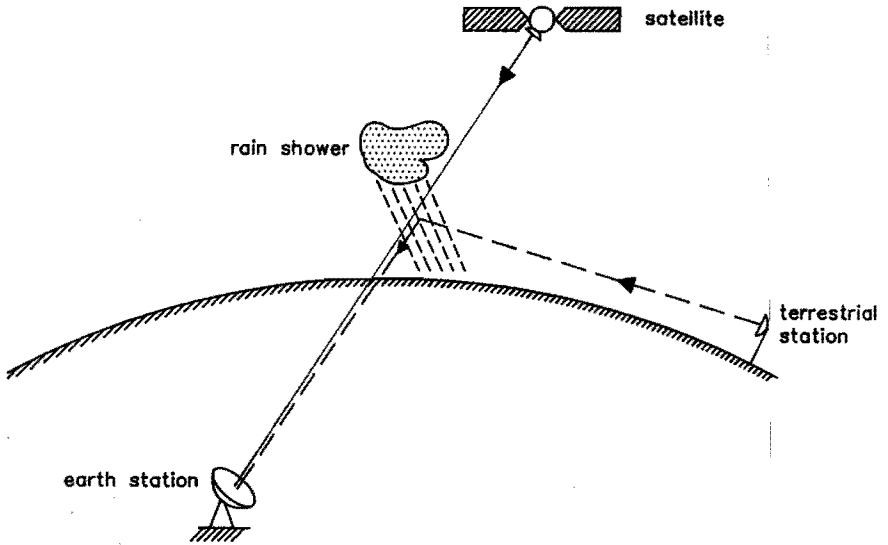


Fig. 3.7. Interference by hydrometeor scatter.

—— wanted path;      - - - - - unwanted path.

appears at the receiver as additional noise imposed on the wanted signal. Reception of this type of interference is therefore difficult to recognize.

i) Aircraft scatter. Interference by signals scattered from aircraft becomes effective when an aircraft crosses the intersection of the (main) beams of two stations. Only qualitative results have been published on this effect [14, sec. 6]. The probability of this type of interference into an earth station is assumed to be very low, as long as the main beam of the earth station does not cross much-used flight paths, such as runway extensions near airports.

### 3.4. Relative importance of the mechanisms

The mechanisms responsible for interference due to transhorizon propagation have been briefly reviewed in sec. 3.3. Several mechanisms can, of course, occur simultaneously. For example, during superrefractive conditions the effective earth radius (in the straight-ray model) increases; consequently, the scatter angle  $\theta$  (see fig. 3.4) is reduced, and the troposcatter signal is enhanced.

For the calculation of interference exceeded for small time percentages, ducting and hydrometeor scatter are of most interest, because these mechanisms yield the highest interference levels. Below about 5 GHz, ducting is the dominant propagation mechanism, especially along sea paths. Above 5 GHz, hydrometeor scatter becomes increasingly important, and statistically dominates over ducting on land paths and — above 10 GHz — also on most sea paths.

It is pointed out that these two dominant propagation mechanisms seldom occur simultaneously along the same path. The weather conditions necessary for hydrometeor scatter (rain showers, etc.) do not support ducting, which is active mainly in clear-sky conditions. The probabilities of exceeding a certain interference level due to each of the mechanisms are therefore additive.

The ducting mechanism is studied quantitatively in the next chapter.

### 3.5. References

- [1] CCIR, Plenary Assembly, "Determination of co-ordination area", *Recommendations and Reports of the CCIR*, vol. IV/IX-2, Rep. 283-5, Geneva, 1986.
- [2] D.E. Kerr, ed., *Propagation of short radio waves*, Dover, New York, 1951.

- [3] M.P.M. Hall, "*Effects of the troposphere on radio communication*", Peter Peregrinus, Stevenage, 1979.
- [4] C.L. Pekeris, "Accuracy of the earth-flattening approximation in the theory of microwave propagation", *Phys. Rev.*, vol. 70, no. 7-8, pp. 518-522, 1946.
- [5] CCIR, Plenary Assembly, "Propagation data and prediction methods required for line-of-sight radio-relay systems", *Recommendations and Reports of the CCIR*, vol. V, Rep. 338-5, Geneva, 1986.
- [6] K. Hacking, "U.H.F. propagation over rounded hills", *Proc. IEE*, vol. 117, no. 3, pp. 499-511, 1970.
- [7] CCIR, Plenary Assembly, "Propagation by diffraction", *Recommendations and Reports of the CCIR*, vol. V, Rep. 715-2, Geneva, 1986.
- [8] J. Deygout, "Multiple knife-edge diffraction of micro-waves", *IEEE Trans. Ant. Prop.*, vol. AP-14, no. 4, pp. 480-489, 1966.
- [9] J. Dijk, I.V. Brūža and L.J.M. Wijdemans, "*Microwave propagation studies, measurements and education in Surabaya, Indonesia*", Report of cooperation project ITS-EUT, ISBN 90-6144-999-5, Eindhoven University of Technology, Eindhoven, 1983.
- [10] B.R. Bean and E.J. Dutton, "*Radio meteorology*", US Dept. of Commerce, NBS Monograph 92, Washington, 1966.
- [11] O. Rue, "A new clear-air interference prediction method for small time percentages", *Proc. Int. Conf. Ant. Prop. (ICAP)*, *IEE Conf. Publ.*, no. 274, pp. 343-346, 1987.
- [12] A.J. Giger and J. Shapira, "Interference caused by ground scattering in terrestrial microwave radio systems", *IEEE Intern. Conf. Comm. (ICC)*, paper E2.8, 1983.
- [13] A.J. Giger, "Interference caused by ground and building scattering", *XXII<sup>nd</sup> General Assembly of URSI*, session F2, paper 4b, 1987.

- [14] CCIR, Plenary Assembly, "The evaluation of propagation factors in interference problems between stations on the surface of the earth at frequencies above about 0.5 GHz", *Recommendations and Reports of the CCIR*, vol. V, Rep. 569-3, Geneva, 1986.



## 4. CLEAR-AIR TRANSHORIZON PROPAGATION

### 4.1. Introduction

Two categories of transhorizon-propagation mechanisms have been distinguished in chapter 3: clear-air mechanisms and scatter mechanisms. The former category is studied quantitatively in the present chapter, notably the ducting mechanism, which has been shown to be the most important one from an interference point of view.

Most attention will be given to prediction models of clear-air interference, which are essential to coordination procedures. Existing models (mainly empirical or semi-empirical), including the CCIR model [1], are reviewed in sec. 4.2. Measurements have been carried out to test the validity of this CCIR model; results are presented in sec. 4.3. A theoretical model of the ducting mechanism is studied in sec. 4.4, and applied to a specific duct type. The possibility of employing this theory to develop an alternative interference-prediction model is discussed.

Finally, a possible framework of a general interference-prediction procedure, which is at present being developed by the European COST-210 project [2], is briefly described in sec. 4.5.

### 4.2. Review of clear-air interference-prediction models

#### 4.2.1. General remarks

In this section, we discuss prediction models for occasional clear-air interference, i.e., sporadic interference due to propagation mechanisms in the great-circle plane (table 3.1). As argued in sec. 3.3.3, ducting is the most important clear-

air mechanism for low time percentages. Therefore, this mechanism plays a central role in the clear-air interference-prediction models, although other mechanisms are also included in some of the models. Most of the models are partly or completely based on measured radio propagation data, because of the difficulties in theoretically modelling the atmospheric processes involved (e.g. the general lack of sufficient radiometeorological data).

The current CCIR clear-air interference-prediction model [1], which is widely used in interference calculations, is reviewed here in sec. 4.2.2. Other prediction models recently reported in the literature are briefly reviewed in sec. 4.2.3.

#### 4.2.2. CCIR interference-prediction model

The CCIR describes in its Rep. 569-3 [1] a procedure for the calculation of the path loss for a terrestrial path and for low time percentages ( $p < 1\%$ ). For permanent interference mechanisms (responsible for interference during higher time percentages, i.e.,  $p > 1\%$ ), the reader is referred to other CCIR Reports: [3] for diffraction, [4] for troposcatter. (Unfortunately, neither [3] nor any other CCIR Report includes information on the time variability of diffraction loss.) Terrain-scatter is not considered in Rep. 569-3. However, the "permanent" line-of-sight mechanism has been included in this report, because this mechanism occasionally yields enhanced signal levels. Furthermore, the report includes all occasional mechanisms shown in table 3.1.

The occasional scatter mechanisms are dealt with separately in Rep. 569-3; they are not discussed here. The various occasional clear-air mechanisms are treated together, "because of the similarity of the mathematical functions involved", as stated in [1]. This treatment, known as the "CCIR ducting model", is described in some detail below.

The CCIR ducting model. On a path longer than line-of-sight, superrefraction and ducting (or elevated-layer reflection) are assumed to be the dominant clear-air mechanisms for occasional interference ( $p < 1\%$ ). For such a path, the excess path attenuation  $L_m$  is predicted in [1] by the form

$$L_m = -10 \log d + (\gamma_o + \gamma_w + \gamma_d + \gamma_h)d + A_c + A_s \quad (\text{dB}). \quad (4.1)$$

Here,  $d$  is the path length (in km);  $\gamma_o$  and  $\gamma_w$  are the specific attenuations (in dB/km) due to absorption by oxygen and by water vapour, respectively;  $\gamma_d$  is the "specific attenuation" (in dB/km) of the assumed duct;  $\gamma_h$  is the specific attenuation (in dB/km) due to terrain roughness;  $A_c$  is known as the "coupling loss";  $A_s$  is the additional diffraction loss due to terrain shielding of one or both terminals. Empirical formulas are available in [1] for the four specific attenuations (assumed to be constant along the path) and for  $A_c$ , as a function of frequency and time percentage. The expression in [1] for  $A_s$  is taken from [3]. The maximum values of  $A_s$  and  $\gamma_h d$  have been limited in [1] to 30 dB. It is stated that, whenever one of these limits applies, diffraction [3] or troposcatter [4] may become the dominant interference mechanism, even for  $p < 1\%$ .

If we isolate the proper "ducting terms" in (4.1) from the terms representing other mechanisms (i.e., gaseous absorption and terrain shielding), we get the pure CCIR ducting model:

$$L_m = -10 \log d + (\gamma_d + \gamma_h)d + A_c \quad (\text{dB}). \quad (4.2)$$

The *distance* dependence in (4.2) is clear. The *frequency* dependence is implicitly present in  $\gamma_d$ . According to [1], one has



$$\gamma_d = [C_1 + C_2 \log(f + C_3)] p^{C_4}, \quad (4.3)$$

where  $f$  is the frequency in GHz,  $p$  is the time percentage and  $C_i$  ( $i=1, \dots, 4$ ) are constants given in tabular form in [1]. The dependence of (4.2) on *time percentage* is present in  $\gamma_d$  (see eq. (4.3)) and in  $A_c$ . The quantities  $\gamma_d$  and  $A_c$  also depend on the "radioclimatic zone" [1] in which the path is located. Finally,  $\gamma_h$  is a function of the *terrain roughness* of the path. Note that no *antenna-height* dependence is assumed in (4.2).

The CCIR ducting model (4.2) clearly assumes propagation in a ground-based duct. The logarithmic distance-dependent term in (4.2) corresponds to the cylindrical spreading of the power flux in a duct, as distinct from spherical spreading in free space. The terms  $\gamma_d d$  and  $\gamma_h d$  in (4.2) represent the losses at the top and at the bottom of the duct, respectively, assuming this to be a ground-based duct. The term  $A_c$  represents the losses due to imperfect coupling of energy into and out of the duct, when one or both antennas are located above the duct. The presence of all these terms in a ducting model is justified on physical grounds, but the quantitative evaluation of these terms is based on empirical relations. A more fundamental approach to the ducting mechanism is presented in sec. 4.4.

#### 4.2.3. Other clear-air interference-prediction models

Four recent clear-air interference-prediction models are briefly reviewed in this section. Although each of these models improves on specific aspects of the CCIR ducting model [1], most of them have other weaknesses, so the CCIR has not adopted any of these models as a replacement or alternative for its ducting model.

In 1983, Rotheram [5] proposed a new ducting model for Western Europe, in which the paths are classified according to angular distance  $d_a$  (see fig. 3.2). This

model is completely empirical and has been developed by analyzing the cumulative distributions  $L_b(p)$  of the path loss measured on 106 different paths. The model includes a dependence on distance, frequency, terrain roughness and terminal heights. The data are mainly taken from measurements in Europe in the UHF band; thus the model has not been validated outside that band and outside Western Europe. Because of the empirical nature of the model, extrapolation to other paths is difficult, if no measurements on such paths are available.

Ong [6] assumes that the dominant propagation mechanism on land paths is obstacle diffraction in a superrefractive atmosphere. The stronger the degree of superrefraction, the larger is the effective earth-radius factor  $k$  (see sec. 3.2.2), and the smaller are the diffraction angles and hence the diffraction losses. Statistics of measured refractivity gradients are used for the determination of an "effective  $k$ -factor" of a path, which is a fictitious, fixed value of  $k$  along the path. This effective  $k$ -factor is introduced to account for the actual variations in the refractivity gradient along the path. An empirical relation is given in [6] between the path length and the effective  $k$ -factor for  $p=1\%$ . The path loss is predicted by drawing the path profile with the prescribed effective earth radius ( $a_e = ka$ ), from which the diffraction angles and hence the diffraction losses can be determined. The model has been developed for the UK, but can, in principle, be extended to cover other areas and other values of  $p$  as well.

In France, a new model has been developed and proposed [7] as an improvement of the CCIR ducting model (4.2). The model [7] also employs the concept of angular distance (see fig. 3.2) and can thus take into account information on antenna heights. Furthermore, a frequency dependence by  $f^{1/3}$  is assumed in the model, different from the logarithmic frequency dependence in (4.2), and more in accordance with recently measured data. This model is currently being assessed by Working Group 1 (WG1) of the COST-210 project [2].

Recently, yet another model has been proposed by Rue [8], who assumes that elevated-layer reflection, rather than ducting, is the dominant interference mechanism along overland paths. The reflection mechanism is claimed to be much more probable, because the layer has to be present only at the intersection of the horizon rays, whereas an atmospheric duct should extend along the entire path to form an effective interference mechanism. Using available data of European transhorizon paths, a preliminary prediction model has been developed, based on the layer-reflection mechanism. This model is currently also under investigation within the COST-210 project [2].

#### 4.3. Transhorizon-propagation experiments

##### 4.3.1. Measurement programme and equipment

The COST-210 project [2] includes an extensive measurement programme to obtain an adequate database on transhorizon propagation. Because of seasonal and year-to-year variabilities, most experiments have to be carried out continuously for several years. The experiments are aimed at investigating either clear-air mechanisms or the hydrometeor-scatter mechanism; some combined experiments are carried out as well.

The clear-air mechanisms are studied by WG1 of the project. About 40 new transhorizon links have been established, covering wide ranges of path lengths, frequencies, antenna heights and terrain features. The Eindhoven University of Technology (EUT) is actively involved in this measurement programme by operating four receiver stations. Due to the specific location of Eindhoven, these experiments are particularly useful for COST-210 to study clear-air transhorizon propagation over flat land in a coastal climate.

The block diagram of the receiving and data-logging equipment is shown in fig. 4.1. Each receiver amplifies the incoming beacon signal and converts it to an intermediate frequency (IF). The IF signal is passed through a narrow bandpass filter (to limit the noise) into a detector. The resulting baseband signal is offered to a logarithmic amplifier, which yields a DC output voltage proportional to the RF power of the incoming beacon signal. The DC output of the receiver is fed to the data-logging system. This system is centred around a microcomputer, which samples the DC signal every second. The samples that exceed certain preselected threshold values (corresponding to specific values of  $L_m$ , which are chosen in steps of 5 dB) are counted every hour; these hourly totals are printed. Strip-chart recordings of the receiver output signals are also made, to allow separation of any spurious interference or other disturbances from the genuine signals. The printed hourly totals, corrected (if necessary) by visual inspection of the strip-chart recordings, are totalled for the entire measurement period in two ways: for each hour of the day separately (to obtain the diurnal distribution of  $L_m$ ), and for all hours of the day together (to obtain the cumulative distribution of  $L_m$ ).

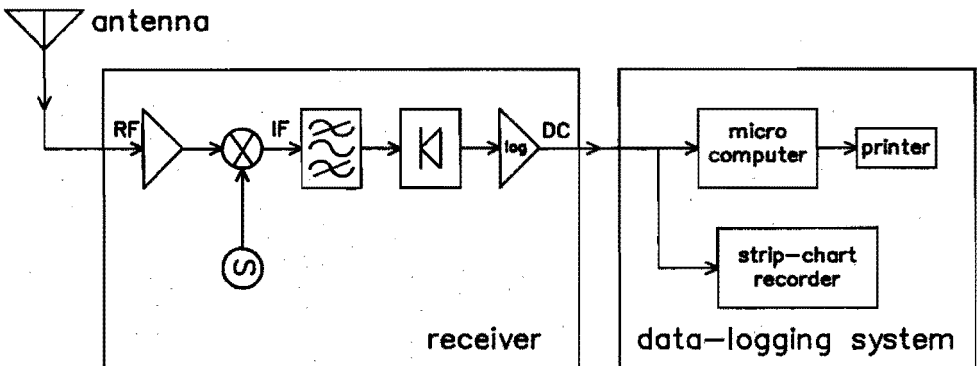


Fig. 4.1. Block diagram of the measurement system for each transhorizon link.

4.3.2. Experimental results obtained at EUT

The four COST-210 transhorizon links to Eindhoven are tabulated in table 4.1, and a map of the paths is shown in fig. 4.2. The parameters of the first two links ("EHV1A" and "EHV1B") are almost identical, with only the receive-antenna heights being different; the path passes partly over sea and partly over flat land. The third link ("EHV2") is operated at the same frequency band (1.3 GHz), but over a shorter distance and rather hilly terrain. The 11.7 GHz link ("EHV3") has a path that passes entirely over flat land.

The cumulative distributions of  $L_m$  measured on these links are shown in fig. 4.3, together with the CCIR predictions for ducting/superrefraction and troposcatter, given in Rep. 569-3 [1] and Rep. 238-5 [4], respectively. The application of the ducting model is relatively straightforward (see sec. 4.2.2), but the troposcatter model is somewhat ambiguous: the result depends on the "climate type" of the path. These climate types are not clearly defined in [4]; especially, the climate

LINK CODE	TRANSMITTER			RECEIVER			FREQUENCY (GHz)	PATH LENGTH (km)	REPORTED MEASUREMENT PERIOD**
	organization	location	antenna height (m a.s.l.)*	organization	location	antenna height (m a.s.l.)*			
EHV1A	BTRL	Martlesham Heath, UK	80	EUT	Eindhoven, NL	61	1.3	298	May 1981 - May 1988
EHV1B	BTRL	Martlesham Heath, UK	80	EUT	Eindhoven, NL	77	1.3	298	June 1986 - May 1988
EHV2	FI/DBP	Köln, FRG	230	EUT	Eindhoven, NL	77	1.3	115	July 1987 - May 1988
EHV3	DNL	Leidschen-dam, NL	44	EUT	Eindhoven, NL	71	11.7	104	April 1987 - May 1988

Table 4.1. Clear-air transhorizon links to Eindhoven.

\* m a.s.l. = meters above sea level; \*\* all experiments are continuing.

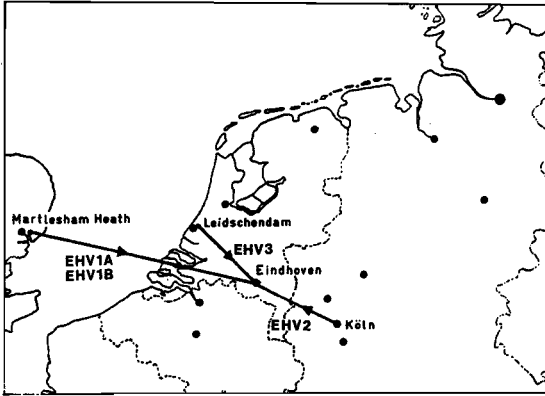


Fig. 4.2. Map showing COST-210 transhorizon links to Eindhoven.

type for the "EHV2" link is ambiguous, and thus two different troposcatter predictions ("continental temperate" and "maritime temperate") may be given.

Measured diurnal distributions (averaged over the entire measurement period) are shown in fig. 4.4; they are displayed for each link at two fixed values of  $L_m$ , corresponding to a high and a low signal level, respectively. A moving average (calculated with a 7-hour square window) is also included.

Typical chart recordings of signal enhancements (known as "events") obtained at EUT are shown in fig. 4.5. Here, a strong correlation is observed between the recordings of the "EHV1A" and "EHV1B" link, which occurred during the entire common measurement period. The correlation between events on the other links is significantly smaller.

#### 4.3.3. Discussion of the experimental results

Referring to fig. 4.3, we compare the measured cumulative distributions of  $L_m$  with the CCIR predictions [1,4], using the additional information supplied by the diurnal distributions (fig. 4.4) and the chart recordings (fig. 4.5).

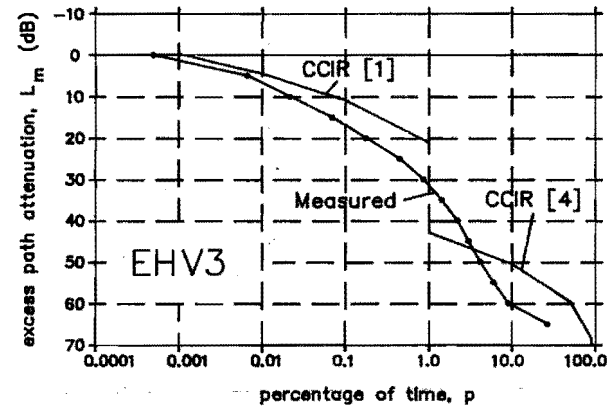
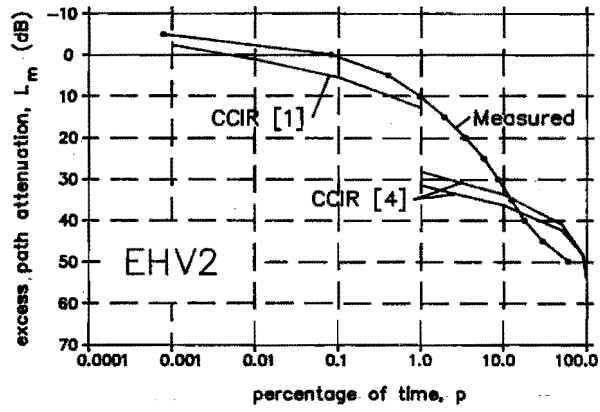
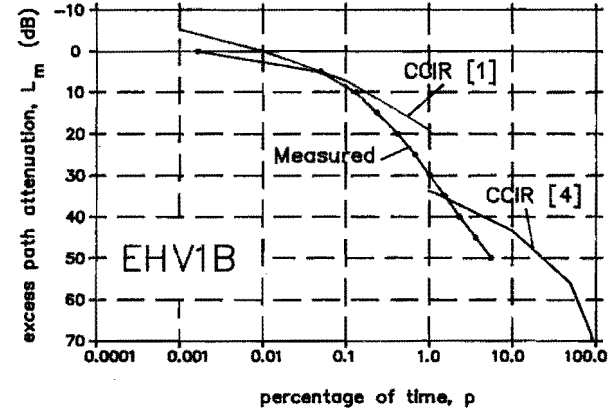
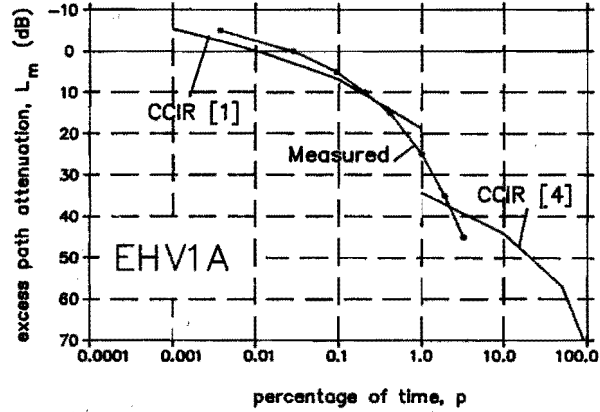


Fig. 4.3.

Measured cumulative distributions of  $L_m$  on the COST-210 transhorizon links to Eindhoven, compared to the CCIR predictions in Rep. 569-3 [1] and Rep. 238-5 [4] for ducting/superrefraction and troposcatter, respectively.

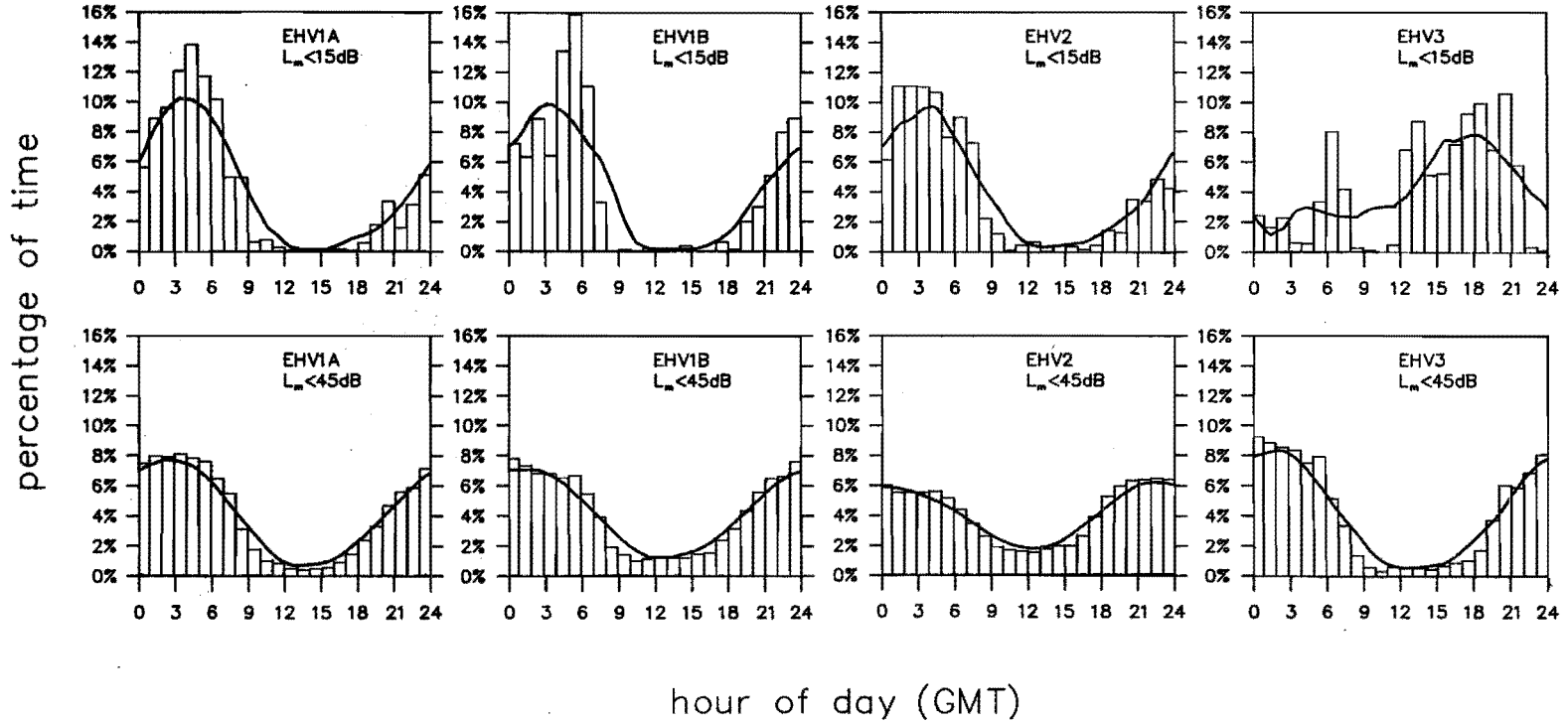


Fig. 4.4. Measured diurnal distributions on the COST-210 transhorizon links to Eindhoven for  $L_m = 15$  dB (i.e., high signal level) and for  $L_m = 45$  dB (i.e., low signal level). Solid line: 7-hour moving average.



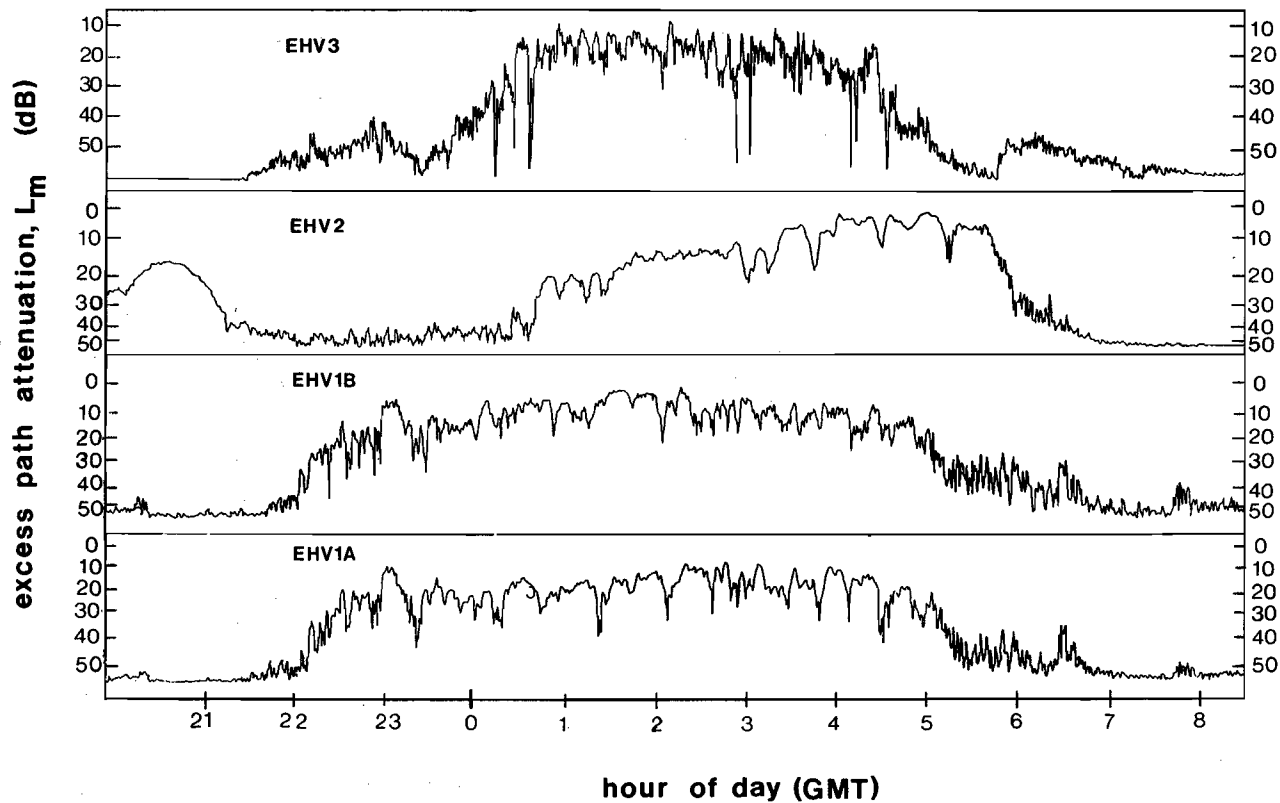


Fig. 4.5. Chart recordings of typical events occurring on the COST-210 transhorizon links to Eindhoven, recorded on June 13th/14th, 1988.

The CCIR predictions cover two adjacent time-percentage ranges:  $0.001\% \leq p < 1\%$  for the ducting model [1] and  $1\% \leq p < 99\%$  for the troposcatter model [4]. The "predicted" discontinuity at  $p=1\%$  is of course not observed in the measured distributions. In general, three regions can be distinguished in these distributions: the "ducting" region with signal levels close to the free-space level (given by  $L_m = 0$  dB), the "troposcatter" region with signal levels more than 40 dB below the free-space level, and a transition region in between. These regions correspond roughly to the time-percentage ranges  $0.001\% < p < 1\%$ ,  $p > 10\%$  and  $1\% < p < 10\%$ , respectively.

In the high time-percentage range, the received signals are mainly due to troposcatter. This is concluded from the observed rapid signal fluctuations, which are typical for the troposcatter mechanism (see sec. 3.3.2). Examples of troposcatter signals are the low-level signals shown in fig. 4.5. The cumulative distributions measured on the links "EHV2" and "EHV3" in the troposcatter region lie significantly below the CCIR predictions. The median troposcatter level cannot be measured on the "EHV1" links (due to insufficient sensitivity of the receiving stations); nevertheless, the corresponding cumulative distributions show the same tendency of falling below the CCIR predictions. Similar discrepancies have been observed on many other COST-210 transhorizon links [9]. We conclude therefore that the CCIR troposcatter model [4] is inadequate for the purpose of interference prediction.

At the low time-percentage range, ducting and superrefraction are assumed to be responsible for the transhorizon propagation. The corresponding strong signals are relatively stable in time, although some fluctuation is always present, see fig. 4.5. In addition, some deep fades are observed in these signals. This is a consequence of phasing effects between individual contributions to the received field, which are known as propagation "modes" (see sec. 4.4.2). Considerably more fading is observed

in the 11.7 GHz signal ("EHV3") than in the 1.3 GHz signals, indicating that the number of contributing "modes" increases with increasing frequency. This fact is confirmed by the mode theory (sec. 4.4.2). The ducting mechanism is mainly active during the nights, as is seen from the diurnal distributions for  $L_m < 15$  dB (fig. 4.4). The strongest ducting events occur during stable, cloudless nights, probably by radiation of heat from the earth. This radiation may cause a temperature inversion in the lower troposphere, implying a strong negative refractive-index gradient, which supports superrefraction and ducting [10, sec. 4.4.2].

In the transition region ( $1\% < p < 10\%$ ), several mechanisms (whether or not occurring simultaneously) are responsible for the transhorizon propagation. The diurnal distributions for  $L_m < 45$  dB (fig. 4.4) show that, in addition to nocturnal radiation, some propagation mechanisms are active during the day. In fact, with increasing  $L_m$ , a gradual transition has been observed from the highly unbalanced distributions of the strong ducting signals to the flat distributions of the weak troposcatter signals. Modelling of the propagation mechanisms corresponding to this time-percentage range is obviously very difficult, and no adequate prediction model for this range is currently available from CCIR.

From an interference point of view, the cumulative distributions for  $p \leq 10\%$ , and in particular for  $p \leq 1\%$ , are of primary interest. The measured distributions for the two "EHV1" links in the range  $p \leq 1\%$  are very similar and reasonably close to the CCIR prediction [1]. No significant antenna-height dependence is observed on these links, possibly because the difference in receive-antenna heights is relatively small (see table 4.1). The small differences between the cumulative distributions may be attributed to the difference in measurement periods. In the "EHV2" experiment, a large transmit-antenna height is used. This probably explains the relatively high signal levels measured on this link, which exceed the CCIR "ducting" predictions (As mentioned in sec. 4.2.2, no antenna-height dependence is included in the CCIR

ducting model.) The 11.7 GHz link ("EHV3") may suggest another weakness of the current CCIR ducting model, namely its unreliability at higher frequencies.

Although the measurement periods of the last two links (see table 4.1) have not been long enough yet to draw any detailed conclusions during this study, it is nevertheless clear that the current CCIR interference-prediction models [1,4] are unsatisfactory in several respects.

#### 4.4. Theoretical ducting model

##### 4.4.1. Review of tropospheric-propagation theory

Theoretical models of tropospheric propagation are only tractable if a number of simplifications is made. Usually, the flat-earth model (see sec. 3.2.2) is adopted, in which the troposphere is characterized by the modified refractive index  $m$ . Horizontal variations in  $m$  are neglected, and the vertical gradient of  $m$  is assumed to be small (i.e.,  $m$  varies only slightly within a vertical distance of one wavelength); in other words, the troposphere is assumed *quasi-homogeneous*. Effects of obstacles or terrain roughness, as well as imperfect conductivity of the earth surface, are usually (though not necessarily) neglected. The geometry of the resulting boundary-value problem is shown in fig. 4.6. Here, the interface between the earth and the troposphere is given by the plane  $z=0$ , and the source is supposed to be located in the vicinity of the  $z$ -axis.

The geometry of the source of the radiation determines the necessary number of dimensions of this problem. The general problem is three-dimensional in nature. If the source is a point source or a vertical line source along the  $z$ -axis, the problem reduces to a rotationally symmetric one. Examples of the latter problem have been treated by Jones [11, sec. 6.25] and by Freehafer in [12, sec. 2.6]. If, on the other

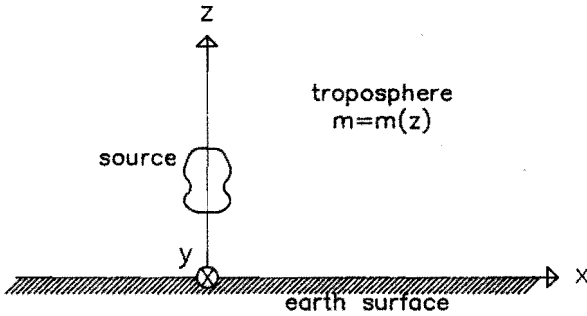


Fig. 4.6. Model for tropospheric wave propagation above a perfectly conducting earth.

hand, the source is a horizontal line source parallel to the  $y$ -axis, the problem becomes two-dimensional. Examples of the latter problem are dealt with by Budden [13, chapters 11–12]. Normalization of the actual field strength to the free-space field strength generally yields the same answer for all sources [12, p. 59; 13, p. 195], hence in effect the excess path attenuation  $L_m$  (eq. (3.4)) is independent of the type of the source and, consequently, of the number of dimensions involved. In this thesis, excitation by a horizontal line-source is considered.

The assumption of a quasi-homogeneous atmosphere enables us to treat the wave-propagation problem by means of the scalar wave equation [11, sec. 6.28; 12, sec. 2.6]. The solution of this equation (with appropriate boundary conditions) can be represented by a discrete and/or continuous spectrum of "modes", hence the name *mode theory*. The mode theory is reviewed in sec. 4.4.2 and applied to a specific problem in sec. 4.4.3.

4.4.2. Review of mode theory

Referring to fig. 4.6, we consider the excitation by a line source of strength  $U_0$  located at  $x=0, z=z_T$  ("transmitter height"). An  $\exp(j\omega t)$  time dependence is tacitly assumed. The resulting electromagnetic field is described by the general field variable  $U=U(x,z)$ , where  $U=E_y$  for TE-waves (electric polarization) and  $U=H_y$  for TM-waves (magnetic polarization). Then the field  $U(x,z)$  must satisfy the inhomogeneous scalar wave equation

$$\frac{\partial^2 U(x,z)}{\partial x^2} + \frac{\partial^2 U(x,z)}{\partial z^2} + k_0^2 m^2(z)U(x,z) = -U_0 \delta(x)\delta(z-z_T), \quad (4.4a)$$

where  $k_0=2\pi/\lambda$  is the free-space wavenumber. The boundary conditions associated with the model under consideration are

$$U(x,0) = 0 \quad \text{for TE-waves,} \quad (4.4b)$$

$$\left. \frac{\partial U(x,z)}{\partial z} \right|_{z=0} = 0 \quad \text{for TM-waves,}$$

$$U(x,z) \rightarrow 0 \quad \text{as } \sqrt{x^2+z^2} \rightarrow \infty. \quad (4.4c)$$

Equation (4.4b) expresses the assumed perfect conductivity of the earth. In the formulation of the radiation condition (4.4c) it is understood that  $k_0$  is complex with a small negative imaginary part (as when the medium is slightly dispersive). In the final result for  $U(x,z)$ , the limit for  $\text{Im}\{k_0\} \rightarrow 0$  can be taken, corresponding to  $k_0$  real. The solution of the boundary-value problem (4.4) can be obtained in two different ways.

i) The first method is described by Jones [11, secs. 6.25 and 6.28]. Introduce the Fourier transform

$$\Phi(z, \alpha) = \int_{-\infty}^{\infty} U(x, z) \exp(-j\alpha x) dx, \quad (4.5a)$$

with the corresponding inverse transform

$$U(x, z) = \frac{1}{2\pi} \int_{-\infty}^{\infty} \Phi(z, \alpha) \exp(j\alpha x) d\alpha. \quad (4.5b)$$

Then by Fourier transformation of (4.4) we are led to the following problem for  $\Phi(z, \alpha)$ :

$$\frac{d^2 \Phi(z, \alpha)}{dz^2} + [k_0^2 m^2(z) - \alpha^2] \Phi(z, \alpha) = -U_0 \delta(z - z_T), \quad (4.6a)$$

$$\Phi(0, \alpha) = 0 \quad \text{for TE-waves,} \quad (4.6b)$$

$$\left. \frac{d\Phi(z, \alpha)}{dz} \right|_{z=0} = 0 \quad \text{for TM-waves,}$$

$$\Phi(z, \alpha) \rightarrow 0 \quad \text{as } z \rightarrow \infty. \quad (4.6c)$$

The transformed problem (4.6) should be solved for a given refractive-index profile  $m(z)$ . The field  $U(x, z)$  is then evaluated from (4.5b) by means of contour integration and residue calculus. Consider  $\Phi(z, \alpha)$  for fixed  $z$  as a function of  $\alpha$  in the complex  $\alpha$ -plane. Suppose that this function is analytic, apart from simple poles at  $\alpha = \pm \alpha_n$ ,  $n=1, 2, 3, \dots$ , with  $\text{Im}\{\alpha_n\} < 0$ . The integration contour in (4.5b) is closed by a semi-circle of radius  $R$  in the upper (lower) half of the  $\alpha$ -plane if  $x > 0$  ( $x < 0$ ). Under the assumption that the contribution from the semi-circle to the integral in (4.5b) vanishes as  $R \rightarrow \infty$  (which should be checked for the particular function  $\Phi(z, \alpha)$ ), the result for  $U(x, z)$  can be expressed as a series of residues at the poles of  $\Phi(z, \alpha)$ , viz.

$$U(x,z) = j \sum_{n=1}^{\infty} \text{Res}_{\alpha=-\alpha_n} \Phi(z, \alpha) \exp(-j\alpha_n |x|). \quad (4.7)$$

This solution can be interpreted as a discrete spectrum of modes. If, in addition to poles,  $\Phi(z, \alpha)$  also has branch cuts in the complex  $\alpha$ -plane, integrals around these branch cuts should be added to the solution for  $U(x,z)$ , corresponding to a continuous spectrum of modes.

ii) The second method is described by Budden [13, chapter 11], based on earlier work of Booker and Walkinshaw [14]. They consider first the source-free problem, in which the right-hand side of (4.4a) and (4.6a) is equal to zero. This problem can be regarded as an eigenvalue problem: for specific values of  $\alpha$  (the eigenvalues), the problem has a non-trivial solution  $\Phi(z)$  (the eigenfunctions). The following assumptions on the eigenvalues and eigenfunctions are made, but cannot be proved in general:

- the spectrum of eigenvalues, denoted by  $\alpha_n$ , is discrete (without loss of generality we set  $\text{Im}\{\alpha_n\} < 0$ );
- the eigenfunctions  $\Phi_n(z)$  form a complete set.

With these assumptions, the field  $U(x,z)$  can be written as a sum of modes,

$$U(x,z) = \sum_{n=1}^{\infty} C_n \Phi_n(z) \exp(-j\alpha_n |x|), \quad (4.8)$$

where the excitation factors  $C_n$  are determined by the particular source in (4.4a). To calculate these factors, we first integrate (4.4a) with respect to  $x$  over a vanishingly small interval around  $x=0$ , yielding

$$\left. \frac{\partial U(x,z)}{\partial x} \right|_{x=+0} - \left. \frac{\partial U(x,z)}{\partial x} \right|_{x=-0} = -2j \sum_{n=1}^{\infty} \alpha_n C_n \Phi_n(z) = -U_0 \delta(z-z_T). \quad (4.9)$$



Next, by use of the orthogonality relation [13, pp. 191-192]

$$\int_0^{\infty} \Phi_n(z) \Phi_m(z) dz = 0 \quad \text{for } n \neq m, \quad (4.10)$$

the factor  $C_n$  is found to be

$$C_n = \frac{U_0}{2j\alpha_n} \frac{\Phi_n(z_T)}{\int_0^{\infty} \Phi_n^2(z) dz}. \quad (4.11)$$

Comparison of (4.8) and (4.11) with the result (4.7) of the previous method shows that both methods yield the same answer if

$$\text{Res}_{\alpha=-\alpha_n} \Phi(z, \alpha) = - \frac{U_0}{2\alpha_n} \frac{\Phi_n(z_T) \Phi_n(z)}{\int_0^{\infty} \Phi_n^2(z) dz}. \quad (4.12)$$

The symmetry of  $z_T$  and  $z$  in (4.12) is obvious, and could be expected because of reciprocity.

The first method is more laborious than the second one, but it has a sounder mathematical basis. The nature of the spectrum (discrete or continuous) can be established directly from the particular function  $\Phi(z, \alpha)$ . Justification of the assumptions in the second method (discreteness of the spectrum and completeness of the set of eigenfunctions) is not always possible, see e.g. [11, p. 398], [12, p. 65-66] and [13, p. 191]. In the next section, the first method is applied to a specific example.

It has been observed [15] that for both methods it may be necessary to assume a small loss of the atmosphere, mathematically expressed by  $k_0$  being complex with a small negative imaginary part. In this way, some mathematical difficulties are

avoided. In the final result for  $U(x,z)$  the limit for  $\text{Im}\{k_0\} \rightarrow 0$  can be taken, corresponding to  $k_0$  real.

To calculate the excess path attenuation  $L_m$ , we note that the free-space field of the line source in (4.4a) is given by [11, sec. 3.8]

$$U_{fs}(r) = \frac{j}{4} U_0 H_0^{(2)}(k_0 r), \quad (4.13)$$

where  $r = \sqrt{x^2 + (z - z_T)^2}$  is the distance of the observation point to the source and  $H_0^{(2)}(\cdot)$  is the Hankel function of the second kind. For  $|x| \gg |z - z_T|$ , one has  $r \approx |x|$  and  $H_0^{(2)}(\cdot)$  can be replaced by its asymptotic approximation [16, sec. 9.2]; hence, (4.13) becomes

$$U_{fs}(x,z) = \frac{jU_0}{4\pi} \sqrt{\frac{\lambda}{|x|}} \exp[-j(k_0|x| - \pi/4)]. \quad (4.14)$$

The ratio of  $U(x,z)$  and  $U_{fs}(x,z)$  yields an expression for  $L_m$ ,

$$L_m = -20 \log |U(x,z)/U_{fs}(x,z)| \quad (\text{dB}), \quad (4.15)$$

which, by use of (4.8), (4.11) and (4.14), becomes

$$L_m = -20 \log \left| 2\pi \sqrt{\frac{|x|}{\lambda}} \sum_{n=1}^{\infty} \frac{\Phi_n(z_T) \Phi_n(z)}{\alpha_n \int_0^{\infty} \Phi_n^2(z) dz} \exp(j\alpha_n|x|) \right| \quad (\text{dB}). \quad (4.16)$$

The function  $\Phi_n(z)$  is known as the *height-gain function* of mode  $n$ ;  $\alpha_n$  is the corresponding (complex) propagation constant. The *specific attenuation*  $\gamma_n$  of mode  $n$  is defined as

$$\gamma_n = -\text{Im}\{\alpha_n\} \text{ Neper/m} = -\frac{2 \cdot 10^4}{\ln 10} \text{Im}\{\alpha_n\} \text{ dB/km,} \quad (4.17)$$

with  $\alpha_n$  expressed in  $\text{m}^{-1}$ . Usually, the modes are arranged in the order of increasing  $\gamma_n$ . Hence, the higher-order modes contribute little to the sum (4.7) or (4.8) and only a finite number of modes has to be taken into account, provided that the series is convergent (which is normally true for  $|x| \gg z_T$  and  $|x| \gg z$ ).

For the presentation of numerical results, it is convenient to introduce the *normalized height-gain function*  $g_n(z)$ , defined by

$$g_n(z) = \Phi_n(z) \left[ \alpha_n \int_0^{\infty} \Phi_n^2(z) dz \right]^{-1/2}. \quad (4.18)$$

Using (4.18) in (4.16), it is found that  $L_m$  is given by

$$L_m(x,z) = -20 \log \left| 2\pi \sqrt{\frac{|x|}{\lambda}} \sum_{n=1}^{\infty} g_n(z_T) g_n(z) \exp(-j\alpha_n |x|) \right| \text{ (dB)}. \quad (4.19)$$

The mode theory can be applied to describe the propagation in a tropospheric duct, if the refractive-index profile  $m(z)$  is known. However, analytical solutions of the boundary-value problem (4.6) are only possible for idealized profiles. In general, the problem (4.6) must be solved numerically; an early method was given as early as 1946 [17]. Approximate solutions can be obtained by modelling a realistic profile by a piecewise linear one. The latter can be handled analytically; an example is treated in the next section.

4.4.3. Tropospheric ducting produced by an elevated inversion layer

As an example, we apply the mode theory to the problem of wave-propagation in a quasi-homogeneous atmosphere with the modified refractive-index profile  $m(z)$  shown in fig. 4.7. This profile is an idealized model of the profile that occurs when an elevated inversion layer is present in the troposphere at a height  $z_h$  above the surface of the earth. The profile contains a discontinuity at  $z=z_h$ ; the source is located at  $z=z_T < z_h$ . The profile is described analytically by

$$\begin{aligned} m(z) &= 1 + z/a_e & (0 < z < z_h), \\ m(z) &= 1 - \Delta + z/a_e & (z_h < z < \infty), \end{aligned} \tag{4.20}$$

where  $a_e$  is the effective earth radius (see sec. 3.2.2). At large height  $z$ , this model is invalid, but it is reasonable to assume that the precise form of  $m(z)$  as  $z \rightarrow \infty$  has a negligible influence on the propagation in the lower troposphere ( $z \ll a_e$ ). In the latter region,  $m^2(z)$  is approximated by

$$\begin{aligned} m^2(z) &= 1 + 2z/a_e & (0 < z < z_h), \\ m^2(z) &= 1 - 2\Delta + 2z/a_e & (z_h < z < \infty). \end{aligned} \tag{4.21}$$

The profile (4.21) has been investigated by Wait and Spies [18]. They have calculated the specific attenuations  $\gamma_n$  of the first four modes, as a function of the parameters  $a_e$ ,  $\Delta$  and  $\lambda$ , with  $z_h=1$  km. In [19], the corresponding height-gain functions  $\Phi_n(z)$  have been calculated. Both papers only treat the source-free problem; there is no discussion of the excitation of the individual modes by a given source. Furthermore, only the first four modes are considered in [18,19].

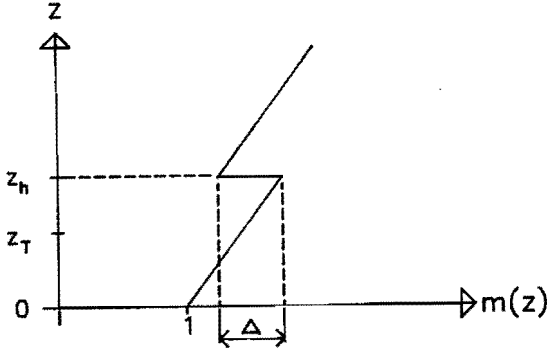


Fig. 4.7. Refractive-index discontinuity produced by an elevated inversion layer.  $z_h$  : layer height;  $z_T$  : source height.

Here, we solve the complete problem (4.4), including the source term in (4.4a), by the first method described in sec. 4.4.2; this allows the determination of the excitation factors. In addition, the mode sum (cf. (4.7)) is calculated for a layer height  $z_h=100$  m, and realistic terminal heights  $z_T$  and  $z$  and path length  $|x|$ .

For convenience, we first introduce some notations and symbols:

$$\zeta = (k_0 a_e / 2)^{2/3} 2z / a_e, \tag{4.22a}$$

$$\zeta_h = (k_0 a_e / 2)^{2/3} 2z_h / a_e, \tag{4.22b}$$

$$\zeta_T = (k_0 a_e / 2)^{2/3} 2z_T / a_e, \tag{4.22c}$$

$$t = (k_0 a_e / 2)^{2/3} (\alpha^2 / k_0^2 - 1), \tag{4.22d}$$

$$T = (k_0 a_e / 2)^{2/3} 2\Delta, \tag{4.22e}$$

$$w_1(\tau) = -j\sqrt{\pi} [Ai(\tau) + jBi(\tau)], \tag{4.22f}$$

$$w_2(\tau) = j\sqrt{\pi} [Ai(\tau) - jBi(\tau)]. \tag{4.22g}$$

Here, the Airy functions  $Ai(\tau)$  and  $Bi(\tau)$  are independent solutions of the Airy equation [16, sec. 10.4]

$$w''(\tau) - \tau w(\tau) = 0, \quad (4.23)$$

with the Wronskian relation

$$Ai(\tau)Bi'(\tau) - Bi(\tau)Ai'(\tau) = \pi^{-1}. \quad (4.24)$$

We observe that  $\zeta$ ,  $\zeta_h$ ,  $\zeta_T$  and  $T$  are dimensionless, real, non-negative quantities;  $t$  is in general complex.

Now, we take the source to be a line current  $I \exp(j\omega t) \hat{e}_y$ , located at  $x=0$ ,  $z=z_T$ . Then the resulting electromagnetic field is a TE-wave, which can be described by the electric-field component  $E_y = E(x, z)$ . Similarly to (4.4),  $E(x, z)$  is determined as the solution of the boundary-value problem

$$\frac{\partial^2 E(x, z)}{\partial x^2} + \frac{\partial^2 E(x, z)}{\partial z^2} + k_0^2 m^2(z) E(x, z) = jk_0 Z_0 I \delta(x) \delta(z - z_T), \quad (4.25a)$$

$$E(x, 0) = 0, \quad (4.25b)$$

$$E(x, z) \rightarrow 0 \quad \text{as} \quad \sqrt{x^2 + z^2} \rightarrow \infty, \quad (4.25c)$$

where  $Z_0 = \sqrt{\mu_0/\epsilon_0}$  is the intrinsic impedance of free space. By introducing the Fourier transform

$$\Phi(z, \alpha) = \int_{-\infty}^{\infty} E(x, z) \exp(-j\alpha x) dx \quad (4.26)$$

and by substitution of (4.21) for  $m^2(z)$ , we are led to the transformed problem, expressed in the notations (4.22) as

$$\Phi''(\zeta) - (t-\zeta)\Phi(\zeta) = jk_0 Z_0 I (2k_0^2/a_e)^{-1/3} \delta(\zeta-\zeta_T) \quad (0 < \zeta < \zeta_h), \quad (4.27a)$$

$$\Phi''(\zeta) - (t+T-\zeta)\Phi(\zeta) = 0 \quad (\zeta_h < \zeta < \infty), \quad (4.27b)$$

$$\Phi(0) = 0, \quad (4.27c)$$

$$\Phi(\zeta) \rightarrow 0 \quad \text{as } \zeta \rightarrow \infty. \quad (4.27d)$$

The solution of (4.27a) that satisfies the boundary condition (4.27c) is given by

$$\Phi(\zeta) = [AAi(t-\zeta_T) - BBi(t-\zeta_T)] [Ai(t-\zeta) - \beta(t)Bi(t-\zeta)] \quad (0 < \zeta < \zeta_T), \quad (4.28a)$$

$$\Phi(\zeta) = [Ai(t-\zeta_T) - \beta(t)Bi(t-\zeta_T)] [AAi(t-\zeta) - BBi(t-\zeta)] \quad (\zeta_T < \zeta < \zeta_h), \quad (4.28b)$$

where  $\beta(t) = Ai(t)/Bi(t)$ ,  $B = j\pi k_0 Z_0 I (2k_0^2/a_e)^{-1/3} + A\beta(t)$ , and the constant A is still to be determined. The general solution of (4.27b) is given by

$$\Phi(\zeta) = C w_1(t+T-\zeta) + D w_2(t+T-\zeta) \quad (\zeta_h < \zeta < \infty), \quad (4.29)$$

where C and D are arbitrary constants. From the asymptotic expansions of the functions  $w_1(\tau)$  and  $w_2(\tau)$  (cf. [16, sec. 10.4]), it readily follows that  $w_1(t+T-\zeta) \rightarrow 0$  and  $w_2(t+T-\zeta) \rightarrow \infty$  as  $\zeta \rightarrow \infty$  (if  $k_0$  is taken complex with a small negative imaginary part). Hence, to satisfy the radiation condition (4.27d), it is required that  $D=0$ .

Next we require continuity of  $\Phi(\zeta)$  and  $d\Phi(\zeta)/d\zeta$  at the transition height  $\zeta = \zeta_h$ , using the solutions (4.28b) and (4.29). Then the constants A and C can be determined. For brevity we introduce the functions

$$\chi_A(t) = Ai'(t-\zeta_h)w_1(t+T-\zeta_h) - Ai(t-\zeta_h)w_1'(t+T-\zeta_h), \quad (4.30a)$$

$$\chi_B(t) = Bi'(t-\zeta_h)w_1(t+T-\zeta_h) - Bi(t-\zeta_h)w_1'(t+T-\zeta_h). \quad (4.30b)$$

The solution for  $\Phi(\zeta)$  is then given by

$$\Phi(\zeta) = j\pi k_0 Z_0 I \left[ \frac{2k_0^2}{a_e} \right]^{-1/3} \frac{\text{Ai}(t-\zeta_T)\chi_B(t) - \text{Bi}(t-\zeta_T)\chi_A(t)}{\chi_A(t) - \beta(t)\chi_B(t)} [\text{Ai}(t-\zeta) - \beta(t)\text{Bi}(t-\zeta)]$$

( $0 < \zeta < \zeta_T$ ), (4.31a)

$$\Phi(\zeta) = j\pi k_0 Z_0 I \left[ \frac{2k_0^2}{a_e} \right]^{-1/3} \frac{\text{Ai}(t-\zeta_T) - \beta(t)\text{Bi}(t-\zeta_T)}{\chi_A(t) - \beta(t)\chi_B(t)} [\text{Ai}(t-\zeta)\chi_B(t) - \text{Bi}(t-\zeta)\chi_A(t)]$$

( $\zeta_T < \zeta < \zeta_h$ ), (4.31b)

$$\Phi(\zeta) = jk_0 Z_0 I \left[ \frac{2k_0^2}{a_e} \right]^{-1/3} \frac{\text{Ai}(t-\zeta_T) - \beta(t)\text{Bi}(t-\zeta_T)}{\chi_A(t) - \beta(t)\chi_B(t)} w_1(t+T-\zeta)$$

( $\zeta_h < \zeta < \infty$ ). (4.31c)

Consider now  $\Phi(\zeta)$  for fixed  $\zeta$  as a function of  $t$ . This function is analytic apart from simple poles at  $t=t_n$ , determined by

$$\chi_A(t_n) - \beta(t_n)\chi_B(t_n) = 0. \quad (4.32)$$

By setting  $\beta(t)=0$ , eq. (4.32) becomes identical to eq. (11) in [19]. However, the approximation  $\beta(t)\approx 0$  is not generally valid. We shall therefore retain the second term of (4.32) in our calculations.

From the mode equation (4.32) (also known as the dispersion relation), the poles  $t_n$  should be determined; this requires numerical computations. Each pole  $t=t_n$  of  $\Phi(\zeta)$  corresponds to two poles  $\alpha=\pm\alpha_n$  of  $\Phi(z,\alpha)$ , where  $\text{Im}\{\alpha_n\}<0$ , as is seen from (4.22d). The corresponding residues of  $\Phi(z,\alpha)$  are given by



$$\text{Res}_{\alpha=\pm\alpha_n} \Phi(z, \alpha) = j\pi k_0 Z_0 I \left[ \frac{2k_0^2}{a_e} \right]^{-1/3} \frac{\text{Ai}(t_n - \zeta_T) \chi_B(t_n) - \text{Bi}(t_n - \zeta_T) \chi_A(t_n)}{\chi_A'(t_n) - \beta(t_n) \chi_B'(t_n) - \beta'(t_n) \chi_B(t_n)} \cdot$$

$$\cdot \frac{\text{Ai}(t_n - \zeta) - \beta(t_n) \text{Bi}(t_n - \zeta)}{\left. \frac{dt}{d\alpha} \right|_{\alpha=\pm\alpha_n}} \quad (0 < z < z_T), \quad (4.33a)$$

$$\text{Res}_{\alpha=\pm\alpha_n} \Phi(z, \alpha) = j\pi k_0 Z_0 I \left[ \frac{2k_0^2}{a_e} \right]^{-1/3} \frac{\text{Ai}(t_n - \zeta_T) - \beta(t_n) \text{Bi}(t_n - \zeta_T)}{\chi_A'(t_n) - \beta(t_n) \chi_B'(t_n) - \beta'(t_n) \chi_B(t_n)} \cdot$$

$$\cdot \frac{\text{Ai}(t_n - \zeta) \chi_B(t_n) - \text{Bi}(t_n - \zeta) \chi_A(t_n)}{\left. \frac{dt}{d\alpha} \right|_{\alpha=\pm\alpha_n}} \quad (z_T < z < z_h), \quad (4.33b)$$

$$\text{Res}_{\alpha=\pm\alpha_n} \Phi(z, \alpha) = j\pi k_0 Z_0 I \left[ \frac{2k_0^2}{a_e} \right]^{-1/3} \frac{\text{Ai}(t_n - \zeta_T) - \beta(t_n) \text{Bi}(t_n - \zeta_T)}{\chi_A'(t_n) - \beta(t_n) \chi_B'(t_n) - \beta'(t_n) \chi_B(t_n)} \cdot$$

$$\cdot \frac{w_1(t_n + T - \zeta)}{\left. \frac{dt}{d\alpha} \right|_{\alpha=\pm\alpha_n}} \quad (z_h < z < \infty). \quad (4.33c)$$

These expressions can be simplified by means of the following relations, which follow from the mode equation (4.32), the definitions (4.30) of  $\chi_A(t)$  and  $\chi_B(t)$ , the Wronskian relation (4.24), the Airy equation (4.23), and the definition (4.22d) of  $t$ :

$$\chi_A(t_n) = \pi^{-1} \beta(t_n) w_1(t_n + T - \zeta_h) [\text{Ai}(t_n - \zeta_h) - \beta(t_n) \text{Bi}(t_n - \zeta_h)]^{-1}, \quad (4.34a)$$

$$\chi_B(t_n) = \pi^{-1} w_1(t_n + T - \zeta_h) [\text{Ai}(t_n - \zeta_h) - \beta(t_n) \text{Bi}(t_n - \zeta_h)]^{-1}, \quad (4.34b)$$

$$\chi_A'(t_n) - \beta(t_n) \chi_B'(t_n) = -T w_1(t_n + T - \zeta_h) [\text{Ai}(t_n - \zeta_h) - \beta(t_n) \text{Bi}(t_n - \zeta_h)], \quad (4.34c)$$

$$\beta(t_n) = -\pi^{-1} [\text{Bi}(t_n)]^{-2}, \quad (4.34d)$$

$$\left. \frac{dt}{d\alpha} \right|_{\alpha=\pm\alpha_n} = \pm 2\alpha_n (2k_0^2/a_e)^{-2/3}. \quad (4.34e)$$

Using (4.34) in (4.33), we find

$$\operatorname{Res}_{\alpha=\pm\alpha_n} \Phi(z, \alpha) = \frac{\mp j k_0 Z_0 I}{2\alpha_n \Psi_n} \frac{\operatorname{Ai}(t_n - \zeta_T) - \beta(t_n) \operatorname{Bi}(t_n - \zeta_T)}{[\operatorname{Ai}(t_n - \zeta_h) - \beta(t_n) \operatorname{Bi}(t_n - \zeta_h)]^2} [\operatorname{Ai}(t_n - \zeta) - \beta(t_n) \operatorname{Bi}(t_n - \zeta)]$$

$$(0 < z < z_h), \quad (4.35a)$$

$$\operatorname{Res}_{\alpha=\pm\alpha_n} \Phi(z, \alpha) = \frac{\mp j k_0 Z_0 I}{2\alpha_n \Psi_n} \frac{[\operatorname{Ai}(t_n - \zeta_T) - \beta(t_n) \operatorname{Bi}(t_n - \zeta_T)] w_1(t_n + T - \zeta)}{[\operatorname{Ai}(t_n - \zeta_h) - \beta(t_n) \operatorname{Bi}(t_n - \zeta_h)] w_1(t_n + T - \zeta_h)}$$

$$(z_h < z < \infty), \quad (4.35b)$$

where  $\Psi_n$  is given by

$$\Psi_n = \left[ \frac{2k_0^2}{a e} \right]^{-1/3} \{ T - \pi^{-2} [\operatorname{Bi}(t_n)]^{-2} [\operatorname{Ai}(t_n - \zeta_h) - \beta(t_n) \operatorname{Bi}(t_n - \zeta_h)]^{-2} \}. \quad (4.36)$$

To express the residues in the form (4.12), we must define the height-gain function  $\Phi_n(z)$ . The results (4.35) suggest the definition

$$\Phi_n(z) = \frac{\operatorname{Ai}(t_n - \zeta) - \beta(t_n) \operatorname{Bi}(t_n - \zeta)}{\operatorname{Ai}(t_n - \zeta_h) - \beta(t_n) \operatorname{Bi}(t_n - \zeta_h)} \quad (0 < z < z_h), \quad (4.37a)$$

$$\Phi_n(z) = \frac{w_1(t_n + T - \zeta)}{w_1(t_n + T - \zeta_h)} \quad (z_h < z < \infty). \quad (4.37b)$$

This function is in fact a solution of the corresponding homogeneous problem (having the right-hand side of (4.27a) replaced by zero), and has in addition the following properties:

$$\Phi_n(z_h) = 1, \tag{4.38a}$$

$$\left. \frac{d\Phi_n(z)}{dz} \right|_{z=0} = \left[ \frac{2k_0^2}{a_e} \right]^{1/3} \pi^{-1} [\text{Bi}(t_n)]^{-1} [\text{Ai}(t_n - \zeta_h) - \beta(t_n) \text{Bi}(t_n - \zeta_h)]^{-1}, \tag{4.38b}$$

$$\int_0^\infty \Phi_n^2(z) dz = \Psi_n. \tag{4.38c}$$

The latter property can be proved as follows, using (4.27):

$$\begin{aligned} \int_0^\infty \Phi_n^2(z) dz &= \left[ \frac{2k_0^2}{a_e} \right]^{-1/3} \left\{ \int_0^{\zeta_h} \Phi_n^2(\zeta) d\zeta + \int_{\zeta_h}^\infty \Phi_n^2(\zeta) d\zeta \right\} \\ &= \left[ \frac{2k_0^2}{a_e} \right]^{-1/3} \left\{ [(\Phi_n(\zeta))^2 - (t_n - \zeta)\Phi_n^2(\zeta)] \Big|_0^{\zeta_h} + [(\Phi_n(\zeta))^2 - (t_n + T - \zeta)\Phi_n^2(\zeta)] \Big|_{\zeta_h}^\infty \right\} \\ &= \left[ \frac{2k_0^2}{a_e} \right]^{-1/3} \left\{ T\Phi_n^2(\zeta_h) - [\Phi_n(\zeta)]_{\zeta=0}^2 \right\} \\ &= \left[ \frac{2k_0^2}{a_e} \right]^{-1/3} \left\{ T - \left[ \frac{2k_0^2}{a_e} \right]^{-2/3} \left[ \left. \frac{d\Phi_n(z)}{dz} \right|_{z=0} \right]^2 \right\} = \Psi_n. \end{aligned}$$

By using (4.37) and (4.38c) in (4.35), the residue in (4.35) can be written concisely as

$$\text{Res}_{\alpha = \pm \alpha_n} \Phi(z, \alpha) = \mp \frac{1}{2} j k_0 Z_0 I \frac{\Phi_n(z_T) \Phi_n(z)}{\alpha_n \int_0^\infty \Phi_n^2(z) dz} \quad (0 < z < \infty), \tag{4.39}$$

which is equivalent to (4.12).

We are now able to evaluate the inverse Fourier transform, ~~by the method of sec. 4.4.2~~ (4.40)

$$E(x,z) = \frac{1}{2\pi} \int_{-\infty}^{\infty} \Phi(z,\alpha) \exp(j\alpha x) d\alpha, \tag{4.40}$$

by contour integration and residue calculus. We close the integration contour by a semi-circle of radius R, as described in sec. 4.4.2. It has been shown [15] by asymptotic expansion of the Airy functions that the contribution from the semi-circle to the integral in (4.40) vanishes as  $R \rightarrow \infty$ , if  $|x| \gg z+z_T$ , which is the case of interest. Thus we find that the field  $E(x,z)$  is represented by the modal expansion

$$\begin{aligned} E(x,z) &= j \sum_{n=1}^{\infty} \text{Res}_{\alpha=-\alpha_n} \Phi(z,\alpha) \exp(-j\alpha_n |x|) \\ &= -\frac{1}{2} k_0 Z_0 I \sum_{n=1}^{\infty} \frac{\Phi_n(z_T) \Phi_n(z)}{\alpha_n \int_0^{\infty} \Phi_n^2(z) dz} \exp(-j\alpha_n |x|). \end{aligned} \tag{4.41}$$

The same result would have been obtained by the second method of sec. 4.4.2. It has been verified that for  $|x| \gg z+z_T$ , the series in (4.41) is convergent [15].

Finally, the excess path attenuation  $L_m$  follows from (4.41) by normalization of  $E(x,z)$  to the free-space field  $E_{fs}(x,z)$ , as in sec. 4.4.2. Expressed in terms of the normalized height-gain functions  $g_n(z)$  defined by (4.18), we obtain the result

$$L_m(x,z) = -20 \log \left| 2\pi \sqrt{\frac{|x|}{\lambda}} \sum_{n=1}^{\infty} g_n(z_T) g_n(z) \exp(-j\alpha_n |x|) \right| \quad (\text{dB}), \tag{4.42}$$

which is identical to (4.19).

#### 4.4.4. Numerical results

The main problem in obtaining numerical results from the mode theory concerns the determination of the poles  $t_n$  from the mode equation. In our example (sec. 4.4.3) we need to numerically solve eq. (4.32) in the complex plane. Newton's method has been employed for this task. The iterative procedure is considerably facilitated if good initial values are available. The latter can be obtained by starting from the special cases  $\Delta=0$  or  $z_h=0$  (which can be handled analytically) and then gradually increasing  $\Delta$  and/or  $z_h$ . Initial values can also be obtained by asymptotic expansion of the functions in (4.32) for large mode number  $n$ . Details can be found in appendix B. Here we present numerical results for  $z_h=100$  m,  $\Delta=10^{-5}$ ,  $\lambda=10$  cm,  $a_e=8493$  km,  $x=100$  m and  $z_T=50$  m, with  $z$  variable.

The first ten poles  $t_n$  have been tabulated in table 4.2, together with the corresponding specific attenuations  $\gamma_n$ . The modes have been arranged by increasing  $\gamma_n$ . It can be seen that  $\gamma_n$  is very small for the first few modes; the calculated values of  $\gamma_n$  for  $n \leq 4$  turn out to be almost independent of  $z_h$  (for  $z_h \geq 100$  m) and agree with those reported by Wait and Spies [18] for  $z_h=1$  km. For  $n \geq 7$ , the value of  $\gamma_n$  is no longer small compared to unity and increases steadily with increasing  $n$ . Therefore, when  $|x|$  is large, we may expect the modes with  $n \geq 7$  to contribute only little to the mode sum.

The corresponding normalized height-gain functions  $g_n(z)$ ,  $n=1,2,\dots,8$ , are plotted in fig. 4.8. It is seen that for the lower-order modes the field is concentrated in a region just below  $z=z_h$ . This type of modes is known as "trapped" or "locked" modes [13, sec. 9.5]. For  $n \geq 7$  the field increases rapidly with height ("leaky" modes), although eventually  $g_n(z) \rightarrow 0$  as  $z \rightarrow \infty$  (if a small negative imaginary part of  $k_0$  is assumed).

n	Re{t <sub>n</sub> }	Im{t <sub>n</sub> }	γ <sub>n</sub> (dB/km)	n	Re{t <sub>n</sub> }	Im{t <sub>n</sub> }	γ <sub>n</sub> (dB/km)
1	7.79	-1.91 · 10 <sup>-10</sup>	1.26 · 10 <sup>-10</sup>	6	1.21	-9.12 · 10 <sup>-2</sup>	6.01 · 10 <sup>-2</sup>
2	6.06	-5.17 · 10 <sup>-7</sup>	3.40 · 10 <sup>-7</sup>	7	2.62	-2.38	1.57
3	4.65	-1.08 · 10 <sup>-4</sup>	7.12 · 10 <sup>-5</sup>	8	3.49	-3.90	2.57
4	3.42	-4.05 · 10 <sup>-3</sup>	2.66 · 10 <sup>-3</sup>	9	4.19	-5.14	3.38
5	2.30	-3.32 · 10 <sup>-2</sup>	2.18 · 10 <sup>-2</sup>	10	4.81	-6.23	4.10

Table 4.2. The poles t<sub>n</sub> (n=1,2,...,10) determined from the mode equation (4.32), with the corresponding values of the specific attenuation γ<sub>n</sub>.  
Parameters: z<sub>n</sub>=100 m, Δ=10<sup>-5</sup>, λ=10 cm, a<sub>e</sub>=8493 km.

The excess path attenuation L<sub>m</sub>, calculated from (4.42), is shown in fig. 4.9a for an observation point (x,z) with |x|=100 km. As expected, the modes with n≥7 could be ignored in the mode sum. For n≤6, the magnitude of exp(-jα<sub>n</sub>|x|) is close to unity, so the magnitude of each term in (4.42) is mainly determined by |g<sub>n</sub>(z<sub>T</sub>)| and |g<sub>n</sub>(z)|. Hence, it depends on the terminal heights z<sub>T</sub> and z which mode yields the largest contribution.

Because of phasing effects between the individual modes, the function L<sub>m</sub>(z) shows some deep nulls. Similar results have been reported in the literature [20,21]. However, such nulls are not observed in measurements, see [20] and sec. 4.3.3. This discrepancy is believed to be caused by spatial irregularities in the duct, and by temporal atmospheric fluctuations due to turbulence. As a consequence, coherent phasing of the individual modes is unlikely to be maintained during the measurement time (which in practice is always finite). Rather, each mode arrives at the observation point with a more or less random phase. Thus it is more realistic to take a power sum of the modes [21] instead of the phasor sum (4.42), i.e.,

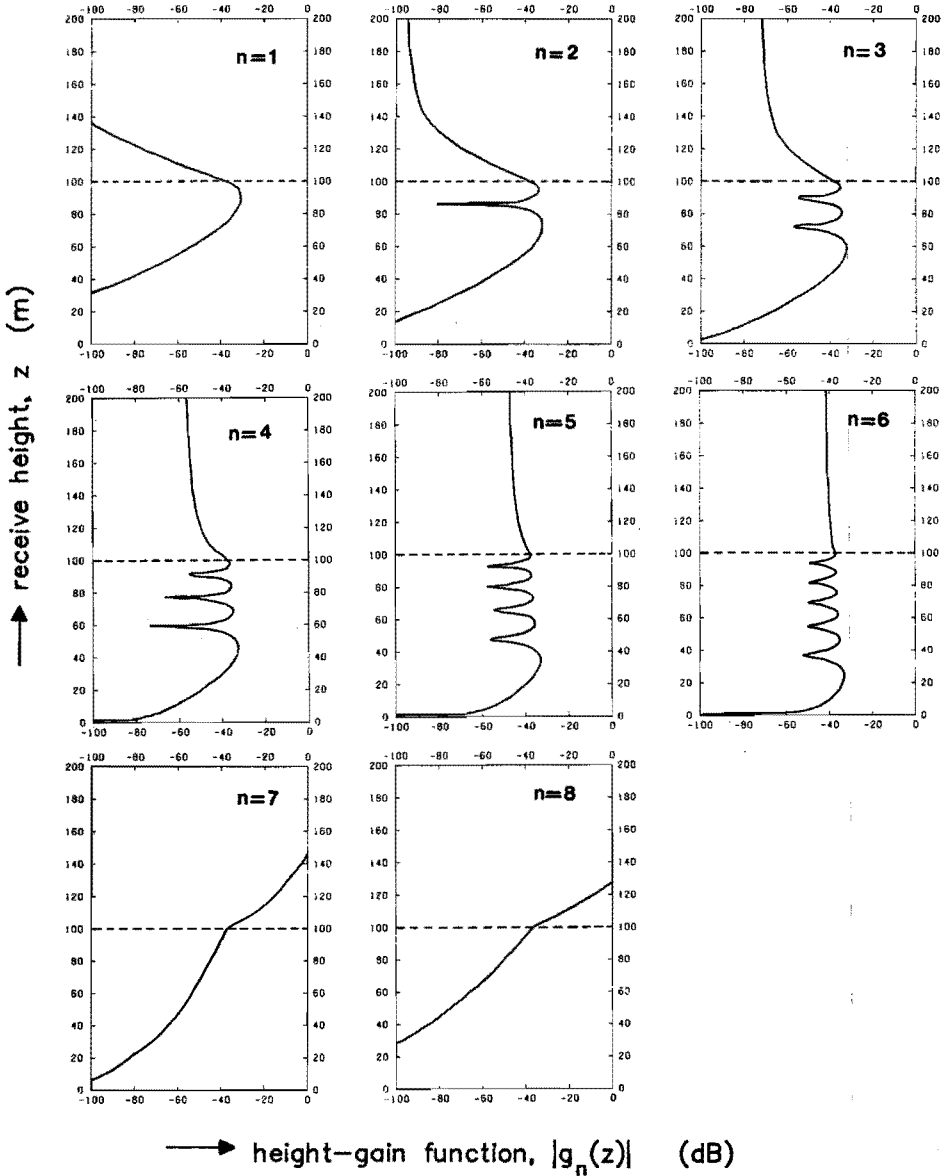


Fig. 4.8. Normalized height-gain functions  $|g_n(z)|$ ,  $n=1,2,\dots,8$ , for propagation in a duct, caused by a layer with refractive-index discontinuity  $\Delta$  at height  $z_h$  (dashed line).

Parameters:  $z_h=100$  m,  $\Delta=10^{-5}$ ,  $\lambda=10$  cm,  $a_e=8493$  km.

$$L_m(x,z) = -10 \log \left[ 4\pi^2 \frac{|x|}{\lambda} \sum_{n=1}^{\infty} |g_n(z_T)g_n(z)\exp(-j\alpha_n|x|)|^2 \right] \quad (\text{dB}). \quad (4.43)$$

The result of (4.43) is shown in fig. 4.9b. The function  $L_m(z)$ , calculated from (4.43), is much smoother, which is more in agreement with measured (time-averaged) data.

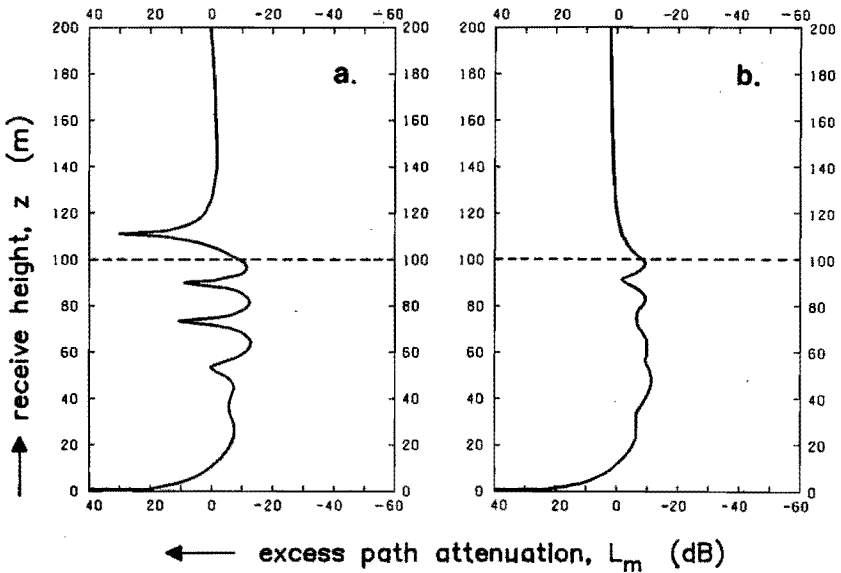


Fig. 4.9. Excess path attenuation  $L_m$  as a function of the receive height  $z$  (with fixed transmit height  $z_T$ ), for a path of length  $x$  in a duct, caused by a layer with refractive-index discontinuity  $\Delta$  at height  $z_h$  (dashed line). Parameters:  $z_h=100$  m,  $\Delta=10^{-5}$ ,  $\lambda=10$  cm,  $a_e=8493$  km,  $x=100$  km and  $z_T=50$  m.  
 a) Phasor sum (4.42); b) power sum (4.43).



4.4.5. Prediction model based on mode theory

According to the mode theory, the excess path attenuation is given by (4.19). This formula is, in general, not suited for practical applications. The calculation of the height-gain functions  $g_n(z)$  is time-consuming, and should, in principle, be carried out for each mode. For some typical ground-based-duct configurations, it has been shown that only one mode is responsible for the transmission [20,22]. In this case, it is possible to formulate a simple prediction model [22] similar to the CCIR ducting model [1]. Based on (4.19), with the receiver located at  $|x|=d$ ,  $z=z_R$ , and with only mode  $n$  taken into account, the model yields

$$L_m = -51.2 - 10 \log d - 10 \log f + \gamma_n d - 20 \log |g_n(z_T)| - 20 \log |g_n(z_R)| \quad (\text{dB}), \quad (4.44)$$

with  $d$  in km and  $f$  in GHz.

This formula is comparable with the CCIR ducting model (4.2). Ignoring the effect of terrain roughness in (4.2) (i.e., setting  $\gamma_h=0$ ), the CCIR ducting model is given by

$$L_m = -10 \log d + \gamma_d d + A_c \quad (\text{dB}). \quad (4.45)$$

The differences between (4.44) and (4.45) are the following:

- The frequency dependence of (4.45) is contained in  $\gamma_d$ , which increases logarithmically with increasing frequency, see (4.3). The frequency dependence of (4.44) is more complex: the  $-10 \log f$  term and the  $\gamma_n d$  term decrease with increasing frequency (the latter is illustrated e.g. in [18]), but

the height-gain function  $g_n(z)$  also depends implicitly on the frequency. The overall frequency dependence of (4.44) is therefore not evident.

- The coupling loss  $A_c$  in the CCIR model (4.45) has been refined in (4.44) into the sum of the logarithms of the height-gain functions at the transmitter and the receiver. The absence of any height-gain information in (4.45) is remarkable.

These differences may be explained as follows [23]. The empirical CCIR coupling-loss term ( $A_c$ ) contains no frequency dependence and height dependence. In the CCIR model, the higher losses observed at higher frequencies are attributed to a larger  $\gamma_d$ . However, the model (4.44) suggests that these higher losses may be caused by poorer coupling into the duct from terminals outside the duct, instead of by higher  $\gamma_d$ . An alternative explanation for the apparent increase of  $\gamma_d$  at higher frequencies might be the enhanced effects at these frequencies of surface roughness and of scattering out of the duct due to atmospheric inhomogeneities.

In general, a number of limitations is inherent in the mode-theory prediction model (4.44):

- The actual number of modes that must be taken into account depends strongly upon the link parameters. For elevated ducts (sec. 4.4.3), the single-mode model (4.44) is often unrealistic.
- The solution of the mode equation and the calculation of the height-gain functions are, in general, time-consuming, because an analytic solution is usually not possible. Application of the mode-theory model is therefore not attractive in interference calculations.
- The mode theory neglects horizontal variations in the refractive-index profile. This assumption is often too crude on long transhorizon paths.
- The model requires a detailed specification of the refractive-index profile of the duct. This information is difficult to obtain in practice, because the

atmosphere varies permanently and because there is a lack of sufficient radiometeorological data.

- The excitations of the individual modes are affected by horizontal inhomogeneities in the refractive index; at such inhomogeneities, other modes can be excited (*mode conversion* [24]).

It is recognized that the mode theory may yield valuable qualitative insight into various physical aspects of tropospheric ducting. However, for the purpose of quantitative interference prediction a more useful model will necessarily be of a semi-empirical nature.

#### 4.5. General transhorizon-interference prediction procedure

From the preceding sections, it is clear that the current CCIR interference-prediction models [1,3,4] are unsatisfactory in several respects:

- The models may produce considerable prediction errors for certain path parameters (see sec. 4.3.2).
- Most of the models do not include any information on their accuracy; therefore, the user does not know the reliability of the predictions obtained from these models.
- The CCIR does not give a clear, straightforward, unambiguous prediction procedure. The relevant information is scattered in several Reports which are not completely complementary. For example, in Rep. 569-3 [1], a user who has to do with very rough paths is referred to Rep. 715-2 [3] for diffraction calculations, as mentioned earlier in sec. 4.2.2. The latter Report does not consider any time-variability, hence the user is left with his problem of interference predictions for low time percentages.

- Several terms in the CCIR models contradict theoretical considerations (see for example sec. 4.4.5), or intuitive physical insights (e.g., the absence of any antenna-height dependence in the CCIR ducting model (4.1)).
- Some interference mechanisms (e.g. terrain scatter) are hardly or not at all included in the models.

Improvements in the current CCIR prediction models are only possible at the cost of a considerable effort. The development of a general interference-prediction procedure, which is unambiguous, straightforward, widely applicable and reasonably accurate, is probably outside the scope of a single national telecommunication administration. Such a task is better suited to a cooperative international project, like COST 210 [2]. It is not claimed that the latter project will succeed in completing such a general prediction procedure, but a considerable step forward may be set.

A possible framework of a general interference-prediction procedure is illustrated in fig. 4.10 [9]. Here the user input is translated into a parameter array, with the help of additional information from three databases. These databases contain the relevant radiometeorological and terrain information and can also produce, as by-products, path profiles and maps. The parameter array should give an indication of the relevant propagation mechanism(s) on the path of interest. Each mechanism has its own sub-model, and the output of these sub-models is then combined in the user output interface to produce the final prediction results.

The realization of such a general prediction procedure would be an important step forward for interference calculations; the straightforward, unambiguous character allows for computerization of the procedure.

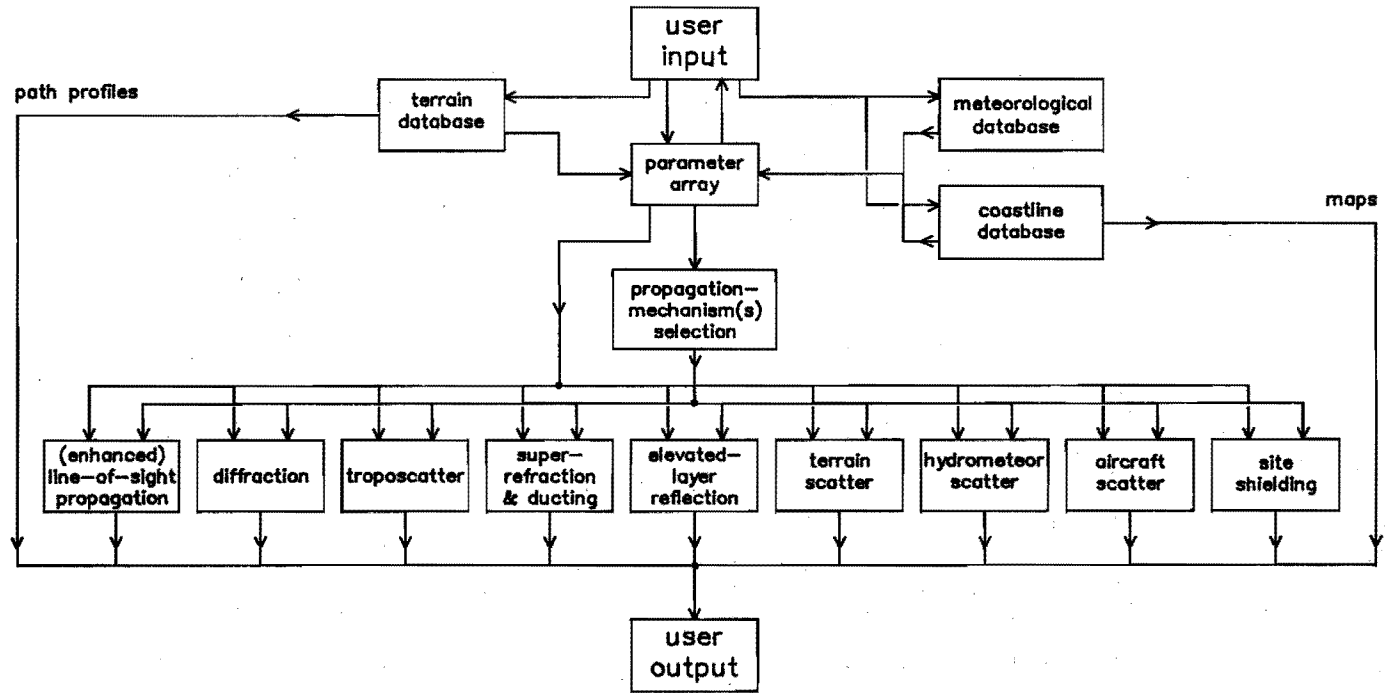


Fig. 4.10. Possible framework of a general interference-prediction procedure [9].

#### 4.6. References

- [1] CCIR, Plenary Assembly, "The evaluation of propagation factors in interference problems between stations on the surface of the earth at frequencies above about 0.5 GHz", *Recommendations and Reports of the CCIR*, vol. V, Rep. 569-3, Geneva, 1986.
- [2] COST 210 Management Committee, "COST 210 activities to model trans-horizon cochannel interference paths in Europe", Proc. Int. Conf. Ant. Prop. (ICAP), *IEE Conf. Publ.*, no. 274, pp. 352-354, 1987.
- [3] CCIR, Plenary Assembly, "Propagation by diffraction", *Recommendations and Reports of the CCIR*, vol. V, Rep. 715-2, Geneva, 1986.
- [4] CCIR, Plenary Assembly, "Propagation data and prediction methods required for transhorizon radio-relay systems", *Recommendations and Reports of the CCIR*, vol. V, Rep. 238-5, Geneva, 1986.
- [5] S. Rotherham, "A radio interference model for Western Europe", *Agard Conf. Proc.*, no. 346, pp. 21/1-21/15, 1983.
- [6] J.T. Ong, "An estimation of microwave interference levels over land in clear-air conditions", EMC Conf., *IERE Publ.*, no. 60, pp. 119-123, 1984.
- [7] "Evaluation of interference on the great-circle path (MODE 1)", *CCIR document 5/273-E* (France), June 1985.
- [8] O. Rue, "A new clear-air interference prediction method for small time percentages", Proc. Int. Conf. Ant. Prop. (ICAP), *IEE Conf. Publ.*, no. 274, pp. 343-346, 1987.
- [9] COST 210, internal communications, 1984-1988.
- [10] B.R. Bean and E.J. Dutton, "*Radio Meteorology*", US Dept. of Commerce, NBS Monograph 92, Washington, 1966.
- [11] D.S. Jones, "*The theory of electromagnetism*", Pergamon, Oxford, 1964.

- [12] D.E. Kerr, ed., "*Propagation of short radio waves*", Dover, New York, 1951.
- [13] K.G. Budden, "*The wave-guide mode theory of wave propagation*", Logos, London, 1961.
- [14] H.G. Booker and W. Walkinshaw, "The mode theory of tropospheric refraction and its relation to waveguides and diffraction", *Meteorological factors in radio wave propagation*, Conf. Rep., Phys. Soc. & Royal Meteor. Soc., London, pp. 80-127, 1946.
- [15] J. Boersma, EUT, private communications, 1988.
- [16] M. Abramowitz and I.A. Stegun, "*Handbook of mathematical functions*", Dover, New York, 1965.
- [17] D.R. Hartree, J.G.L. Michel and P. Nicholson, "Practical methods for the solution of the equations of tropospheric refraction", *Meteorological factors in radio wave propagation*, Conf. Rep., Phys. Soc. & Royal Meteor. Soc., London, pp. 127-168, 1946.
- [18] J.R. Wait and K.P. Spies, "Internal guiding of microwaves by an elevated tropospheric layer", *Radio Science*, vol. 4, no. 4, pp. 319-326, 1969.
- [19] P. Scheeren and R. Prasad, "Tropospheric ducting of radio waves produced by a refractive-index discontinuity", *Proc. ANSTI EE'86 Conf.*, Dar es Salaam, pp. G.1.1-G.1.11, 1986.
- [20] R.A. Pappert and C.L. Goodhart, "Case studies of beyond-the-horizon propagation in tropospheric ducting environments", *Radio Science*, vol. 12, no. 1, pp. 75-87, 1977.
- [21] S.W. Marcus, "A model to calculate e.m. fields in tropospheric-duct environments at frequencies through SHF", *Radio Science*, vol. 17, no. 5, pp. 895-901, 1982.

- [22] J. Dijk, J. van Tiggelen and J. Neessen, "Modelling on interference due to ducting at frequencies above 1 GHz", *Agard Conf. Proc.*, no. 332, pp. 17.1-17.13, 1982.
- [23] K.H. Craig, Rutherford Appleton Laboratory, private communications, 1986.
- [24] J.R. Wait, "Theory for the excitation and propagation of electromagnetic waves guided by an elevated refractive-index discontinuity in the troposphere", *Can. Journ. Phys.*, vol. 52, pp. 1852-1860, 1974.





## 5. INTERFERENCE-REDUCTION TECHNIQUES

### 5.1. Introduction

In the previous chapters, it has been shown that successful frequency sharing between radiocommunication systems can be severely hampered by RF-interference effects. In these cases, interference-reduction techniques are essential. These are designed to reduce the mutual interference between frequency-sharing systems (inter-system interference) to acceptable levels. In addition, techniques for reduction of radio interference within an individual network (intra-system interference) may be essential to allow frequency reuse within that network.

Most spectrum users have a common interest in adhering to the allocated frequency bands, and in an efficient utilization of the radio-frequency spectrum. The ultimate *common* goal of employing interference-reduction techniques is the improvement of the spectrum efficiency. In addition, an *individual* system operator may apply interference-reduction techniques to improve the quality of his links. The latter applications are often a-posteriori (sometimes even ad-hoc) solutions in a specific interference situation, whereas the former are often (though not necessarily) planned a priori.

The situation is different in a military "friend/foe" scenario, where there is no such thing as a common interest. Here deliberate jamming of the enemy's links, and power battles between transmitters (to "burn through" the interference of the adversary), do not improve but in fact reduce the spectrum efficiency. The individual interests in interference-reduction techniques still exist in such a situation.

Many techniques for interference reduction have been described in the literature; these techniques are reviewed in sec. 5.2 from a general point of view. In this

thesis, we are especially interested in reduction of a specific type of interference, namely transhorizon interference from terrestrial stations into satellite earth stations. Reduction of this type of interference has been studied by the author in the framework of Working Group 3 of the COST-210 project [1], and is discussed in sec. 5.3.

Two interference-reduction techniques have been investigated in more detail. A typical a-posteriori application of interferometric cancellation of a specific interference type is described in sec. 5.4; the site-shielding technique is studied in depth in chapters 6-8.

## 5.2. Review of interference-reduction techniques

### 5.2.1. *General survey*

Consider the schematic, simplified interference situation (with only one interferer) shown in fig. 5.1. Here, the wanted signal is transmitted by the wave  $U^w$  and the interfering (unwanted) signal by the wave  $U^i$ . We assume that the wanted RF signal  $x^w(t)$  and the interfering RF signal  $x^i(t)$  are uncorrelated [2, p. 108], so that superposition of signal powers and definition of signal-to-interference ratios are allowed. For the evaluation of the performance of the interfered-with communication system, we can thus write:

$$S/I = \frac{P_t^w G_t^w L_b^i G_r^w}{P_t^i G_t^i L_b^w G_r^i} G_{\text{mod}}^{w,i} G_{\text{proc},r}^{w,i} G_{\text{proc},n} \quad (5.1)$$

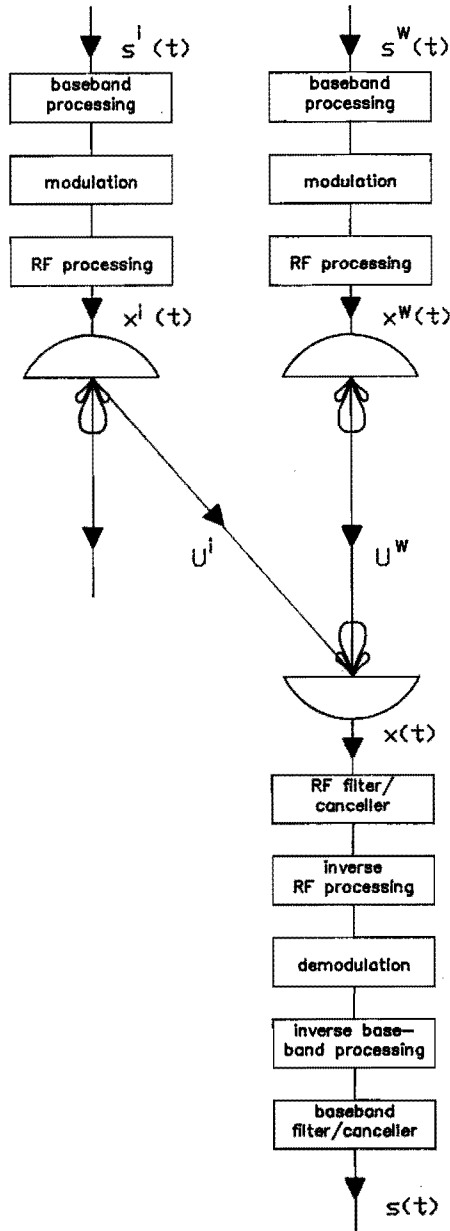


Fig. 5.1. Simplified interference situation with one interferer.  
 $s(t)$ : baseband signal,  $x(t)$ : RF signal,  $U$ : electromagnetic wave;  
superscripts  $w$  and  $i$  denote "wanted" and "interfering"  
(i.e., unwanted), respectively.

Here,

- $S/I$  is the signal-to-interference ratio at the receiver output;
- $P_t^{w,i}$  denotes transmit power of the wanted (w) and interfering (i) carrier, respectively;
- $G_t^{w,i}$  denotes transmit-antenna gain in the direction of the receive station;
- $L_b^{w,i}$  is the basic transmission loss (see sec. 3.2.2) along the propagation path of  $U^w$  and  $U^i$ , respectively;
- $G_r^{w,i}$  denotes receive-antenna gain in the direction of the incoming wave ( $U^w$  or  $U^i$ , respectively);
- $G_{mod}^{w,i}$  is the gain in  $S/I$  from RF level to baseband level, due to a particular choice of the modulation/demodulation methods of  $x^w(t)$  and (in cooperative systems) of  $x^i(t)$ ;
- $G_{proc,r}^{w,i}$  is the gain in  $S/I$  due to *reciprocal* signal processing of the wanted and/or unwanted signals (either at baseband or at RF) at the transmitter, including the inverse processing at the receiver;
- $G_{proc,n}$  is the gain in  $S/I$  due to *non-reciprocal* signal processing at the receiver (either at baseband or at RF), i.e., filtering or cancellation.

It has been assumed in (5.1) for simplicity that all factors exist and can be treated independently. In reality, some of these factors may be interrelated, in particular if the involved processes are non-linear (modern digital modulation types are generally linear, whereas classical FM exhibits non-linear threshold effects [2, pp. 334-337]).

Interference reduction can be based on any of the seven factors in (5.1), corresponding respectively to the following techniques:

- i) superior transmit power of the wanted signal;
- ii) antenna discrimination at the transmitting stations;
- iii) propagation screening of the interfering signal;
- iv) antenna discrimination at the receiving station;

- v) improved modulation/demodulation methods;
- vi) reciprocal processing of wanted and/or interfering signals;
- vii) non-reciprocal signal processing.

These techniques are now introduced briefly before they are described in more detail in the following sections.

*ad (i).* Increasing the transmit power  $P_t^w$  of the wanted signal is a well-known practice in military warfare, which can become very costly. For the mutual coordination of (cooperative) radiocommunication systems, this brute-force method is of little value, because the enhanced transmit power may cause more interference into other stations. This method is therefore not further considered.

*ad (ii) and (iv).* Antenna discrimination is effective if the unwanted radiation is transmitted or received via an antenna sidelobe (the wanted radiation is generally transmitted or received by the main lobe). Increasing the antenna gain in the main direction, i.e., increasing  $G_t^w$  or  $G_r^w$ , is generally not an attractive solution, as it implies a larger antenna. It is more cost-effective to reduce the sidelobe gains  $G_r^i$  and (in a cooperative system)  $G_t^i$ , which is known as *antenna-sidelobe suppression*, see sec. 5.2.2.

*ad (iii).* The ratio  $L_b^i/L_b^w$  cannot be increased by reducing the path loss  $L_b^w$  of the wanted signal, as this loss is already minimized for properly designed links. However, propagation screening of the interfering signal can increase the loss  $L_b^i$ , due to extra diffraction losses along the unwanted propagation path. This kind of obstacle diffraction has been discussed previously (sec. 3.3.2). Screening by (natural or artificial) obstacles close to the receiving station is known as *site shielding*, see sec. 5.2.3. Modelling of the latter technique is more difficult; in the vicinity of the receive antenna, the obstacle diffraction loss and antenna gain can no longer be treated independently, as has been assumed in (5.1). This problem is studied in depth in chapter 7.

*ad (v) and (vi).* Modulation is the conversion of the baseband signal to an RF signal, and is in fact a specific, indispensable form of reciprocal signal processing in radiocommunication (other signal-processing techniques are more or less optional). Modulation and reciprocal signal processing always require the inverse operation at the other end of the communication link, in order to recover the desired baseband information. These techniques can therefore not be used for interference reduction if one terminal of the wanted link is inaccessible (e.g. in the case of an already orbiting satellite), or when it can not be changed for other reasons (e.g. the transmitter in a point-to-multipoint distribution system). A brief discussion of these techniques is presented in sec. 5.2.4.

*ad (vii).* Non-reciprocal signal-processing techniques are applied at the receive terminal only, and do not require an inverse operation. Like all signal-processing techniques, these techniques exploit specific properties of the wanted and interfering signals.

*Filters* are, in general, applicable only if the cochannel interference (i.e., the part of the interference spectrum overlapping the spectrum of the wanted signal) has sufficiently narrow bandwidth, compared to the bandwidth of the wanted signal. Adjacent-channel interference can, in principle, be eliminated by filters, although cost is often a limiting factor if the filter skirts are to be steep.

*Interferometric cancellers* are more powerful than filters and can eliminate both cochannel interference and adjacent-channel interference. A general description of interferometric cancellation methods is given in sec. 5.2.5; a specific application is described in sec. 5.4.

### 5.2.2. Antenna-sidelobe suppression

In principle, an antenna is a spatial filter if the main-lobe gain is higher than the sidelobe gain. If the unwanted radiation is transmitted or received via a sidelobe (and the wanted radiation via the main lobe), the antenna discrimination between wanted and unwanted signals can be increased by sidelobe suppression. The ways of achieving this suppression greatly depend on the type of antenna used.

We restrict the present discussion to earth-station antennas, although many of the conclusions are also valid for antennas in satellite stations or terrestrial stations. For large earth-station antennas ( $100 < D/\lambda < 150$ ), the majority (90%) of the sidelobes should be below the CCIR reference curve [3,4], i.e.,

$$\begin{aligned} G(\theta) &= 32 - 25 \log \theta \quad (\text{dBi}), & 1^\circ \leq \theta \leq 48^\circ, \\ G(\theta) &= -10 \quad (\text{dBi}), & 48^\circ \leq \theta \leq 180^\circ, \end{aligned} \tag{5.2}$$

where  $\theta$  is the angle (in degrees) relative to the main direction. The type of antenna which is most often used in large earth stations is the axisymmetric Cassegrain antenna. In [5], the principal sources of sidelobe radiation from such an antenna (fig. 5.2) are identified as:

- a) main-reflector aperture distribution, including blockage by the subreflector;
- b) primary-feed spillover;
- c) subreflector edge diffraction of the primary-feed radiation (*c1*) and of the main-reflector radiation (*c2*);
- d) main-reflector edge diffraction;
- e) strut scattering of the subreflector radiation (*e1*) and of the main-reflector radiation (*e2*);
- f) main-reflector profile errors.



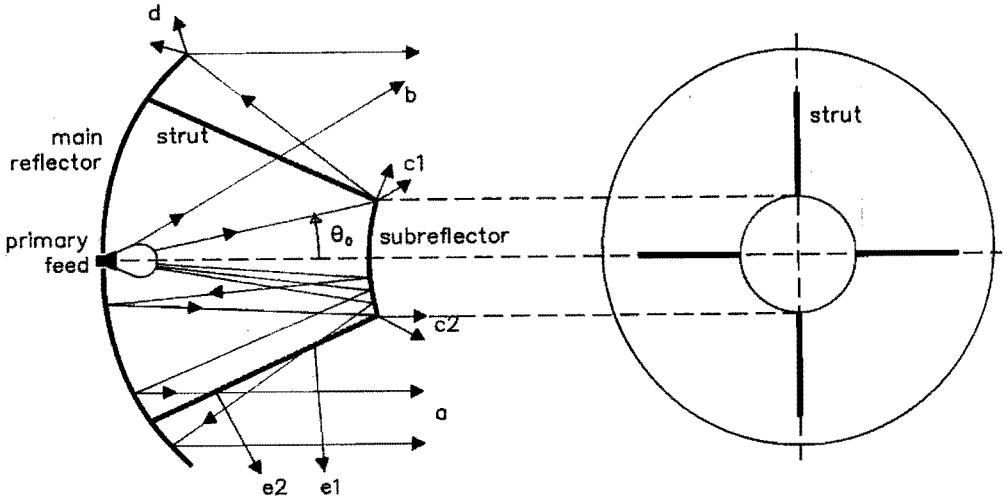


Fig. 5.2. Principal sources of sidelobe radiation from an axisymmetric Cassegrain antenna, as listed on page 115.

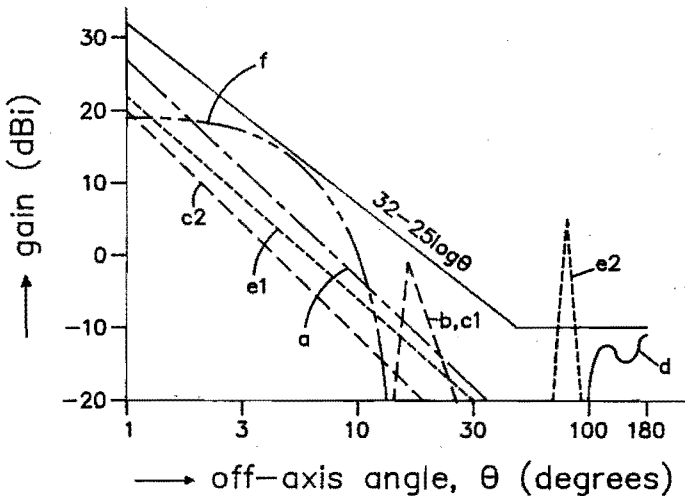


Fig. 5.3. Contribution to the overall sidelobe performance of earth-station antennas (from [5]), as listed on page 115.

The relative significance of these factors depends, of course, on the specific antenna considered. For a typical earth-station antenna, the contributions from these factors to the overall sidelobe performance are illustrated in fig. 5.3 [5].

As suggested by fig. 5.3, the overall sidelobe performance of an antenna can be improved by the following techniques.

i) The *aperture distribution* (*a*) is responsible for the sidelobes at small angles  $\theta$  (i.e., a few degrees). These sidelobes can be reduced by tapering the illumination levels at the edge of the main reflector and at the edge of the region blocked by the subreflector. This can be achieved by choosing an appropriate primary-feed pattern and/or by the utilization of shaped reflectors [6].

ii) *Main-reflector profile errors* (*f*) determine the sidelobe level up to  $\theta \approx 10^\circ$ . Such errors arise, among other things, from gravitational forces, wind and thermal expansions, as well as from errors in the manufacturing and alignment of individual reflector panels. Obtaining antennas with better surface accuracies is limited mainly by costs.

iii) *Primary-feed spillover* (*b*) and *diffraction of this radiation past the subreflector* (*c1*) are important for  $\theta_0 \leq \theta < 30^\circ$  (approx.), where  $\theta_0$  is the angle subtended by the subreflector (fig. 5.2). The corresponding sidelobes can be reduced by applying a low-sidelobe feed and tapering the subreflector illumination. Alternatively, the subreflector edge diffraction can be reduced by attaching a microwave absorber around the edge [7].

iv) *Main-reflector edge diffraction* (*d*) determines the sidelobe level for  $\theta > 90^\circ$ . This effect can also be reduced by tapering the illumination, or by attaching a microwave absorber around the edge [7].

v) *Scattering from struts* (*e*) can result in sidelobe radiation into various specific directions, depending on the actual strut geometry. Attaching a microwave absorber to the struts reduces the scatter effect, but can cause a significant increase in the

antenna noise temperature. A better solution is the use of microwave-scattering material, which scatters the incident radiation more or less isotropically. Alternatively, the sidelobe level may be reduced by an improved strut design [8].

Some of the above mentioned techniques are relatively easily implemented. For this reason, the CCIR [4] has recently formulated a more demanding design criterion for large earth-station antennas (i.e., those with  $D/\lambda > 100$ ) installed after 1991: at least 90% of the sidelobe peaks should not exceed the new reference curve

$$G(\theta) = 29 - 25 \log \theta \quad (\text{dBi}), \quad 1^\circ \leq \theta \leq 20^\circ. \quad (5.3)$$

Further reduction of sidelobe levels in axisymmetric Cassegrain antennas is difficult to achieve. A better solution is the adoption of an offset configuration [9, chapter 2], which does not suffer from aperture blockage by struts or by the subreflector. According to [5], a much lower envelope of sidelobes should then be feasible, namely

$$G(\theta) = 26 - 33 \log \theta \quad (\text{dBi}), \quad 1^\circ \leq \theta \leq 12.4^\circ. \quad (5.4)$$

The above discussion deals with *general* sidelobe suppression. Suppression of *specific* sidelobes is an alternative way of reducing interference from certain specific, nominally fixed, directions. This can be achieved by attaching microwave absorbers at appropriate points on the reflector surface [10]. More complicated techniques, known as *sidelobe cancellation* or "*nulling*", closely resemble the interferometric-cancellation techniques, and are treated together with the latter in sec. 5.2.5. Most sidelobe-cancellation techniques are especially suited for the reduction of near-in sidelobes ( $\theta$  small), e.g. in order to raise the satellite occupancy of the geostationary orbit.

### 5.2.3. *Site shielding*

In this thesis, we define site shielding as the screening of a receiving station against interference from transmitting stations, by means of an obstacle located in the vicinity of the receiving station. This technique cannot be applied if the unwanted radiation is received from a direction so close to the main-beam direction that the wanted radiation cannot pass unhindered. However, this technique is well suited for combatting wide-angle interference. Site shielding is, therefore, often employed to protect earth stations against harmful interference from terrestrial stations (fig. 5.4), if this interference is of the "clear-air" type (see sec. 3.3.1).

The *shielding effectiveness* or *site-shielding factor* (SSF) of an obstacle is defined as the ratio of the powers of the received (unwanted) signal in the absence and presence of the obstacle, respectively. This factor depends, among other things, on the shielding medium. The shielding obstacle can be either natural or man-made. The following possibilities have been suggested [11]:

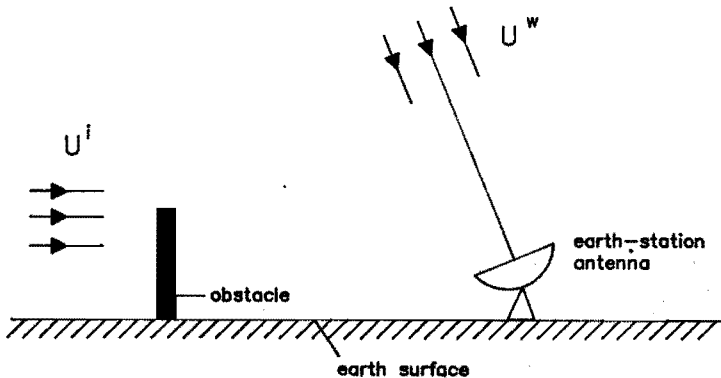


Fig. 5.4. Site shielding of an earth station against interference from a terrestrial station.  $U^w$ : wanted radiation (from a satellite station);  $U^i$ : interfering radiation (from a terrestrial station).

i) Shielding by *terrain* (hills, volcanic craters, embankments or pits) is a well-known technique in the radio-astronomy service [12] for the protection of the sensitive receivers used in that service. Shielding by embankments or pits has also been employed for satellite earth stations, using either natural [13] or artificial [14] structures. Good protection has been observed in these cases: measured SSFs range from 20 dB up to 50 dB. However, ideal natural shielding is seldom available. The construction of artificial pits is expensive and requires a considerable area, which may not be available if the earth station is to be located close to a large population centre.

ii) *Vegetation* is another natural shielding medium, which can provide an estimated protection [11] of 10 to 40 dB, depending on the situation. Shielding by vegetation is rather unreliable, because of:

- very strong influence of rain and wind;
- seasonal variability of the SSF, especially for deciduous vegetation;
- possible changes or removal of the trees during the lifetime of the earth station.

Only little is known about the effect of vegetation at microwave frequencies. The available data [15] suggest that a wood or forest may be treated as a more or less opaque obstacle at these frequencies.

iii) Shielding by *walls* or *fences* around an antenna is a well-known practice for high-power radars [16] to reduce ground-clutter effects (and to protect personnel). The same technique has been applied for satellite earth stations. If the mesh of the fence is small enough (less than  $0.1 \lambda$ ), a SSF of typically 25 dB can be achieved with a knife-edge fence (or wall). Extra protection can be obtained by treating the top edge with serrations [16] or absorbing material, or by rounding the top edge of the fence.

*iv) Buildings* and other (existing) man-made structures can also provide shielding for earth-station antennas. This technique is especially useful for small earth stations (e.g. for "business" satellite services), as these are often located in urban areas. The protection afforded by an individual building can be estimated by diffraction theory, considering a building as a knife-edge obstacle. However, in an urban area, prediction of the SSF is more complicated, because (multiple) reflections and scatter effects by other buildings severely affect the received-signal level. Propagation in an urban environment is, at present, of special interest in land mobile radio services [17], which operate below 1 GHz. Experience with urban propagation at higher frequencies is limited to measurements made for the planning of terrestrial broadcasting services in the 12 GHz band [18]. Obviously, shielding by buildings shows a great variability in shielding effectiveness, depending on the actual situation. In-situ measurements may be required for each proposed installation of an earth station. As with vegetation, buildings may be modified or even vanish (or others be erected) during the lifetime of an earth station.

*v) Screens* [19] can be used to protect a receiving antenna against interference from specific, fixed directions. Such screens are installed at a given (short) distance from the antenna, or mounted on it (this technique can therefore also be regarded as a special case of sidelobe suppression). With a simple screen, the interference is only reduced if it is received from a fixed, well-defined direction. More complex screens (e.g. a double-ring screen) have a somewhat wider suppression region. Antenna-mounted screens reduce the sidelobe radiation in particular sectors of the off-axis angle  $\theta$ . Care must be taken that scattering at the edges of screens does not cause interference into other directions.

#### 5.2.4. (Reciprocal) signal processing, including (de)modulation

The choice of a modulation method in a specific communication system is determined (among other things) by the properties of the communication channel. Classical (mainly analogue) modulation methods were designed to be optimum for idealized channels with additive white Gaussian noise, thus neglecting possible interference in the channel, or considering it a minor perturbation [2, sec. 7.4]. Modern modulation methods (increasingly digital) should be chosen for optimum transmission in a channel with noise plus interference. In general, two aspects of interference are important for the selection of the modulation method: minimum receiver susceptibility to interference, and minimum transmitter interference caused into other stations. Both aspects are included in studies of modern (digital) modulation methods, see e.g. [20].

Even when a choice of modulation system at the transmitter has been made, interference reduction is still possible in a receiver by improving the demodulator structure. This topic has received only very little attention in the literature. The following studies have been reported:

- a new FM–demodulator structure [21];
- optimum detection of a BPSK signal [22, 23].

Apart from the modulation method, additional signal processing can assist in improving the signal–to–interference ratio at the receiver output, see eq. (5.1). Again, two aspects can be distinguished: processing of the wanted signal for minimum susceptibility to interference, and processing of the unwanted signal so that it causes minimum (harmful) interference. For both signals, the processing can be carried out either at baseband or at radio frequency; the inverse operation is required after or before the demodulation process, respectively.

RF processing is employed in modern *spread-spectrum communications* [24]. Here, the modulated wanted signal  $x^w(t)$  with bandwidth  $B_x$  is spread over a much wider RF bandwidth  $B_y$  by a process  $\hat{P}$ ,

$$y^w(t) = \hat{P} x^w(t), \quad (5.5)$$

before transmission. The received signal is subject to the inverse spreading operator  $\hat{P}^{-1}$  to obtain the wanted signal  $x^w(t)$ . Generally, the operator  $\hat{P}$  is chosen such that  $\hat{P}^{-1} = \hat{P}$  [2, pp. 325–328]. Thus, any interfering signal  $x^i(t)$  at the receiver input is spread over the same bandwidth  $B_y$  by the operator  $\hat{P}^{-1} = \hat{P}$ , thereby reducing the spectral density of the interfering signal by a factor

$$G_{\text{proc},r} \approx B_y / B_x. \quad (5.6)$$

Spread-spectrum techniques are much used in military communications. In addition to "jamming" protection, they also yield protection against unwanted detection by the "enemy", because the spectral density of the wanted signal is reduced to a level difficult or impossible to detect, as long as the spreading operator  $\hat{P}$  is unknown to the adversary.

A typical baseband signal-processing technique is *energy dispersal* [25]. In this technique, the baseband signal is spread out evenly over its entire available bandwidth, to keep its spectral density low. This is especially important if the baseband signal can temporarily be absent because in this case the RF energy is concentrated at the carrier frequency. Energy dispersal then reduces the harmfulness of the unmodulated carrier to other receivers. The technique is well known in analogue FM systems for telephony and television [25]. For digital systems, energy dispersal is designed to ensure that the pulse train is sufficiently random, as any



repetitive pattern causes peaks in the spectrum of the signal. Transforming a pulse train to a pseudo-random sequence is known as *scrambling*; this is functionally similar to (5.5).

An essential technique in digital communication systems is *coding* [26]. Two main kinds of coding can be distinguished. *Source coding* is generally designed to reduce the required dynamic range and bandwidth of the transmitted signal, thereby increasing the efficiency of channel use. A review of source-coding techniques for satellite telephony is given in [27]. *Channel coding* has more or less the opposite purpose, in that it adds redundancy to the information to be transmitted, in order to make it less vulnerable to noise, interference or other imperfections in the channel. The added redundancy can be utilized to detect or even correct errors in the detection process by means of suitable algorithms [28].

A special type of coding is *correlative coding*, which is in fact a combination of coding and modulation (known as "codulation"). A typical example is *minimum-shift keying* (MSK), in which the phase transitions of the carrier are built up gradually during a bit period, thereby avoiding high-frequency components in the RF spectrum [20, sec. 5.3].

#### 5.2.5. Interferometric cancellation

Interferometric-cancellation techniques (including the sidelobe-cancellation techniques mentioned at the end of sec. 5.2.2) are all based on the same principle (see fig. 5.5). A replica of the unwanted signal, provided by a reference source, is properly weighted (in amplitude and phase) and subtracted from the wanted plus unwanted signals provided by the main source, in such a way that the unwanted signal is cancelled. The differences between the individual techniques follow mainly

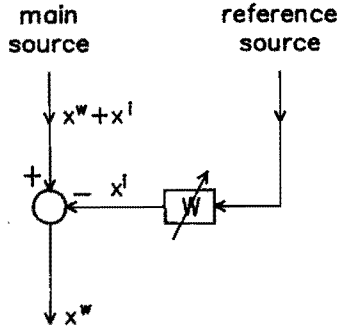


Fig. 5.5. Principle of interferometric cancellation.

$W$ : complex weighting (i.e., in amplitude and phase);

$x^w$ : = wanted signal;  $x^i$  = interfering (unwanted) signal.

from the way in which the required reference source is obtained. The following four methods can be distinguished.

i) Envelope detection. This method can only be applied for angle-modulated signals. The reference signal is obtained by simple envelope detection of the main signal, as shown in [29]. Up to 15 dB of interference cancellation has been measured in the laboratory, but the practical feasibility of the method is still to be determined.

ii) Sidelobe cancellation. The sidelobe-cancellation techniques mentioned in sec. 5.2.2 obtain the required reference signal by adaptation of the receiver antenna.

Williams [30] has suggested to use a phase-reversed, selected, ring-shaped area of the antenna aperture as a source of the reference signal. The correct amplitude weighting factor is obtained by selecting the proper width of the ring. This system can be implemented with a lens antenna and  $180^\circ$  phase shifters.

For satellite earth-terminals, sidelobe cancellation by an auxiliary feed in a reflector antenna [31,32] has been proposed. This (defocused) feed is placed in the

focal region of the antenna, in such a way that the corresponding scanned main lobe points towards the interference source. The output signal of the auxiliary feed is the required reference signal.

These sidelobe-cancellation techniques appear suited for the reduction of fixed, near-in sidelobes which complicate frequency sharing between links to closely spaced satellites (see sec. 2.2.3). However, these techniques have, to our knowledge, not yet been applied in practice.

*iii) Auxiliary antenna.* The most obvious way of obtaining the required reference signal is the utilization of a second (auxiliary) antenna, which is pointed at the interfering source. The auxiliary antenna can be smaller than the main antenna, because the main-lobe gain of the former only has to exceed the sidelobe gain of the latter. This fact makes the technique very attractive for reduction of wide-angle interference, such as (clear-air) terrestrial interference into satellite earth stations.

Interference cancellers of this type (fig. 5.6a) are simple and cheap, and are applicable whenever the direction of the interfering source is known and fixed. However, in practice, differential variations in the received signals require continuous adjustment of the weighting of the reference signal, and this is only feasible by making the system adaptive by means of a correlation process, see fig. 5.6b. Such an adaptive interference canceller is more complicated (and hence more expensive) than the static type of fig. 5.6a, but can yield excellent results: more than 50 dB of cancellation has been measured [33,34]. Application of adaptive interference cancellers for communications-satellite earth stations is receiving increasing attention [35-37]. A different application of this technique is presented in sec. 5.4.

Recently, it has been suggested that, instead of an auxiliary antenna, an auxiliary reflector (in addition to the antenna main reflector) can be used as an alternative way of obtaining the required reference signal [38].

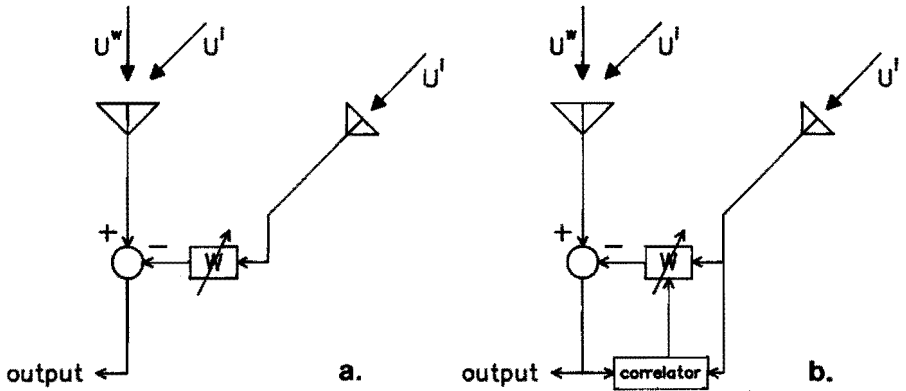


Fig. 5.6. Interference cancellation by means of an auxiliary antenna.  
 a) Static interference canceller; b) adaptive interference canceller.

$W$ : complex weighting,  $U^w$ : wanted radiation,  $U^i$ : interfering radiation.

*iv) Phased array.* A phased array goes a step further than the auxiliary-antenna method, by using a large number of (most often identical) antennas, known as array elements. The many degrees of freedom can be utilized to cancel simultaneously a large number of interfering signals. The outputs of all elements are properly weighted in amplitude and phase and added together to produce the final array output, see fig. 5.7. In an *adaptive array* [39], the weights can be controlled automatically to reach an optimum signal-to-interference ratio. As distinct from the previous technique of one auxiliary antenna, adaptive arrays are capable of reducing several interfering signals simultaneously. Furthermore, adaptive arrays are very flexible, because they can adapt themselves very quickly (by electronic means) to a rapidly-changing interference environment. Electronic beam steering is another capability of adaptive arrays, which makes them especially attractive for military radars [40, chapter 8]. Adaptive arrays are inherently limited in bandwidth and are quite expensive. They are, therefore, less attractive for communications-satellite earth stations.

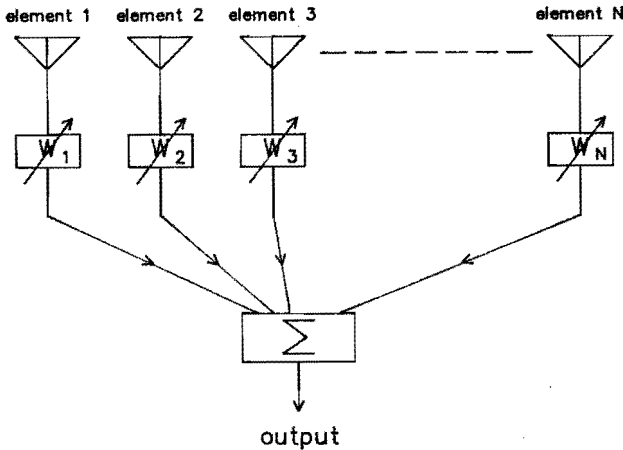


Fig. 5.7. Phased array. The output signal is a complex weighting of N individual signals from the array elements.

### 5.3. Reduction of transhorizon interference in satellite earth stations

In sec. 5.2, various interference-reduction techniques have been presented. The choice of a technique in a specific interference situation depends on numerous factors. In the present section, methods for the reduction of transhorizon interference (from terrestrial stations) into a satellite earth station are studied. This interference situation has been discussed earlier (sec. 2.2.4) and is illustrated in fig. 5.8.

Suppose that the transmitting satellite station and the interfering terrestrial station are given and cannot be changed – a common operational limitation. If a *new* earth station is planned, the options of choosing an optimum antenna and receiver are available and should definitely be considered. For such considerations, interference-prediction models (see chapter 4) are essential. However, if interference

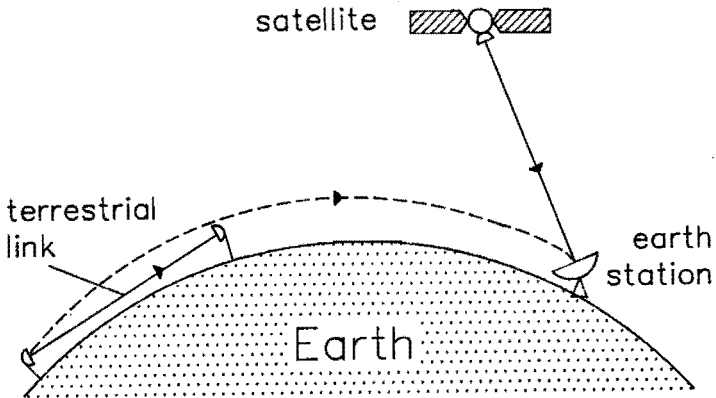


Fig. 5.8. Transhorizon interference from a terrestrial station into an earth station. ——— wanted links; - - - unwanted link.

is to be reduced in an *existing* earth station, replacement of the existing equipment may be too expensive, and other solutions should be sought.

The latter case is examined here in more detail. Survey of the interference-reduction techniques in sec. 5.2 reveals that in this case only the following techniques deserve consideration:

- i) site shielding (see sec. 5.2.3);
- ii) interference cancellation by auxiliary feeds (sec. 5.2.5, item (ii));
- iii) interference cancellation by auxiliary antennas (sec. 5.2.5, item (iii)).

The preferred choice among these options depends, *inter alia*, on the characteristics of the interfering signal(s). The most important characteristics are:

- the angle of arrival (relative to the main beam);
- the bandwidth;
- the rate of change, i.e., the short-term temporal behaviour;
- the number of interference sources which are active (either at the same time or at different times).

The relevance of the angle of arrival is obvious. Bandwidth limitations exist in all cancellation techniques. The rate of change may be a limiting factor in *adaptive* cancellation techniques: too rapid signal fluctuations (in amplitude or phase) may prevent proper adaptation. Such rapid signal fluctuations occur in troposcatter and — especially — hydrometeor-scatter interference, as mentioned in sec. 3.3. Finally, the number of interference sources is also a limiting factor in interference cancellation, because for each interfering source a corresponding reference signal is required. The auxiliary-antenna method is, in this respect, more flexible than the auxiliary-feed method, as the latter is geometrically fixed and cannot adapt to a changing interference geometry unless several auxiliary feeds with an adaptive network are employed [32].

These interfering-signal properties limit the applicability of the three types of interference-reduction techniques (i)–(iii), as summarized in table 5.1. It can be seen from this table that site shielding has only one principle limitation: the interference should arrive at relatively large angles off-axis. This is normally the case for clear-air interference into earth terminals; therefore, site shielding is a powerful means of combatting this type of interference, especially if the number of potential interfering sources is large. Interference cancellation has more limitations, but is especially attractive if interference from a few, relatively strong sources is suffered.

The exact limitations of interference-cancellation techniques are not yet known and are currently intensive research topics [41–44]. The comparison in table 5.1 is therefore only of a qualitative nature.

TECHNIQUES	Interference-reduction techniques		Site shielding	Interferometric cancellation	
				Aux. feed	Aux. antenna
REDUCTION	Interference-reduction feasible (dB)		10 - 40	5 - 15	25 - 50
INTERFERENCE	Angle rel. to boresight	zero small large	- - +	- + -	- - +
	Bandwidth	small large	+ +	+ -	+ -
	Rate of change	small medium large	+ + +	+ + -	+ - -
	Number of sources	few, fixed few, moving many	+ + +	+ - -	+ + -

Table 5.1. Qualitative comparison of the interference-reduction techniques.

" - ": application impossible, " + ": application possible.

#### 5.4. Application of interference cancellation for the protection of cable networks against radio pirates

Interference cancellation by an auxiliary antenna (sec. 5.2.5, item (iii)) is well suited for the protection of cable television (CATV) distribution networks against interference from unauthorized broadcasting by so-called "ether pirates". A detailed study on this application in the event of FM radio pirates has been carried out and published earlier [45]. This publication is reproduced here to illustrate the engineering approach involved in designing a canceller for a given interference scenario.



**R**elaying of radio and TV broadcast programs by cable networks is a much-used technique for improving the local reception conditions in urban and suburban areas. Community receive stations at the cable head-end allow both a wider range of offered programs and a better reception quality than is technically or economically feasible for individual households. These advantages have already resulted in very high national CATV subscription percentages in some Western European countries, as well as ambitious plans for cabling in other countries.

At present, more than 70 percent of all Belgian and Dutch households are connected to local cable networks, many of whom offer 10 to 15 TV channels and 7 to 12 FM (stereo) channels received off the air from domestic and foreign broadcast organizations. Some of the world's largest private broadcast cable networks are operating in this part of Europe. For example, the Amsterdam cable operator KTA has more than 340,000 subscribers.

However, a parallel development in Europe during the last decade has been an explosive increase in the number of unauthorized broadcasters, so-called "ether pirates." Without having obtained official frequency assignments, they engage in radio transmitting activities and thus willfully infringe the Broadcasting Act, Telecommunications Regulations or Copyright Laws in force in a particular country. As a consequence, it is necessary to conduct such pirate transmissions in a clandestine way; this is greatly facilitated by the availability and low cost of high-power VHF components, audio and video equipment, and remote-control technology.

Typical motives for broadcast piracy in Western Europe appear to range from "freedom-of-expression" partisanship (often addressed against the official public broadcast systems), over rather freakish technical interests, to mere commercial enterprise. Evident sponsorship of such illegal TV and radio transmissions, say by advertising, cannot be prosecuted under some European penal codes, unless the sponsor has been caught red-handed during a financial transaction with the actual violator of the radio spectrum. Such legal difficulties and modern technology have provided a more than adequate soil for a steady growth of pirate business over the last 10 years in many European nations.

Obviously, this trend toward more disorderly use of the broadcast bands threatens not only the functions of public broadcast stations, but also those of the private cable networks. These must now often operate in severe interference conditions unforeseen during their design five or ten years ago. Moreover, official direction-finding and confiscation of the pirate stations will be concentrated against disturbances of the national public services (including most of the air broadcasters in Europe) and against threats to public safety or national security, whereas the successful operation of private cable companies may not enjoy a similar official priority. Thus, a local cable operator may find little effective support from the authorities if his subscribers complain about degraded reception of their desired channels—or if copyright owners hold him legally responsible for unintentional relaying of pirate transmissions to thousands of households, perhaps never intended

## Interference Protection of Cable Networks Against Radio Pirates

Peter M. J. Scheeren  
Jens C. Ambak

The problem of radio-frequency interference from unauthorized transmitters into the cable distribution networks used for community reception of public broadcasts in densely populated areas in Western Europe is discussed

to be reached by the clandestine transmitter in the first place! In several ensuing civil court cases in the Netherlands, judges have tended to rule that the cable operator can be held responsible for the (type and quality of) services offered in his contract; he cannot invoke an act of God, where only ether pirates are at play.

This novel social and legal situation in turn results in a new technical problem—can (community) reception of radio-frequency broadcasts be protected adequately from interference by clandestine ether pirates operating in the same frequency band? We shall review this interference problem and discuss a possible technical remedy in this article. In so doing, we leave aside both the possibility of changing the legal and regulatory environment to be less conducive to ether piracy, as well as the possible ultimate technical solution: an international broadband (optical-fiber) telecommunications network extending immune audio and video connections to all (fixed) subscribers. The European Economic Community (EEC) is studying such a future network in its RACE program.

The next section outlines the dynamic RF interference environment created by typical ether pirates. The related interference management problem is different from that encountered in classical frequency sharing between different radio services (for example, satellite and terrestrial microwave links) and provided for by the ITU Radio Regulations [1], because a pirate is not very cooperative in his choice of technical parameters. Yet the pirate problem cannot be analyzed as a zero-sum game of electronic warfare between (military) adversaries, who ultimately may attempt everything in their power to maximize damage to each other. In fact, the collective activity of individual ether pirates is characterized by a social "pecking order," which favors mutual separation in space, time, or frequency) of strong competitors for broadcast spectrum.

The section titled "Technical Means of Protection Against RF Interference" discusses the generic technical means of protection against the strong isolated radio interference entries resulting from such an environment of "pecking" pirates. The section titled "Adaptive Interference Canceller for the FM Broadcasting Band" describes the principle of an adaptive interference canceller developed for the FM broadcast band (88-108 MHz), while the section titled "A Practical Reference Antenna for the Adaptive Interference Canceller" outlines the design of an antenna improving the adaptation to dynamic developments in the pirate environment. The resulting performance of the total interference

cancellation system is analyzed and evaluated in "Overall System Performance."

## Characteristics of a Pirate Scenario

### The Dutch History

To illustrate the relevant features of broadcast piracy, we shall briefly outline the recent developments in the Netherlands. Table I shows the number of confiscated FM and TV transmitters, nationwide and in Amsterdam, during 1975-1984.

TV pirates were mainly active in the early 1980s. Most of them cannot mount sufficient transmit power to cover a significant part of a city like Amsterdam, and so exploited the existing cable networks for distribution of their programs by targeting their clandestine transmissions into the community antennas. (This also reduced the risk of being spotted by RF direction finding, relative to omnidirectional broadcasting). In most cases, this practice was confined to vacant TV channels in metropolitan cable networks, probably for want of sufficient power to suppress the public broadcast transmissions or to avoid annoying their audiences. However, late-night pirate shows after closing hours of the public TV stations attracted a considerable cable audience, especially with all kinds of popular and "blue" movies infringing Dutch laws of copyright or public decency. In this period, electric power stations noted an unexpected extra load late at night when the TV pirates were most active, at times indicating that more than 10 percent of the cable subscribers were still watching. However, in May 1982, a government decree forced Dutch CATV network operators to switch off their channels in the absence of authorized broadcasts, and so most TV pirates disappeared.

The occurrence of (FM) radio pirates survived this official intervention. These ether pirates generally have sufficient transmit power to cover considerable areas without the need for a cable network as an intermediary. Table II shows the distribution of "useful" ranges of typical illegal FM ether transmitters in the Netherlands, derived from an interesting study of piracy for the Dutch Government Policy Council [2].

The activities of FM pirates obviously may cause harmful interference to the proper reception of authorized broadcasts, in particular for the more distant domestic and foreign public programs. These often cannot be received satisfactorily without the advanced receiving capabilities of a cable network. Thus, the local FM

TABLE I  
CONFISCATIONS OF ILLEGAL BROADCAST TRANSMITTERS IN THE NETHERLANDS 1975-1984 (Courtesy: Dutch PTT).

Type of confiscation	Year										
	1975	76	77	78	79	80	81	82	83	84	
FM transmitters											
-nationwide	264	517	688	954	1168	1398	2178	2735	2326	2225	
-Amsterdam	36	60	70	24	85	42	89	86	80	225	
TV transmitters											
-nationwide							75	55	31	16	
-Amsterdam							8	5	—	—	

TABLE II  
RADIUS OF COVERAGE AREA OF ILLEGAL FM TRANSMITTERS,  
FROM [2].

Range (km)	Percentage of pirate stations
<11	36
11-15	14
16-20	13
21-35	9
26-50	19
51-100	7
>100	2

pirates tend to disturb precisely those radio stations for which the cable network was intended to provide the greatest advantages. Hence, a large number of complaints are being lodged about FM ether pirates, both directly by the general public and by cable subscribers and operators.

During 1982-1984, the annual number of *successful* complaints in the city of Amsterdam has continuously exceeded hundred cases of FM-pirate interference. There is no decreasing trend, which suggests that official action does not terminate the activities of an FM pirate, but only forces him to seek new transmit locations from time to time, to avoid (or following) confiscation of his FM transmitters.

### Operational Characteristics of FM Pirate Transmissions

The dynamic interference environment caused by FM pirates is confirmed by Table III, which shows the short operational "lifetime" of illegal FM transmitters in the Netherlands [2]. Obviously, the daily and weekly fluctuations of FM pirate activities add to the complexity of the interference environment in which Dutch cable networks now have to operate. Table IV shows the diurnal variations of the transmit activity.

From Table II-IV, it is evident that technical means of interference protection must be extremely flexible and adaptable, in order to cope with the great variety and variability of FM pirate signals. It should be noted, however, that the strongest and most professional (commercial) pirate transmissions far exceed the great majority of illegal stations, both in radiated power and permanence. Their emissions are normally located in slots of the radio spectrum with little competition from

TABLE III  
LENGTH OF OPERATIONAL PERIOD OF ILLEGAL  
FM TRANSMITTERS, FROM [2].

Time that transmitter has been operational (years)	Percentage of pirate stations
<½	40
½-1	27
1-2	19
2-3	9
3-4	3
>4	2

TABLE IV  
DAILY DISTRIBUTIONS OF FM PIRATE TRANSMISSION, FROM [2].

Time of day	Percentage of transmitters active		
	Working days	Week-end	Total
0-8 hrs	6	5	6
9-11 hrs	11	19	14
12-14 hrs	9	24	15
15-17 hrs	18	19	18
18-21 hrs	40	24	34
22-24 hrs	16	9	13
	100	100	100

nearby high-powered public broadcast stations; also, they tend to avoid permanent interference with each other (probably to protect their business). Less professional FM pirates may be up to 30 or 40 dB weaker upon reception and spread more evenly all over the FM spectrum; also they tend not to worry too much about using the internationally agreed FM-parameters (peak deviation 75 kHz, RF bandwidth 210 kHz). In contrast, the dominant professional pirates will continuously attempt to select all transmission parameters such as to optimize reception quality for their audience. This includes proper deviation, stereo transmission, and avoidance of interference from stronger local transmitters.

In practice, this behavior of FM pirates results in a dynamic interference scenario in which the strong FM pirates continue to organize themselves more or less in accordance with the CCIR frequency raster all over the band 88-108 MHz, thereby avoiding both strong official assignments and the competition from even more dominant pirates. Although this natural pecking order may not be adhered to by the majority of (weak) FM pirates, their numbers and inferior transmit powers will allow modeling of the resulting interferences as a more or less uniform background of Gaussian noise. In contrast, the frequency assignments of official public broadcasts may be disturbed by two strong adjacent-channel pirate interferers, one on either side of the official assignment. Weaker (that is distant) public broadcasts may, in addition, be completely overlapped by one co-channel pirate interferer. Although the latter is normally received through a sidelobe of the community antenna, its receiver input level can be 20 to 30 dB above that of the distant desired broadcast signal received through the mainlobe.

It should be realized that the resulting scenario is essentially different from the interference situations postulated in most studies of electronic counter-counter measures (ECCM) for radio networks. In particular, the popular FM pirates seldom attempt to "jam" the cable network deliberately or to broadcast by targeting only on the community antenna. This is so, because the majority of their audience is not receiving FM radio via cable subscriptions, but use portable or car radio receivers. We denote the few weak FM pirates who may be attempting to broadcast via the cable "first class" interferers; the majority will be "second class" interferers, that is, not specially targeted against the cable network.

## Technical Means of Protection Against RF Interference

### General Discussion

Consider the interference scenario with one interferer sketched in Fig. 1. In general, adequate protection of the wanted radio channel against RF-interference from an unwanted source requires a minimum value of the signal-to-interference ratio at the output of the receiver:

$$\frac{P_w}{P_i} = \frac{G_R(O)}{G_R(\theta)} \frac{L_i}{L_w} \frac{EIRP_w}{EIRP_i} G_{proc} \cong \left(\frac{P_w}{P_i}\right)_{min} \quad (1)$$

- where:  $P$  is the signal power at the receiver input;  
 $G_R(\theta)$  is the receiver antenna gain at the angle  $\theta$  off boresight;  
 $L$  is the path loss between transmitter and receiver;  
 $EIRP$  is the equivalently isotropically radiated power;  
 $G_{proc}$  is the process gain, defined by the receiver improvement of the signal-to-interference ratio,

and the subscripts  $w$  and  $i$  denote wanted and interfering signals, respectively.

Technical means of protection of radio channels are based on enhancing the protection ratio  $P_w/P_i$ . Equation (1) shows that the increase of any of the following factors improves the interference immunity of the wanted channel:

- **Antenna discrimination:**  $G_R(O)/G_R(\theta)$ .  
The receiving antenna acts as a spatial filter and may therefore discriminate between wanted and interfering signals, provided that these signals arrive from different directions ( $\theta \neq 0$ ). In addition, the antenna may discriminate between signals with different polarizations.
- **Propagation control:**  $L_i/L_w$ .  
The path loss  $L_i$  of the unwanted signal can be increased by the introduction of obstacles on the propagation path in order to cause extra diffraction losses. This possibility, known as site shielding, is often inherently available in urban areas.
- **Superior transmitting stations:**  $EIRP_w/EIRP_i$ .  
A brute-force method of suppressing interference effects in one's own system is simply to avail oneself

of extra equivalent radiated power, by increasing either the output power of the transmitter or the transmitting antenna gain. This is a common countermeasure in military electronic warfare, which, however, can soon lead to escalations from an adversary ("power battle").

- **Signal processing:**  $G_{proc}$ .  
Often, signal processing will be the most effective and flexible technique for improving the system protection ratio. Processing can be carried out before, during, or after the demodulation process, depending on the system that has been adopted at the transmitter side. Examples are spread spectrum techniques [3], energy disposal [4], and error-correcting codes [5]. In all events, signal processing is required on both the transmitter and the receiver side.

### Traditional Technical Means of Protection Against FM Interference

A CATV network operator, exploring the technical possibilities to protect his network against RF interference from FM pirates, has only control of the receiver side of the radio channel. He cannot change the properties of the broadcast stations. Therefore, the latter two techniques mentioned in the section titled "General Discussion" are inapplicable in this situation. Furthermore, he experiences the problem that typical pirates transmit from various, unpredictable locations with variable powers and times on-air. This makes systematic shielding by buildings unreliable, and increases the difficulty of protection by antenna discrimination.

Apart from simply switching off the CATV network (thereby not only preventing FM pirates to reach the subscribers, but of course also making the distribution of authorized programs impossible), most CATV network operators have only the principle of diversity as a defense against FM pirates. One possibility could be frequency diversity: switching to another broadcast transmitter when the original frequency is suffering from interference. However, this will generally mean a degradation of the wanted signal quality, if the frequency choice for a desired program was optimum without pirates.

On the other hand, site diversity has proven to be a useful principle to avoid interference from FM pirates. Here, a second antenna, situated on a "secret" spot elsewhere in the city, is used for the reception of the wanted signals when the normal reception is made impossible. This system works well against pirates of the "first class" (see the section "Operational Characteristics of FM Pirate Transmission"), who use directional antennas to radiate directly into the CATV antenna. However, FM pirates of the "second class" use omnidirectional antennas and stronger transmitters, in order to broadcast to most parts of the city (see Table II), and as a consequence will often disturb both CATV antennas simultaneously. Only if the second antenna is more than, say, 50 km away from the city, it may be beyond the reach of the strongest broadcasting FM pirates in the city. It is useful to position this second antenna closer to the desired broadcast stations to improve the signal quality. At present, however, carrying legal broadcasts from

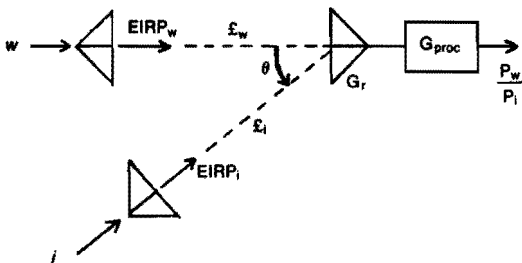


Fig. 1. General interference scenario (with one interferer),  $w$  = wanted signal,  $i$  = interfering signal.

outside the municipal boundaries via relay needs a special permission from the Dutch authorities, because the PTT carrier monopoly is involved.

### Interference Cancellers

Recently, new technical means of protection have been developed. Originally, these were employed for protection of military or diplomatic communications against deliberate disturbance by an opponent, but are increasingly being applied outside the government to raise the efficiency of spectrum usage. These techniques, known as interference cancellation, are able to discriminate and eliminate an interfering signal from the wanted signal.

The basic principle is shown in Fig. 2. An auxiliary antenna, pointed toward the interfering source is used as a "reference" antenna to obtain a copy of the interference received by the main antenna. After complex weighting (in amplitude and phase), the signal from the reference antenna is subtracted from the main antenna signal in such a way that the interference is eliminated. Such a static interference canceller is applicable whenever the direction of the interfering source is known and fixed, and different from the direction of the wanted source. Static systems are simple and cheap and are in use by many U.S. CATV network operators for nulling out local broadcast stations. In the USA, these are generally situated on fixed and known locations, since low-power commercial FM is an authorized mode of operation in American states.

Because of the far more chaotic receiving situation in the Netherlands, where the (unauthorized) interference is continuously changing, a Dutch CATV operator would need an automatically controlled version of such an interference canceller, unless he is willing to spend a lot of manpower in continuous manual control. The principle of such an adaptive interference canceller is shown in Fig. 3. Here, the complex weighting is

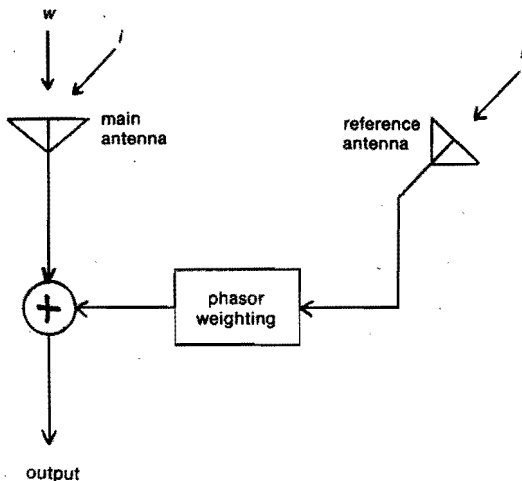


Fig. 2. Principle of interference canceller,  $w$  = wanted signal,  $i$  = interfering signal.

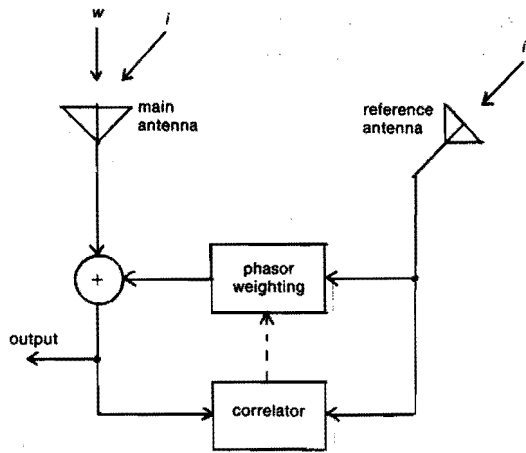


Fig. 3. Principle of adaptive interference canceller,  $w$  = wanted signal,  $i$  = interfering signal.

controlled by the output of a correlator, which compares the output signal of the system and the reference signal. The correlator adjusts the phasor modulator in such a way that the correlation between the input signals of the correlator is minimized, which is the case when there is no interference present in the output (provided that the reference antenna receives a "clean" interfering signal).

Such an adaptive interference canceller can suppress unwanted signals up to about 50 dB, according to a CCIR Report [6] and an earlier application by the British Post Office [7]. In the following sections, the design and performance of a relatively cheap adaptive interference cancellation system, suited for protection of a Dutch CATV receiving station, will be described.

### Adaptive Interference Canceller for the FM Broadcasting Band

#### Design

The design of the adaptive interference canceller was based on the cancellation system built by the British Post Office [7]; its block diagram is given by CCIR [6], see Fig. 4. For an interference canceller to be used for protection of a Dutch CATV receiving station, changes to this basic system are necessary to cope with the great variations in the interference environment, and to obtain a low-cost design. The block diagram of the modified design is shown in Fig. 5 [8]. The heart of the system is the complex phasor modulator (CPM), a commercially available electronic device that controls the RF input signal, both in amplitude and in phase, dependent on two DC control signals. These control signals are derived by correlating both quadrature components of the reference signal with the output signal, by means of two synchronous detectors. The output signals of these detectors are integrated and then fed into the control inputs of the CPM. An automatic gain control (AGC) is used to guarantee a constant level of the reference signal at the inputs of the detectors. The IF bandpass filters are

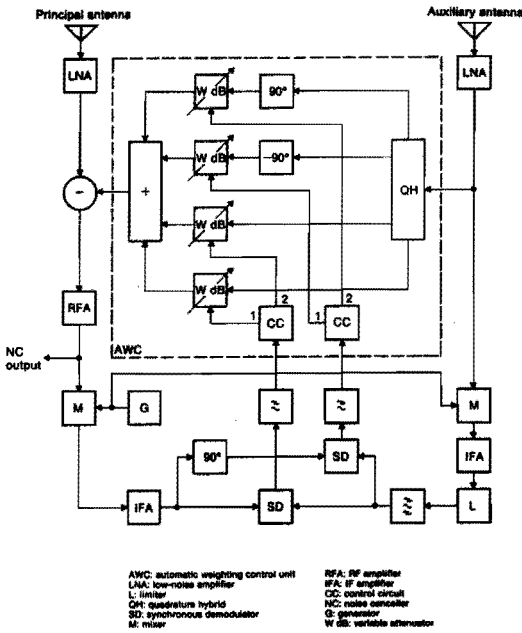


Fig. 4. Block diagram of basic adaptive interference canceller, from [6].

is dependent on the signal-to-noise ratios of the two input signals to be processed by the canceller.

Figure 7 shows a typical result at baseband. For simplicity, the wanted signal is in this case an unmodulated carrier, while the unwanted signal is FM modulated on exactly the same RF frequency (95.0 MHz), with a power level at the output exceeding the wanted signal power by 16.5 dB in the absence of the canceller. In this case the process gain is almost 50 dB, as determined by the crosstalk components of the demodulated carrier.

In general, the process gain of the system will drop when the reference signal is not quite "clean" (that is contains some wanted signal), because of correlation with the wanted signal. This justifies a search for a very selective reference antenna, which is the subject of the next section.

### A Practical Reference Antenna for the Adaptive Interference Canceller

The design of a reference antenna for the interference canceller, useful for protection of a Dutch CATV receiving station against interference from FM pirates,

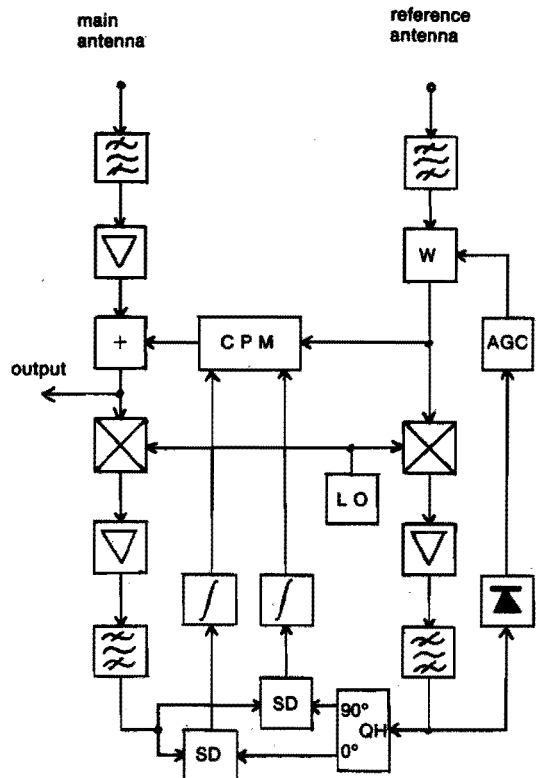


Fig. 5. Block diagram of modified interference canceller, from [8]. CPM: complex phasor modulator, SD: synchronous detector, AGC: automatic gain control, QH: quadrature hybrid, LO: local oscillator.

needed to define the channel to be protected; this can be varied by adjusting the local oscillator. The RF bandpass filters protect the broadband amplifiers against saturation by signals outside the frequency band to be protected. These filters must be changed or retuned whenever the local oscillator frequency is changed.

### Realized Canceller Performance

A breadboard version of the described design has been realized, in which RF bandpass filters have been omitted and the control signals for the CPM are directly derived from the RF signals. Because of the resulting absence of selectivity in the reference branch, for measuring purposes the interfering signal should be supplied artificially by an FM-modulated generator instead of an auxiliary antenna. The wanted signal can be supplied either by another FM modulator or directly by means of a suitable antenna and any desired broadcasting transmitter. The dynamic range of the AGC (which determines the dynamic range of the whole system) is limited to 45 dB, which is sufficient to cope with the variety of interference levels met in practice (see the section titled "Operational Characteristics of FM Pirate Transmissions.")

Figure 6 shows a typical result of the measurements. Without the canceller, the interference is 16.2 dB stronger than the wanted signal. The system suppresses the interference 39.7 dB in this case. As will be shown in the section "Overall System Performance," the suppression

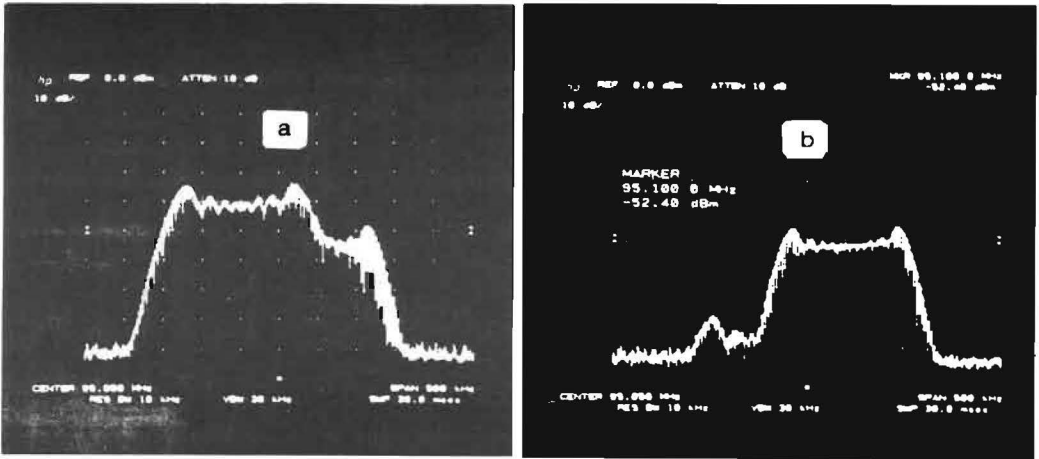


Fig. 6. Signal spectrum; FM interference at the left, wanted FM signal at the right. a) Signal spectrum at main antenna input. b) Signal spectrum at the output of the canceller. The original copy of this figure was not available at the time of printing. We apologize for the degraded quality of this image.

should be based on two principles. Because of the unpredictability and variety of the interference sources, the reference antenna should be sensitive in all horizontal directions. As an exception, however, the antenna should not receive any signals from the boresight direction of the main antenna, because the canceller needs a clean reference signal to be correlated with the output signal. The ideal radiation pattern of the reference antenna is therefore a circular symmetric pattern, with a very sharp null in the direction of the wanted signal. To realize this minimum, the directivity of the main antenna can be exploited: Subtract a suitable fraction of the main antenna signal from the output signal of an "omnidirectional" antenna, in such a way that the wanted signal

is eliminated in the combined output, see Fig. 8. The required 180° phase shift is most easily achieved by interchanging the connecting wires of the auxiliary antenna, provided that the path lengths from both antennas to the summing network are equal.

For calculations to demonstrate the resulting pattern, a typical CATV VHF antenna pattern for an array of eight Yagi-antennas has been used. The radiation pattern is shown in Fig. 9. For the auxiliary antenna a hypothetical antenna with a horizontally circular-symmetric radiation pattern has been assumed. This can be realized approximately by two crossed dipole antennas.

Figure 10 shows some radiation patterns for a reference antenna achieved in this way. It can be seen that the null in the main direction can be made very narrow, by positioning the auxiliary antenna at a suitable spacing  $d$  from the main antenna in the same (horizontal) plane.

## Overall System Performance

### Theory

The system performance that can be achieved with the described interference canceller, in combination with the reference antenna system set out in Section 5, can be calculated using the theory of adaptive array antennas [9].

Referring to Fig. 11, we can derive formulas for the signal to interference-plus-noise ratios that will be reached with or without the use of the cancellation system. These formulas are (see Appendix):

$$(SINR)_{\text{unprotected}} = (SNR)_0 \frac{1}{1 + \gamma_2 g_1^2(\theta)} \quad (2)$$

$$(SINR)_{\text{protected}} = (SNR)_0 \frac{1 + \gamma_2 g_2^2(\theta)}{1 + \gamma_2 g_1^2(\theta) + \gamma_2 g_2^2(\theta)} \quad (3)$$

where:  $g_1(\theta)$  is the voltage gain of the main antenna in the direction  $\theta$ ;

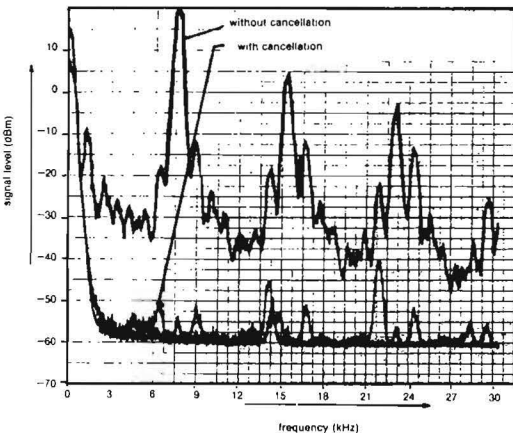
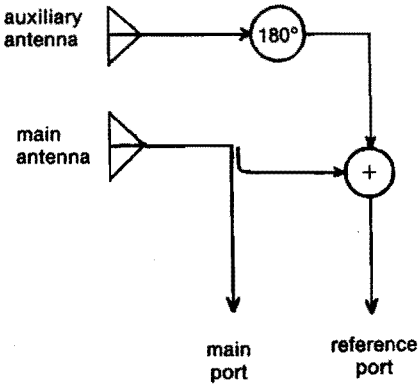
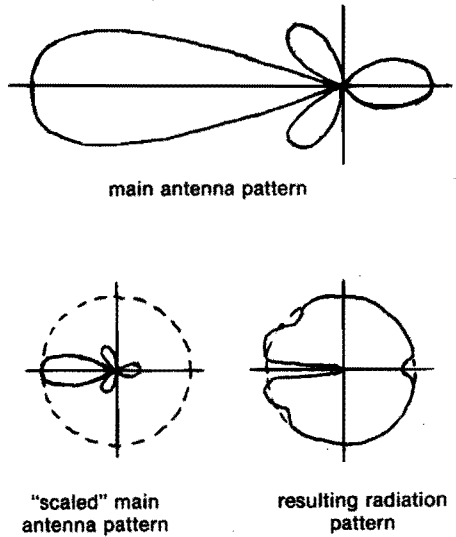


Fig. 7. Baseband spectra of unprotected and protected unmodulated carrier, due to crosstalk from a co-channel FM pirate. The original copy of this figure was not available at the time of printing. We apologize for the degraded quality of this image.



(a)



(b)

Fig. 8. Design of a reference antenna for the adaptive interference canceller. a) principle. b) antenna patterns.

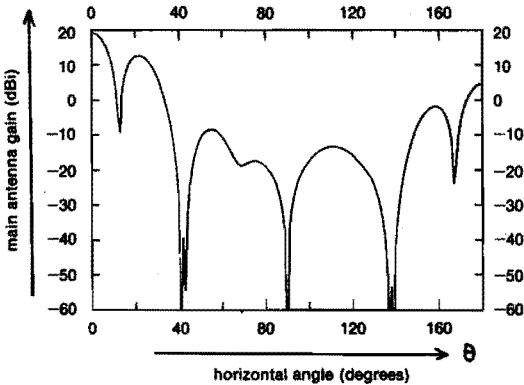


Fig. 9. Main antenna radiation pattern (horizontal plane).

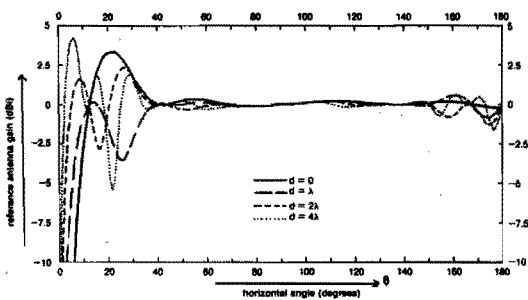


Fig. 10. Reference antenna radiation pattern for different spacings  $d$  between main and auxiliary antenna.

$g_2(\theta)$  is the voltage gain of the reference antenna in the direction  $\theta$ ;  
 $\gamma_1, \gamma_2$  are the signal-to-noise ratios of unwanted and interfering signals, respectively;  
 $(SNR)_0 = \gamma_1 g_1^2(0)$  is the signal-to-noise ratio at the output in the absence of interference;  
 SINR is the signal to interference-plus-noise ratio.

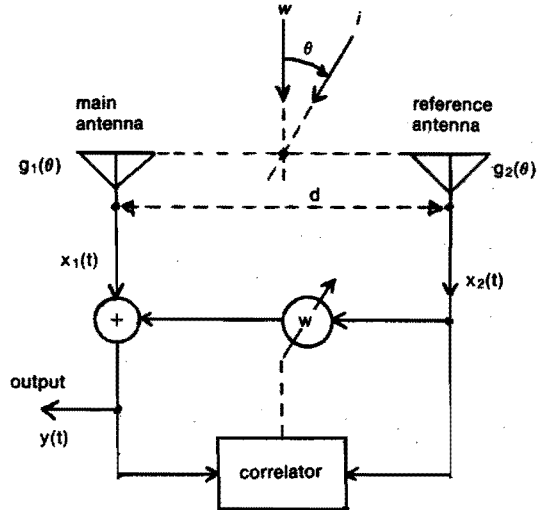


Fig. 11. Adaptive interference canceller using an ideal reference antenna.



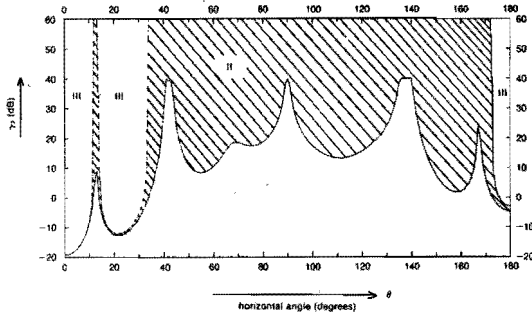


Fig. 12. Mapping of characteristics of FM pirates causing a SINR-degradation in the wanted signal of less than 3 dB. (Signal-to-noise ratio of wanted signal:  $\gamma_1 = 21$  dB)  
 I: Range of pirate signals without protection by the canceller  
 II: Range of pirate signals with protection by the canceller  
 III: Range of unacceptable pirate signals, that is, those causing more than 3 dB degradation of SINR.  
 (In practice the upper boundary of region II will be limited by the dynamic range of the A.G.C.)

For high interference-to-noise ratios ( $\gamma_2 \gg 1$ ), the SINR for the protected system becomes independent of the interference level:

$$SINR_{\text{protected}} \cong (SNR)_o \frac{1}{1 + g^2(\theta)/g^2(\theta)} \quad (4)$$

From (2) and (3), the overall improvement in the SINR, afforded by the entire cancellation system, is easily calculated.

Results

Using (2) and (3), the influence of pirates can be "mapped" according to their incident angles and powers. This is shown in Fig. 12 for a realistic situation, using the main antenna and reference antenna (with spacing  $d = 0$ ) described in the section "A Practice Reference Antenna for the Adaptive Interference Canceller" and choosing a 3 dB degradation in the SINR as the limit for acceptable operation in the presence of a dominant pirate signal. It has been assumed that the noise level is completely determined by man-made noise, resulting in an antenna noise figure of 22 dB at FM-band (88-108 MHz) in a city like Amsterdam, according to CCIR [10]. Figure 12 shows that if a degradation of 3 dB in the SINR can be accepted, the majority of FM pirate

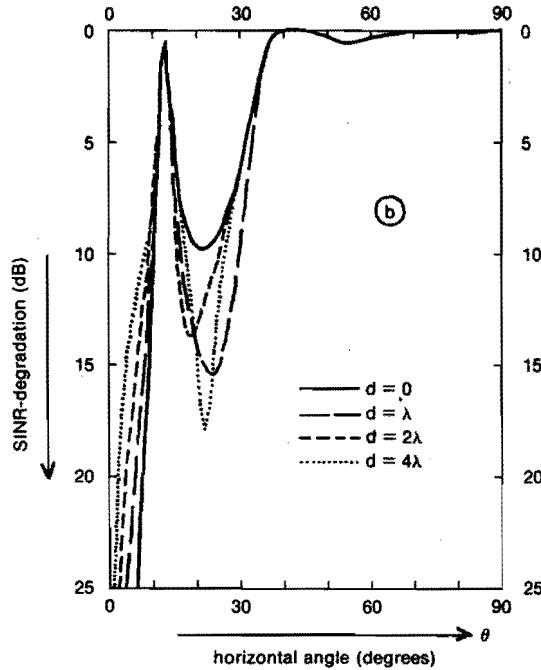
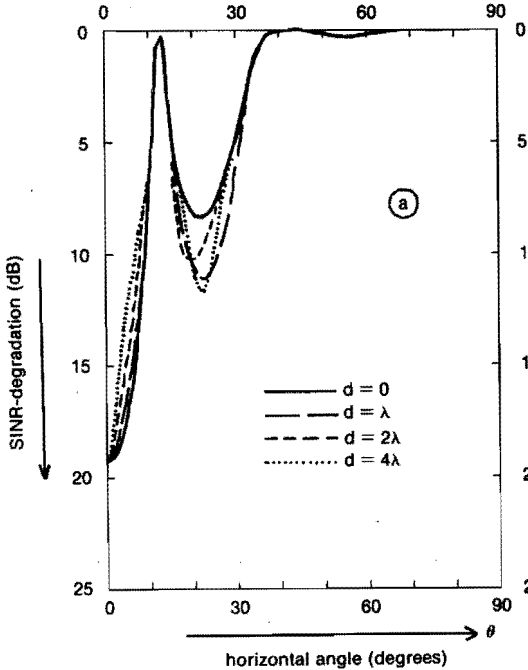


Fig. 13. SINR-degradation as a function of incident angle of interference, for different spacings  $d$  between main and auxiliary antenna. Signal-to-noise ratio of wanted signal:  $\gamma_1 = 21$  dB. Signal-to-noise ratio of interfering signal:  
 a:  $\gamma_2 = 0$  dB  
 b:  $\gamma_2 \cong 20$  dB

broadcasts encountered in practice will be suppressed by the interference canceller, except for pirate signals incident in the main lobe, the first sidelobe, and the back-lobe of the main antenna.

Figure 13 shows the SINR-degradation as a function of the incident angle of the interference, for different reference antenna configurations (that is, different horizontal spacings  $d$ ), assuming fixed values of the interference power. It can be seen that the range of incident angles in which the pirate signals will be suppressed can be enlarged by increasing the distance  $d$  between main and auxiliary antenna, at the cost of a reduction of the performance in the first sidelobe. Accepting a maximum SINR-degradation of 18 dB at this single spot gives the possibility to protect the system against harmful interference from an FM pirate in all other directions, except in a very narrow sector (a few degrees) around the main direction.

### Conclusions

An adaptive interference canceller, suitable for suppression of FM pirate signals in Dutch CATV networks, has been designed, realized, and evaluated. This canceller is able to suppress an interfering signal by about 50 dB. The canceller requires a reference antenna providing a "clean" pirate signal. An ideal reference antenna can be approached by use of a combination of the existing CATV antenna and an antenna with a horizontally circular symmetric radiation pattern. Using this reference antenna, the cancellation system turns out to be able to suppress the majority of pirate signals encountered in practice so that reasonably good reception of the desired authorized FM broadcasts can be maintained in the exigent operational conditions of an urban Dutch CATV network.

### Acknowledgments

The authors wish to express their gratitude to Mr. S.H.L. Herman of the Frequency Management Authority of the Netherlands PTT for making available official information about Dutch pirate activity.

Furthermore, they like to thank Eric F.C.J.M. Tijssen, who developed and measured the breadboard cancellation system, Ger W.P.M. Bakker and Jean-Paul M.G. Linartz, who contributed to the system calculations, and Ms. Doret Pellegrino for her patience in typing the manuscript.

### Appendix

Referring to the symbols in Fig. 11, we can write the following expressions for the antenna output signals  $x_1(t)$  and  $x_2(t)$ :

$$\begin{aligned} x_1(t) &= g_1(\theta) w(t) + g_1(\theta) i(t) e^{-ju} + n_1(t) \\ x_2(t) &= g_2(\theta) w(t) + g_2(\theta) i(t) e^{+ju} + n_2(t) \end{aligned} \quad (A.1)$$

where

$$u = \frac{\Delta}{\lambda} \pi d \sin \theta.$$

The noise components  $n_1(t)$  and  $n_2(t)$  are assumed to be uncorrelated and are representing white additive Gaussian noise, with the same noise power in both antennas:

$$|\overline{n_1^2}| = |\overline{n_2^2}| = |\overline{n^2}| \quad (A.2)$$

The signal-to-noise ratios of both input signals are:

$$\begin{aligned} \gamma_1 &= \frac{\Delta}{|\overline{n^2}|} |\overline{w^2}| / |\overline{n^2}| \\ \gamma_2 &= \frac{\Delta}{|\overline{n^2}|} |\overline{i^2}| / |\overline{n^2}| \end{aligned} \quad (A.3)$$

The output signal  $y(t)$  can be written as:

$$y(t) = x_1(t) + W x_2(t) \quad (A.4)$$

The complex weighting factor  $W$  is adjusted in such a way that the correlation between  $y(t)$  and  $x_2(t)$  is minimized. From (A.4) it follows that the "steady-state" value of  $W$  will then be:

$$W = - \frac{E[x_1 x_2^*]}{E[|x_2|^2]} \quad (A.5)$$

where  $E$  denotes the expectation value and the asterisk denotes the complex conjugate.

From these formulas, the powers of the wanted signal ( $P_w$ ), the interfering signal ( $P_i$ ), and the noise ( $P_n$ ) in the output signal  $y(t)$  can be calculated. For an ideal reference antenna ( $g_2(\theta) = 0$ ) the results are:

$$P_w = |\overline{w^2}| g_1^2(\theta) \quad (A.6)$$

$$P_i = |\overline{i^2}| g_1^2(\theta) \left[ \frac{1}{(1+g_1^2(\theta)\gamma_2^2)} \right] \quad (A.7)$$

$$P_n = |\overline{n^2}| \frac{(1+g_1^2(\theta)\gamma_2^2) + g_1^2(\theta)g_2^2(\theta)\gamma_2^2}{(1+g_1^2(\theta)\gamma_2^2)} \quad (A.8)$$

From (A.6), (A.7) and (A.8) the SINR follows from:

$$\text{SINR}_{\text{protected}} = \frac{\Delta}{P_i + P_n} P_w$$

The result is (3).

Without the cancellation system, the output powers follow from (A.6), (A.7) and (A.8) by taking  $g_2(\theta) = 0$ . The result for the unprotected SINR is then given by (2).

### References

- [1] I.T.U., *Radio Regulations*, Geneva, 1982.
- [2] *Etherpirates in the Netherlands*, Study performed by Intomart B.V., The Hague: Netherlands Government Publ., 1982. W.R.R. (Netherlands Government Policy Council): Preparatory studies and backgrounds of Media policy, M6. ISBN 90-12-04001-9 (in Dutch).
- [3] R. C. Dixon, *Spread Spectrum Techniques*, IEEE Press, New York, 1976.
- [4] CCIR, Plenary Assembly, "Energy dispersal in the fixed-satellite service," Rep. 384-4, vol. IX-1, Geneva, 1982.
- [5] F. J. Mac Williams, and N. J. A. Sloane, *The Theory of Error-Correcting Codes*, North-Holland, 1978.
- [6] CCIR, Plenary Assembly, "Use of interference cancellers in order to increase spectrum usage," Rep. 830, Vol. I, Geneva, 1982.
- [7] N. White, et al. "The application of interference cancellation to an earth station," *IEE Conf. Publ.*, 126, Sat. Comm. Syst. Techn., pp. 233-238, 1975.

- [8] E. F. C. J. M. Tijssen, "Realization of an interference suppressor for the FM broadcast band," Master's thesis, Eindhoven University of Technology, Dept. of Electrical Engineering, Oct. 1984 (in Dutch).
- [9] R. A. Monzingo and T. W. Miller, *Introduction to Adaptive Arrays*, John Wiley & Sons, 1980.
- [10] CCIR, Plenary Assembly, "Man-made radio noise," Rep. 258-4, vol. VI, Geneva, 1982.

**Jens Arnbak** held a chair of telecommunications at Eindhoven University of Technology, The Netherlands.

He worked on international integrated services networks for the North Atlantic Treaty Organization in the 1970s. Since 1982, he has participated in various telecommunication policy studies commissioned by the Dutch Government, including committees dealing with computer and communications crime, and with the structure and status of the Netherlands PTT. He has published numerous papers on electromagnetic wave propagation, satellite communication systems and packet radio. He advised the Amsterdam Court of Justice on the feasibility of technical protection of CATV networks against pirate interference.

Since May 1986, he is professor of tele-information systems at Delft University of Technology, the Netherlands. ■

**Peter Scheeren** received the M.S. degree in Electrical Engineering from the Eindhoven University of Technology, Eindhoven, The Netherlands, in 1981. Since 1984 he is working at the same Institute in the field of radio frequency interference in telecommunication networks.

Note: The following corrections to the foregoing paper are pointed out:

On page 10:

- Formula (1) should read:

$$\frac{P_w}{P_i} = \frac{G_R(0) L_i}{G_R(\theta) L_w} \frac{EIRP_w}{EIRP_i} G_{proc} \geq \left[ \frac{P_w}{P_i} \right]_{min}$$

where the subscript "min" means minimum acceptable.

- Line 27, first column, should read:

• *Antenna discrimination:*  $G_R(0)/G_R(\theta)$ .

- Line 31, first column: replace " $\theta \neq 0$ " by " $\theta \neq 0$ " ( $\theta$  not equal to zero).
- Line 14, second column: replace "disposal" by "dispersal".

On page 15: line 13, second column: "Practice" should be "Practical".

## 5.5. References

- [1] COST 210 Management Committee, "COST 210 activities to model trans-horizon cochannel interference paths in Europe", Proc. Int. Conf. Ant. Prop. (ICAP), *IEE Conf. Publ.*, no. 274, pp. 352-354, 1987.
- [2] A.B. Carlson, "*Communication Systems*", 3rd ed., McGraw-Hill, New York, 1986.
- [3] CCIR, Plenary Assembly, "Reference earth-station radiation pattern for use in coordination and interference assessment in the frequency range from 2 to about 30 GHz", *Recommendations and Reports of the CCIR*, vol. IV-1, Rec. 465-2, Geneva, 1986.
- [4] CCIR, Plenary Assembly, "Radiation diagrams for use as design objectives for antennas of earth stations operating with geostationary satellites", *Recommendations and Reports of the CCIR*, vol. IV-1, Rec. 580-1, Geneva, 1986.
- [5] A.B. Harris, B. Claydon and K.M. Keen, "Reducing the sidelobes of earth-station antennas", *Conf. Rcd. ICC*, Boston, vol. I, pp. 6.6.1-6.6.5, 1979.
- [6] P.J. Wood, "*Reflector antenna analysis and design*", Peter Peregrinus, London, 1980.
- [7] CCIR, Plenary Assembly, "Earth-station antennas for the fixed-satellite service", *Recommendations and Reports of the CCIR*, vol. IV-1, Rep. 390-5, Geneva, 1986.
- [8] G. Schindler, "Reduction of sidelobe level by improved strut design for low F/D Cassegrain antennas", *Electr. Letters*, vol. 21, no. 5, pp. 203-204, 1985.
- [9] R. Mittra, W.A. Imbriale and E.J. Maanders, ed., "*Satellite communication antenna technology*", North-Holland, Amsterdam, 1983.

- [10] J.M. Janky, B.B. Lusignan, L.S. Lee, E. Chong Ha and E.F. Reinhart, "New sidelobe envelopes for small aperture earth stations", *IEEE Trans. Broadcast.*, vol. BC-22, no. 2, pp. 39-44, 1976.
- [11] R.G. Gould and C. Schmidt, "Interference-reduction techniques for satellite earth stations", *IEEE EMC Conf.*, Montreux, pp. 285-292, 1977.
- [12] J.B. Hagen, "Communication techniques in radio physics and astronomy", *IEEE Comm. Magaz.*, vol. 24, no. 10, pp. 16-20, 1986.
- [13] G.H. Hagn, M.G. Keenen and H.A. Turner, "Pit shielding for communication satellite ground-terminal antennas", *IEEE Trans. Electromagn. Comp.*, vol. EMC-7, no. 2, pp. 93-103, 1965.
- [14] E.F. Lucia, Jr., "Artificial site shielding for communications satellite earth stations", *IEEE Trans. Aerospace & Electr. Syst.*, vol. AES-6, no 5, pp. 612-619, 1970.
- [15] CCIR, Plenary Assembly, "Influence of terrain irregularities and vegetation on tropospheric propagation", *Recommendations and Reports of the CCIR*, vol. V-1, Rep. 236-6, Geneva, 1986.
- [16] J. Ruze, F.I. Sheftman and D.A. Cahlander, "Radar ground-clutter shields", *Proc. IEEE*, vol. 54, no. 9, pp. 1171-1183, 1966.
- [17] J. van Rees, "Measurements of impulse response of a wideband radio channel at 910 MHz from a moving vehicle", *Electr. Letters*, vol. 22, no. 5, pp. 246-247, 1986.
- [18] CCIR, Plenary Assembly, "Propagation data required for terrestrial broadcasting in the frequency bands above 10 GHz", *Recommendations and Reports of the CCIR*, vol. V, Rep, 562-2, Geneva, 1986.
- [19] CCIR, Plenary Assembly, "Use of special screens to improve interference immunity in radio links", *Recommendations and Reports of the CCIR*, vol. I, Rep. 831, Geneva, 1986.

- [20] K. Feher, *"Digital modulation techniques in an interference environment"*, Don White Cons. Inc., Germantown, 1977.
- [21] Z.D. Stojanović, M.L. Dukić and I.S. Stojanović, "A new demodulation method improving FM system interference immunity", *IEEE Trans. Comm.*, vol. COM-29, no. 7, pp. 1001-1011, 1981.
- [22] M.J. Wilmot and L.L. Campbell, "Signal detection in the presence of cochannel interference and noise", *IEEE Trans. Comm.*, vol. COM-20, no. 6, pp. 1153-1198, 1972.
- [23] J. Goldman, "Detection in the presence of spherically symmetric random vectors", *IEEE Trans. Inf. Th.*, vol. IT-22, no. 1, pp. 52-59, 1976.
- [24] R. Dixon, *"Spread spectrum techniques"*, IEEE Press, New York, 1976.
- [25] CCIR, Plenary Assembly, "Energy dispersal in the fixed-satellite service", *Recommendations and Reports of the CCIR*, vol. IV-1, Rep. 384-5, Geneva, 1986.
- [26] A.J. Viterbi and J.K. Omura, *"Principles of digital communication and coding"*, McGraw-Hill, Tokyo, 1979.
- [27] G.R. Welti and R.K. Kwan, "Comparison of signal processing techniques for satellite telephony", *Conf. Rcd. NTC*, pp. 05.1.1-05.1.6, 1977.
- [28] F.J. MacWilliams, *"The theory of error-correcting codes"*, North-Holland, Amsterdam, 1977.
- [29] B.A. Pontano, "Methods of interference cancellation for improved orbit and spectrum utilization", *Conf. Rcd. NTC*, pp. 33.4.1-33.4.5, Houston, 1980.
- [30] W.F. Williams, "Reduction of near-in sidelobes using phase reversal aperture rings", *JPL Quarterly Technical Review*, vol. 1, no. 4, pp. 34-42, 1972.
- [31] J. Arnbak, M.H.A.J. Herben and R.A.C.M. van Spaendonk, "Interference rejection by auxiliary feeds in Cassegrain earth terminals", *Agard Conf.*

- Proc.*, no. 332, pp. 38.1-38.11, 1982. See also: "Improved orbit utilization using auxiliary feeds in existing earth terminals", *Space Comm. Broadcast.*, no. 1, pp. 405-416, 1983.
- [32] M.L. Burrows, "Closer spacing of geostationary satellites through adaptive nulling at the ground terminal", *IEEE Trans. Ant. Prop.*, vol. AP-35, no. 7, pp. 870-873, 1987.
- [33] CCIR, Plenary Assembly, "Use of the interference cancellers in order to increase spectrum usage", *Recommendations and Reports of the CCIR*, vol. I, Rep. 830-1, Geneva, 1986.
- [34] CCIR, Plenary Assembly, "A survey of interference cancellers for application in the fixed-satellite service", *Recommendations and Reports of the CCIR*, vol. IV-1, Rep. 875, Geneva, 1986.
- [35] N. White, D. Brandwood and G. Raymond, "The application of interference cancellation to an earth station", *Int. Conf. Sat. Comm. Syst. Techn.*, *IEE Conf. Publ.*, no. 126, pp. 233-238, 1975.
- [36] P.D. Lubell and F.D. Rebhun, "Suppression of co-channel interference with adaptive cancellation devices at communications satellite earth stations", *Conf. Rcd. ICC*, vol. 3, pp. 49.3.284-49.3.289, 1977.
- [37] T. Kaitsuka and T. Inoue, "Interference cancellation system for satellite communication earth station", *IEEE Trans. Comm.*, vol. COM-32, no. 7, pp. 796-803, 1984.
- [38] P.T. Lam, S.W. Lee, K.C. Lang and D.C.D. Chang, "Sidelobe reduction of a parabolic reflector with auxiliary reflectors", *IEEE Trans. Ant. Prop.*, vol. AP-35, no. 12, pp. 1367-1374, 1987.
- [39] R.A. Monzingo and T.W. Miller, "*Introduction to adaptive arrays*", John Wiley, New York, 1980.

- [40] M.I. Skolnik, *"Introduction to radar systems"*, McGraw-Hill, New York, 1980.
- [41] C.H.M. Clemens and M.H.A.J. Herben, "Bandwidth and propagation limitations in antenna sidelobe suppression systems for satellite communications", *Conf. Rcd. ICC*, pp. 345-350, 1984.
- [42] R.H. Ott and R.B. Dybdal, "The effects of reflector antenna diffraction on the interference cancellation performance of coherent sidelobe cancellers", *IEEE Trans. Ant. Prop.*, vol. AP-34, no. 3, pp. 432-439, 1986.
- [43] R.B. Dybdal and R.H. Ott, "Time-compensated adaptive interference cancellation", *Conf. Rcd. IEEE-AP Symp.*, paper AP02-8, pp. 74-77, Blacksburg, 1987.
- [44] P.M.J. Scheeren, "Interference reduction techniques", *XXIInd General Assembly of URSI*, session F2, paper 2, Tel Aviv, 1987.
- [45] P.M.J. Scheeren and J.C. Arnbak, "Interference protection of cable networks against radio pirates", *IEEE Comm. Magaz.*, vol. 25, no. 4, pp. 7-17, 1987.





## 6. OBSTACLE DIFFRACTION

### 6.1. Introduction

It has been suggested in chapter 5 that site shielding can be an effective means to reduce transhorizon interference into a receiving earth station. The term site shielding has been restricted to the screening by an obstacle located in the vicinity of the earth-station antenna. The performance of a given obstacle in a specific situation is quantified by the site-shielding factor (SSF), which has been defined in sec. 5.2.3 as the ratio of the received powers in the absence and presence of the obstacle, respectively. The SSF of an opaque obstacle is determined mainly by diffraction at the edge(s) of the obstacle. In this and the next chapter, we intend to model the site-shielding problem, in order to predict the SSF in a given situation.

The site-shielding problem is, in fact, the problem of diffraction by an obstacle in the near-field region of an earth-station antenna. Rayleigh's far-field criterion [1, sec. 5.3.1] is generally employed to separate the near-field and far-field regions of an antenna. The Rayleigh distance of an antenna with diameter  $D$  is given by  $R=D^2/2\lambda$ . At distances  $r>4R$  (the far-field region), the radiation of the antenna can be described by the far-field antenna-gain pattern  $G(\psi,\varphi)$  in a spherical  $(r,\psi,\varphi)$  coordinate system with origin in the antenna phase centre; in other words, the antenna can be treated as a point source. In the near-field region of the antenna ( $r<4R$ ), this procedure is invalid.

For the site-shielding problem, this implies that the obstacle diffraction and the reception by the earth-station antenna cannot be treated independently. Therefore, these aspects are investigated together in chapter 7. However, it is useful to first study the isolated obstacle-diffraction problem (assuming the antenna to be a point

source), as a basis for the analysis of the complete site-shielding problem of chapter 7. This obstacle-diffraction problem is the subject of the present chapter.

### 6.2. Knife-edge diffraction model

Obstacle diffraction of an electromagnetic wave is frequently modelled by the well-known *knife-edge diffraction model*. In this two-dimensional model the obstacle is a perfectly conducting half-plane with its edge perpendicular to the propagation direction of the incident wave. Influences of the ground and of the atmosphere are neglected. These assumptions imply rather gross simplifications of a realistic situation, as discussed in more detail in sec. 6.7.

A cross-section of the knife-edge model is shown in fig. 6.1. The obstacle coincides with the half-plane  $x=0, z \leq z_0$ . The observation point P is described by its Cartesian coordinates  $(x,z)$ , or equivalently by its polar coordinates  $(r,\theta)$ , given by

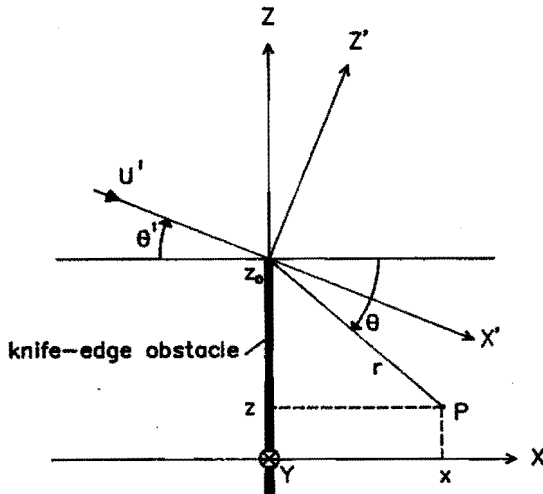


Fig. 6.1. Cross-section of the knife-edge model. The obstacle is located at  $x=0, z \leq z_0$ ; P is the observation point,  $U^i$  is the incident field.

$$r = \sqrt{x^2 + (z_0 - z)^2}, \quad \theta = \arctan[(z_0 - z)/x]. \quad (6.1)$$

The incident electromagnetic field is usually modelled either as a spherical wave (if the location of its source is known) or as a plane wave (if the source is located far away). In the latter case, the amplitude is constant in the transverse direction, corresponding to a uniform plane wave.

If the incident field results from transhorizon propagation (see chapters 3 and 4), then the incident wavefront is of a more complicated form, which depends on the mechanism that is responsible for the transhorizon propagation. To a first approximation, the incident wavefront can be taken as planar, with small phase disturbances superimposed on it. The amplitude is, in general, not constant in the transverse direction. Therefore, a suitable model for the incident field is a plane wave, propagating in the  $x'$ -direction (which makes an angle  $\theta^i$  with the positive  $x$ -axis), with an amplitude that is non-uniform in the transverse  $z'$ -direction. Mathematically, this incident field is expressed as (see fig. 6.1),

$$\text{for E-polarization (TE-waves):} \quad \vec{E}^i = E_y^i \hat{e}_y = E_0(z') \exp(-jk_0 x') \hat{e}_y; \quad (6.2a)$$

$$\text{for H-polarization (TM-waves):} \quad \vec{H}^i = H_y^i \hat{e}_y = H_0(z') \exp(-jk_0 x') \hat{e}_y. \quad (6.2b)$$

Here  $\vec{E}^i$  and  $\vec{H}^i$  are the incident electric and magnetic fields, respectively, with amplitude functions  $E_0(z')$  and  $H_0(z')$ . The time factor  $\exp(j\omega t)$  is tacitly assumed. The magnetic field in the TE case and the electric field in the TM case readily follow from Maxwell's equations. Note that by treating the two polarizations separately, the two-dimensional electromagnetic diffraction problem is reduced to two scalar diffraction problems. This procedure is well known in two-dimensional wave-propagation problems [2, sec. 11.4.1]. The two polarizations can be studied simultaneously by introducing the general field variable  $U$ , where  $U = E_y$  for

TE-waves and  $U=H_y$  for TM-waves. Then, the incident field  $U^i$  is given by

$$U^i(x,z) = U_0(z') \exp(-jk_0 x') . \tag{6.3}$$

### 6.3. Notations and symbols

Before concentrating on the diffraction problem, we introduce some notations and symbols from [3], to be used later on; see fig. 6.2.

The unit vectors  $\hat{k}^i$ ,  $\hat{k}^r$  and  $\hat{k}^d$  denote the direction of propagation of the incident, reflected and diffracted fields, respectively. The angles  $\psi^i$  and  $\psi^r$  are defined as follows:  $|\psi^{i,r}|$  is the angle of rotation around the edge that brings  $\hat{k}^{i,r}$  onto  $\hat{k}^d$  without crossing the obstacle; the angle  $\psi^i$  ( $\psi^r$ ) is negative for an observation point in the lit region and positive for an observation point in the shadow region of the incident (or reflected) field. It is seen from fig. 6.2. that

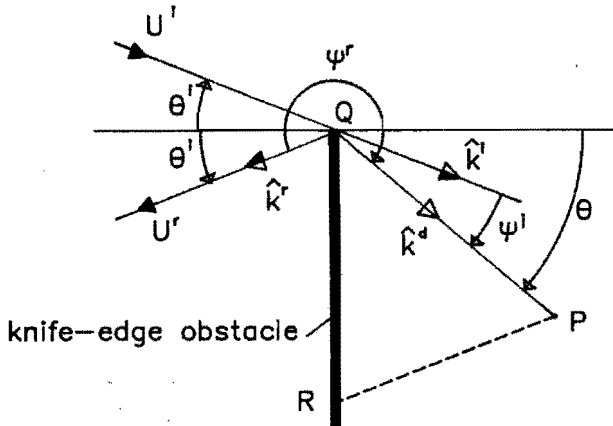


Fig. 6.2. Definition of the unit vectors  $\hat{k}^i$ ,  $\hat{k}^r$  and  $\hat{k}^d$ , and of the angles  $\psi^i$  and  $\psi^r$ . The shadow zones of  $U^i$  and  $U^r$  are indicated by the darkened halves of the arrows of  $\hat{k}^i$  and  $\hat{k}^r$ .

$$\psi^i = \theta - \theta', \quad \psi^r = \pi + \theta + \theta'. \quad (6.4)$$

The *detour parameter*  $\xi^i$  (or  $\xi^r$ ) of the incident (or reflected) field is defined as

$$\xi^{i,r} = \sqrt{2k_0 r} \sin\left(\frac{1}{2}\psi^{i,r}\right). \quad (6.5)$$

Physically,  $(\xi^{i,r})^2$  is interpreted as the difference between the phase along the diffracted ray and the phase along the incident (or reflected) ray through the observation point. The sign of  $\xi^{i,r}$  (like the sign of  $\psi^{i,r}$ ) serves as a "shadow indicator" for the incident (or reflected) field.

We denote the incident field by  $U^i$ , the reflected field by  $U^r$ , and the total field by  $U$ . The fields  $U^i$  and  $U^r$  are defined everywhere in space, not only in the lit regions. By using (6.4), the incident field  $U^i(P)$  at  $P$  can be written from (6.3) as

$$U^i(P) = U_0(P) \exp(-jk_0 r \cos \psi^i). \quad (6.6)$$

The reflected field  $U^r(P)$  is found to be

$$U^r(P) = \mp U_0(R) \exp(-jk_0 r \cos \psi^r), \quad (6.7)$$

where  $R$  is the reflection point corresponding to  $P$  (fig. 6.2), and the upper and lower signs hold for the TE case and the TM case, respectively. The geometrical-optics field  $U^g$  can be represented by

$$U^g(P) = \Theta(-\xi^i)U^i(P) + \Theta(-\xi^r)U^r(P), \quad (6.8)$$

where  $\Theta(\xi)$  is the unit step function, defined by  $\Theta(\xi)=1$  for  $\xi>0$ ,  $\Theta(\xi)=0$  for  $\xi<0$ .

The symmetry between  $U^i$  and  $U^r$  in (6.8) is typical and is emphasized by shortly writing

$$U^g(P) = \Theta(-\xi^i)U^i(P) + \{i \rightarrow r\}, \quad (6.9)$$

where  $\{i \rightarrow r\}$  means repeating all terms after the equality sign with the superscript "i" changed into "r".

Finally, we introduce the three functions  $F(\xi)$ ,  $\bar{F}(\xi)$  and  $\check{F}(\xi)$ , which show up frequently in diffraction theory. The Fresnel integral  $F$  is defined by

$$F(\xi) = \pi^{-1/2} \exp(j\pi/4) \int_{\xi}^{\infty} \exp(-jt^2) dt. \quad (6.10)$$

From [4, sec. 7.3] we deduce the two-term series expansion for  $|\xi| \ll 1$ ,

$$F(\xi) = \frac{1}{2} - \pi^{-1/2} \exp(j\pi/4) \xi + O(\xi^3), \quad |\xi| \rightarrow 0, \quad (6.11)$$

and the asymptotic expansion for  $|\xi| \gg 1$ ,

$$F(\xi) = \Theta(-\xi) + \bar{F}(\xi) + \check{F}(\xi) + O(\xi^{-5}), \quad |\xi| \rightarrow \infty. \quad (6.12)$$

Here we have introduced the functions  $\bar{F}$  and  $\check{F}$ , defined by

$$\bar{F}(\xi) = \pi^{-1/2} \exp(j\pi/4) \exp(-j\xi^2)/2j\xi, \quad (6.13a)$$

$$\check{F}(\xi) = \pi^{-1/2} \exp(j\pi/4) \exp(-j\xi^2)/4\xi^3. \quad (6.13b)$$

#### 6.4. Review of knife-edge diffraction of a uniform plane wave

For a uniform plane wave with constant amplitude  $U_0$ , the incident field follows from (6.6) as

$$U^i(x,z) = U_0 \exp(-jk_0 r \cos \psi^i). \quad (6.14)$$

Several well-known solutions of the corresponding knife-edge diffraction problem exist, and these are now briefly reviewed.

##### 6.4.1. Sommerfeld's solution

The exact solution of the diffraction problem was presented almost 100 years ago by Sommerfeld [5]. His solution reads in our notation:

$$U(P) = F(\xi^i)U^i(P) + \{i \rightarrow r\}. \quad (6.15)$$

This result describes the total field at  $P$  in terms of the incident and reflected fields at  $P$ .

##### 6.4.2. Kirchhoff's approximation

Prior to Sommerfeld's exact solution, Kirchhoff developed an approximate theory for the solution of three-dimensional diffraction problems. For a survey of Kirchhoff's diffraction theory, which is based on the Huygens-Fresnel principle, we refer to e.g. [2, sec. 8.3]. In this section the two-dimensional knife-edge diffraction problem is treated by Kirchhoff's method.



We start from the integral theorem of Helmholtz-Weber for solutions of the two-dimensional Helmholtz equation [6, chapter I, sec. 6.2], viz.

$$U(P) = \frac{-1}{4j} \int_S \left[ U(P_0) \frac{\partial}{\partial n} H_0^{(2)}(k_0 \rho) - H_0^{(2)}(k_0 \rho) \frac{\partial U(P_0)}{\partial n} \right] ds. \quad (6.16)$$

Here,  $S$  is a closed contour around the observation point  $P$  with outward normal  $\hat{n}$ ,  $P_0$  is an arbitrary point on  $S$ , and  $\rho$  is the distance between  $P$  and  $P_0$ . For  $S$  we take the contour formed by the part of the  $z$ -axis occupied by the knife-edge ( $-\infty < z \leq z_0$ ), the positive  $z'$ -axis, and a circular arc of radius  $R$  in the half plane  $x > 0$  (fig. 6.3). The contribution of the latter part to the integral in (6.16) can be argued to vanish as  $R \rightarrow \infty$  [2, sec. 8.3]. Along the remaining two parts we approximate  $U(P_0)$  by Kirchhoff's boundary values, i.e., we replace  $U$  and  $\partial U / \partial n$  by zero on the  $z$ -axis (the shadow side of the knife edge), and by  $U^i$  and  $\partial U^i / \partial n$  on the positive  $z'$ -axis. With this Kirchhoff approximation, (6.16) reduces to

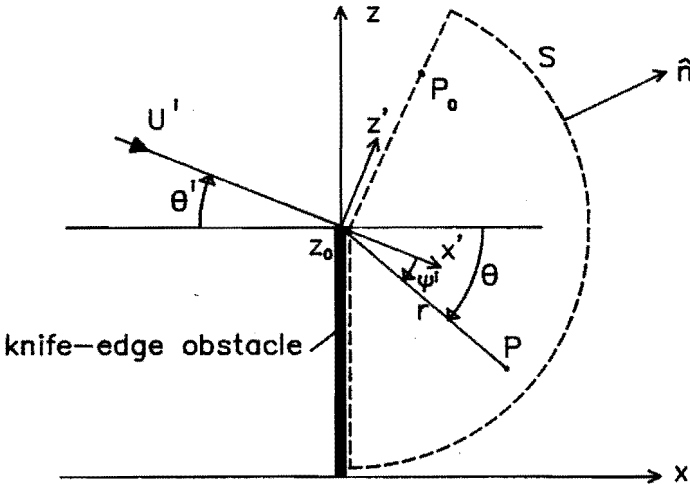


Fig. 6.3. Derivation of Kirchhoff's approximation.

$$U_K(P) = \frac{1}{4j} \int_0^{\infty} \left[ U^i(0, \zeta) \frac{\partial}{\partial x'} H_0^{(2)}(k_0 \rho) - H_0^{(2)}(k_0 \rho) \frac{\partial}{\partial x'} U^i(0, \zeta) \right] d\zeta, \quad (6.17)$$

where the subscript K refers to the Kirchhoff approximation, and the  $z'$ -coordinate of a point  $P_0$  on the  $z'$ -axis has been denoted by  $\zeta$ . The integral in (6.17) can be simplified if  $k_0 r \gg 1$  and  $\psi^i \ll 1$ . To this end we utilize the approximations

$$\begin{aligned} \rho &= \sqrt{x'^2 + (z' - \zeta)^2} = \sqrt{r^2 + \zeta^2 + 2\zeta r \sin \psi^i} \\ &\approx r + 2\zeta \sin(\frac{1}{2}\psi^i) + \frac{\zeta^2}{2r} = r \cos \psi^i + \frac{1}{2r} (2r \sin(\frac{1}{2}\psi^i) + \zeta)^2, \end{aligned} \quad (6.18a)$$

$$H_0^{(2)}(k_0 \rho) \approx \sqrt{\frac{2}{\pi k_0 \rho}} \exp[-j(k_0 \rho - \pi/4)]. \quad (6.18b)$$

We point out that only the vicinity of the end point  $\zeta=0$  contributes significantly to the integral in (6.17). Hence, by use of (6.18) we can approximate (6.17) by

$$\begin{aligned} U_K(P) &= (k_0/4) U_0 \int_0^{\infty} (1+x'/\rho) \sqrt{2/\pi k_0 \rho} \exp[-j(k_0 \rho - \pi/4)] d\zeta \approx \sqrt{k_0/2\pi} \cdot \\ &\cdot \exp(j\pi/4) U_0 \exp(-jk_0 r \cos \psi^i) \int_0^{\infty} \exp\left[-j(k_0/2r)(2r \sin(\frac{1}{2}\psi^i)^2 + \zeta)^2\right] d\zeta, \end{aligned} \quad (6.19)$$

where the additional approximation  $x'/\rho \approx x'/r = \cos \psi^i \approx 1$  has been used. With (6.5), (6.10) and (6.14) we obtain finally

$$U_K(P) = F(\xi^i) U^i(P), \quad (6.20)$$

valid for high frequencies ( $k_0 r \gg 1$ ) and small diffraction angles ( $\psi^i \ll 1$ ). This result

differs from the exact solution only in that the second term in (6.15) is absent here. Under the assumptions made, this term may indeed be neglected.

#### 6.4.3. CCIR formula

In CCIR Report 715-2 [7] a formula for the SSF of a knife-edge obstacle is given, which is based on the Kirchhoff approximation (6.20). Introduce the parameter  $v$  [7] as

$$v = \sqrt{2/\pi} \xi^i = 2 \sqrt{2\tau/\lambda} \sin\left(\frac{1}{2} \psi^i\right). \quad (6.21)$$

Then, the SSF based on (6.20) is given by

$$\text{SSF} = -20 \log |U_K(P)/U^i(P)| = -20 \log |F(\sqrt{\pi/2} v)| \quad (\text{dB}). \quad (6.22)$$

For small values of  $v$  ( $|v| \ll 1$ ), the series expansion (6.11) of the Fresnel integral in (6.22) yields

$$\text{SSF} \approx -20 \log \left| \frac{1}{2} - \frac{1+j}{2} v \right| \approx 20 \log [2(1+v)] \quad (\text{dB}), \quad (6.23)$$

whereas for large positive values of  $v$  ( $v \gg 1$ ), the asymptotic expansion (6.12) of the Fresnel integral yields

$$\text{SSF} \approx -20 \log |\tilde{F}(\sqrt{\pi/2} v)| = 20 \log (\sqrt{2\pi} v) \quad (\text{dB}). \quad (6.24)$$

Both (6.23) and (6.24) are now approximated (somewhat arbitrarily) by

$$\text{SSF} \approx 20 \log \left[ 2.1 \left[ \sqrt{v^2 + 1} + v \right] \right] = 6.4 + 20 \log \left[ \sqrt{v^2 + 1} + v \right] \quad (\text{dB}), \quad (6.25)$$

which is the CCIR formula [7]. The difference between (6.25) and (6.22) is less than 0.5 dB for all  $v > -1$ . For  $v \leq -1$ , the SSF approaches 0 dB (i.e., no influence of the obstacle).

Like the Kirchhoff approximation, the CCIR formula is only valid for small diffraction angles  $\psi^i$ . In [7], an upper limit of  $\psi^i = 12^\circ$  is indicated.

#### 6.4.4. Keller's GTD

Keller's *geometrical theory of diffraction* (GTD) [8] is an extension of geometrical optics which accounts for diffraction. In addition to incident and reflected rays, GTD introduces diffracted rays which are produced whenever an incident ray hits an edge of the diffracting obstacle. Along a diffracted ray, the field varies according to the laws of geometrical optics. The initial value of the diffracted field is obtained by multiplying the incident field at the edge by an appropriate diffraction coefficient.

The application of GTD to the two-dimensional knife-edge diffraction problem is well known, see [8]. The field at P is represented by

$$U(P) = U^g(P) + U^d(P), \quad (6.26)$$

where  $U^g$  is the geometrical-optics field introduced in (6.8) and  $U^d$  is the diffracted field given by

$$U^d(P) = D^i U^i(Q) \exp(-jk_0 r) / \sqrt{r} + \{i - r\}. \quad (6.27)$$

Here,  $U^{i,r}(Q)$  is the incident (reflected) field at the diffraction point  $Q$  (see fig. 6.2), while in our notation the diffraction coefficients  $D^{i,r}$  can be expressed as

$$D^{i,r} = \exp(-j\pi/4) / [\sqrt{8\pi k_0} \sin(\frac{1}{2}\psi^{i,r})] . \quad (6.28)$$

By use of (6.5) and (6.13a), the result (6.27) can be rewritten as

$$U^d(P) = \tilde{F}(\xi^i) U^i(Q) \exp(-jk_0 r \cos \psi^i) + \{i \rightarrow r\} . \quad (6.29)$$

In the case of uniform plane-wave incidence, one has  $U^{i,r}(Q) \exp(-jk_0 r \cos \psi^{i,r}) = U^{i,r}(P)$  in view of (6.14). Thus the GTD solution (6.26) equals the asymptotic expansion (up to order  $k_0^{-1/2}$ ) of the exact solution (6.15).

#### 6.4.5. Uniform theories of edge diffraction

The GTD result (6.29) becomes invalid when the observation point  $P$  is close to or on the shadow boundaries of the incident and reflected fields (where  $\xi^i=0$  and  $\xi^r=0$ , respectively). This shortcoming has been removed in two uniform theories of edge diffraction: the "*uniform geometrical theory of diffraction*" (UTD) [9,10], and the "*uniform asymptotic theory of diffraction*" (UAT) [11-13]. Both theories yield high-frequency asymptotic solutions of the edge-diffraction problem that are uniformly valid in the entire space including the transition regions around the shadow boundaries.

According to UTD, the field at a point  $P$  is represented by

$$U(P) = U^g(P) + U^D(P) , \quad (6.30)$$

where  $U^G$  is the geometrical-optics field and  $U^D$  is a modification of Keller's diffracted field  $U^d$ ; cf. (6.26). For the two-dimensional knife-edge diffraction problem, it is found from [9] that  $U^D$  is given by

$$U^D(P) = F_{KP}((\xi^i)^2) D^i U^i(Q) \exp(-jk_0 r) / \sqrt{r} + \{i \rightarrow r\}, \quad (6.31)$$

with the transition function  $F_{KP}$  defined by (cf. [9, eq. (26)])

$$F_{KP}(\xi^2) = F(|\xi|) / \tilde{F}(|\xi|). \quad (6.32)$$

The transition function  $F_{KP}$  makes the diffracted field finite but discontinuous at the shadow boundaries; this discontinuity precisely compensates the discontinuity of the geometrical-optics field  $U^G$ . Away from the shadow boundaries (i.e., where  $|\xi| \gg 1$ ),  $F_{KP}(\xi^2)$  approaches unity and  $U^D$  reduces to Keller's diffracted field  $U^d$ . The diffracted field  $U^D$  can be written in a form similar to (6.29), namely,

$$U^D(P) = F_{KP}((\xi^i)^2) \tilde{F}(\xi^i) U^i(Q) \exp(-jk_0 r \cos \psi^i) + \{i \rightarrow r\}, \quad (6.33a)$$

or, equivalently, by use of (6.32),

$$U^D(P) = [F(\xi^i) - \Theta(-\xi^i)] U^i(Q) \exp(-jk_0 r \cos \psi^i) + \{i \rightarrow r\}. \quad (6.33b)$$

In the case of uniform plane-wave incidence, one has  $U^{i,r}(Q) \exp(-jk_0 r \cos \psi^{i,r}) = U^{i,r}(P)$ , hence the UTD result from (6.30) equals the exact solution (6.15).

According to UAT, the field at a point P is represented by

$$U(P) = U^G(P) + U^d(P), \quad (6.34)$$

where  $U^d$  is Keller's diffracted field and  $U^G$  is a modification of the geometrical-optics field. It is found from [12] that  $U^G$  is given by

$$U^G(P) = [F(\xi^i) - \bar{F}(\xi^i)] U^i(P) + \{i - r\} . \quad (6.35)$$

Away from the shadow boundaries (i.e., where  $|\xi| \gg 1$ ), one has  $F(\xi) - \bar{F}(\xi) = \Theta(-\xi) + O(k_0^{-3/2})$  in view of (6.12); hence,  $U^G$  reduces to the geometrical-optics field  $U^G$  and the UAT solution (6.34) becomes identical to the GTD solution (6.26). At the shadow boundaries, both  $U^G$  and  $U^d$  become infinite, in such a way that their singular parts cancel and the total field  $U$  is finite and continuous. In the case of uniform plane-wave incidence, the UAT result (6.34) equals the exact solution (6.15), as is easily verified.

## 6.5. Knife-edge diffraction of a non-uniform plane wave

### 6.5.1. Introduction

In this section we extend the knife-edge diffraction theories, presented in sec. 6.4, to the case of an incident non-uniform plane wave given by

$$U^i(x, z) = U_0(z') \exp(-jk_0 x') . \quad (6.36)$$

The amplitude function  $U_0(z')$  is related to the height-gain function (sec. 4.4) in the (transhorizon) propagation mechanism by which the incident field reaches the obstacle. It is pointed out that  $U^i$  in (6.36) satisfies the Helmholtz equation only if  $U_0(z')$  is a linear function. In that case the diffraction problem can be solved exactly (sec. 6.5.2). For a general amplitude function  $U_0(z')$ , the field  $U^i$  is an *optical field*

(in the terminology of [12]), to be interpreted as the dominant term in the high-frequency asymptotic expansion of the true incident field. Although for this case the knife-edge diffraction problem cannot be solved exactly, the Kirchhoff approximation and the high-frequency asymptotic theories (GTD/UTD/UAT) can be extended to cover the general case of non-uniform plane-wave incidence.

6.5.2. Exact solution for the linear case

Consider an incident plane wave with a linear amplitude function  $U_0(z')$ , i.e.,

$$U^i(x,z) = U_0(z') \exp(-jk_0 x') = A z' \exp(-jk_0 x') , \tag{6.37}$$

where A is constant. By use of (6.4) and fig. 6.1, the expression (6.37) is reduced to

$$U^i(P) = - A r \sin\psi^i \exp(-jk_0 r \cos\psi^i) . \tag{6.38}$$

The knife-edge diffraction problem for this incident field can be solved by a method due to Karp and Keller [14]. To this end we rewrite (6.38) as

$$U^i(P) = (A/jk_0) \frac{\partial}{\partial \theta^i} \exp(-jk_0 r \cos\psi^i) , \tag{6.39}$$

i.e.,  $U^i$  is the derivative of the uniform plane wave  $\exp(-jk_0 r \cos\psi^i)$  with respect to  $\theta^i$ . Notice that differentiation with respect to  $\theta^i$  is a linear operation. Therefore, the exact solution of the diffraction problem for the incident field (6.37) is obtained by differentiation of Sommerfeld's solution (6.15) with respect to  $\theta^i$ , viz.

$$U(P) = (A/jk_0) \frac{\partial}{\partial \theta^i} [F(\xi^i) \exp(-jk_0 r \cos\psi^i)] + \{i \rightarrow r\} . \tag{6.40}$$



On evaluating the derivative, the exact solution for the total field  $U(P)$  can be represented by

$$U(P) = [F(\xi^i) - \bar{F}(\xi^i)] U^i(P) + \{i - r\}. \quad (6.41)$$

### 6.5.3. Kirchhoff's approximation for the non-uniform case

The Kirchhoff approximation, described in sec. 6.4.2 for the case of uniform plane-wave incidence, can be applied in the non-uniform case as well. The difference with the former case is that the amplitude function  $U_0(z')$  is no longer constant and should therefore now be placed inside the approximating integral (6.19). Thus, for the non-uniform case, (6.19) becomes

$$U_K(P) = \sqrt{k_0/2\pi} \exp(j\pi/4) \exp(-jk_0 r \cos \psi^i) \cdot \int_0^{\infty} U_0(\zeta) \exp \left[ -j(k_0/2r)(2r \sin(\frac{1}{2}\psi^i) + \zeta)^2 \right] d\zeta. \quad (6.42)$$

Because only the vicinity of the end point  $\zeta=0$  contributes significantly to the integral, we expand  $U_0(\zeta)$  around  $\zeta=0$ , i.e.,

$$U_0(\zeta) = U_0(0) + \zeta U_0'(0) + O(\zeta^2). \quad (6.43)$$

Neglecting the second-order term, we insert (6.43) into (6.42); then the resulting integral can be expressed in terms of  $F(\xi^i)$  and  $\bar{F}(\xi^i)$ . Thus we obtain the Kirchhoff approximation for the total field,

$$U_K(P) = F(\xi^i)U_0(0) \exp(-jk_0 r \cos \psi^i) - [F(\xi^i) - \bar{F}(\xi^i)] r \sin \psi^i U_0'(0) \exp(-jk_0 r \cos \psi^i). \quad (6.44)$$

In the case of uniform plane-wave incidence, one has  $U_0'(0)=0$  and (6.44) reduces to the previous Kirchhoff approximation (6.20). In the case of a linear amplitude function as in (6.37), we have  $U_0(0)=0$  and only the second term in (6.44) remains. Then, by use of (6.38) the Kirchhoff approximation reduces to

$$U_K(P) = [F(\xi^i) - \bar{F}(\xi^i)] U^i(P), \quad (6.45)$$

which is identical to the first term of the exact solution (6.41). As in the uniform case, the contribution related to the reflected field is absent in the Kirchhoff approximation.

The second term in (6.44), which is proportional to the first derivative of  $U_0$  at the edge, is known as the *slope-diffraction* term. Away from the shadow boundary of the incident field (such that  $|\xi^i| \gg 1$ ), this term is of order  $k_0^{-3/2}$ , whereas the first term in (6.44) is of order  $k_0^{-1/2}$ .

#### 6.5.4. Extension of the CCIR formula to the non-uniform case

No CCIR formula for the site-shielding factor (SSF) is presently available in the case of a knife-edge that is hit by a non-uniform plane wave. However, the Kirchhoff approximation (6.44) suggests a simple extension of the CCIR formula for the uniform case as presented in sec. 6.4.3. The extended form of (6.22) reads

$$\begin{aligned} \text{SSF} &= -20 \log |U_K(P)/U^i(P)| \\ &= -20 \log |F(\sqrt{\pi/2} v)U_0(Q)/U_0(P)| \quad (\text{dB}). \end{aligned} \quad (6.46)$$

By applying the same approximations as in sec. 6.4.3, we obtain the extended CCIR formula

$$\text{SSF} = 6.4 + 20 \log \left[ \sqrt{v^2 + 1 + v} \right] - 20 \log |U_0(Q)/U_0(P)| \quad (\text{dB}). \quad (6.47)$$

The final term in (6.47) can be interpreted as (the logarithm of) the ratio of the height-gain functions for the incident field at the observation point P and at the edge point Q. Note that for simplicity the slope-diffraction term in (6.44) has been ignored, so that the formulas (6.46) and (6.47) make sense only if  $U_0(Q) \neq 0$ , or equivalently,  $U^i(Q) \neq 0$ .

#### 6.5.5. High-frequency asymptotic solutions for the non-uniform case

The high-frequency asymptotic methods introduced in secs. 6.4.4 and 6.4.5 (GTD, UTD and UAT) are readily extended to cover the knife-edge diffraction of an incident non-uniform plane wave. Especially if the incident field vanishes at the edge, higher-order terms in the high-frequency expansion of the diffracted field should be taken into account. The most important of these higher-order terms is the slope-diffraction term, which is proportional to the transverse derivative of the incident field  $U^i$  at the edge. It is recalled that UAT [11] provides a systematic procedure to successively determine all higher-order terms, although the actual evaluation of these terms is often laborious or even impractical. Such a procedure is not known in Keller's GTD and in UTD.

We now present the solution of our two-dimensional knife-edge diffraction problem with slope-diffraction terms included. Since UAT inherently includes slope diffraction, the UAT solution (6.34)-(6.35) remains unchanged for an incident non-uniform plane wave. As for GTD, James [15, sec. 5.5] has derived appropriate slope-

diffraction terms in case the incident field vanishes at the edge, i.e.,  $U^i(Q)=0$ . His derivation is based on the UAT approach [11]. He has then extended his results heuristically to obtain the UTD slope-diffraction terms. His results are summarized here in our notation, with some errors corrected [16].

If  $U^i(Q) \neq 0$ , the GTD and UTD solutions for the diffracted field are given by

$$\text{GTD: } U^d(P) = \bar{F}(\xi^i) U^i(Q) \exp(-jk_0 r \cos \psi^i) + \{i \rightarrow r\} + O(k_0^{-3/2}), \quad (6.48a)$$

$$\text{UTD: } U^D(P) = F_{\text{KP}}((\xi^i)^2) \bar{F}(\xi^i) U^i(Q) \exp(-jk_0 r \cos \psi^i) + \{i \rightarrow r\} + O(k_0^{-1}), \quad (6.48b)$$

in accordance with (6.29) and (6.33a).

If  $U^i(Q)=0$ , the GTD and UTD solutions for the diffracted field are given by [15, p. 140-141]

$$\begin{aligned} \text{GTD: } U^d(P) = \frac{1}{jk_0} \frac{\partial}{\partial \theta^i} [\bar{F}(\xi^i) \exp(-jk_0 r \cos \psi^i)] \frac{\partial}{\partial z^i} U^i(Q) \\ + \{i \rightarrow r\} + O(k_0^{-5/2}), \end{aligned} \quad (6.49a)$$

$$\begin{aligned} \text{UTD: } U^D(P) = \frac{1}{jk_0} \frac{\partial}{\partial \theta^i} [F_{\text{KP}}((\xi^i)^2) \bar{F}(\xi^i) \exp(-jk_0 r \cos \psi^i)] \frac{\partial}{\partial z^i} U^i(Q) \\ + \{i \rightarrow r\} + O(k_0^{-3/2}). \end{aligned} \quad (6.49b)$$

The slope-diffraction term in (6.49b) has also been given by Kouyoumjian and Pathak [10]. The differentiation with respect to  $\theta^i$  can be carried out to yield

$$U^D(P) = d^i \frac{\partial}{\partial z^i} U^i(Q) \exp(-jk_0 r) / \sqrt{r} + \{i \rightarrow r\} + O(k_0^{-3/2}), \quad (6.50)$$

where the "slope-diffraction coefficients"  $d^{i,r}$  are found to be

$$\text{UTD: } d^{i,r} = -\exp(-j\pi/4) (2\pi k_0)^{-1/2} r \cos(\frac{1}{2}\psi^{i,r}) [F_{\text{KP}}((\xi^{i,r})^2) - 1]. \quad (6.51a)$$

Away from the shadow boundaries (where  $|\xi^{i,r}| \gg 1$ ), (6.49b) reduces to (6.49a) and (6.51a) passes into

$$\text{GTD: } d^{i,r} = -\frac{1}{4} \exp(j\pi/4) (2\pi)^{-1/2} k_0^{-3/2} \cos(\frac{1}{2}\psi^{i,r}) / \sin^2(\frac{1}{2}\psi^{i,r}). \quad (6.51b)$$

In the special case of grazing incidence ( $\theta^i = \pi/2$ ) this result has also been derived by Karp and Keller [14, eq. (7)].

It is emphasized in [15] that the slope-diffraction term in (6.49) is the leading term in the diffracted-field expansion only if the incident field  $U^i$  vanishes at the edge point Q. If  $U^i(Q) \neq 0$ , the solution (6.48) is the leading term and the slope-diffraction term provides only part of the next higher-order term in the expansion of the diffracted field.

The results (6.49a) and (6.49b) can be written more conveniently in a form similar to (6.29) and (6.33b), namely,

$$\text{GTD: } U^d(P) = -\tilde{F}(\xi^i) \left[ \frac{\partial}{\partial z^i} U^i(Q) \right] r \sin \psi^i \exp(-jk_0 r \cos \psi^i) + \{i \rightarrow r\}, \quad (6.52a)$$

$$\begin{aligned} \text{UTD: } U^D(P) = & -[F(\xi^i) - \Theta(-\xi^i) - \tilde{F}(\xi^i)] \left[ \frac{\partial}{\partial z^i} U^i(Q) \right] \\ & \cdot r \sin \psi^i \exp(-jk_0 r \cos \psi^i) + \{i \rightarrow r\}. \end{aligned} \quad (6.52b)$$

Because of (6.12), it is easily recognized that (6.52a) follows from (6.52b) by replacing  $F(\xi)$  by its asymptotic expansion up to order  $\xi^{-3}$  or  $k_0^{-3/2}$ .

## 6.6. Comparison of knife-edge diffraction theories

In the previous sections, several knife-edge diffraction theories have been presented, namely:

- Sommerfeld's rigorous diffraction theory;
- Kirchhoff's approximation (which underlies the CCIR formula);
- Keller's GTD;
- the uniform theories UTD and UAT.

We now compare the results of these theories when applied to our two-dimensional knife-edge diffraction problem.

For the case of an incident *uniform* plane wave, such a comparison has been reported in [3], and has also been made in sec. 6.4. It was found there that both the UTD solution (6.30)–(6.31) and the UAT solution (6.34)–(6.35) are identical to the exact Sommerfeld solution (6.15). Away from the shadow boundaries, the exact solution is well approximated by Keller's GTD solution (6.26)–(6.27). For small diffraction angles  $\psi^i$ , the solution is well approximated by the Kirchhoff approximation (6.20); the resultant CCIR formula for the site-shielding factor (SSF) has amply sufficient accuracy for practical purposes.

For the case of an incident plan wave with a *linear* amplitude distribution, the exact solution of the diffraction problem is available, see (6.41). For small diffraction angles  $\psi^i$ , this solution is well approximated by the Kirchhoff approximation (6.45). The UAT solution (6.34)–(6.35) equals the exact solution (6.41), since the incident field  $U^i(Q)$  at the edge is zero and consequently,  $U^d(P)$  in (6.34) vanishes. In the UTD result (6.52b), the factor following the square brackets is equal to  $-U^i(P)$  by (6.38), hence the UTD total field  $U^g+U^D$  also equals the exact solution (6.41). Away from the shadow boundaries, the field  $U^D$  can be asymptotically expanded to yield the GTD solution (6.52a) for the diffracted field.

For the case of an incident plane wave with a *general* non-uniform amplitude distribution, no exact solution of the diffraction problem is available. If the higher-order derivatives of the amplitude distribution at the edge are not too large, it is expected that the Kirchhoff approximation and the high-frequency asymptotic methods (GTD/UTD/UAT) still yield reasonably accurate results. Only if both the dominant term and the slope-diffraction term vanish (that is, if both  $U^i(Q)=0$  and  $\partial U^i(Q)/\partial z'=0$ ), the higher-order terms in the expansion of the diffracted field become important. This is very unlikely to occur in practice, and in addition the diffracted field would then be very small (i.e., of order  $k_0^{-5/2}$  away from the shadow boundaries) and therefore negligible.

The results of the various knife-edge diffraction theories for the case of plane-wave incidence are summarized in table 6.1. It is clear from this table that, irrespective of the method adopted, the result for  $U(P)$  strongly depends on the behaviour of the incident field  $U^i(Q)$  at the edge. In its turn, this behaviour depends on the (transhorizon) propagation mechanism that is responsible for the incident radiation. Height-gain information on transhorizon propagation is therefore needed, and should be included in any clear-air interference-prediction model (see chapter 4).

Some graphical results calculated from the expressions of table 6.1, are shown in figs. 6.4 and 6.5 for the two cases of an incident plane wave with a uniform and a linear amplitude distribution, respectively. These results refer to the site-shielding factor (SSF), which is determined by normalizing the power received in the presence of the obstacle to the power received in the absence of the obstacle, i.e.,

$$\text{SSF} = -20 \log |U(P)/U^i(P)| \quad (\text{dB}) . \quad (6.53)$$

$$U^i = U_0 \exp(-jk_0 x')$$

$$\text{Uniform : } U_0 = \text{constant}$$

$$\text{Linear : } U_0 = A z'$$

$$\text{General amplitude distribution : } U_0 = U_0(z')$$

	Uniform : $U_0 = \text{constant}$	Linear : $U_0 = A z'$	General amplitude distribution : $U_0 = U_0(z')$
Exact solution	$F(\xi^i)U^i(P) + \{i \rightarrow r\}$	$[F(\xi^i) - \bar{F}(\xi^i)]U^i(P) + \{i \rightarrow r\}$	
Kirchhoff's approximation	$F(\xi^i)U^i(P)$	$[F(\xi^i) - \bar{F}(\xi^i)]U^i(P)$	$F(\xi^i)U_0(0)\exp(-jk_0 r \cos \psi^i) - [F(\xi^i) - \bar{F}(\xi^i)]r \sin \psi^i U_0'(0)\exp(-jk_0 r \cos \psi^i)$
(Extended) CCIR formula	$[2.1 [\sqrt{v^2+1} + v]]^{-1}  U^i(P) $		$[2.1 [\sqrt{v^2+1} + v]]^{-1}  U_0(0) $
GTD	$[\Theta(-\xi^i) + \bar{F}(\xi^i)]U^i(P) + \{i \rightarrow r\}$	$[\Theta(-\xi^i) + \bar{F}(\xi^i)]U^i(P) + \{i \rightarrow r\}$	$\Theta(-\xi^i)U^i(P) + \bar{F}(\xi^i)U_0(0)\exp(-jk_0 r \cos \psi^i) + \{i \rightarrow r\}$ if $U_0(0) \neq 0$ $\Theta(-\xi^i)U^i(P) - \bar{F}(\xi^i)r \sin \psi^i U_0'(0)\exp(-jk_0 r \cos \psi^i) + \{i \rightarrow r\}$ if $U_0(0) = 0$
UTD	$F(\xi^i)U^i(P) + \{i \rightarrow r\}$	$[F(\xi^i) - \bar{F}(\xi^i)]U^i(P) + \{i \rightarrow r\}$	$\Theta(-\xi^i)U^i(P) + [F(\xi^i) - \Theta(-\xi^i)]U_0(0)\exp(-jk_0 r \cos \psi^i) + \{i \rightarrow r\}$ if $U_0(0) \neq 0$ $\Theta(-\xi^i)U^i(P) - [F(\xi^i) - \Theta(-\xi^i) - \bar{F}(\xi^i)]r \sin \psi^i U_0'(0)\exp(-jk_0 r \cos \psi^i) + \{i \rightarrow r\}$ if $U_0(0) = 0$
UAT	$F(\xi^i)U^i(P) + \{i \rightarrow r\}$	$[F(\xi^i) - \bar{F}(\xi^i)]U^i(P) + \{i \rightarrow r\}$	$[F(\xi^i) - \bar{F}(\xi^i)]U^i(P) + \bar{F}(\xi^i)U_0(0)\exp(-jk_0 r \cos \psi^i) + \{i \rightarrow r\}$

Table 6.1. Comparison of six methods for the solution of the two-dimensional knife-edge diffraction problem, for three amplitude distributions of the incident plane wave. The entries based on the (extended) CCIR formula refer to  $|U(P)|$ , the other entries refer to  $U(P)$  (i.e., the total field at the observation point P. The edge point Q has coordinates  $x'=z'=0$ ).



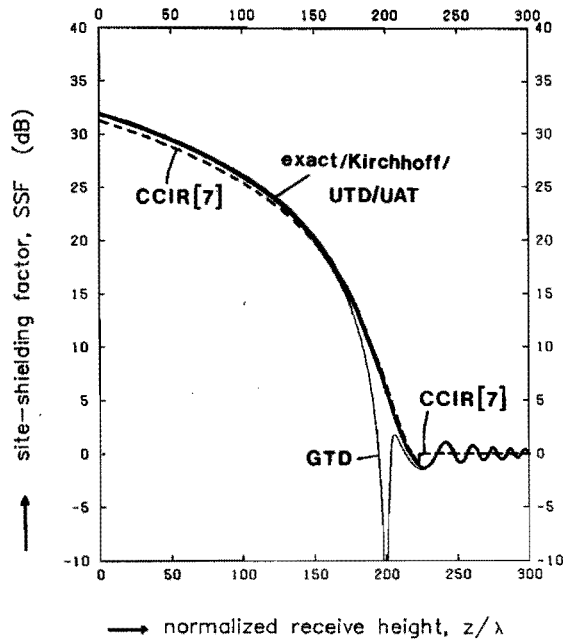


Fig. 6.4. SSF of a knife-edge obstacle, calculated by six different methods (see table 6.1). Incident plane wave has a uniform amplitude distribution.  $\theta^i=0$ ,  $z_0=200\lambda$ ,  $x=1000\lambda$ .

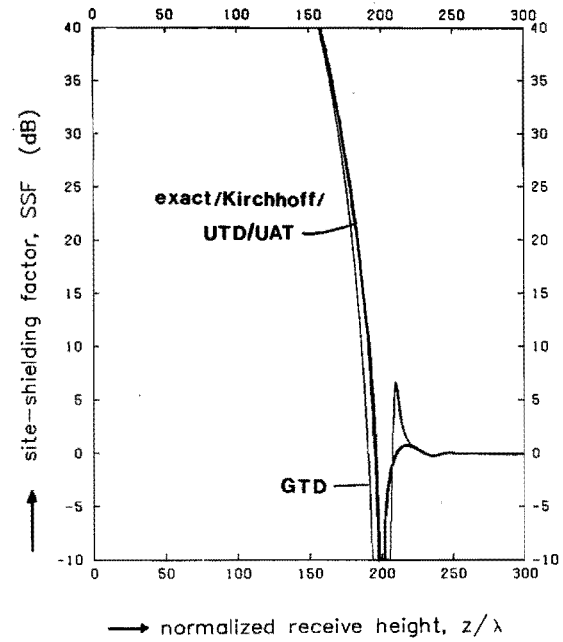


Fig. 6.5. SSF of a knife-edge obstacle, calculated by five different methods (see table 6.1). Incident plane wave has a linear amplitude distribution with a null at the edge.  $\theta^i=0$ ,  $z_0=200\lambda$ ,  $x=1000\lambda$ .

The geometry in the example of figs. 6.4 and 6.5 is typical for a realistic site-shielding situation (see fig. 6.1):  $\theta^i=0$ ,  $z_0=200\lambda$  and  $x=1000\lambda$ . The results are valid for both polarizations of the incident field, because the contribution of the second part of the formulas from table 6.1 (i.e., the contribution related to the reflected field) is found to be negligible. For the same reason, the SSF based on the Kirchhoff approximation has a negligible error. Also, Keller's GTD produces accurate values of the SSF, except in the vicinity of the shadow boundary, as expected. It is clear that in the uniform case, the simple CCIR formula is – for practical purposes – as good as any other SSF–formula based on table 6.1. For the linear case, no CCIR formula is available. The graphical results for this case (fig. 6.5) show that the SSF is now much higher than in the uniform case. The reason is that the incident field has a null at the edge, hence the field at the observation point is determined by slope diffraction only.

## 6.7. Modelling of a realistic site–shielding geometry

In the previous sections the two–dimensional knife–edge diffraction model was applied. In this model various assumptions and simplifications of a realistic site-shielding situation are made which may not always be justified. Here, we examine these assumptions in more detail, and, if possible, procedures are suggested to extend the knife–edge model so as to include more general, realistic situations.

### 6.7.1. Atmospheric influence

We have assumed free–space propagation between the obstacle and the observation point. On the other hand, the incident field reaches the obstacle by transhorizon propagation which is often due to atmospheric effects (see chapter 3).

This apparent inconsistency is justified by the fact that for site shielding of an earth-station antenna, the obstacle is located in the vicinity of the antenna. Consequently, the distance between the obstacle and the receive antenna is much smaller than the total path length. Therefore, since the influence of the inhomogeneous atmosphere on the propagation between the obstacle and the receive antenna is correspondingly smaller, free-space propagation may be assumed here.

### 6.7.2. Influence of the ground

The influence of the ground on the propagation between the obstacle and the receive antenna is neglected in the knife-edge model. This neglect is not always justified, but it is easy to include the effect of ground reflection in the model. If the electromagnetic properties of the earth surface at the reflection point are known, the total field  $U^{\dagger}$  at the observation point P follows from a simple two-ray model (fig. 6.6), i.e.,

$$U^{\dagger}(P) = U(P) + RU(P') . \quad (6.54)$$

Here, P' is the mirror image of P with respect to the earth surface (which is assumed to be flat) and R is the reflection coefficient of the earth surface. Note that the diffracted field is cylindrical wave emanating from the obstacle rim, in accordance with the view-point of GTD.

If the height of P above the ground is large, then the diffraction angle  $\theta'$  for the ray QP' is much larger than the angle  $\theta$  for the ray QP. As a consequence, one has  $U(P') \ll U(P)$ , and the influence of the ground can be neglected. On the other hand, if P lies close to the surface, one has  $\theta' \approx \theta$  and  $U(P') \approx U(P)$ . Then the reflection coefficient R becomes an important parameter. For small angles  $\theta$  not close to the

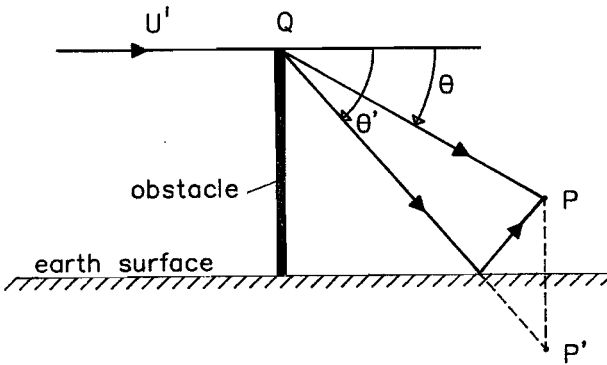


Fig. 6.6. Two-ray model to include the effect of ground reflection.

Brewster angle [17, sec. 9.6], one has  $|R| \approx 1$  and the reflected field  $RU(P')$  is of the same order of magnitude as  $U(P)$ .

### 6.7.3. *Oblique incidence*

An artificial site-shielding obstacle is usually located in such a way that the edge is oriented perpendicularly to the propagation direction of the incident wave. For an existing obstacle this is not always feasible, and oblique incidence occurs in that case. Then, the diffraction problem is no longer two-dimensional.

The exact solution of the diffraction problem for a plane electromagnetic wave obliquely incident on a knife-edge is available, see e.g. [2, sec. 11.6]. This solution is obtained by a decomposition of the incident wave into an E-polarized and an H-polarized part; for each part, the corresponding diffraction problem can be reduced to a scalar problem. Recently, the exact solution has been reformulated in a more convenient form [3], using the notations adopted in this thesis (except that the quantities in [3] are  $\vec{E}$  and  $\vec{H}$  instead of the scalar field quantity  $U$ ). The simplification in [3] is due to insights provided by Keller's GTD [8]. In the latter theory, the general law of edge diffraction states that a ray obliquely incident on an

edge produces a cone of diffracted rays with vertex at the diffraction point and axis tangent to the edge (fig. 6.7a). The semi-angle of this cone is equal to the angle  $\beta$  between the incident ray and the tangent to the edge. In the special case  $\beta = \pi/2$  (i.e., perpendicular incidence), this cone degenerates into a plane (fig. 6.7b).

The exact solution of the diffraction problem is written in [3] in several forms. One of these forms reads

$$\vec{E} = \vec{E}^G + \vec{E}^d, \tag{6.55}$$

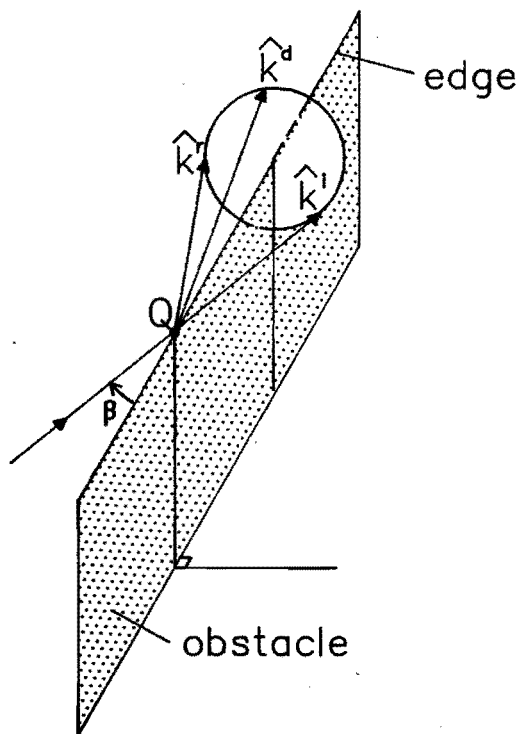


Fig. 6.7a. Cone of diffracted rays at oblique incidence.

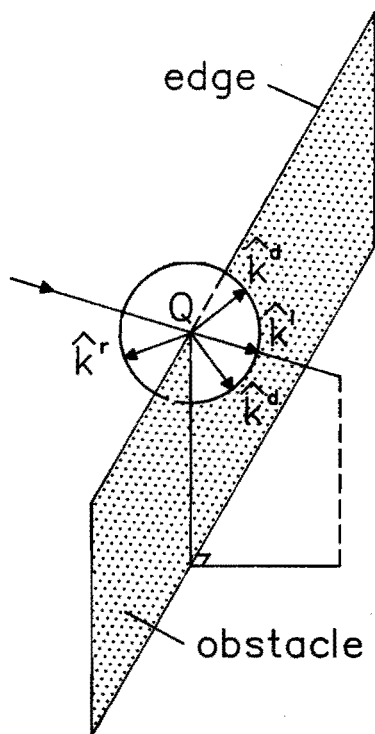


Fig. 6.7b. Plane of diffracted rays at perpendicular incidence.

where  $\vec{E}$  is the total electric field,  $\vec{E}^G$  is a modification of the geometrical-optics field and  $\vec{E}^d$  is Keller's diffracted field. The form (6.55) is similar to the UAT solution (6.34) of the two-dimensional scalar diffraction problem. In fact, the general UAT solution is precisely given by (6.55). Another form of the exact solution reads

$$\vec{E} = \vec{E}^G + \vec{E}^D, \tag{6.56}$$

where  $\vec{E}^G$  is the geometrical-optics field and  $\vec{E}^D$  is a modification of Keller's diffracted field  $\vec{E}^d$ . The representation (6.56) is in the format of the general UTD solution (cf. (6.30) for the two-dimensional scalar case), although UTD does not yield the correct expression for  $\vec{E}^D$ , as is pointed out in [3]. However, the error of UTD is small for observation points far away from the edge ( $k_0 r \gg 1$ ).

In the site-shielding problem considered in the present thesis (see chapter 7), only perpendicular incidence is considered. Therefore, we do not give detailed expressions here for the exact solution of the diffraction problem in the case of oblique incidence. We only point out that the exact solution contains a detour parameter defined by

$$\xi^{i,r} = \sqrt{2k_0 r} \sin \beta \sin\left(\frac{1}{2}\psi^{i,r}\right), \tag{6.57}$$

which is an extension of the detour parameter defined in (6.5) for the two-dimensional problem. This detour parameter also occurs in the general UAT solution and the general UTD solution; the latter is reviewed in detail in sec. 7.5.

#### 6.7.4. Finite obstacles

Up to now the obstacle has been assumed to be infinitely long in the  $y$ -direction, hence only diffraction at the top edge of the obstacle has been considered. However, any realistic obstacle has finite lateral dimensions, and diffraction at the side-edges takes place as well. It depends very much on the geometry of the shielding obstacle whether or not this effect should be taken into account. As a rule, the edge for which the diffraction angle of the observation point is smallest, yields the largest diffracted field. Hence, for a broad, relatively low obstacle (e.g. a row of houses), it is justified to ignore diffraction at the side-edges.

#### 6.7.5. Thickness of the obstacle

The most important artificial site-shielding obstacles are conducting screens, fences or walls. For these obstacles the knife-edge model is certainly realistic. However, other obstacle geometries are possible which cannot be modelled by a knife-edge. Methods for treating the diffraction by "thick" obstacles are now briefly reviewed. Some idealized (two-dimensional) models alternative to the knife-edge model are:

- i) the wedge (fig. 6.8a);
- ii) the square-top obstacle (fig. 6.8b);
- iii) the rounded-top obstacle (fig. 6.8c).

For the *wedge*-diffraction problem in the case of plane-wave incidence, the first uniform asymptotic solution was obtained by Pauli [18]. The leading term in his solution is equal to the UTD solution of sec. 6.4.5, with  $D^i$  in (6.31) replaced by the diffraction coefficient of a wedge [8,9]. Thus, wedge diffraction can be treated by the

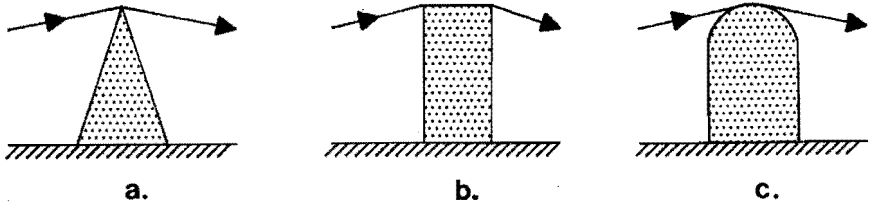


Fig. 6.8. Idealized two-dimensional models of a "thick" obstacle.

- a) Wedge;      b) square-top obstacle;      c) rounded-top obstacle.

high-frequency asymptotic theories (GTD/UTD/UAT), although the solutions obtained are more complicated than those for diffraction by a half-plane.

The *square-top obstacle* can be seen as a configuration of two wedges. A solution of the diffraction problem may be obtained by applying the high-frequency asymptotic theories to the diffraction at each wedge separately (multiple diffraction). Note that the diffracted field due to the first wedge hits the second wedge at grazing incidence. The square-top geometry is typical for a building as shielding obstacle.

For the *rounded-top obstacle*, the canonical problem is that of plane-wave diffraction at an infinitely long circular cylinder. An exact solution of this problem was given by Rayleigh [19], but his series-solution is slowly convergent at high frequencies. More convenient high-frequency asymptotic solutions were derived in the 1950's in terms of "creeping waves" [20] and of diffracted rays [21]; see Jones [22, secs. 8.1-8.4, 8.33] for more details. Keller's solution [21] in terms of diffracted rays is presented in the format of GTD, involving the diffraction coefficient  $B$  and the "decay rate"  $\alpha$  that accounts for the loss of energy in the propagation along the curved surface (fig. 6.8c). The expressions for  $B$  and  $\alpha$  are rather complicated and untractable for practical applications. Fortunately, an alternative, approximate formula for the SSF is available from CCIR [7].



The diffraction loss at a rounded-top obstacle is larger than the loss at a knife-edge obstacle of the same height, owing to the additional loss associated with the decay rate  $\alpha$ . The difference is considerable if the radius of curvature of the obstacle top is large compared to the wavelength; a typical example is a hill or a ridge.

For an *arbitrarily shaped obstacle*, no exact solution of the diffraction problem is available, and one has to resort to some idealized model which resembles the actual geometry.

#### 6.7.6. Surface roughness and finite conductivity of the obstacle

The obstacles considered so far have been assumed to be perfectly conducting. This is a realistic assumption for artificial structures like metallic screens and walls. Imperfect conductivity of a knife-edge obstacle results in a reduced reflected field. In the calculations that underlie figs. 6.4 and 6.5, it has been found that the reflected-field contribution to the SSF is anyway negligible. Therefore, no significant influence of the finite conductivity on the site-shielding properties is expected. For diffraction at rounded-top obstacles, the conductivity may be more important, but no analytical methods for the evaluation of its effect are known.

A similar conclusion can be drawn about the effect of surface roughness of the obstacle. Roughness of the faces of a knife-edge obstacle is expected to have only little influence on the SSF, but roughness of a rounded-top obstacle (e.g. a hill) may be an important factor. Again, analytical calculation methods are not available.

For a wedge, finite conductivity and surface roughness [23,24] can be included heuristically in the UTD wedge-diffraction coefficients. This procedure has shown to yield good results in terrain-diffraction calculations [25-27], where the dimensions of the diffracting obstacles are very large compared to the wavelength (e.g. hills or ridges). Generally, finite conductivity and surface roughness lead to a larger

diffraction loss as compared to the case of a perfectly conducting and smooth obstacle.

Finally, realistic obstacles may be partly transparent to the incident radiation (e.g. a fence, a building with large windows, or vegetation). In this case transmission through the obstacle should be included in the calculations [28]. Obviously, it is impossible to obtain general expressions for the transmission coefficient of an arbitrary, realistic obstacle. Of course, for maximum protection, artificial site-shielding obstacles are usually designed to have a negligible transmission coefficient.

### 6.8. References

- [1] R.H. Clarke and J. Brown, *"Diffraction theory and antennas"*, Wiley, Chichester, 1980.
- [2] M. Born and E. Wolf, *"Principles of optics"*, 3rd ed., Pergamon, Oxford, 1965.
- [3] G.A. Deschamps, J. Boersma and S.W. Lee, "Three-dimensional half-plane diffraction: exact solution and testing of uniform theories", *IEEE Trans. Ant. Prop.*, vol. AP-32, no. 3, pp. 264-271, 1984.
- [4] M. Abramowitz and I.A. Stegun, *"Handbook of mathematical functions"*, Dover, New York, 1965.
- [5] A. Sommerfeld, "Mathematische Theorie der Diffraction", *Math. Ann.*, vol. 47, pp. 317-374, 1896.
- [6] B.B. Baker and E.T. Copson, *"The mathematical theory of Huygens' principle"*, 2nd ed., Oxford Univ. Press, Oxford, 1950.
- [7] CCIR, Plenary Assembly, "Propagation by diffraction", *Recommendations and Reports of the CCIR*, vol. V, Rep. 715-2, Geneva, 1986.

- [8] J.B. Keller, "Geometrical theory of diffraction", *Journ. Opt. Soc. Am.*, vol. 52, no. 2, pp. 116-130, 1962.
- [9] R.G. Kouyoumjian and P.H. Pathak, "A uniform geometrical theory of diffraction for an edge in a perfectly conducting surface", *Proc. IEEE*, vol. 62, no. 11, pp. 1448-1461, 1974.
- [10] R.G. Kouyoumjian and P.H. Pathak, "Authors' reply" to J.D. Cashman, Comments on "A uniform geometrical theory of diffraction for an edge in a perfectly conducting surface", *IEEE Trans. Ant. Prop.*, vol. AP-25, no. 5, pp. 447-451, 1977.
- [11] D.S. Ahluwalia, R.M. Lewis and J. Boersma, "Uniform asymptotic theory of diffraction by a plane screen", *SIAM Journ. Appl. Math.*, vol. 16, no. 4, pp. 783-807, 1968.
- [12] S.W. Lee and G.A. Deschamps, "A uniform asymptotic theory of electromagnetic diffraction by a curved edge", *IEEE Trans. Ant. Prop.*, vol. AP-24, no. 1, pp. 25-34, 1976.
- [13] S.W. Lee, "Uniform asymptotic theory of electromagnetic edge diffraction: a review", in "*Electromagnetic scattering*", P.L.E. Uslenghi, ed., Academic Press, New York, pp. 67-119, 1978.
- [14] S.N. Karp and J.B. Keller, "Multiple diffraction by an aperture in a hard screen", *Optica Acta*, vol. 8, pp. 61-72, 1961.
- [15] G.L. James, "*Geometrical theory of diffraction for electromagnetic waves*", Peter Peregrinus, Stevenage, 1976.
- [16] J. Boersma, EUT, private communications, 1988.
- [17] J.A. Stratton, "*Electromagnetic theory*", McGraw-Hill, New York, 1941.
- [18] W. Pauli, "On asymptotic series for functions in the theory of diffraction of light", *Phys. Rev.*, vol. 54, pp. 924-931, 1938.

- [19] Lord Rayleigh, "On the electromagnetic theory of light", *Phil. Mag.*, vol. 12, pp. 81-101, 1881.
- [20] W. Franz und K. Deppermann, "Theorie der Beugung am Zylinder unter Berücksichtigung der Kriechwelle", *Ann. Phys.*, vol. 10, no. 6/7, pp. 361-373, 1952.
- [21] J.B. Keller, "Diffraction by a convex cylinder", *IRE Trans. Ant. Prop.*, vol. AP-4, no. 3, pp. 312-321, 1956.
- [22] D.S. Jones, "*Acoustic and electromagnetic waves*", Oxford Univ. Press, Oxford, 1986.
- [23] W.D. Burnside and K.W. Burgener, "High-frequency scattering by a thin lossless dielectric slab", *IEEE Trans. Ant. Prop.*, vol. AP-31, no. 1, pp. 104-110, 1983.
- [24] K.A. Chamberlin and R.J. Luebbers, "An evaluation of Longley-Rice and GTD propagation models", *IEEE Trans. Ant. Prop.*, vol. AP-30, no. 6, pp. 1093-1098, 1982.
- [25] R.J. Luebbers, "Finite-conductivity uniform GTD versus knife-edge diffraction in prediction of propagation path loss", *IEEE Trans. Ant. Prop.*, vol. AP-32, no. 1, pp. 70-76, 1984.
- [26] R.J. Luebbers, "Propagation prediction for hilly terrain using GTD wedge diffraction", *IEEE Trans. Ant. Prop.*, vol. AP-32, no. 9, pp. 951-955, 1984.
- [27] R. Grosskopf, "Experiences and results with a fieldstrength prediction method based on GTD", *Int. Conf. Ant. Prop. (ICAP)*, *IEE Conf. Publ.*, no. 274, pp. 35-38, 1987.
- [28] J.C. Arnbak, "Microwave propagation - Some problems and methods in the study of microwave propagation behind terrain-masking obstacles", *Danish Defence Research Establishment*, Rep. no. DDRE 1972/3, Copenhagen, 1972.



## 7. SITE SHIELDING FOR EARTH-STATION ANTENNAS -- THEORY

### 7.1. Introduction

In sec. 5.2.3, site shielding has been defined as the screening of a receiving (earth) station against interference from transmitting (terrestrial) stations, by means of an obstacle located in the vicinity of the receiving antenna. Often site shielding has to be performed in the near-field region of the receiving antenna. This is especially relevant if the antenna needs to be completely surrounded by the screening obstacle (e.g. a wall or a fence), as costs or real-estate availability may be severely limiting factors.

Selection of the site of a (new) receiving earth station in an interference environment, and the design of site-shielding obstacles, always need careful consideration. Relocating existing earth stations or rebuilding inadequate shields is often too expensive to be feasible. Therefore, a reliable prediction model is desirable to estimate a priori the obtainable site-shielding factor (SSF, see sec. 5.2.3) of a given obstacle in specific situations.

The current CCIR site-shielding model [1] will be shown to be inadequate for this purpose. A more fundamental investigation of the site-shielding problem is presented in this chapter. Numerical results of this investigation are presented in chapter 8.

### 7.2. Formulation of the site-shielding problem

The general site-shielding problem is three-dimensional in nature and can involve various geometries. In the present thesis, we are interested in protecting earth-station antennas against transhorizon interference from terrestrial stations.

Earth stations usually employ reflector antennas of the Cassegrain or parabolic type; shielding obstacles (especially artificial ones) can frequently be modelled as conducting knife edges. Therefore, we restrict our investigations to the geometry of fig. 7.1, in which the following assumptions and simplifications are implicitly made:

- The incident field is due to a distant source and can be modelled as a uniform or non-uniform plane wave (as discussed in sec. 6.2).
- The obstacle is a perfectly conducting knife edge, with a horizontal edge perpendicular to the propagation direction of the incident (transhorizon) field. The latter direction is usually taken to be horizontal (i.e.,  $\theta^i=0$ ).
- The earth surface between the obstacle and the antenna is flat, and the influence of the atmosphere in the region in between is negligible.

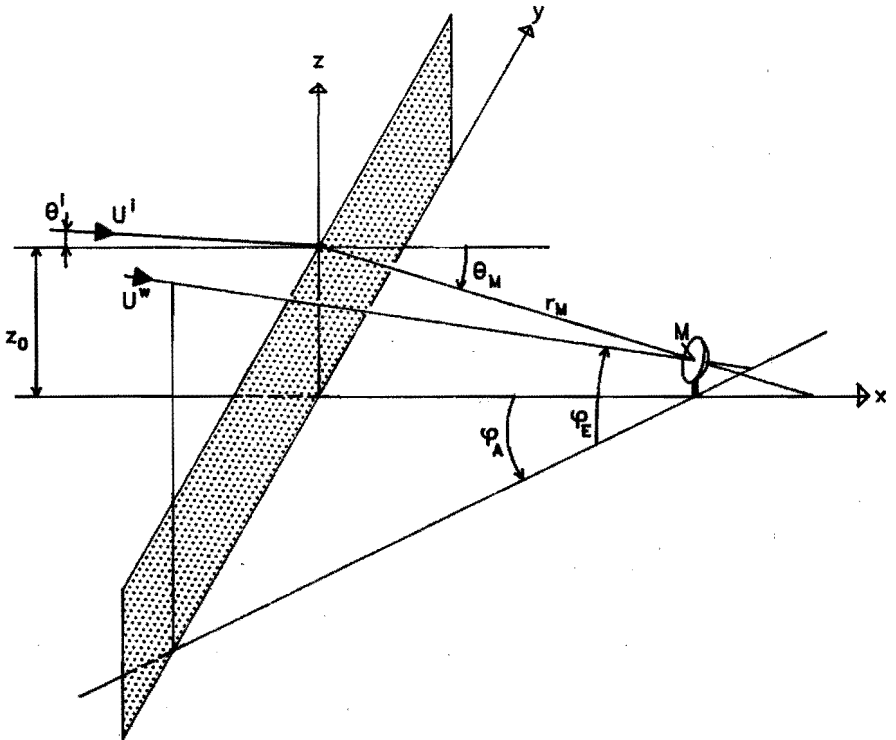


Fig. 7.1. Typical geometry for site shielding of an earth-station antenna.

- The antenna is a reflector antenna with a circular aperture.
- The circular cylinder generated by the aperture ("aperture cylinder") is not obstructed by the obstacle.

For the description of the problem, a Cartesian  $(x,y,z)$  coordinate system is introduced (fig. 7.1). The earth surface is given by the plane  $z=0$ , the obstacle is described by  $x=0, 0 \leq z \leq z_0$ . The unwanted field  $U^i$  (caused by a terrestrial interferer) is incident on the obstacle in a direction parallel to the  $xz$ -plane, at an elevation  $\theta^i$  (with respect to the  $x$ -axis). The wanted field  $U^w$  originates from a satellite station and can be assumed to be unaffected by the obstacle (as will be argued in sec. 7.4.3). The position of the satellite determines the azimuth angle  $\varphi_A$  (with respect to the negative  $x$ -axis) and the elevation angle  $\varphi_E$  (with respect to the  $xy$ -plane) of the earth-station antenna. The angles  $\varphi_A$  and  $\varphi_E$  refer to the antenna phase centre  $M$ ; the "diffraction angle" referring to  $M$  is denoted by  $\theta_M$ . The Cartesian coordinates of  $M$  are  $x=x_M, y=0$  and  $z=z_M$ , with  $x_M > 0$  and  $z_M > 0$ . The height difference  $z_0 - z_M$  is denoted by  $\Delta z$ , where usually  $\Delta z > 0$ . The reflector diameter is denoted by  $D$ .

The site-shielding problem amounts to the determination of the site-shielding factor (SSF), i.e., the ratio of the interference powers received in the absence and the presence of the obstacle, respectively.

### 7.3. Review of the CCIR site-shielding model

#### 7.3.1. Derivation of the CCIR model

The current CCIR site-shielding model, described in Rep. 390-5 [1], is simple and two-dimensional; it is based on a study performed in the early 1970's by the British Post Office [2-4]. The geometry of the model is shown in fig. 7.2, which follows from fig. 7.1 by choosing the azimuth  $\varphi_A = 0$  and the angle of incidence  $\theta^i = 0$ .



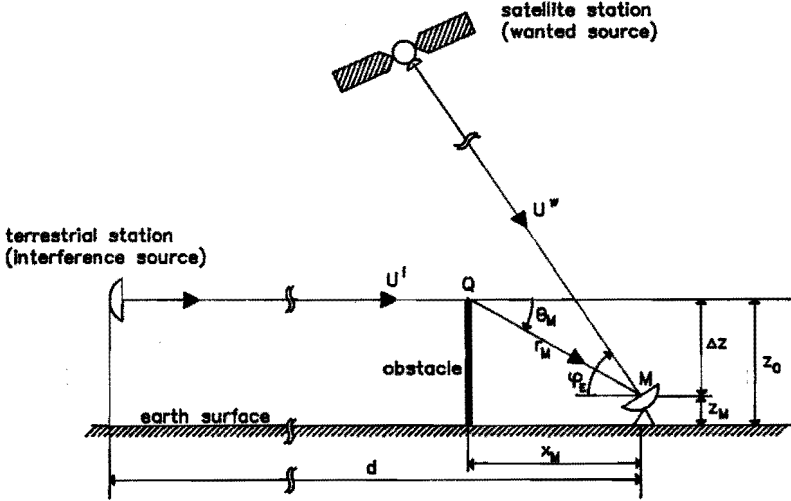


Fig. 7.2. Geometry of the CCIR site-shielding model [1].

In the CCIR model, the SSF consists of two terms. The first term accounts for the diffraction loss due to the obstacle, calculated by the CCIR knife-edge diffraction formula [5]. Referring to the derivation of the latter formula in sec. 6.4.3, the dimensionless parameter  $v$ , defined in (6.21), is approximated by

$$v = 2\sqrt{2r_M/\lambda} \sin(\theta_M/2) \approx \theta_M \sqrt{2x_M/\lambda}, \quad \theta_M \ll 1, \quad (7.1)$$

where  $r_M = \sqrt{x_M^2 + (\Delta z)^2}$  is the distance between the antenna phase centre  $M$  and the obstacle edge point  $Q$ . (We have assumed in fig. 7.2 that  $M$  is located at the centre of the aperture plane. In general, the phase centre lies close to this point [6].) For  $v \gg 1$ , the diffraction loss follows from (6.24) as

$$L = 20 \log(\sqrt{2\pi}v) = 20 \log(2\pi\theta_M \sqrt{x_M/\lambda}) \quad (\text{dB}). \quad (7.2)$$

The second term in the SSF takes account of the changed antenna-sidelobe gain in the presence of the obstacle, compared to the unshielded case. In the shielded case, there is an apparent interference source at the obstacle edge (see chapter 6). If we assume the standard reference sidelobe pattern (5.2) for the earth-station antenna, the correction in antenna gain becomes

$$\begin{aligned} \Delta G &= G(\varphi_E - \theta_M) - G(\varphi_E) \\ &= [32 - 25 \log(\varphi_E - \theta_M)] - [32 - 25 \log(\varphi_E)] = -25 \log(1 - \theta_M / \varphi_E) \quad (\text{dB}). \end{aligned} \quad (7.3)$$

In the CCIR site-shielding model, (7.2) and (7.3) are combined to yield an expression for the SSF [1],

$$\text{SSF} = L - \Delta G = 20 \log \left[ \frac{\pi^2 \theta_M}{90} \sqrt{x_M / \lambda} \right] + 25 \log (1 - \theta_M / \varphi_E) \quad (\text{dB}), \quad (7.4)$$

with  $\theta_M$  and  $\varphi_E$  in degrees.

A computer program has been developed [2] to test the validity of this simple model [3]. This computer program is based on an approximate aperture-integration method and ignores a number of effects [2], but is claimed to show agreement within 5 dB with measurements [2,4]. The differences between the computer calculations and the CCIR model were found to be within 3 dB if the following conditions are fulfilled:

- i)  $x > D^2 / 2\lambda$  : minimum obstacle distance [1,3,4];
- ii)  $\varphi_E - \theta_M > 2^\circ$  : minimum obstacle clearance of aperture cylinder [3,4];
- iii)  $0.5^\circ < \theta_M < 10^\circ$  : limited range of diffraction angle [3,4];
- iv)  $d > 2D^2 / \lambda$  and  $d > 3x_M$  : interference source located in far-field region of antenna and far away from obstacle [3];
- v)  $\Delta z > 1.5D$  : obstacle top well above entire antenna [4].

These constraints are a consequence of the assumptions made in the derivation of (7.4). This will be demonstrated in the next section. We observe that constraint (i) excludes many cases of near-field site shielding, which is a severe practical limitation. It has been shown [3] that for  $x_M < D^2/2\lambda$ , the CCIR model (7.4) predicts an SSF that is much larger than the result of the computer program.

### 7.3.2. Limitations of the CCIR model

An examination of the CCIR site-shielding model (7.4) reveals that it contains a number of assumptions and simplifications:

- a) the azimuth of the antenna (relative to the incident interference) is zero;
- b) the polarization of the unwanted interference is taken as the one most harmful for the earth station, both in the presence and in the absence of the obstacle;
- c) the envelope of the antenna-sidelobe pattern follows the CCIR reference pattern (5.2);
- d) the influence of the ground between the obstacle and the antenna is neglected;
- e) the unwanted field is a horizontally incident uniform plane wave;
- f) the detailed antenna geometry is ignored: instead, the circular aperture is treated as a point source located at the phase centre M;
- g) the "diffraction angle"  $\theta_M$  has a limited range.

The first four assumptions (a-d) have not been clearly indicated in the literature [1,3,4], but may nevertheless severely restrict practical application of the model. The assumptions e-g are expressed to some extent by the constraints i-iv listed in the previous section. The limited range for  $\theta_M$  (assumption g and constraint iii) follows from the approximations in the derivation of (7.1) and (7.2), i.e.,  $\theta_M \ll 1$  and  $v \gg 1$ .

Constraint  $iv$  on the minimum path length  $d$  justifies the assumption  $e$  of an incident plane wave (although not necessarily uniform or horizontally incident). Constraint  $i$  on the minimum distance  $x_M$  allows treatment of the antenna as a point source (assumption  $f$ ), provided that the top edge of the antenna is still well below the edge of the obstacle (constraint  $v$ ). If the latter condition is not fulfilled, the upper part of the reflector is illuminated rather strongly, owing to the rapid increase of the field strength with height near the shadow boundary (see fig. 6.4), and assumption  $f$  will be unrealistic.

A more fundamental study of the site-shielding problem is required to remove the limitations  $a-g$ . Such a study is reported in the sequel.

## 7.4. Fundamental approach to the site-shielding problem

### 7.4.1. General description

As mentioned before, if an obstacle is located in the near-field region of an antenna, the antenna far-field radiation pattern  $G(\varphi_A, \varphi_E)$  cannot be applied; in fact, the antenna gain  $G$  is then also a function of the distance. In this case, the antenna cannot be treated as a point source. Rather, each contribution to the off-angle reception by the antenna should be considered individually. Therefore, in order to assess the off-angle reception, the detailed structure of the antenna should be taken into account as an input datum for the near-field site-shielding problem.

Typical examples of earth-station antennas are the axisymmetric Cassegrain antenna (a dual-reflector system) and the simple parabolic antenna. In sec. 5.2.2, we identified the principal causes of sidelobe reception by a Cassegrain antenna. The present investigation of the site-shielding problem is confined to the simple parabolic antenna. In such an antenna, wide-angle reception is caused mainly by

primary-feed spillover and by reflector-edge diffraction. It will be shown in sec. 7.6.2 that in most cases only two points on the reflector edge yield a contribution to the edge-diffracted field in a given direction. Thus, a three-ray model is, in principle, adequate to describe the wide-angle reception of a parabolic antenna (fig. 7.3): the direct ray  $QF$  from the source point  $Q$  to the feed centre  $F$ , and two edge-diffracted rays  $QP_1F$  and  $QP_2F$ , where  $P_1$  and  $P_2$  are the diffraction points at the reflector edge. The fields along these three rays are weighted by the feed radiation pattern and vectorially added to obtain the received field.

In fig. 7.3, we have assumed that the source is concentrated at the point  $Q$ . For the calculation of the far-field response of the antenna,  $Q$  should be located at infinity, yielding an incident plane wave at the antenna. In our site-shielding problem (fig. 7.1), the obstacle edge behaves as a line source for the field incident on the antenna. In principle, the three-ray model is applicable in all these cases.

Refinements of the model are obtained by including multiple-diffraction and ground-reflection effects. Multiply diffracted rays (e.g.  $QP_1P_2F$  in fig. 7.3) contribute only little to the received field because of the multiple diffraction losses.

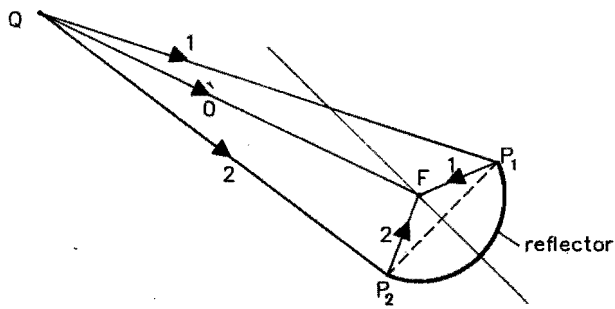


Fig. 7.3. Three-ray model for the wide-angle reception by a parabolic antenna. F: feed phase centre; Q: source point;  $P_1$  and  $P_2$ : diffraction points; "0": direct ray; "1" and "2": diffracted rays.

It has been shown [7–9] by comparison with measured results [10] that higher-order diffraction can often be neglected. Ground-reflected rays can simply be included by the method of sec. 6.7.2. In principle, this implies the extension of the three-ray model to a six-ray model. In the following calculations, we have ignored multiple diffraction, and — for reasons of simplicity of discussion and physical interpretation — also ground reflections.

The geometrical theory of diffraction (GTD) is well suited for the calculation of the diffracted rays and the associated diffracted fields. The GTD and its modifications UTD and UAT have been described in chapter 6 for the two-dimensional knife-edge diffraction problem. A more general formulation of these theories is needed to handle the reflector-edge diffraction problem. We have selected UTD for the solution of the latter diffraction problem, because it is more easily applied and provides more physical insight than UAT, although the latter may be slightly preferable on theoretical grounds. For axially symmetric reflector antennas, the differences between UTD and UAT have been shown to be insignificant from an engineering viewpoint [11]. The general GTD/UTD formulation is described in sec. 7.5.

#### 7.4.2. Description of the earth-station antenna

For simplicity, we restrict the investigation of the site-shielding problem to earth-station antennas of the axisymmetric parabolic type. Such an antenna consists of a single parabolic reflector and a feed located at the paraboloid focus, see fig. 7.4. The feed struts and the reflector-support structure are ignored in our calculations; these structures can have various geometries and are difficult to include in a general analysis.

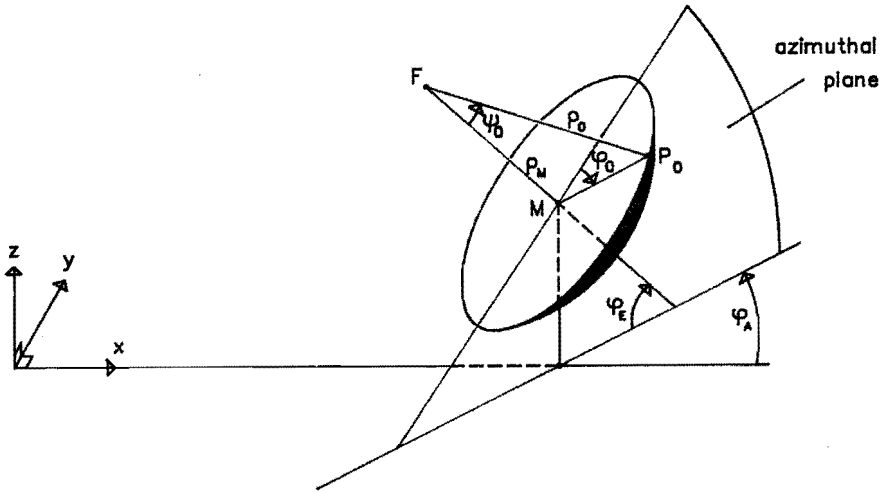


Fig. 7.4. Geometry of the parabolic earth-station antenna.

Because of the relatively small size of the feed, the reflector may be assumed to lie in the far-field zone of the feed. Hence, the radiation of the feed can be described by the far-field radiation pattern  $G_f(\psi)$ , which is assumed to be rotationally symmetric around the axis of the antenna. This pattern  $G_f(\psi)$  induces a weighting of each ray-optical field arriving at the feed.

To describe the geometry of the parabolic antenna, we employ a spherical  $(\rho, \psi, \varphi)$  coordinate system with its origin at the focus F. Here,  $\psi$  is the angle with the axis of symmetry of the antenna; the angle  $\varphi$  is measured with respect to the azimuthal plane, i.e., the plane through the antenna axis perpendicular to the  $xy$ -plane (fig. 7.4). The azimuthal plane, and the plane through the antenna axis perpendicular to the azimuthal plane, are the *principal planes* of the antenna. The location of the antenna with respect to the obstacle is indicated by the position of the centre M of the aperture plane. Thus, M is described either by its spherical coordinates  $\rho = \rho_M$ ,  $\psi = 0$ , or by its Cartesian coordinates  $x = x_M$ ,  $y = 0$ ,  $z = z_M$ . A typical point  $P_0$  at the reflector edge has spherical coordinates  $\rho = \rho_0$ ,  $\psi = \psi_0$ ,  $\varphi = \varphi_0$ .

The distances  $\rho_M$  and  $\rho_0$  and the subtended angle  $\psi_0$  are readily expressed in terms of the reflector diameter  $D$  and the focal distance  $f$ , which determine the reflector surface completely (see appendix C). Specifically, one has

$$\rho_M = f - D^2/16f, \tag{7.5a}$$

$$\rho_0 = f + D^2/16f, \tag{7.5b}$$

$$\psi_0 = 2 \arctan(D/4f). \tag{7.5c}$$

Next, we need to specify the far-field radiation pattern  $G_f(\psi)$  of the antenna feed. A feed that is frequently employed in practice, is the corrugated horn. Its radiation pattern can be modelled well by a power of a cosine in the forward directions, and by a constant in the rear directions [9; 12, sec. 5.2]. As a first approximation, the phase of  $G_f(\psi)$  may be assumed to be constant (it will turn out in sec. 7.6.4 that the phase is unimportant for site-shielding calculations). Hence, we take  $G_f(\psi)$  as

$$G_f(\psi) = G_0(a + \cos^m \psi), \quad 0 \leq \psi \leq \pi/2, \tag{7.6a}$$

$$G_f(\psi) = G_0 a, \quad \pi/2 \leq \psi \leq \pi. \tag{7.6b}$$

Here, the dimensionless constant  $a$  determines the relative sidelobe level for  $\psi \geq \pi/2$ , with  $a < 1$  (and usually  $a \ll 1$ ), and  $G_f(0) = G_0(1+a)$  is the forward voltage gain of the feed. The exponent  $m$  determines the amplitude taper over the reflector, in particular the relative edge illumination  $G_f(\psi_0)/G_f(0)$ . Because any voltage radiation pattern  $G_f(\psi, \varphi)$  must satisfy the directivity relation [13, sec. 2.3]

$$\int_0^\pi \int_0^{2\pi} G_f^2(\psi, \varphi) \sin \psi \, d\psi \, d\varphi = 4\pi, \tag{7.7}$$



the three parameters  $G_0$ ,  $a$  and  $m$  are not independent. Substitution of (7.6) into (7.7) leads to the relation

$$G_0 = \left[ a^2 + \frac{a}{m+1} + \frac{1}{4m+2} \right]^{-1/2} \quad (7.8)$$

In our numerical calculations, we have chosen  $a=0.00316$  and  $m=3.368$ . The corresponding pattern  $G_f(\psi)$  (fig. 7.5) has a relative rear-sidelobe level of  $-50$  dB, with a relative edge illumination of  $-20$  dB for a reflector with subtended angle  $\psi_0=60^\circ$  (corresponding to  $f/D=0.433$ ); the feed gain in the forward direction amounts to  $11.9$  dBi.

Finally, the polarization of the antenna is an important input datum. In satellite communications, both linear polarization and circular polarization are commonly applied. For simplicity, we assume linear polarization in our calculations. Circular polarization can be obtained from a suitable combination of two linear polarizations.

The polarization of the antenna is determined by the polarization of the feed. The latter is taken as the polarization of a Huygens source. For the antenna in transmit mode, such a source produces a linearly polarized reflected field in the antenna aperture. Then two independent orthogonal polarizations can be

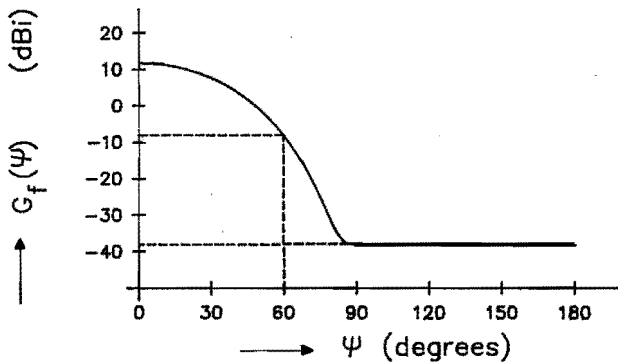


Fig. 7.5. Feed radiation pattern  $G_f(\psi)$  used in the numerical calculations.

distinguished: vertical and horizontal antenna polarization, corresponding to a reflected field in the aperture parallel and perpendicular to the azimuthal plane, respectively. (Strictly speaking, the terminology "vertical" polarization is correct only for antenna elevation  $\varphi_E=0$ .)

If we denote by  $\hat{e}_{\text{pol}}$  the unit vector in the direction of the electric field radiated by the feed, we can specify the feed polarization in the spherical  $(\rho, \psi, \varphi)$  coordinate system (fig. 7.4) by [12, sec. 5.2]

$$\hat{e}_{\text{pol}} = \cos\varphi \hat{e}_{\psi} + \sin\varphi \hat{e}_{\varphi} \quad \text{for vertical antenna polarization,} \quad (7.9a)$$

$$\hat{e}_{\text{pol}} = \sin\varphi \hat{e}_{\psi} - \cos\varphi \hat{e}_{\varphi} \quad \text{for horizontal antenna polarization.} \quad (7.9b)$$

For the antenna operating in receive mode, these polarization properties apply by reciprocity to the field received by the feed.

### 7.4.3. Influence of the obstacle on the wanted radiation

In sec. 7.2 we stated that the wanted radiation can be assumed to be unaffected by the obstacle. For an earth-station antenna of the parabolic type (as described in the previous section), this assumption is justified under certain conditions, to be derived now.

Intuitively it is expected that the wanted radiation  $U^W$  is unaffected if the antenna aperture cylinder sufficiently clears the obstacle. The worst case is likely to occur for azimuth  $\varphi_A=0$ , shown in fig. 7.6, because in this case the clearance is minimal. Here, the aperture cylinder is unobstructed if

$$\sin(\varphi_E - \theta_M) > D/2r_M. \quad (7.10)$$

s of gainboqer  
 lenby lathum  
 boores at r  
 hoinbr  
 stanf

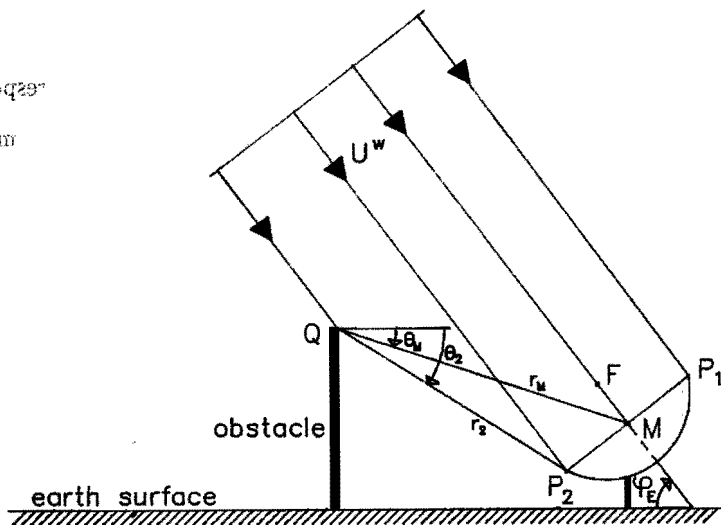


Fig. 7.6. Influence of the obstacle on the wanted radiation ( $\varphi_A=0$ ).

However, (7.10) does not guarantee that the obstacle has no influence, because the obstacle edge causes diffraction of the incident field  $U^w$ . The diffracted field may affect the received field on the entire reflector, but the strongest influence occurs at the nearest edge point  $P_2$ . For a rough estimate of this effect, the simple CCIR knife-edge diffraction formula [5], derived in sec. 6.4.3, can be applied. The relevant formula (6.25) contains the dimensionless parameter  $v$ , introduced in (6.21). For  $v \ll -1$ , the influence of the obstacle is negligible.

Hence, the field at  $P_2$  (and thus everywhere on the reflector) can be assumed to be unaffected by the obstacle if the corresponding parameter value  $v_2$  satisfies

$$v_2 = 2\sqrt{2r_2/\lambda} \sin\left[\frac{1}{2}(\theta_2 - \varphi_E)\right] < -1, \tag{7.11a}$$

that is, if

$$2 \sin\left[\frac{1}{2}(\varphi_E - \theta_2)\right] > \sqrt{\lambda/2r_2}, \tag{7.11b}$$

where  $r_2$  and  $\theta_2$  are the polar coordinates of  $P_2$ . These are related to the polar coordinates  $r_M$  and  $\theta_M$  of  $M$  by

$$r_2^2 = (r_M \sin \theta_M + \frac{1}{2} D \cos \varphi_E)^2 + (r_M \cos \theta_M - \frac{1}{2} D \sin \varphi_E)^2, \quad (7.12a)$$

$$\tan \theta_2 = \frac{r_M \sin \theta_M + \frac{1}{2} D \cos \varphi_E}{r_M \cos \theta_M - \frac{1}{2} D \sin \varphi_E}. \quad (7.12b)$$

However, condition (7.11) is often unnecessarily stringent, because the diffracted field at  $P_2$  contributes only little to the total received field, especially if the aperture illumination is tapered (as in fig. 7.5). In the latter case, the received wanted field at  $F$  mainly results from the field incident on the central part of the reflector. It is therefore more realistic to impose the condition  $v < -1$  on the parameter value  $v_M$  (corresponding to  $M$ ) instead of  $v_2$  as in (7.11a). Then, (7.11b) can be replaced by

$$2 \sin \left[ \frac{1}{2} (\varphi_E - \theta_M) \right] > \sqrt{\lambda / 2 r_M}. \quad (7.13)$$

In conclusion, the obstacle influence on the wanted radiation  $U^w$  is insignificant if the conditions (7.10) and (7.13) are met; a stricter condition is given by (7.11). These conditions are fulfilled in many practical site-shielding geometries. In particular, if a minimum obstacle clearance  $(\varphi_E - \theta_M)$  of  $2^\circ$  is assumed (as in the CCIR site-shielding model - see constraint *ii* in sec. 7.3.1), the conditions (7.10), (7.11) and (7.13) are normally all satisfied.

## 7.5. Review of the geometrical theory of diffraction for a curved edge

### 7.5.1. *Introduction*

The geometrical theory of diffraction (GTD) and its extension, the uniform geometrical theory of diffraction (UTD), have been described in secs. 6.4.4 and 6.4.5 for the two-dimensional knife-edge diffraction problem. These descriptions are inadequate for the present reflector-edge diffraction problem, because

- i) the present problem is vectorial and cannot be reduced to a diffraction problem for a single scalar field quantity;
- ii) the field incident on the reflector edge is, in general, not a plane wave;
- iii) the diffracting edge is curved, and its curvature should be taken into account.

The required extensions of GTD and UTD, as presented in the sequel, are adopted from [14–16]; the notation is taken mainly from [16].

### 7.5.2. *Fundamentals of the general GTD*

In the general GTD, the diffracting obstacle is a curved wedge that consists of two curved surfaces intersecting along a curved edge. The justification of GTD is that high-frequency diffraction is a *local* phenomenon. Locally, the obstacle can be approximated by a straight wedge, whose surfaces are tangent to the surfaces of the curved wedge at the diffraction point. In addition, any incident field can be approximated locally by a plane wave. Thus, the theory for a straight wedge can be applied to the general wedge as well. In the required extension the curvatures of the wedge surfaces, of the edge, and of the incident wavefront have to be taken into account.

This approach is similar to the extension of the geometrical-optics method for electromagnetic reflection by a plane surface to reflection by a curved surface. For scalar fields this extension is described in e.g. [17].

Furthermore, it is required to extend GTD for diffraction of a scalar field to diffraction of a vector field. This extension may seem trivial, but the actual computation is much more complex. (The same holds for the reflection problem mentioned above, see [18].)

Apart from these extensions, the principles of GTD remain unchanged. Thus, it is again assumed that a ray (obliquely) incident on an edge produces a cone of diffracted rays (fig. 6.7a) with axis tangent to the edge (law of edge diffraction). Along a diffracted ray, the field varies according to the laws of geometrical optics. The curvatures of the diffracted wavefront are to be determined from the curvatures of the incident wavefront and of the edge.

### 7.5.3. Description of the electromagnetic fields

The general site-shielding problem is vectorial in nature and cannot be described in terms of a single scalar field quantity  $U$ . Instead, we require a complete description in terms of the electric field  $\vec{E}$  and the magnetic field  $\vec{H}$ . We assume that each electromagnetic field is locally a plane wave, mathematically expressed by

$$\vec{E}(\vec{r}) \cdot \hat{k} = 0, \quad \vec{H}(\vec{r}) = \frac{1}{Z_0} \hat{k} \times \vec{E}(\vec{r}), \quad (7.14)$$

where  $Z_0 = \sqrt{\mu_0/\epsilon_0}$  is the intrinsic impedance of free space and  $\hat{k}$  is the unit vector in the propagation direction of the field. For the description it is customary to concentrate on the electric field only. As in chapter 6, we use superscripts  $g, i, r, d$  and  $D$  for geometrical-optics, incident, reflected, diffracted and modified diffracted

fields, respectively. Thus,  $\vec{E}^D$  is the UTD modification of the diffracted field  $\vec{E}^d$  of GTD.

The electromagnetic field propagates along rays which are straight lines in the direction  $\hat{k}$ . These rays are orthogonal to the surfaces of constant phase, called wavefronts. At a typical point P of a wavefront, the principal directions of the wavefront are denoted by  $\hat{x}_1$  and  $\hat{x}_2$ , with corresponding principal radii of curvature  $R_1$  and  $R_2$ ; these radii measure the distances to the two foci of the wavefront at P. Let  $\sigma$  denote the abscissa along the ray through P in the direction  $\hat{k}$ . Then the field amplitude variation along the ray is described by the function  $a(\sigma, R_1, R_2)$  defined by

$$a(\sigma, R_1, R_2) = \left[ (1 + \sigma/R_1)^{1/2} (1 + \sigma/R_2)^{1/2} \right]^{-1}, \quad (7.15)$$

where the principal values of the square roots are meant. When the origin is taken at one of the foci and the other focus lies at  $\sigma = -R_c$  (where  $R_c$  is the interfocal distance), the amplitude variation along the ray is described by the function  $b(\sigma, R_c)$  defined by

$$b(\sigma, R_c) = \left[ \sigma^{1/2} (1 + \sigma/R_c)^{1/2} \right]^{-1}. \quad (7.16)$$

At the foci, the functions  $a(\sigma, R_1, R_2)$  and  $b(\sigma, R_c)$  become infinite and are no longer adequate for the description of the fields; these focal points (caustics) should be dealt with separately.

With (7.15) and (7.16), the fields  $\vec{E}^i$ ,  $\vec{E}^r$  and  $\vec{E}^d$  can generally be represented by

$$\vec{E}^i(\sigma \hat{k}^i) = \vec{E}^i(0) a(\sigma, R_1^i, R_2^i) \exp(-j\mathbf{k}_0 \sigma), \quad (7.17a)$$

$$\vec{E}^r(\sigma \hat{k}^r) = \vec{E}^r(0) a(\sigma, R_1^r, R_2^r) \exp(-j\mathbf{k}_0 \sigma), \quad (7.17b)$$

$$\vec{E}^d(\sigma \hat{k}^d) = \vec{E}^d(0) b(\sigma, R_c) \exp(-j\mathbf{k}_0 \sigma), \quad (7.17c)$$

where the origin has been taken at the edge point P, which is a focus of the diffracted field  $\vec{E}^d$ . The coordinate  $\sigma$  is measured from P in the directions  $\hat{k}^i$ ,  $\hat{k}^r$  and  $\hat{k}^d$ , respectively. Notice that  $\vec{E}^d(0)$  in (7.17c) is merely a fictitious initial value of the diffracted field  $\vec{E}^d$ ; the actual diffracted field becomes infinite at the edge.

The principal directions of  $\vec{E}^r$  and  $\vec{E}^d$  and the corresponding principal radii of curvature, as well as the initial values  $\vec{E}^r(0)$  and  $\vec{E}^d(0)$ , depend on the parameters of the incident field  $\vec{E}^i$  and on the geometry of the curved edge. Therefore, a detailed description of the edge is required.

#### 7.5.4. Description of the curved edge and the reflector surface

In GTD, the diffracting obstacle is modelled as a curved wedge with interior wedge angle  $(2-n)\pi$ . For a reflector antenna this wedge reduces to an infinitely thin surface with a sharp edge, i.e.  $n=2$ ; see fig. 7.7a. The reflector surface is denoted by  $\Sigma$ , its unit normal (pointing outward from the convex face of  $\Sigma$ ) by  $\hat{n}^\Sigma$ , and its principal directions by  $\hat{x}_1^\Sigma$  and  $\hat{x}_2^\Sigma$ , with corresponding principal radii of curvature  $R_1^\Sigma$  and  $R_2^\Sigma$ . Let P be a typical point of the curved edge  $\Gamma$  of the surface. At P we introduce the unit tangent vector  $\hat{t}$  to  $\Gamma$  and the unit vector  $\hat{n}^\Gamma$  normal to  $\Gamma$  pointing away from the centre of curvature; the radius of curvature of  $\Gamma$  at P is denoted by  $R^\Gamma$ , with  $R^\Gamma > 0$ .

The incident field  $\vec{E}^i$  at P propagates in the direction  $\hat{k}^i$ , which makes an angle  $\beta$  with  $\hat{t}$  (fig. 7.7b). The plane spanned by  $\hat{t}$  and  $\hat{k}^i$  is known as the *edge-fixed plane of incidence*. The principal direction  $\hat{x}_1^i$  of the incident wavefront at P makes an angle  $\Omega^i$  with this plane. Similarly, the *edge-fixed plane of reflection* is defined as the plane spanned by  $\hat{t}$  and  $\hat{k}^r$ , and the principal direction  $\hat{x}_1^r$  of the reflected wavefront at P makes an angle  $\Omega^r$  with the latter plane (not shown in fig. 7.7b). The propagation direction  $\hat{k}^r$  of the reflected field  $\vec{E}^r$  follows by Snell's law, i.e.,



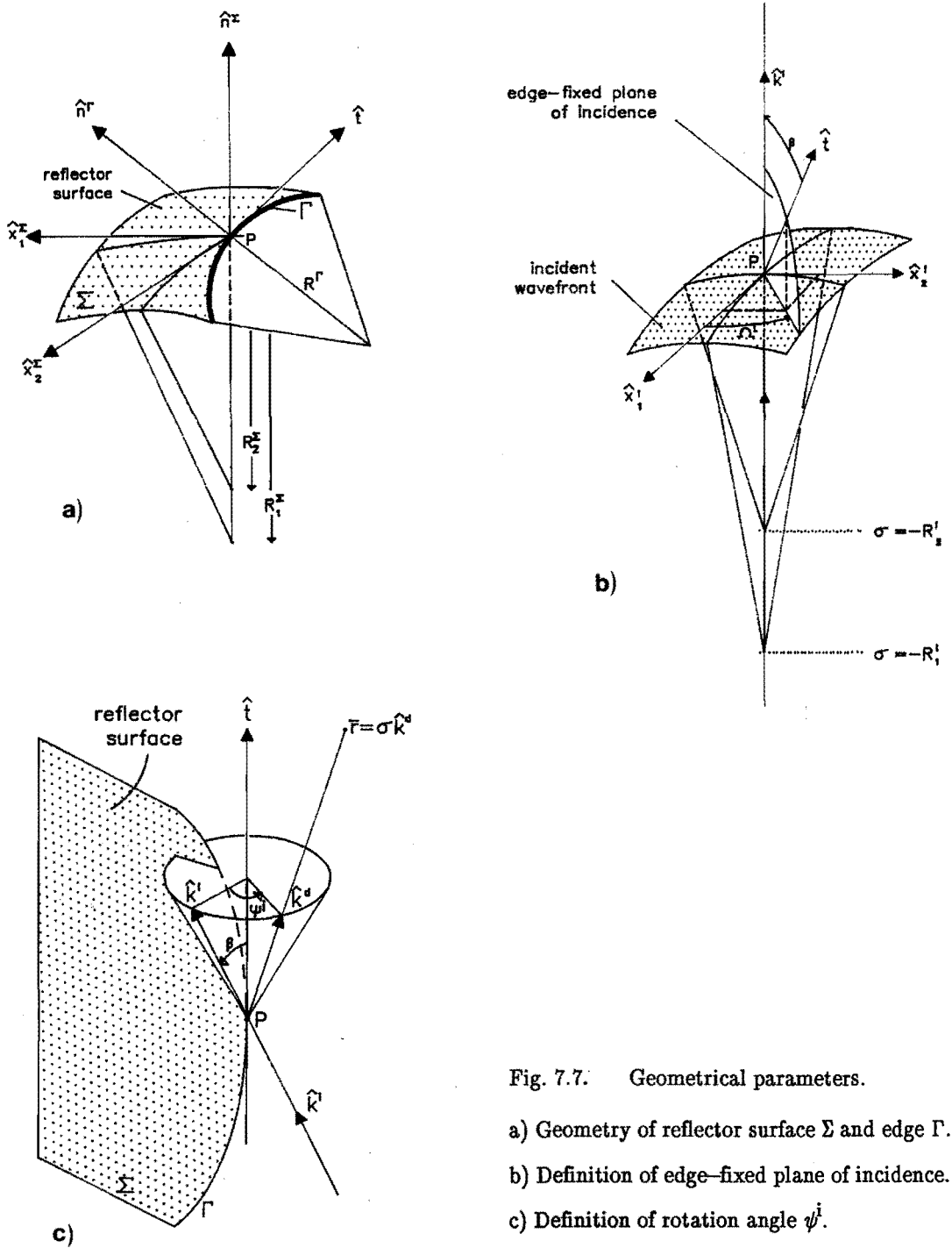


Fig. 7.7. Geometrical parameters.

a) Geometry of reflector surface  $\Sigma$  and edge  $\Gamma$ .

b) Definition of edge-fixed plane of incidence.

c) Definition of rotation angle  $\psi^i$ .

$$\hat{k}^r = \hat{k}^i - 2(\hat{k}^i \cdot \hat{n}^\Sigma) \hat{n}^\Sigma. \quad (7.18)$$

According to the law of edge diffraction (see sec. 7.5.2), the incident ray at P gives rise to a circular cone of diffracted rays (fig. 7.7c) with axis  $\hat{t}$  and semi-angle  $\beta$ . A specific diffracted ray propagates in the direction  $\hat{k}^d$ , which follows from  $\hat{k}^i$  by a rotation around  $\hat{t}$  through an angle  $\psi^i$  (as defined in sec. 6.3), or equivalently, by a rotation of  $\hat{k}^r$  around  $\hat{t}$  through an angle  $\psi^r$ . This rotation operation is mathematically expressed as [16]

$$\hat{k}^d = \text{rot}(\hat{t}, \psi^i) \hat{k}^i = \text{rot}(\hat{t}, \psi^r) \hat{k}^r. \quad (7.19)$$

#### 7.5.5. Auxiliary parameters

For a complete description of the reflected and diffracted fields, the principal directions  $\hat{x}_{1,2}^{r,d}$  of the wavefronts are needed, as well as the corresponding principal radii of curvature  $R_{1,2}^r$  and  $R_c$ ; see (7.17). In addition, an expression is needed for the detour parameter  $\xi^{i,r}$ , which is defined (as in sec. 6.3) as the square root of the difference between the phase along the diffracted ray and the phase along the incident (or reflected) ray through the observation point. These auxiliary parameters can be calculated from the parameters of the incident field. Omitting further details, we quote the necessary formulas from the literature.

i) Parameters related to  $\hat{E}^r$ . The parameters  $\hat{x}_{1,2}^r$  and  $R_{1,2}^r$  are determined by geometrical optics. The general procedure is rather laborious, but it is well described by Lee [18]. Introduce the 2x2 curvature matrices  $\bar{Q}^i$  and  $\bar{Q}^\Sigma$ , the 2x2 matrix  $\bar{P}$  and the scalar  $p_{33}$  as

$$Q_{11}^{i,\Sigma} = 1/R_1^{i,\Sigma}, \quad Q_{22}^{i,\Sigma} = 1/R_2^{i,\Sigma}, \quad Q_{12}^{i,\Sigma} = Q_{21}^{i,\Sigma} = 0; \quad (7.20a)$$

$$P_{mn} = \hat{x}_m^i \cdot \hat{x}_n^\Sigma, \quad m, n = 1, 2; \quad p_{33} = \hat{k}^i \cdot \hat{n}^\Sigma. \quad (7.20b)$$

Next, we define the preliminary unit vectors  $(\hat{x}_{1,2}^r)'$  by

$$(\hat{x}_{1,2}^r)' = \hat{x}_{1,2}^i - 2 (\hat{x}_{1,2}^i \cdot \hat{n}^\Sigma) \hat{n}^\Sigma. \quad (7.21)$$

In general, the vectors  $(\hat{x}_{1,2}^r)'$  are not the principal directions of the reflected wavefront. It has been shown by Deschamps [19] that the curvature matrix  $\bar{Q}^r$  of the reflected wavefront can now be calculated from

$$\bar{Q}^r = \bar{Q}^i - 2 p_{33} (\bar{P})^{-T} \bar{Q}^\Sigma (\bar{P})^{-1}, \quad (7.22)$$

where  $(\bar{P})^{-1}$  is the inverse of  $\bar{P}$  and  $(\bar{P})^{-T}$  is the transposed of  $(\bar{P})^{-1}$ . If  $\bar{Q}^r$  happens to be diagonal, the vectors  $(\hat{x}_{1,2}^r)'$  coincide with the principal directions  $\hat{x}_{1,2}^r$ . Otherwise, a diagonalization of  $\bar{Q}^r$  yields  $\hat{x}_{1,2}^r$  and the corresponding radii of curvature  $R_{1,2}^r$ . By carrying out this diagonalization as in [14, appendix 1], we obtain the results

$$1/R_{1,2}^r = \frac{1}{2} (Q_{11}^r + Q_{22}^r) \pm \frac{1}{2} \left[ (Q_{11}^r - Q_{22}^r)^2 + 4(Q_{12}^r)^2 \right]^{1/2}, \quad (7.23a)$$

$$\hat{x}_1^r = \left[ (Q_{22}^r - 1/R_1^r)(\hat{x}_1^r)' - Q_{12}^r(\hat{x}_2^r)' \right] \left[ (Q_{22}^r - 1/R_1^r) + (Q_{12}^r)^2 \right]^{-1/2}, \quad (7.23b)$$

$$\hat{x}_2^r = -\hat{k}^r \times \hat{x}_1^r. \quad (7.23c)$$

Here, the elements  $Q_{11}^r$ ,  $Q_{22}^r$  and  $Q_{12}^r = Q_{21}^r$  of the curvature matrix  $\bar{Q}^r$  follow from (7.22) as

$$Q_{11}^r = \frac{1}{R_1^i} - \frac{2P_{33}}{|\bar{P}|^2} \left[ \frac{P_{22}^2}{R_1^\Sigma} + \frac{P_{21}^2}{R_2^\Sigma} \right], \quad (7.24a)$$

$$Q_{12}^r = Q_{21}^r = \frac{2P_{33}}{|\bar{P}|^2} \left[ \frac{P_{22}P_{12}}{R_1^\Sigma} + \frac{P_{11}P_{21}}{R_2^\Sigma} \right], \quad (7.24b)$$

$$Q_{22}^r = \frac{1}{R_2^i} - \frac{2P_{33}}{|\bar{P}|^2} \left[ \frac{P_{12}^2}{R_1^\Sigma} + \frac{P_{11}^2}{R_2^\Sigma} \right], \quad (7.24c)$$

ii) Parameters related to  $\hat{E}^d$ . Proceeding along the diffracted ray through the edge point P in the direction  $\hat{k}^d$ , the principal directions of the diffracted wavefront remain the same. These directions are given by  $\hat{x}_1^d = \hat{x}_2^d \times \hat{k}^d$  and  $\hat{x}_2^d = (\hat{k}^d \times \hat{t})/\sin\beta$ , and the corresponding principal radii of curvature of the wavefront at P are given by  $R_1^d = R_c$  and  $R_2^d = 0$ , where  $R_c$  is the interfocal distance. The latter can be calculated by means of [16, eq. (4.7)], viz.

$$\frac{1}{R_c} = \frac{1}{R_0^i} - \frac{(\hat{k}^i - \hat{k}^d) \cdot \hat{n}^r}{R^i \sin^2\beta} = \frac{1}{R_0^r} - \frac{(\hat{k}^r - \hat{k}^d) \cdot \hat{n}^r}{R^r \sin^2\beta}, \quad (7.25)$$

where  $R_0^{i,r}$  is the radius of curvature of the incident or reflected wavefront in the edge-fixed plane of incidence or reflection (see fig. 7.7b), given by [16, eq. (4.6)], viz.

$$\frac{1}{R_0^{i,r}} = \frac{\cos^2\Omega^{i,r}}{R_1^{i,r}} + \frac{\sin^2\Omega^{i,r}}{R_2^{i,r}}. \quad (7.26)$$

iii) The detour parameter. The general expression for the detour parameter  $\xi^{i,r}$  is rather difficult to handle. However, it will turn out that an expression is needed only for  $|\psi^{i,r}| \ll 1$ , i.e., near the shadow boundaries. In these regions,  $\xi^{i,r}$  is well

approximated by [16, eq. (6.3) and appendix A]

$$\xi^{i,r} = \sin\beta \sin\left(\frac{1}{2}\psi^{i,r}\right) \sqrt{2k_0} \frac{a(\sigma, R_1^{i,r}, R_2^{i,r})}{b(\sigma, R_0^{i,r})}. \quad (7.27)$$

The sign of  $\xi^{i,r}$  (like the sign of  $\psi^{i,r}$ ) serves as a shadow indicator of  $\vec{E}^i$  or  $\vec{E}^r$ , just as in the two-dimensional knife-edge diffraction problem (see sec. 6.3).

A problem occurs if  $a(\sigma, R_1^{i,r}, R_2^{i,r})$  or  $b(\sigma, R_0^{i,r})$  is imaginary. This may happen with converging wavefronts, when  $R_{1,2}^{i,r} < 0$ ; see (7.15), (7.16) and fig. 7.7b. The proper handling of this case is not well understood in the literature [14, sec. VB; 15; 16, sec. VA]. We return to this problem in secs. 7.5.7 and 7.6.1.

#### 7.5.6. The GTD solution

Referring to (7.17), the only parameters of  $\vec{E}^r$  and  $\vec{E}^d$  which are still unknown are the initial values  $\vec{E}^r(0)$  and  $\vec{E}^d(0)$  at the diffraction point P. These values can be calculated from the incident field  $\vec{E}^i(0)$  at P.

The initial value of  $\vec{E}^r$  follows from the boundary condition for a perfectly conducting surface; thus,  $\vec{E}^r(0)$  is the mirror image of  $\vec{E}^i(0)$  with respect to the normal  $\hat{n}^\Sigma$ , i.e.,

$$\vec{E}^r(0) = -\vec{E}^i(0) + 2(\vec{E}^i(0) \cdot \hat{n}^\Sigma) \hat{n}^\Sigma. \quad (7.28)$$

The "initial" value  $\vec{E}^d(0)$  according to GTD can be written as [16]

$$\vec{E}^d(0) = D^i \text{rot}(\hat{t}, \psi^i) \vec{E}^i(0) + \{i \rightarrow r\}, \quad (7.29)$$

where the rotation operator is defined in (7.19), and the notation  $\{i \rightarrow r\}$  means repeating all terms after the equality sign with the superscript "i" changed into "r". The diffraction coefficient  $D^{i,r}$  is given by

$$D^{i,r} = \frac{\exp(-j\pi/4)}{\sqrt{8\pi k_0} \sin\beta \sin(\frac{1}{2}\psi^{i,r})}, \quad (7.30)$$

which is equal to the diffraction coefficient of a knife edge for an obliquely incident plane wave, see sec. 6.7.3.

Thus, the GTD solution of the curved-edge diffraction problem can be summarized as follows. The total field  $\vec{E}$  is given by

$$\vec{E} = \vec{E}^g + \vec{E}^d, \quad (7.31a)$$

consisting of the geometrical-optics field

$$\vec{E}^g = \Theta(-\xi^i) \vec{E}^i + \{i \rightarrow r\} \quad (7.31b)$$

(where  $\Theta(\xi)$  is the unit step function), and the diffracted field

$$\vec{E}^d(\sigma \hat{k}^d) = D^i \text{rot}(\hat{t}, \psi^i) \vec{E}^i(0) b(\sigma, R_c) \exp(-jk_0 \sigma) + \{i \rightarrow r\}. \quad (7.31c)$$

These formulas are of the same form as the scalar formulas (6.26), (6.9) and (6.27), respectively.

7.5.7. The UTD solution

The GTD solution (7.31) becomes infinite at the shadow boundaries where  $\psi^{i,r}=0$ . As in the case of two-dimensional knife-edge diffraction (sec. 6.4.5), UTD removes these singularities by means of the transition function  $F_{KP}$ , defined in (6.32). Thus, to obtain the UTD solution,  $\vec{E}^d$  in (7.31) is replaced by  $\vec{E}^D$ , given by

$$\vec{E}^D(\sigma \hat{k}^d) = F_{KP}((\xi^i)^2) D^i \text{rot}(\hat{t}, \psi^i) \vec{E}^i(0) b(\sigma, R_c) \exp(-jk_0 \sigma) + \{i \rightarrow r\}. \quad (7.32)$$

With the transition function  $F_{KP}$ , the total field  $\vec{E}$  is continuous across the shadow boundaries, whereas away from these boundaries (where  $(\xi^{i,r})^2 \gg 1$ ), one has  $F_{KP} \approx 1$  and  $\vec{E}^D$  reduces to  $\vec{E}^d$ . Thus, the evaluation of  $F_{KP}((\xi^{i,r})^2)$  is only required in the vicinity of the shadow boundaries.

A problem occurs in the case of a converging incident or reflected wavefront, when a focus is located at the shadow boundary. Then,  $\xi^{i,r}$  is imaginary (see the end of sec. 7.5.5) and the function  $F_{KP}$ , as defined in (6.32), can no longer be used. For this case, the following continuation of  $F_{KP}$  has been suggested [14,15]:

$$F_{KP}(-|\xi|^2) = F_{KP}^*(|\xi|^2), \quad (7.33)$$

where the asterisk denotes the complex conjugate. Kouyoumjian and Pathak [14,15] have reported good numerical results with (7.33), but they admit that it lacks a satisfactory theoretical justification.

The continuation (7.33) of  $F_{KP}$  has been constructed in such a way that it has the proper behaviour for  $|\xi| \rightarrow \infty$  (i.e., approaching unity) and for  $|\xi| \rightarrow 0$  (i.e., yielding continuity of  $\vec{E}$  across the shadow boundaries). However, it has been shown by Brown [20] that the choice of (7.33) does not guarantee continuity of  $\vec{E}$  in every

case. Instead of (7.33), an alternative continuation of  $F_{KP}$  ensures continuity of  $\vec{E}$ , although this continuation also lacks theoretical justification [20].

These problems occur if a focus of the converging incident or reflected wavefronts is located at the shadow boundary. It will be argued in sec. 7.6.1 that such a situation does not arise in the site-shielding problem as described in sec. 7.2. Therefore, we do not elaborate any further on this matter.

Slope diffraction is not included in the UTD solution (7.32), nor in the GTD solution (7.31). Its effect depends on the spatial variation of  $\vec{E}^{i,r}$  in the vicinity of the edge, and becomes important for small  $\vec{E}^{i,r}(0)$ . In case  $\vec{E}^{i,r}(0)=0$ , appropriate expressions for the slope-diffraction terms are available [15; 21, sec. 5.5], which are similar to the expressions presented for the two-dimensional knife-edge diffraction problem (sec. 6.5.5). Usually these terms are small compared to the dominant terms given in (7.31) or (7.32). Therefore, we have not included slope diffraction in our calculations.

#### 7.5.8. Limitations of the GTD/UTD solution

We conclude our description of the general GTD/UTD by pointing out some limitations of these theories:

i) In the vicinity of the shadow boundaries, the GTD solution becomes invalid and should be replaced by the (more complicated) UTD solution.

ii) Both theories fail at caustics of  $\vec{E}^i$ ,  $\vec{E}^r$  or  $\vec{E}^d$ . The fields at caustic points are to be determined by a separate analysis [22-26].

iii) Close to grazing incidence towards the reflector, UTD cannot be applied to determine the diffracted field in the vicinity of the shadow boundaries; see [14, sec. VA]. No problems arise at observation points away from these boundaries, where the diffracted field can be determined by means of GTD.



iv) In the case of a converging wavefront, the detour parameter (7.27) may become imaginary and the transition function  $F_{KP}$  of UTD cannot be applied. The proper handling of this case is not well understood. As in (iii), this causes no problem away from the shadow boundaries, because GTD can be applied there.

v) An appropriate expression for the slope-diffraction terms is not available, unless  $\vec{E}^i(0)$  vanishes, see sec. 6.5.5. If  $\vec{E}^i(0)$  is not too small, slope diffraction can be neglected. In practice, the slope-diffraction terms for  $\vec{E}^i(0) \neq 0$  are often approximated by the corresponding terms for  $\vec{E}^i(0) = 0$  [15; 21, sec. 5.5].

## 7.6. Application of GTD/UTD to the site-shielding problem

### 7.6.1. *General considerations*

As argued in sec. 7.4, the site-shielding problem of sec. 7.2 consists of a knife-edge diffraction problem at the obstacle rim and a reflector-edge diffraction problem at the antenna. The former problem can be solved by the methods of chapter 6. The latter problem is now solved by the general GTD/UTD described in sec. 7.5.

The incident field  $\vec{E}^i$  at the antenna is the field diffracted by the obstacle edge which is an apparent line source of  $\vec{E}^i$ . The field  $\vec{E}^i$  causes a reflected field  $\vec{E}^r$  and an edge-diffracted field  $\vec{E}^d$  (or  $\vec{E}^D$ ).

The incident field  $\vec{E}^i(F)$  at the paraboloid focus can be calculated directly by the methods of chapter 6. The field  $\vec{E}^i(F)$  is weighted by the radiation pattern of the antenna feed. In addition, possible blockage of the direct ray by the reflector should be taken into account.

Owing to the antenna pointing, the reflected field  $\vec{E}^r$  at  $F$  is zero. This follows from the parabolic shape of the reflector: a reflected ray reaches  $F$  if, and only if, the corresponding incident ray is parallel to the axis of the antenna. Thus, for wide-angle

reception the focus  $F$  is always in the shadow region of  $\vec{E}^r$ , and not close to the shadow boundary of  $\vec{E}^r$ .

The diffracted rays emanate from the reflector edge. Any diffracted ray through  $F$  is perpendicular to the tangent  $\hat{t}$  to the edge. Therefore, according to the law of edge diffraction, the corresponding incident ray also makes an angle  $\beta=\pi/2$  with  $\hat{t}$ . This property is utilized in sec. 7.6.2 to determine the location of the diffraction points on the reflector edge. The fact that  $\beta=\pi/2$  implies that the cone of diffracted rays degenerates into a plane perpendicular to  $\hat{t}$  (see sec. 6.7.3).

Just like the direct ray to the feed, a ray incident on a diffraction point may be blocked by some part of the reflector (fig. 7.8). In this case, the corresponding diffracted ray results from double diffraction, which has been neglected in our calculations, as mentioned in sec. 7.4.1.

We observe that the limitations of GTD/UTD (items  $i-v$  in sec. 7.5.8) appear to be unimportant for the present application. In particular, the feed centre  $F$  is never located on a caustic of  $\vec{E}^i$ ,  $\vec{E}^r$  or  $\vec{E}^d$  (item  $ii$ ), because of the wide-angle incidence

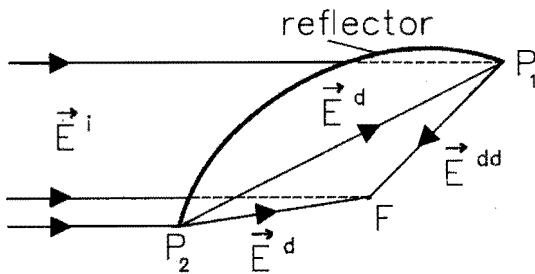


Fig. 7.8. Blockage of incident rays by the reflector.

$F$ : focal point;  $P_1$  and  $P_2$ : diffraction points;  $\vec{E}^i$ : incident field;  $\vec{E}^d$ : (singly) diffracted field;  $\vec{E}^{dd}$ : doubly diffracted field.

of  $\vec{E}^i$ . At grazing incidence (item *iii*), F is not located in the vicinity of a shadow boundary. The problem with a converging wavefront of  $\vec{E}^r$  (item *iv*), which arises for example for azimuth  $\varphi_A=0$ , is unimportant, because F is not located close to the shadow boundary of  $\vec{E}^r$ . Finally, slope diffraction (item *v*) is neglected in the present application, as explained in sec. 7.5.7.

7.6.2. Determination of the diffraction points

Any point P on the reflector edge is characterized by its spherical coordinates  $(\rho, \psi, \varphi)$ , with  $\rho=\rho_0=f+D^2/16f$  and  $\psi=\psi_0=2\arctan(D/4f)$ , see sec. 7.4.2. We introduce the unit vectors  $\hat{e}_0$  and  $\hat{e}_{\pi/2}$  in the aperture plane (fig. 7.9), with  $\hat{e}_0$  lying in the half-plane  $\varphi=0$  and  $\hat{e}_{\pi/2}$  in the half-plane  $\varphi=\pi/2$ . With respect to the Cartesian  $(x,y,z)$  coordinate system, these vectors have components

$$\hat{e}_0 = \begin{pmatrix} \sin\varphi_E \cos\varphi_A \\ \sin\varphi_E \sin\varphi_A \\ \cos\varphi_E \end{pmatrix}, \quad \hat{e}_{\pi/2} = \begin{pmatrix} \sin\varphi_A \\ -\cos\varphi_A \\ 0 \end{pmatrix}. \quad (7.34)$$

The position of the focal point F of the paraboloid is then given by

$$\vec{x}_F = \vec{x}_M - \rho_M (\hat{e}_0 \times \hat{e}_{\pi/2}), \quad (7.35)$$

where  $\rho_M=f-D^2/16f$ . The aperture centre M has Cartesian coordinates  $x=x_M, y=0, z=z_M$ . The position of the point P at the reflector edge is determined by

$$\vec{x}_P = \vec{x}_M + \frac{1}{2}D\cos\varphi \hat{e}_0 + \frac{1}{2}D\sin\varphi \hat{e}_{\pi/2}. \quad (7.36)$$

The tangent  $\hat{t}$  to the reflector edge at P can be represented by

$$\hat{t} = \sin\varphi \hat{e}_0 - \cos\varphi \hat{e}_{\pi/2} \quad (7.37)$$

In the presence of the knife-edge obstacle, the incident field  $\vec{E}^i$  at the antenna is due to an apparent line source at the obstacle edge. Then the direction  $\hat{k}^i$  of the incident ray through P is perpendicular to the y-axis. Thus, the corresponding "source point"  $Q_P$  (fig. 7.9) has coordinates  $x=0, y=y_P, z=z_0$ , and  $\hat{k}^i$  follows from

$$\hat{k}^i = \frac{\vec{x}_P - \vec{x}_{Q_P}}{|\vec{x}_P - \vec{x}_{Q_P}|} = [x_P^2 + (z_0 - z_P)^2]^{-1/2} \begin{pmatrix} x_P \\ 0 \\ z_P - z_0 \end{pmatrix} \quad (7.38)$$

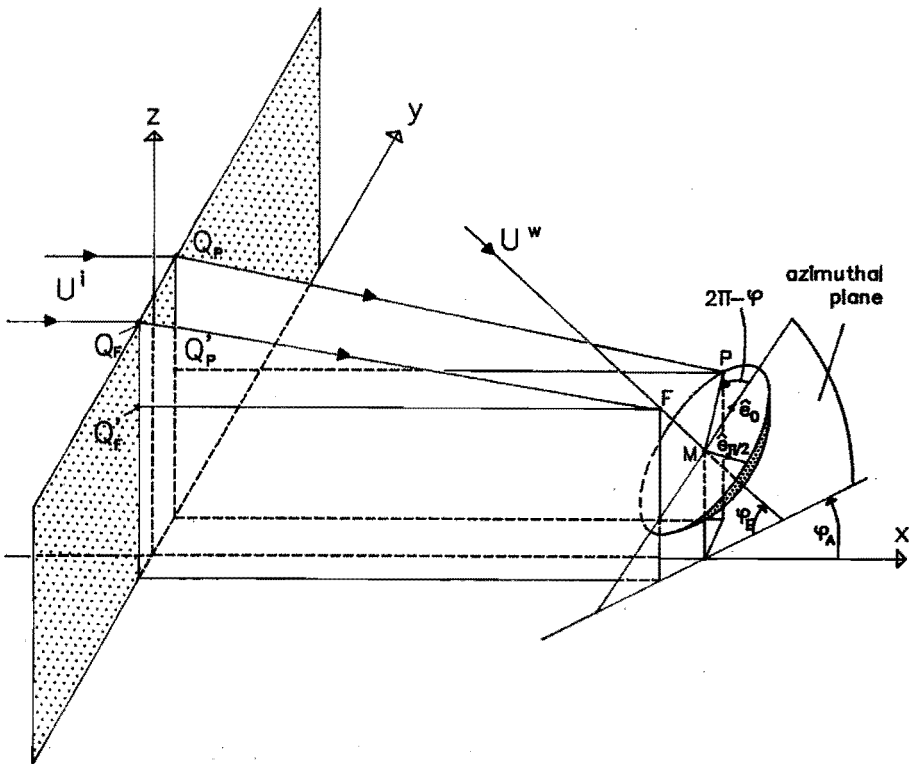


Fig. 7.9. Introduction of the unit vectors  $\hat{e}_0$  and  $\hat{e}_{\pi/2}$  in the aperture plane, and of the "source points"  $Q_P, Q'_P, Q_F$  and  $Q'_F$  in the yz-plane.

The condition for the point P to be a diffraction point can now be expressed as

$$\cos\beta = (\hat{\mathbf{k}}^i \cdot \hat{\mathbf{t}}) = 0. \quad (7.39)$$

Substitution of (7.36)–(7.38) into (7.39) yields an equation for  $\varphi$ , which determines the diffraction point P. This equation can be written as

$$A_1 \cos\varphi + A_2 \sin\varphi + A_3 \cos 2\varphi + A_4 \sin 2\varphi = 0, \quad (7.40)$$

where (7.34) has been used, and the constants  $A_1$ – $A_4$  are defined by

$$\begin{aligned} A_1 &= x_M \sin\varphi_A, \\ A_2 &= \Delta z \cos\varphi_E - x_M \sin\varphi_E \cos\varphi_A, \\ A_3 &= \frac{1}{2} D \sin\varphi_E \sin\varphi_A \cos\varphi_A, \\ A_4 &= \frac{1}{4} D (\sin^2\varphi_E \sin^2\varphi_A - \cos^2\varphi_A). \end{aligned} \quad (7.41)$$

In general, eq. (7.40) has four solutions for  $\varphi$ , corresponding to four diffraction points. However, if the antenna aperture cylinder clears the obstacle, then only two solutions for  $\varphi$  are real. This is illustrated by considering the special case  $\varphi_A = 0$ . Then, from (7.41) we obtain  $A_1 = A_3 = 0$ ,  $A_2 = -r_M \sin(\varphi_E - \theta_M)$  and  $A_4 = -D/4$ ; thus (7.40) becomes

$$[r_M \sin(\varphi_E - \theta_M) + \frac{1}{2} D \cos\varphi] \sin\varphi = 0. \quad (7.42)$$

If the aperture cylinder is unobstructed (see (7.10)), the factor in square brackets in (7.42) is positive for all  $\varphi$ . The only real solutions of (7.42) are then  $\varphi = 0$  and  $\varphi = \pi$ , corresponding to the upper and lower points  $P_1$  and  $P_2$  of the reflector edge.

For  $\varphi_A=0$ , the aperture cylinder just clears the obstacle if  $\varphi_E$  assumes the critical value determined by  $r_M \sin(\varphi_E - \theta_M) = D/2$ ; cf. (7.10). In that case, eq. (7.42) has the solutions  $\varphi=0$  and  $\varphi=\pi$ , where the latter solution corresponds to three coalescing diffraction points at  $P_2$ . It can be shown that along the reflected/diffracted ray  $P_2F$  both the reflected wavefront and the diffracted wavefront have a focus at the feed centre  $F$ . In this case the GTD/UTD description of the field breaks down in the vicinity of  $F$  and one should apply an appropriate caustic correction factor [25,26]. The same difficulty arises if the elevation angle  $\varphi_E$  is close to the critical value determined above. In the sequel we shall stick to a realistic obstacle clearance as expressed by (7.13), when only two diffraction points need to be considered.

An analytic solution of (7.40) is, in general, impossible to obtain. However, eq. (7.40) can easily be solved numerically, e.g. by the bisection method. For  $0 \leq \varphi_A \leq \pi$ , one diffraction point ( $P_1$ ) with polar angle  $\varphi = \varphi_1$  is located on the right half of the reflector edge ( $0 \leq \varphi_1 \leq \pi$ ) and the other one ( $P_2$ ) with polar angle  $\varphi = \varphi_2$  is located on the left half of the reflector edge ( $\pi \leq \varphi_2 \leq 2\pi$ ). These points are in general not diametrically opposite.

In the absence of the knife-edge obstacle, the incident field  $\vec{E}^i$  at the antenna is a (non-)uniform plane wave that propagates in the direction  $\hat{k}^i = \hat{e}_x$ . The condition (7.39) for the point  $P$  to be a diffraction point can now be written as

$$\sin \varphi_A \cos \varphi - \sin \varphi_E \cos \varphi_A \sin \varphi = 0. \quad (7.43)$$

The latter equation has two solutions  $\varphi = \varphi_1$  and  $\varphi = \varphi_2 = \varphi_1 + \pi$ , with  $0 \leq \varphi_1 \leq \pi$ . Thus, in the absence of the obstacle, the corresponding diffraction points  $P_1$  and  $P_2$  are exactly diametrically opposite.

7.6.3. Calculation of the diffracted field

In this section we present expressions for the geometrical and auxiliary parameters that are needed to determine the geometrical-optics reflected field and the diffracted field according to GTD/UTD (see secs. 7.5.4–7.5.7). We employ the obstacle-fixed Cartesian  $(x, y, z)$  coordinate system shown in fig. 7.9.

In the absence of the obstacle, the *incident field*  $\vec{E}^i$  at the antenna is a (non-) uniform plane wave, propagating in a direction parallel to the  $x$ -axis. Its parameters are

$$\begin{aligned} \vec{E}^i(P_n) &= E^i(P_n) \hat{e}_{\text{pol}} = \vec{E}^i(Q_p) \exp(-jk_0 r \cos \theta_n); \\ \hat{k}^i &= \hat{e}_x; \\ \hat{x}_1^i &= \hat{e}_y, \quad \hat{x}_2^i = \hat{e}_z; \\ R_1^i &= R_2^i = \infty; \\ \hat{e}_{\text{pol}} &= \hat{x}_1^i (\hat{x}_2^i) \text{ for horizontal (vertical) polarization.} \end{aligned} \tag{7.44}$$

Here,  $P_n$  ( $n=1,2$ ) is the reflector-edge diffraction point;  $P_n$  has polar coordinates  $(r_n, \theta_n)$  with respect to the obstacle edge, which can be determined from (7.36);  $Q_p$  is the projection of  $P_n$  on the  $yz$ -plane (fig. 7.9);  $\hat{e}_{\text{pol}}$  is the polarization vector of  $\vec{E}^i$ . The remaining symbols in (7.44) have been defined in sec. 7.5.

In the presence of the knife-edge obstacle, the obstacle edge serves as an apparent line source of  $\vec{E}^i(P_n)$ . Then, (7.44) should be replaced by

$$\begin{aligned} \vec{E}^i(P_n) &= E^i(P_n) \hat{e}_{\text{pol}} = \mathcal{S}\{\vec{E}^i(Q_p)\}; \\ \hat{k}^i &= \cos \theta_n \hat{e}_x - \sin \theta_n \hat{e}_z; \\ \hat{x}_1^i &= \hat{e}_y, \quad \hat{x}_2^i = \sin \theta_n \hat{e}_x + \cos \theta_n \hat{e}_z; \\ R_1^i &= \infty, \quad R_2^i = r_n; \\ \hat{e}_{\text{pol}} &= \hat{x}_1^i (\hat{x}_2^i) \text{ for horizontal (vertical) polarization.} \end{aligned} \tag{7.45}$$

Here,  $Q_P$  is the projection of  $P_n$  on the obstacle edge (fig. 7.9) and  $\mathcal{D}$  stands for the knife-edge diffraction operator. The latter can be evaluated by the methods of chapter 6.

The incident field  $\vec{E}^i(F)$  at the feed centre is determined in the same manner as  $\vec{E}^i(P_n)$ . In fig. 7.9, the "source points"  $Q_P'$  and  $Q_P$  corresponding to  $F$  have been indicated: these points are the projections of  $F$  on the  $yz$ -plane and on the obstacle edge, respectively. If the incident ray concerned is blocked by the reflector,  $\vec{E}^i(P_n)$  or  $\vec{E}^i(F)$  is set equal to zero.

The *reflector surface* and its edge at  $P$  are described by the following parameters (see appendix C):

$$\begin{aligned}
 \hat{n}^\Sigma &= \sin(\psi_0/2) (\cos\varphi \hat{e}_0 + \sin\varphi \hat{e}_{\pi/2}) + \cos(\psi_0/2) (\hat{e}_0 \times \hat{e}_{\pi/2}) ; \\
 \hat{x}_1^\Sigma &= \sin\varphi \hat{e}_0 - \cos\varphi \hat{e}_{\pi/2} ; \\
 \hat{x}_2^\Sigma &= \cos(\psi_0/2) (\cos\varphi \hat{e}_0 + \sin\varphi \hat{e}_{\pi/2}) - \sin(\psi_0/2) (\hat{e}_0 \times \hat{e}_{\pi/2}) ; \\
 R_1^\Sigma &= 2f/\cos(\psi_0/2) , \quad R_2^\Sigma = 2f/\cos^3(\psi_0/2) ; \\
 \hat{t} &= \sin\varphi \hat{e}_0 - \cos\varphi \hat{e}_{\pi/2} ; \\
 \hat{n}^\Gamma &= \cos\varphi \hat{e}_0 + \sin\varphi \hat{e}_{\pi/2} ; \\
 R^\Gamma &= D/2 .
 \end{aligned} \tag{7.46}$$

Here,  $D$ ,  $f$  and  $\psi_0$  are antenna parameters related by (7.5c), whereas  $\hat{e}_0$  and  $\hat{e}_{\pi/2}$  are defined by (7.34);  $\varphi$  is the polar angle of  $P$  (fig. 7.9).

The parameters of the *reflected field*  $\vec{E}^r$  can now be calculated by the method of sec. 7.5. In particular, we determine the propagation direction  $\hat{k}^r$  from (7.18), the principal directions  $\hat{x}_{1,2}^r$  with corresponding principal radii of curvature  $R_{1,2}^r$  from (7.20)–(7.24), and the initial value  $\vec{E}^r(P)$  from (7.28).

The *diffracted field*  $\vec{E}^d$  at  $F$  propagates in the direction  $\hat{k}^d$ , which follows from (7.35)–(7.36) as



$$\hat{\mathbf{k}}^d = \frac{\vec{\mathbf{x}}_F - \vec{\mathbf{x}}_P}{|\vec{\mathbf{x}}_F - \vec{\mathbf{x}}_P|} = -\rho_0^{-1} \left[ \frac{1}{2} D \cos \varphi \hat{\mathbf{e}}_0 + \frac{1}{2} D \sin \varphi \hat{\mathbf{e}}_{\pi/2} + \rho_M (\hat{\mathbf{e}}_0 \times \hat{\mathbf{e}}_{\pi/2}) \right]. \quad (7.47)$$

The corresponding interfocal distance  $R_c$  for the diffracted wavefront is obtained from (7.25) with  $\beta = \pi/2$ , viz.

$$\frac{1}{R_c} = \frac{1}{R_0^i} - \frac{(\hat{\mathbf{k}}^i - \hat{\mathbf{k}}^d) \cdot \hat{\mathbf{n}}^\Gamma}{R^\Gamma}. \quad (7.48)$$

Here  $R_0^i$  is given by (7.26), which for  $\beta = \pi/2$  becomes (see fig. 7.7b)

$$\frac{1}{R_0^i} = \frac{(\hat{\mathbf{t}} \cdot \hat{\mathbf{x}}_1^i)^2}{R_1^i} + \frac{(\hat{\mathbf{t}} \cdot \hat{\mathbf{x}}_2^i)^2}{R_2^i}. \quad (7.49)$$

The rotation angles  $\psi^i$  and  $\psi^r$  are determined as follows. In the present case where  $\beta = \pi/2$ , the vectors  $\hat{\mathbf{k}}^i$ ,  $\hat{\mathbf{k}}^r$  and  $\hat{\mathbf{k}}^d$  all lie in the plane through the diffraction point P perpendicular to the tangent  $\hat{\mathbf{t}}$ . A cross-section of this plane with the reflector surface  $\Sigma$  is shown in fig. 7.10. Clearly, the line through P in the direction  $\hat{\mathbf{k}}^i$  (or  $\hat{\mathbf{k}}^r$ ) and the surface  $\Sigma$  divide the cross-section into three regions, two of which belong to the lit zone of  $\hat{\mathbf{E}}^i$  (or to the shadow zone of  $\hat{\mathbf{E}}^r$ ). For  $\hat{\mathbf{k}}^d$  in each region, the angles  $\psi^i$  and  $\psi^r$  are given in table 7.1.

We are now able to calculate the GTD solution  $\hat{\mathbf{E}}^d$  from (7.31c), i.e.,

$$\hat{\mathbf{E}}^d(\mathbf{F}) = \hat{\mathbf{E}}^d(\rho_0 \hat{\mathbf{k}}^d) = D^i \text{rot}(\hat{\mathbf{t}}, \psi^i) \hat{\mathbf{E}}^i(P) b(\rho_0, R_c) \exp(-jk_0 \rho_0) + \{i \rightarrow r\}, \quad (7.50)$$

which should be evaluated for both diffraction points  $P_1$  and  $P_2$ .

For the calculation of the UTD solution  $\hat{\mathbf{E}}^D$  from (7.32), we need the detour parameters  $\xi^{i,r}$ . From (7.27) we obtain

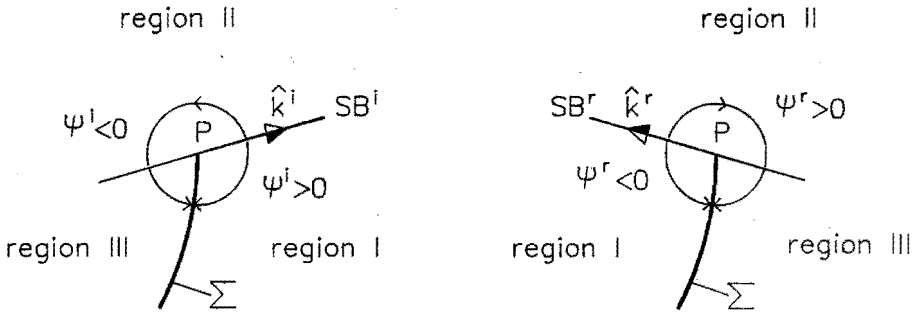


Fig. 7.10. Determination of the rotation angles  $\psi^i$  and  $\psi^r$ .

region	INCIDENT FIELD		REFLECTED FIELD	
I	shadow	$\psi^i = \arccos(\hat{k}^i \cdot \hat{k}^d) > 0$	lit	$\psi^r = -\arccos(\hat{k}^r \cdot \hat{k}^d) < 0$
SB	SB <sup>i</sup>	$\psi^i = 0$	SB <sup>r</sup>	$\psi^r = 0$
II	lit	$\psi^i = -\arccos(\hat{k}^i \cdot \hat{k}^d) < 0$	shadow	$\psi^r = \arccos(\hat{k}^r \cdot \hat{k}^d) > 0$
III	lit	$\psi^i = \arccos(\hat{k}^i \cdot \hat{k}^d) - 2\pi < 0$	shadow	$\psi^r = 2\pi - \arccos(\hat{k}^r \cdot \hat{k}^d) > 0$

Table 7.1. Determination of the rotation angles  $\psi^i$  and  $\psi^r$  in the regions I–III of fig. 7.10. The shadow boundary (SB) separates the lit zone and the shadow zone of  $\vec{E}^i$  or  $\vec{E}^r$ .

$$\xi^{i,r} = \sin\left(\frac{1}{2}\psi^{i,r}\right) \sqrt{2k_0} a(\rho_0, R_1^{i,r}, R_2^{i,r}) / b(\rho_0, R_0^{i,r}), \quad (7.51)$$

where the only unknown parameter  $R_0^i$  is determined in the same way as  $R_0^r$  from (7.49). For  $(\xi^{i,r})^2 > 10$ , we approximate  $F_{KP}((\xi^{i,r})^2)$  by unity, in which case  $\vec{E}^D$  reduces to  $\vec{E}^d$ .

7.6.4. Summation of the ray-optical fields at the feed

The three ray-optical fields arriving at the feed centre should be properly weighted by the radiation pattern  $G_f(\psi)$  of the feed and vectorially added, taking into account the polarization of the feed (sec. 7.4.2). This polarization is related to the polarization of the antenna (either vertical or horizontal), as expressed by (7.9), and is accounted for by taking the proper component of the arriving (transverse) fields.

In (7.9), the polarization vector  $\hat{e}_{\text{pol}}$  of the feed is expressed in terms of the unit vectors  $\hat{e}_\psi$  and  $\hat{e}_\varphi$  of the spherical  $(\rho, \psi, \varphi)$  coordinate system. For our calculations it is more convenient to rewrite  $\hat{e}_{\text{pol}}$  in terms of the antenna-fixed orthogonal unit vectors  $\hat{e}_0$ ,  $\hat{e}_{\pi/2}$  and  $\hat{e}_0 \times \hat{e}_{\pi/2}$  (see fig. 7.9); these vectors have components given by (7.34), with respect to the obstacle-fixed Cartesian  $(x, y, z)$  coordinate system. It is easily shown that (7.9) is equivalent to

$$\hat{e}_{\text{pol}} = (\cos\psi\cos^2\varphi - \sin^2\varphi) \hat{e}_0 + (1+\cos\psi) \sin\varphi\cos\varphi \hat{e}_{\pi/2} - \sin\psi\cos\varphi (\hat{e}_0 \times \hat{e}_{\pi/2}) \quad \text{for vertical antenna polarization,} \quad (7.52a)$$

$$\hat{e}_{\text{pol}} = (1+\cos\psi) \sin\varphi\cos\varphi \hat{e}_0 + (\cos\psi\sin^2\varphi - \cos^2\varphi) \hat{e}_{\pi/2} - \sin\psi\sin\varphi (\hat{e}_0 \times \hat{e}_{\pi/2}) \quad \text{for horizontal antenna polarization,} \quad (7.52b)$$

where the angles  $\psi$  and  $\varphi$  describe the direction of the relevant ray towards the feed centre F.

Thus, the received field  $E_0^R$  due to the directly incident field  $\vec{E}^i(F)$  is found to be

$$E_0^R = G_f(\psi) \vec{E}^i(F) \cdot \hat{e}_{\text{pol}}, \quad (7.53)$$

where  $\psi$  and  $\varphi$  are determined from the direction  $\hat{\mathbf{k}}^i$  of the direct ray (ray "0") towards F. In the Cartesian coordinate system this direction is given by

$$\hat{\mathbf{k}}^i = \hat{\mathbf{e}}_x, \quad (7.54a)$$

$$\hat{\mathbf{k}}^i = \frac{\vec{\mathbf{x}}_F - \vec{\mathbf{x}}_Q}{|\vec{\mathbf{x}}_F - \vec{\mathbf{x}}_Q|} = \left[ x_F^2 + (z_0 - z_F)^2 \right]^{-1/2} \begin{pmatrix} x_F \\ 0 \\ z_F - z_0 \end{pmatrix}, \quad (7.54b)$$

in the absence or presence of the obstacle, respectively, where  $\vec{\mathbf{x}}_F$  is given by (7.35). The angles  $\psi$  and  $\varphi$  are then readily obtained from

$$\cos \psi = -\hat{\mathbf{k}}^i \cdot (\hat{\mathbf{e}}_0 \times \hat{\mathbf{e}}_{\pi/2}), \quad (7.55a)$$

$$\cos \varphi = -(\hat{\mathbf{k}}^i \cdot \hat{\mathbf{e}}_0) / \sin \psi, \quad \sin \varphi = -(\hat{\mathbf{k}}^i \cdot \hat{\mathbf{e}}_{\pi/2}) / \sin \psi. \quad (7.55b)$$

The diffracted field  $\vec{\mathbf{E}}^d(F)$ , as determined in (7.50), arises at the diffraction points  $P_n$  ( $n=1,2$ ) on the reflector edge. Similarly to (7.53), the corresponding received field  $E_n^R$  ( $n=1,2$ ) can be expressed as

$$E_n^R = G_f(\psi_0) \vec{\mathbf{E}}^d(F) \cdot \hat{\mathbf{e}}_{\text{pol}}, \quad (7.56)$$

where  $\psi_0$  is the subtended angle of the reflector, given by (7.5c); the angle  $\varphi = \varphi_n$  is determined from (7.40) or (7.43) in the presence or absence of the obstacle, respectively.

The total received field  $E^R$  is the sum of at most three ray-optical fields that propagate along the direct ray "0" towards F and the diffracted rays "1" and "2" emanating from  $P_1$  and  $P_2$ , respectively (fig. 7.3). Let  $E_n^R$  denote the contribution associated with ray  $n$  ( $n=0,1,2$ ); then  $E^R$  can be written as

$$E^R = \sum_{n=0}^2 E_n^R. \quad (7.57)$$

The three terms  $E_n^R$  are in general complex, with amplitudes that are often of comparable magnitude, but with very different phases. Whereas  $|E_n^R|$  is normally a smooth function of the geometrical parameters (e.g.  $\varphi_A$ ,  $\varphi_E$ ,  $x_M$  or  $\Delta z$ ), the function  $\arg(E_n^R)$  varies rapidly. Hence,  $|E^R|$  calculated from (7.57) fluctuates rapidly with small changes of the geometry, because of constructive or destructive phasing effects between the individual contributions (unless one term is significantly larger than the other two). Therefore, a single value of  $|E^R|$  is not very meaningful, certainly not if the earth station performs limited tracking of the satellite, in which case  $\varphi_A$  and  $\varphi_E$  vary systematically within a small interval.

A more useful result is obtained by taking the average of  $|E^R|$  over a small interval of some geometrical parameter. Such an average result is conveniently represented by the power sum  $E_P^R$  of the individual terms  $E_n^R$  instead of the phasor sum (7.57), i.e.,

$$E_P^R = \left[ \sum_{n=0}^2 |E_n^R|^2 \right]^{1/2}. \quad (7.58)$$

This power sum behaves much more smoothly than the phasor sum calculated from (7.57). An exception is made in the transition region where the direct ray towards F gets blocked by the reflector; here, the phases of the individual contributions need to be included in order that  $E^R$  remains continuous. Only in this region, we employ the phasor sum (7.57).

The use of the power sum (7.58) implies that the phase pattern of the feed (which has been assumed to be constant, see sec. 7.4.2) becomes unimportant. Note

that the present use of the power sum resembles the use of the mode sum (4.43) instead of (4.42) in the theory of propagation in a tropospheric duct, see sec. 4.4.4.

Another approach would be to take the envelope of the maxima of the fluctuating function  $|E^R|$  calculated from (7.57), which is a well-known approach in the description of antenna sidelobes [27]. However, a precise definition of the envelope is difficult to present. In addition, we expect that comparison of the envelope of  $|E^R|$  for the shielded case with that for the unshielded case (in order to obtain the site-shielding factor) will yield approximately the same result as found by comparing the two power sums. Therefore, the latter approach is adopted in this thesis.

## 7.7. References

- [1] CCIR, Plenary Assembly, "Earth-station antennas for the fixed-satellite service", *Recommendations and Reports of the CCIR*, vol. IV-1, Rep. 390-5, Geneva, 1986.
- [2] P.J. Humphrey and D.H. Shinn, "Site shielding for antennas for satellite ground stations", *Marconi Technical Report*, MTR 72/116, 1972.
- [3] M.A. Streete and D.H. Shinn, "Site shielding for earth-station antennas", *Electr. Lett.*, vol. 10, no. 8, pp. 120-121, 1974.
- [4] D.I. Dalgleish, "The influence of interference on the siting of earth stations", *Proc. Int. Conf. Sat. Comm. Syst. Techn.*, *IEE Conf. Publ.*, no. 126, pp. 21-27, 1975.
- [5] CCIR, Plenary Assembly, "Propagation by diffraction", *Recommendations and Reports of the CCIR*, vol. V, Rep. 715-2, Geneva, 1986.
- [6] D. Carter, "Phase centers of microwave antennas", *IRE Trans. Ant. Prop.*, vol. AP-4, no. 3, pp. 597-600, 1956.

- [7] R.G. Kouyoumjian and P.A.J. Ratnasiri, "The calculation of the complete pattern of a reflector antenna", *Proc. Int. Electr. Conf. and Exhibition*, pp. 152-153, Toronto, 1969.
- [8] W.V.T. Rusch and O. Sorensen, "The geometrical theory of diffraction for axially symmetric reflectors", *IEEE Trans. Ant. Prop.*, vol. AP-23, no. 3, pp. 414-419, 1975.
- [9] C.A. Mentzer and L. Peters, "A GTD analysis of the far-out sidelobes of Cassegrain antennas", *IEEE Trans. Ant. Prop.*, vol. AP-23, no. 5, pp. 702-709, 1975.
- [10] M.S. Afifi, "Radiation from the paraboloid of revolution", *Electromagnetic wave theory* - part 2, J. Brown, ed., Pergamon, New York, pp. 669-687, 1967.
- [11] E. Yazgan and M. Safak, "Comparison of UTD and UAT in axially symmetric reflectors", *IEEE Trans. Ant. Prop.*, vol. AP-35, no. 1, pp. 113-116, 1987.
- [12] P.J.B. Claricoats and A.D. Olver, "*Corrugated horns for microwave antennas*", Peter Peregrinus, Stevenage, 1984.
- [13] R.E. Collin and F.J. Zucker, "*Antenna theory*" - part 1, McGraw-Hill, New York, 1969.
- [14] R.G. Kouyoumjian and P.H. Pathak, "A uniform geometrical theory of diffraction for an edge in a perfectly conducting surface", *Proc. IEEE*, vol. 62, no. 11, pp. 1448-1461, 1974.
- [15] R.G. Kouyoumjian and P.H. Pathak, "Authors' reply" to J.D. Cashman, Comments on "A uniform geometrical theory of diffraction for an edge in a perfectly conducting surface", *IEEE Trans. Ant. Prop.*, vol. AP-25, no. 5, pp. 447-451, 1977.

- [16] S.W. Lee and G.A. Deschamps, "A uniform asymptotic theory of electromagnetic diffraction by a curved edge", *IEEE Trans. Ant. Prop.*, vol. AP-24, no.1, pp. 25-34, 1976.
- [17] J.B. Keller, R.M. Lewis and B.D. Seckler, "Asymptotic solution of some diffraction problems", *Comm. Pure Appl. Math.*, vol. 9, pp. 207-265, 1956.
- [18] S.W. Lee, "Electromagnetic reflection from a conducting surface: geometrical optics solution", *IEEE Trans. Ant. Prop.*, vol. AP-23, no. 3, pp. 184-191, 1975.
- [19] G.A. Deschamps, "Ray techniques in electromagnetics", *Proc. IEEE*, vol. 60, no. 9, pp. 1022-1035, 1972.
- [20] K. Brown, Electromagnetics Institute, Technical University of Denmark, private communications, 1987.
- [21] G.L. James, "*Geometrical theory of diffraction for electromagnetic waves*", Peter Peregrinus, Stevenage, 1976.
- [22] I. Kay and J.B. Keller, "Asymptotic evaluation of the field at a caustic", *Journ. Appl. Phys.*, vol. 25, pp. 876-883, 1954.
- [23] D. Ludwig, "Uniform asymptotic expansions at a caustic", *Comm. Pure Appl. Math.*, vol. 19, pp. 215-250, 1966.
- [24] K. Pontoppidan, "General analysis of dual offset reflector antennas", *ESTEC Contract*, No. 2874/76/NL/AK, TICRA Rep. S-66-02, Copenhagen, 1977.
- [25] N.C. Albertsen, P. Balling and N.E. Jensen, "Caustics and caustic corrections to the field diffracted by a curved edge", *IEEE Trans. Ant. Prop.*, vol. AP-25, no. 3, pp. 297-303, 1977.
- [26] K. Brown, "Analysis of defocused reflector antennas using the complex ray technique and caustic correction factors", *Proc. Int. Conf. Ant. Prop. (ICAP)*, *IEE Conf. Publ.*, no. 274, pp. 451-454, 1987.



- [27] CCIR, Plenary Assembly, "Radiation diagrams for use as design objectives for antennas of earth stations operating with geostationary satellites", *Recommendations and Reports of the CCIR*, vol. IV-1, Rec. 580-1, Geneva, 1986.

## 8. SITE SHIELDING FOR EARTH-STATION ANTENNAS - RESULTS

### 8.1. Introduction

The theoretical results derived in the previous chapter on the basis of GTD/UTD, have been implemented in a computer programme. The implementation is rather laborious but straightforward. Once completed, the computer programme readily provides numerical results. The required computing time is very limited, as no time-consuming integration procedures are needed. This is an obvious advantage of the approach using GTD/UTD.

In addition, we propose an approximate engineering approach to the site-shielding problem, based on the GTD/UTD method. From this engineering approach we deduce a modification of the CCIR site-shielding model [1], which removes the main limitations of the latter.

Finally, the effect of site-shielding on the coordination area of an earth station is illustrated by a specific example.

### 8.2. Numerical results obtained by GTD/UTD

#### 8.2.1. Radiation pattern of the parabolic antenna

Because of reciprocity, the radiation pattern of an antenna in transmit mode is equal to the pattern in receive mode. The latter is obtained by calculating the received field due to uniform plane-wave incidence on the antenna from a variable direction. Here we have calculated the radiation pattern in receive mode in the horizontal plane, by considering horizontal incidence ( $\theta^i=0$ ) on an unshielded parabolic antenna with elevation  $\varphi_E=0$  and variable azimuth  $\varphi_A$ . We employ

GTD/UTD as described in the previous chapter. These theories cannot be applied around the forward ( $\varphi_A=0$ ) and rear ( $\varphi_A=180^\circ$ ) directions, since these directions coincide with a caustic of the diffracted field. Therefore, we have restricted the computations to the range  $10^\circ \leq \varphi_A \leq 170^\circ$ .

Because  $\varphi_E=0$ , the horizontal plane coincides with a principal plane of the antenna (see sec. 7.4.2). For vertical antenna polarization, this plane is known as the H-plane, for horizontal antenna polarization as the E-plane. Because of symmetry, no cross-polarized field is received if the incident field is also vertically or horizontally polarized, respectively. Hence, in the following results only one antenna polarization is considered, equal to the polarization of the incident field.

The correctness of the computer programme has been tested by calculating the H-plane pattern of a small parabolic antenna with a dipole feed, for which calculated and measured results are available in the literature [2,3]. This particular antenna has parameters  $D/\lambda=10.65$  and  $f/D=0.25$  (corresponding to  $\psi_0=90^\circ$ ); the feed pattern is uniform in the plane under consideration, i.e.,  $G_f(\psi)=1$ .

In fig. 8.1a, the individual contributions  $E_n^R$  ( $n=0,1,2$ ) to the received field are shown, together with the phasor sum  $E^R$  calculated from (7.57). Blockage of the direct ray "0" occurs for  $\varphi_A > 90^\circ$ , while ray "1" is blocked for  $90^\circ < \varphi_A < 135^\circ$ . The discontinuity in  $E_0^R$  is compensated by a change of sign in  $E_2^R$  at  $\varphi_A=90^\circ$ . The discontinuities in  $E_1^R$  are not compensated, because double diffraction is not included in our calculations; however, these discontinuities occur in a region where  $|E_1^R| \ll |E_2^R|$  and are therefore hardly observed.

The phasor sum  $E^R$  is compared in fig. 8.1b with the radiation pattern calculated by Kouyoumjian and Ratnasiri [2] by means of GTD/UTD applied to the same antenna in transmit mode. By employing the aperture-integration method [4] in the forward directions and the equivalent edge-currents method [5] in the rear directions, these authors were able to calculate the radiation pattern over the

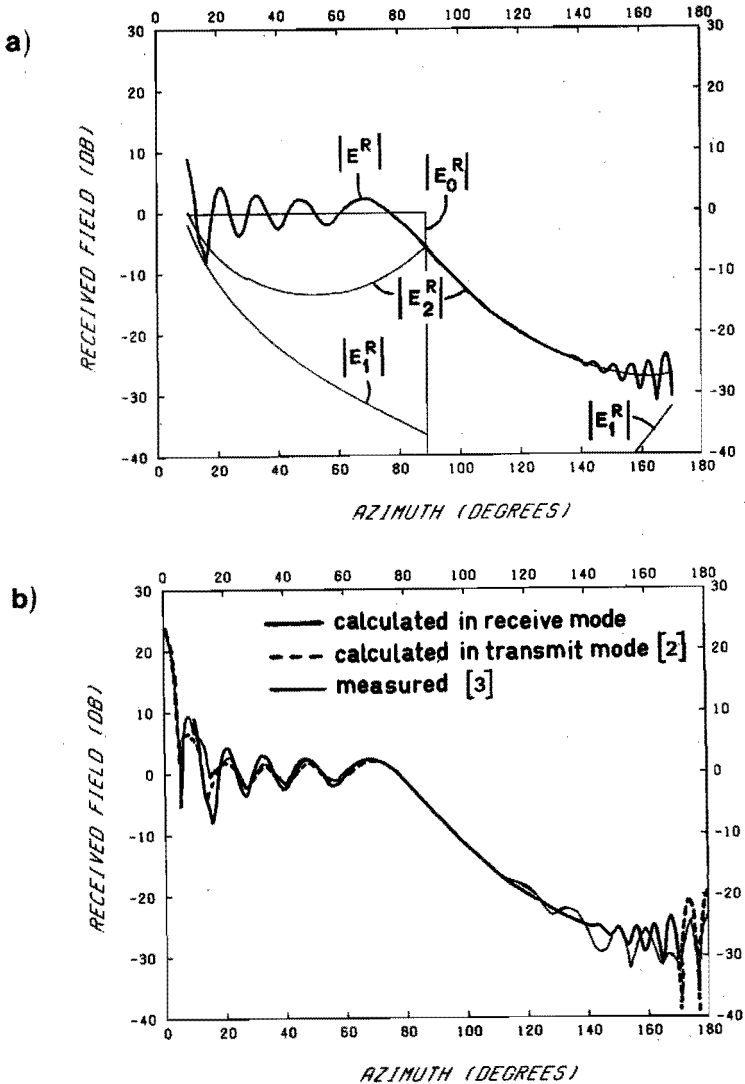


Fig. 8.1. H-plane pattern of a small parabolic antenna with a dipole feed ( $D/\lambda=10.65$ ,  $f/D=0.25$ ).

a) Individual contributions  $E_n^R$  ( $n=0,1,2$ ) and phasor sum  $E^R$ , calculated in receive mode.

b) Comparison of the pattern in receive mode (fig. 8.1a) with the calculated pattern in transmit mode [2] and the measured pattern [3].

complete range  $0^\circ \leq \varphi_A \leq 180^\circ$ . Good agreement between the two calculated patterns is observed, apart from small deviations in the range  $10^\circ < \varphi_A < 60^\circ$ , where the pattern is strongly frequency dependent. This agreement confirms the correctness of our computer programme. Also shown in fig. 8.1b is the pattern measured by Afifi [3]. The agreement between calculated and measured patterns is good; the discrepancies in the region  $\varphi_A > 140^\circ$  can be partly attributed [2] to measurement inaccuracies at the corresponding low levels of the received signal.

Fig. 8.1 refers to a small antenna. We have also calculated the radiation patterns of a large ( $D/\lambda=100$ ) and a very large ( $D/\lambda=400$ ) parabolic antenna. For both antennas we have taken  $f/D=0.433$  (corresponding to  $\psi_0=60^\circ$ ). The feed is a corrugated horn and its radiation pattern is modelled by (7.6), with parameters  $a=0.00316$  and  $m=3.368$  (as in fig. 7.5). The results are shown in figs. 8.2–8.3 and figs. 8.4–8.5, respectively. The E-plane patterns in figs. 8.2 and 8.4 correspond to horizontal polarization of the incident field  $\vec{E}^i$ , while the H-plane patterns in figs. 8.3 and 8.5 correspond to vertical polarization of  $\vec{E}^i$ . Part (a) of each figure shows the three individual contributions to the received field, part (b) compares the phasor sum (7.57) and the power sum (7.58).

The results in figs. 8.2–8.5 give rise to the following comments:

- i) The direct ray "0" to the feed is blocked for  $\varphi_A > 120^\circ$  (in general, for  $\varphi_A > 180^\circ - \psi_0$ ).
- ii) Ray "1" is blocked for  $90^\circ < \varphi_A < 120^\circ$  (in general, for  $90^\circ < \varphi_A < 90^\circ + \psi_0/2$ ).
- iii) The discontinuity in  $E_0^R$  at  $\varphi_A = 120^\circ$  is properly compensated by a change of sign in  $E_2^R$ ; the discontinuities in  $E_1^R$  are not compensated, but are less important.
- iv) The power sum  $E_p^R$  yields a much smoother result than the phasor sum  $E^R$ .
- v) For most azimuths, the received field is well below the CCIR reference level (5.2), which is at  $-10$  dB or above.

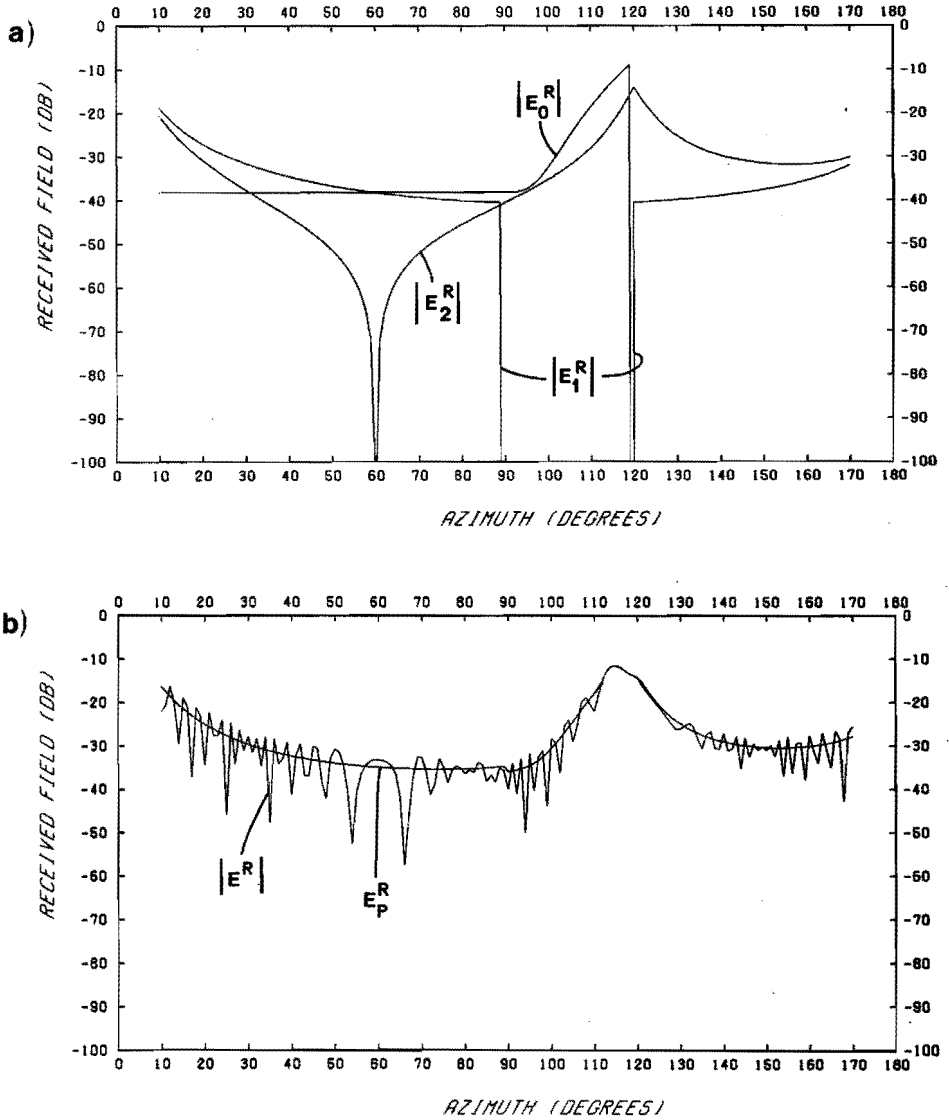


Fig. 8.2. E-plane pattern of a large parabolic antenna ( $D/\lambda = 100$ ,  $f/D = 0.433$ ).  
a) Individual contributions  $E_n^R$  ( $n=0,1,2$ ).  
b) Comparison between phasor sum  $E^R$  and power sum  $E_P^R$  of the individual contributions.

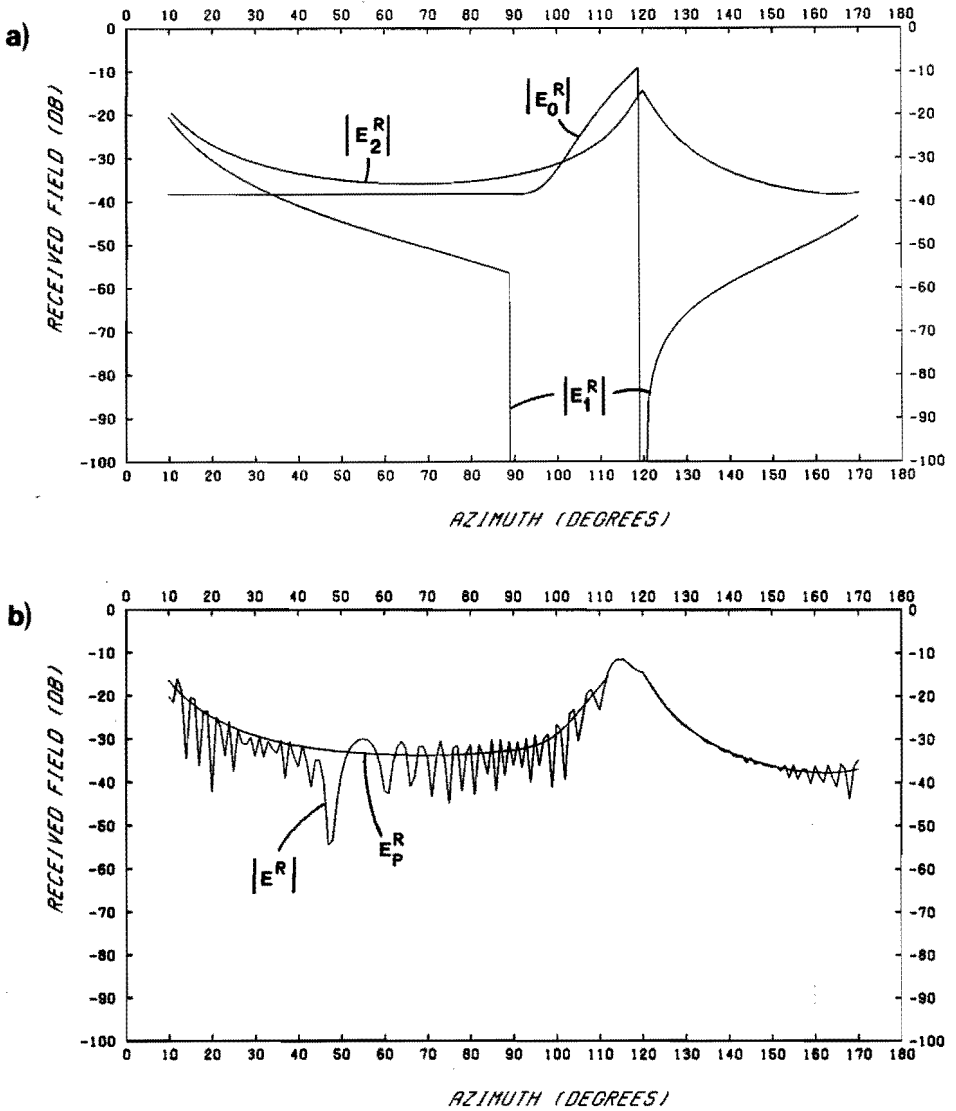


Fig. 8.3. H-plane pattern of a large parabolic antenna ( $D/\lambda=100$ ,  $f/D=0.433$ ).  
a) Individual contributions  $E_n^R$  ( $n=0,1,2$ ).  
b) Comparison between phasor sum  $E^R$  and power sum  $E_P^R$  of the individual contributions.

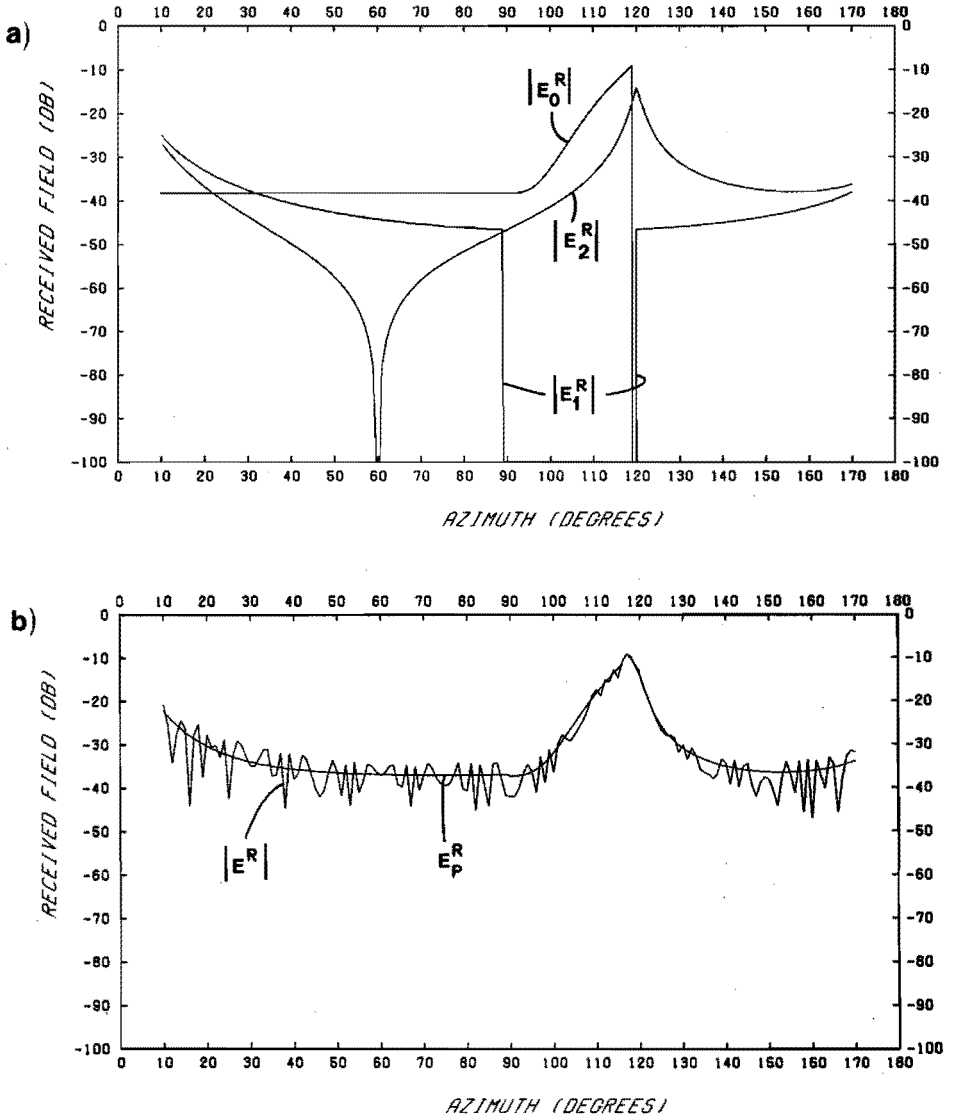


Fig. 8.4. E-plane pattern of a very large parabolic antenna ( $D/\lambda=400$ ,  $f/D=0.433$ ).

a) Individual contributions  $E_n^R$  ( $n=0,1,2$ ).

b) Comparison between phasor sum  $E^R$  and power sum  $E_P^R$  of the individual contributions.



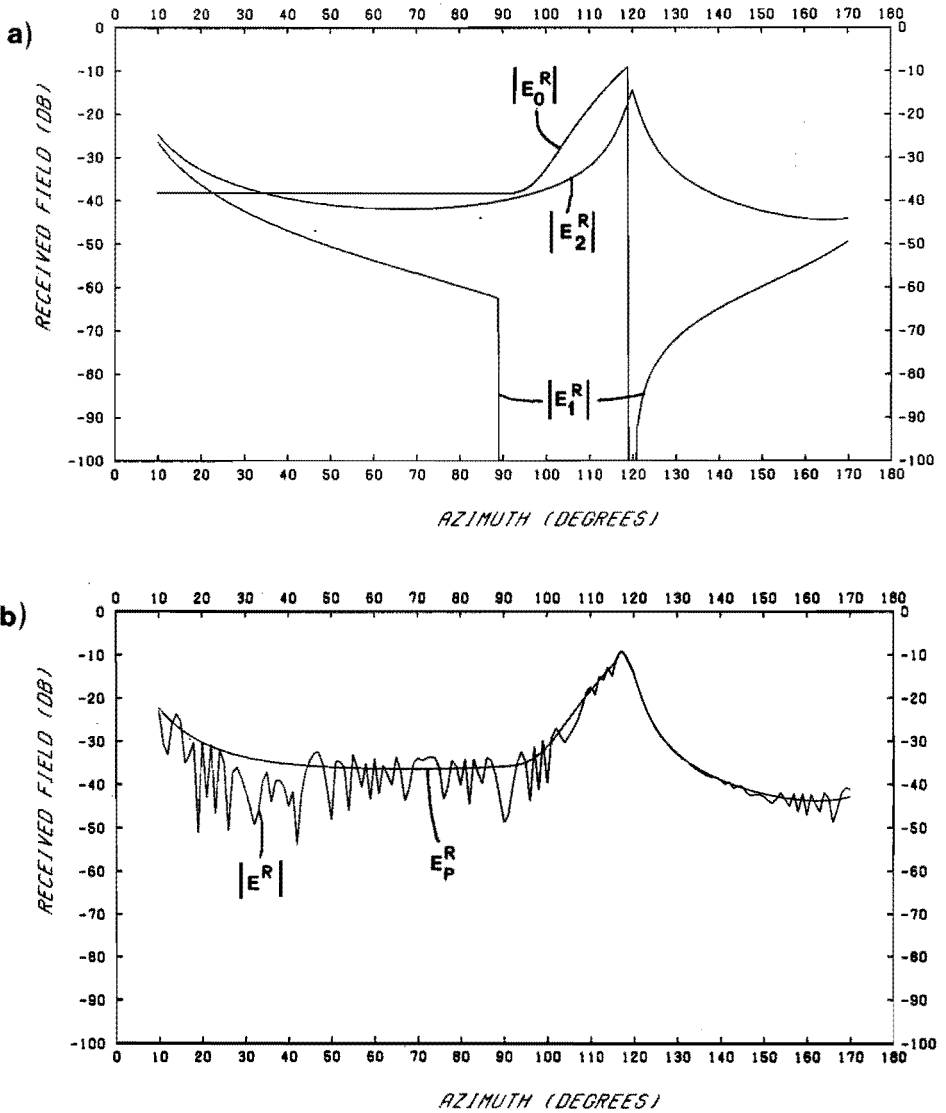


Fig. 8.5. H-plane pattern of a very large parabolic antenna ( $D/\lambda=400$ ,  $f/D=0.433$ ).

a) Individual contributions  $E_n^R$  ( $n=0,1,2$ ).

b) Comparison between phasor sum  $E^R$  and power sum  $E_P^R$  of the individual contributions.

vi) Only a slight difference is observed between the E-plane and H-plane patterns.

It is clear from figs. 8.2–8.5 that for large antennas ( $D/\lambda \geq 100$ ), the power sum yields more useful results than the phasor sum. Therefore, the calculations in the sequel are restricted to the power sum. As a further restriction, the incident field  $\vec{E}^i$  is supposed to be a uniform plane wave of horizontal polarization.

### 8.2.2. SSF as a function of elevation

The site-shielding factor (SSF) of an obstacle is defined as the ratio of the power received in the absence of the obstacle to the power received in the presence of the obstacle. We consider the shielding of an antenna at azimuth  $\varphi_A=0$ , as a function of the elevation  $\varphi_E$  of the antenna. Then, the direction of incidence varies in the azimuthal plane of the antenna, which is a principal plane of the antenna (sec. 7.4.2). Hence, no cross-polarized field is received (just as in sec. 8.2.1). Here we present results for horizontal polarization of the incident field  $\vec{E}^i$  and of the antenna. The choice  $\varphi_A=0$  also underlies the CCIR model [1] (see sec. 7.3) and the work of the British Post Office [6–8]. Following [7], we describe the position of the shielding knife-edge obstacle by its distance  $x_M$  to the antenna-aperture centre M and by the associated "diffraction angle"  $\theta_M$ . The height  $\Delta z$  of the obstacle above M is related to these parameters by (see fig. 7.2)

$$\Delta z = x_M \tan \theta_M . \quad (8.1)$$

For the very large parabolic antenna configuration described in sec. 8.2.1, we have calculated the SSF of the knife-edge obstacle as a function of  $\varphi_E$ , with  $x_M$  and  $\theta_M$  as parameters. Figs. 8.6a and 8.6b show the results for  $\theta_M=1^\circ$  and  $\theta_M=4^\circ$ ,

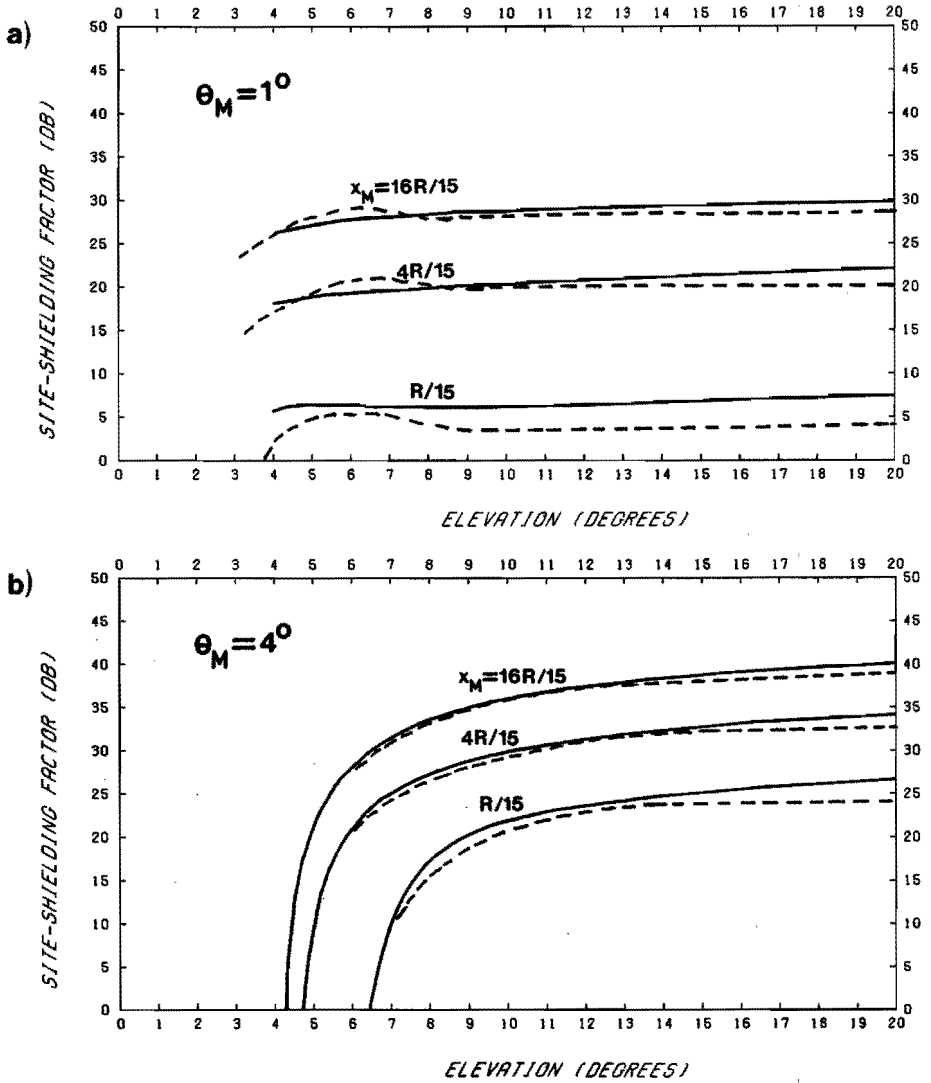


Fig. 8.6. Site-shielding factor for a very large antenna ( $D/\lambda=400$ ) at azimuth  $\varphi_A=0$  as a function of elevation  $\varphi_E$ , with obstacle "diffraction angle"  $\theta_M$  and obstacle distance  $x_M$  as parameters. Horizontal polarization of the incident field.  $R=D^2/2\lambda=80000\lambda$  is the Rayleigh distance.

———— Calculated by GTD/UTD for a parabolic antenna.  
 - - - - - Calculated by Streete and Shinn [7] for a Cassegrain antenna.

a)  $\theta_M=1^\circ$ ,  $x_M$  variable.      b)  $\theta_M=4^\circ$ ,  $x_M$  variable.

respectively. Also shown in these figures are the results reported by Streete and Shinn [7] for a Cassegrain antenna of the same size. In [7] the received field  $E^R$  is calculated by an aperture-integration method [6], whereupon the envelope of the maxima of the function  $|E^R|$  is employed to determine the received power. The results in [7] are in reasonable agreement (within 5 dB) with measurements [6,8]. The close agreement between the results in [7] and our results suggests that for  $\varphi_A=0$ , the type of earth-station antenna (whether parabolic or Cassegrain) is not of primary importance in site-shielding calculations.

### 8.2.3. SSF in relation to antenna polarization

In the geometries considered so far, the direction of the (linearly polarized) incident field relative to the antenna axis varies in a principal plane of the antenna. As a consequence, no "cross-polarized" field is received by the (also linearly polarized) antenna. Here, we define the "cross-polarized" field as the field received by a vertically (horizontally) polarized antenna in the case of horizontal (vertical) polarization of the (unwanted) incident field. In the results presented in the next section (where  $\varphi_A \neq 0$  and  $\varphi_E \neq 0$ ), the direction of incidence lies no longer in a principal plane of the antenna, hence both antenna polarizations need to be considered.

The relative "cross-polarization" level depends on the angles  $\varphi_A$  and  $\varphi_E$  of the antenna and on the "diffraction angle"  $\theta_M$  of the obstacle. An illustrative example of "cross-polarization" reception is shown in fig. 8.7a. Here we have plotted the received field  $E_P^R$  for both antenna polarizations in the absence and in the presence of a knife-edge obstacle, for fixed elevation  $\varphi_E=20^\circ$  and variable azimuth  $\varphi_A$ ; the incident field  $E^i$  is horizontally polarized, the obstacle has parameters  $\Delta z=150\lambda$ ,  $x_M=1000\lambda$ , and the antenna configuration (with  $D/\lambda=100$ ) is described in sec. 8.2.1.

From fig. 8.7a we observe that the "cross-polarized" field may have a magnitude comparable to the magnitude of the "co-polarized" field.

The important consequence for engineering practice is that, in general, polarization discrimination in an earth-station antenna does not provide significant protection against wide-angle interference from a terrestrial station. A local minimum in the received interference power for one polarization (as in fig. 8.7a) is not observed for the other polarization. Hence, an earth-station that uses circular polarization (which is a suitable combination of horizontal and vertical polarizations) benefits only partly from such a minimum. For a satellite-earth link with two orthogonal linear polarizations (frequency reuse), only one polarization direction (and thus only one of the two wanted signals) can be protected against terrestrial interference by means of polarization discrimination.

In order to assess the SSF for the two linear antenna polarizations simultaneously, it is useful to consider the sum of the received powers for vertical and horizontal antenna polarization, instead of each of these powers individually. Therefore, we introduce the "polarization-independent power sum"  $E_{PP}^R$ , defined by

$$E_{PP}^R = \left[ (E_P^{R,V})^2 + (E_P^{R,H})^2 \right]^{1/2}, \quad (8.2)$$

where  $E_P^{R,V}$  and  $E_P^{R,H}$  are the power sums (7.58) for vertical and horizontal antenna polarization, respectively. The results for  $E_{PP}^R$  are more meaningful for an arbitrary antenna polarization than the results for  $E_P^{R,V}$  or  $E_P^{R,H}$  only. As an illustration, we have plotted in fig. 8.7b the "polarization-independent power sum"  $E_{PP}^R$  as a function of azimuth for the numerical example of fig. 8.7a. Clearly, the polarization-independent local minima in  $E_P^R$  are absent in  $E_{PP}^R$ .

The use of  $E_{PP}^R$  instead of  $E_P^R$  implies that the actual antenna polarization is ignored. This approach resembles the ignoring of the phases of the individual

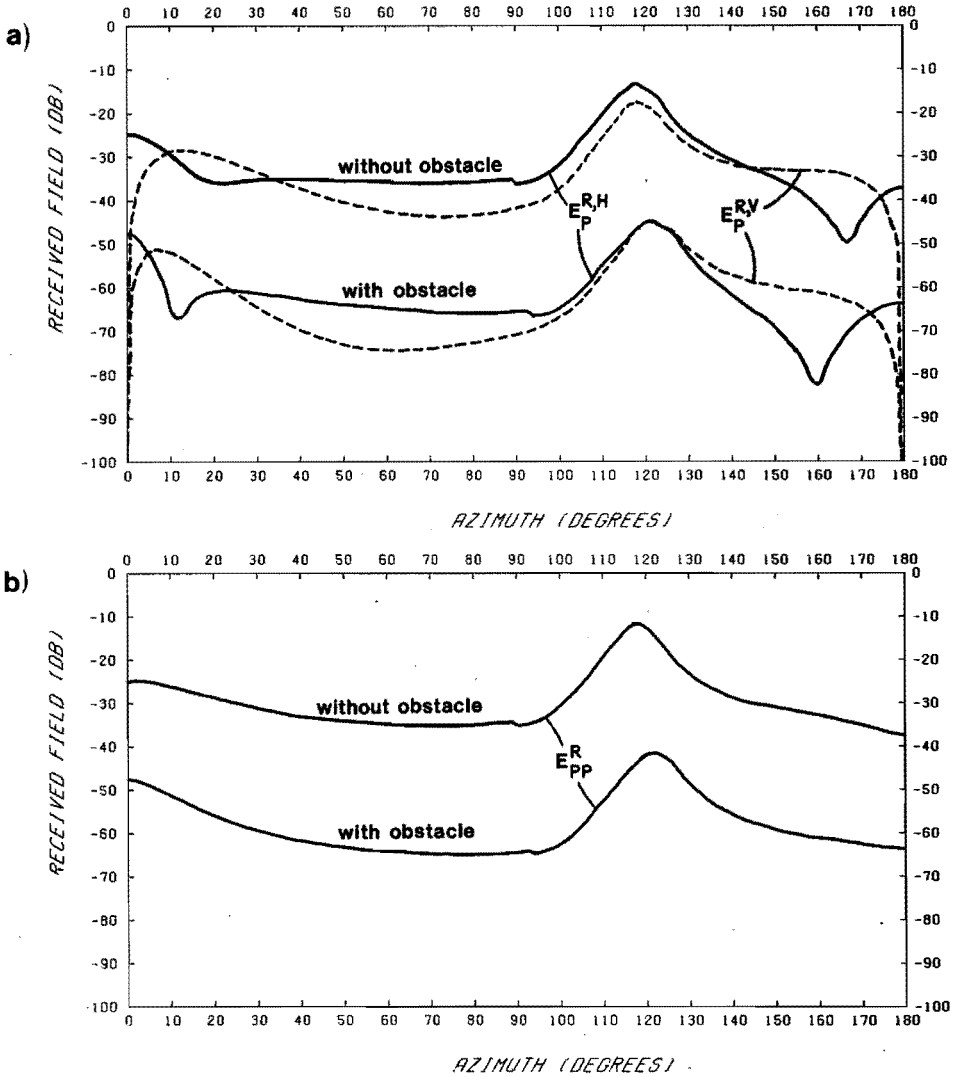


Fig. 8.7. Effect of antenna polarization on the field received by a large parabolic antenna ( $D/\lambda=100$ ) at elevation  $\varphi_E=20^\circ$ , in the absence (upper and presence (lower curves) of an obstacle with distance  $x_M=1000\lambda$  and height  $\Delta z=150\lambda$ . Horizontal polarization of the incident field.

a) Power sum  $E_P^R$  for horizontal ( $E_P^{R,H}$ ) and vertical ( $E_P^{R,V}$ ) antenna polarization.

b) Polarization-independent power sum  $E_{PP}^R$ .

contributions  $E_n^R$  to the actual received field  $E^R$ , as expressed by the power sum (7.58). In fact, in  $E_{PP}^R$  both the phases and the orientations of the individual contributions to the received field are "averaged out". The relation between  $E_{PP}^R$  and the individual contributions  $E_n^R$  follows from (8.2) and (7.58), viz.

$$E_{PP}^R = \left[ \sum_{n=0}^2 (E_n^{R,V})^2 + (E_n^{R,H})^2 \right]^{1/2}, \quad (8.3)$$

where  $E_n^{R,V}$  and  $E_n^{R,H}$  denote the individual contributions  $E_n^R$ ,  $n=0,1,2$  (cf. (7.53) and (7.56)) for vertical and horizontal antenna polarization, respectively.

In the sequel, we employ the "polarization-independent power sum"  $E_{PP}^R$  to calculate a polarization-independent value of the SSF, by comparing the values of  $E_{PP}^R$  in the absence and in the presence of the obstacle, respectively.

#### 8.2.4. SSF as a function of azimuth

For antenna configurations with azimuth  $\varphi_A \neq 0$ , no results for the SSF of a knife-edge obstacle have been reported in the literature. In this section we consider the shielding of an antenna at a fixed elevation  $\varphi_E = 20^\circ$ , for varying azimuth  $\varphi_A$ . Notice that the direction of incidence does not lie in a principal plane of the antenna. Therefore, the calculation of the SSF is based on the "polarization-independent power sum" introduced in sec. 8.2.3. The antenna configurations (with reflector diameters  $100\lambda$  and  $400\lambda$ ) are described in sec. 8.2.1. We have calculated the SSF of the knife-edge obstacle as a function of  $\varphi_A$ , for several values of the obstacle parameters  $\Delta z$  and  $x_M$ . The results for the  $100\lambda$  antenna are shown in fig. 8.8a (for  $\Delta z = 150\lambda$ ,  $x_M$  variable) and fig. 8.8b (for  $x_M = 1000\lambda$ ,  $\Delta z$  variable), while the results for the  $400\lambda$  antenna are shown in fig. 8.9a (for  $\Delta z = 300\lambda$ ,  $x_M$  variable) and fig. 8.9b (for  $x_M = 2000\lambda$ ,  $\Delta z$  variable).

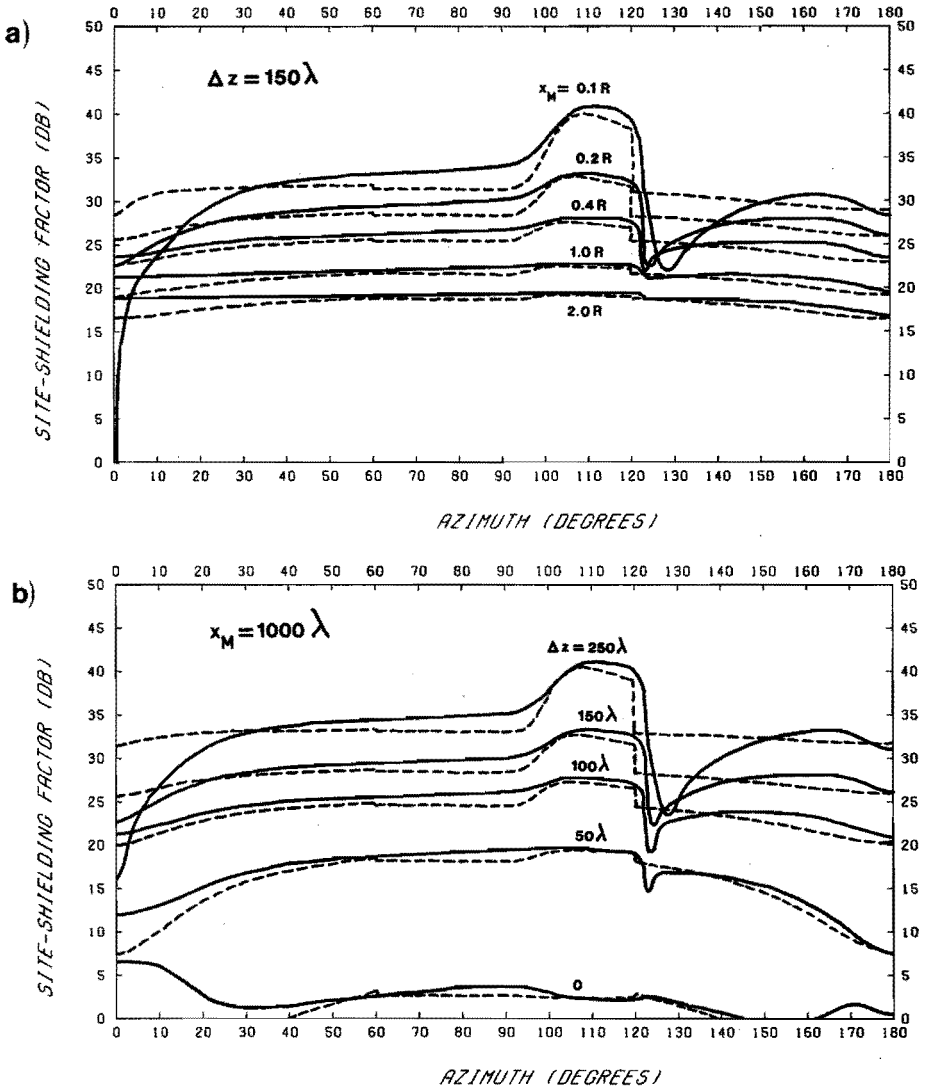


Fig. 8.8. Site-shielding factor for a large parabolic antenna ( $D/\lambda=100$ ) at elevation  $\varphi_E=20^\circ$  as a function of azimuth  $\varphi_A$ , with obstacle height  $\Delta z$  and obstacle distance  $x_M$  as parameters. Horizontal polarization of the incident field.  $R=D^2/2\lambda=5000\lambda$  is the Rayleigh distance.

———— Calculated by GTD/UTD.  
 - - - - Calculated by engineering method (sec. 8.3.2).

a)  $\Delta z=150\lambda$ ,  $x_M$  variable.      b)  $x_M=1000\lambda$ ,  $\Delta z$  variable.



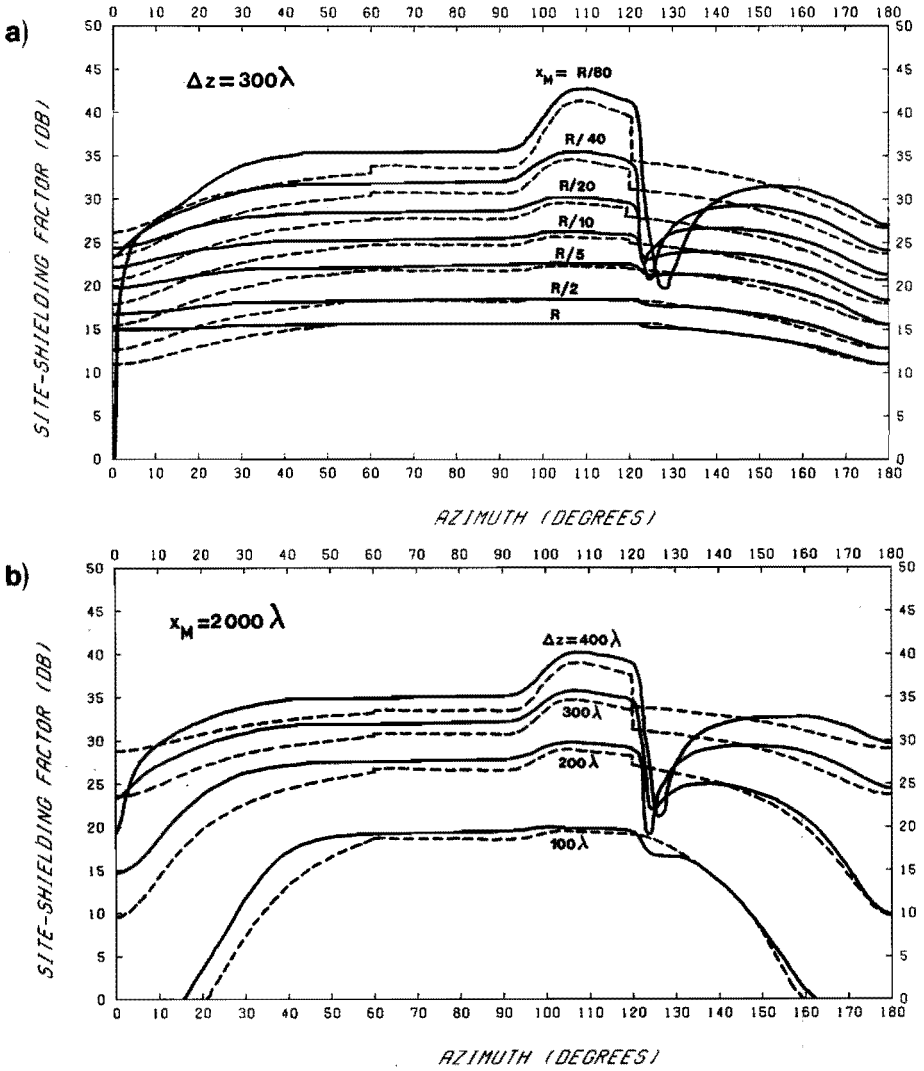


Fig. 8.9. Site-shielding factor for a very large parabolic antenna ( $D/\lambda=400$ ) at elevation  $\varphi_E=20^\circ$  as a function of azimuth  $\varphi_A$ , with obstacle height  $\Delta z$  and obstacle distance  $x_M$  as parameters. Horizontal polarization of the incident field.  $R=D^2/2\lambda=80000\lambda$  is the Rayleigh distance.

———— Calculated by GTD/UTD.

- - - - Calculated by engineering method (sec. 8.3.2).

a)  $\Delta z=300\lambda$ ,  $x_M$  variable.

b)  $x_M=2000\lambda$ ,  $\Delta z$  variable.

From these figures we observe that for most azimuths the SSF increases with increasing obstacle height  $\Delta z$  or decreasing obstacle distance  $x_M$ , because of the increasing associated "diffraction angle"  $\theta_M$ . Exceptions occur at azimuths around  $\varphi_A=0$  and around  $\varphi_A=\varphi_{A, tr}$ , where  $\varphi_{A, tr} \approx 120^\circ$  is the transition value at which the direct ray to the feed gets blocked by the reflector. Around  $\varphi_A=0$ , the obstacle clearance ( $\varphi_E - \theta_M$ ) may become too small for the obstacle to provide adequate protection. The irregularities around  $\varphi_A=\varphi_{A, tr}$  are related to the gradual increase of  $\varphi_{A, tr}$  with increasing  $\theta_M$ .

### 8.2.5. Discussion of the numerical results

The numerical results obtained in the previous sections and depicted in figs. 8.2–8.9, give rise to the following comments:

i) Useful protection against wide-angle interference is observed for many practical geometries. The SSF typically has values between 20 and 40 dB, but is significantly lower for small azimuth and/or elevation angles ( $\varphi_A$  and  $\varphi_E$ , respectively).

ii) The azimuthal dependence of the SSF is somewhat irregular around  $\varphi_A=\varphi_{A, tr}$ , where  $\varphi_{A, tr}$  is the transition value at which the direct ray to the feed gets blocked by the reflector. This behaviour is especially manifest for large "diffraction angles"  $\theta_M$ , owing to the increase of  $\varphi_{A, tr}$  with increasing  $\theta_M$ . Outside the range of small  $\varphi_A$  and the range around  $\varphi_A=\varphi_{A, tr}$ , the SSF depends only slightly on  $\varphi_A$  (figs. 8.8–8.9).

iii) The SSF increases for increasing  $\theta_M$ . Hence, except around  $\varphi_A=0$  and  $\varphi_A=\varphi_{A, tr}$ , very good protection can be obtained for relatively small obstacle distances  $x_M$  and feasible obstacle heights  $\Delta z$  (figs. 8.8–8.9).

iv) For  $\varphi_A=0$ , the SSF is relatively low and increases only slightly with increasing antenna elevation  $\varphi_E$ , except in the range of very small  $\varphi_E$ . For  $\theta_M$  fixed, the SSF increases with increasing  $x_M$  and hence increasing  $\Delta z$  (fig. 8.6). For large protection in the direction  $\varphi_A=0$ , the shielding obstacle should be high and far away. For artificial shields, this will seldom be feasible in practice.

v) No significant difference is observed between the results for horizontal and for vertical polarization of the incident field (figs. 8.2-8.5).

vi) Outside the ranges of small  $\varphi_A$  and small  $\varphi_E$ , the "cross-polar" level is of the same order of magnitude as the "co-polar" level (fig. 8.7). Hence, polarization discrimination cannot be relied upon to protect an earth-station antenna against wide-angle interference from a terrestrial station.

### 8.3. An engineering prediction model for site shielding

#### 8.3.1. Description of the engineering model

The CCIR site-shielding model [1], described in sec. 7.3, has been shown to contain a number of limitations. In particular, the validity of the model is restricted to large obstacle distances ( $x_M > R$ , where  $R = D^2/\lambda$  is the Rayleigh distance) and zero azimuth ( $\varphi_A = 0$ ), as well as to uniform plane-wave incidence. Based on the preceding GTD/UTD analysis, we now present a modification of the CCIR model to remove these limitations.

In the CCIR model (7.4), the SSF is given by

$$\text{SSF} = L_M - \Delta G \quad (\text{dB}), \quad (8.4)$$

where  $L_M$  represents the diffraction loss of the ray-optical field towards the aperture

centre  $M$ , and  $\Delta G$  is the correction in antenna gain due to the changed arrival angle in the presence of the obstacle. This formulation becomes invalid for near-field site shielding, because in that case the antenna can no longer be modelled as a point source. Instead, the individual contributions  $E_n^R$  to the received field  $E^R$  should be considered separately.

Roughly, the field  $E^R$  can be approximated by the largest of the three contributions  $E_n^R$ ,  $n=0, 1$  or  $2$ . Suppose now that this  $E_n^R$  is the dominant contribution both in the absence and in the presence of the obstacle; this assumption is realistic for wide-angle incidence. Then, instead of taking the diffraction loss of the ray-optical field towards  $M$ , we replace the first term in (8.4) by the diffraction loss  $L_n$  of the dominant ray-optical field, and neglect the two other contributions. The diffraction loss  $L_n$  is calculated by the simple CCIR knife-edge diffraction formula (6.25), or – if necessary – by the extended CCIR formula (6.47) in case of non-uniform plane-wave incidence.

The second term in (8.4) takes into account the changed arrival angle of the ray-optical field towards  $M$ , relative to boresight. We replace this term  $\Delta G$  by a term  $\Delta G_n$ , which represents the correction in feed-antenna gain due to the change in arrival angle of the dominant ray-optical field at the feed. Then we obtain, as a modification of the CCIR model (8.4), the formula

$$SSF = L_n - \Delta G_n \quad (\text{dB}), \quad (8.5)$$

where the subscript  $n$  refers to the dominant ray-optical field.

The dominant ray-optical field can be determined by a comparison of the magnitudes of the contributions  $|E_n^R|$ ,  $n=0,1,2$ . On the other hand, the question which ray-optical field is dominant can also be settled a priori by a physical

consideration. For example, for a parabolic antenna, the direct ray-optical field towards the feed normally yields the dominant contribution if the feed centre is located in the vicinity of the shadow boundary cast by the reflector edge, because of the large feed-antenna gain in this region. If the feed centre is away from this shadow boundary, one of the two edge-diffracted fields is dominant, normally the one emanating from the diffraction point with the smallest diffraction angle. This is illustrated by fig. 8.10, where the individual contributions  $E_n^R$  ( $n=0,1,2$ ), averaged for the two antenna polarizations (cf. (8.3)), are shown both in the absence and in the presence of the obstacle.

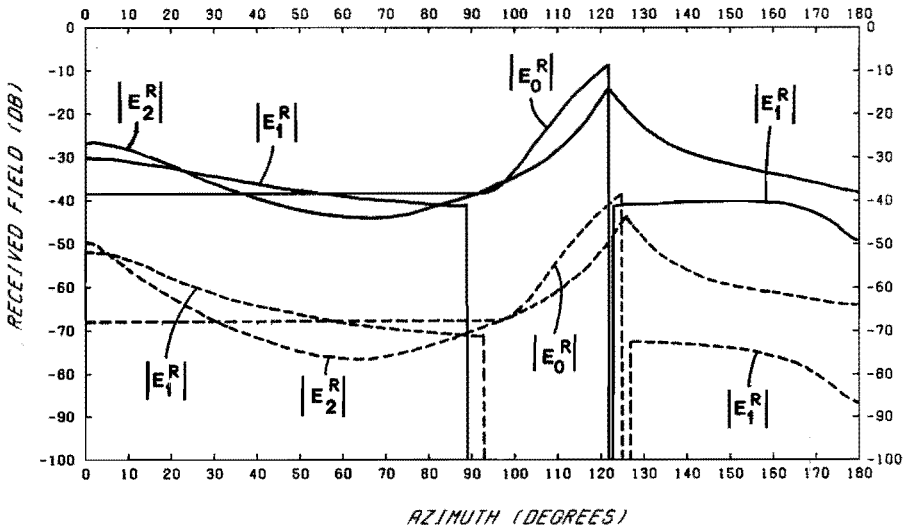


Fig. 8.10. The three individual contributions  $E_n^R$  ( $n=0,1,2$ ), averaged for the two antenna polarizations, to the field received by a large parabolic antenna ( $D/\lambda=100$ ) at elevation  $\varphi_E=20^\circ$ . Horizontal polarization of the incident field.

— Without obstacle;  
 - - - with obstacle of height  $\Delta z=150\lambda$  at a distance  $x_M=1000\lambda$ .

Although the preceding approach is rather crude, it is believed to be satisfactory for engineering purposes as a method to predict the SSF in many cases where the CCIR model [1] does not apply. An illustrative example is discussed in the next section.

### 8.3.2. Application of the engineering model to a specific example

In this section the proposed engineering approach is elaborated for a specific example, namely, the site-shielding problem for a large parabolic antenna at an elevation  $\varphi_E=20^\circ$ . The antenna is completely surrounded by a screen with height  $\Delta z$  at a distance  $x_M$ , which are parameters in the present problem (cf. figs. 8.8 and 8.9). The incident field is a uniform plane wave of horizontal polarization.

From fig. 8.10 we observe that we can roughly distinguish three ranges of the azimuth angle  $\varphi_A$ . In the ranges  $0^\circ < \varphi_A < 60^\circ$  and  $120^\circ < \varphi_A < 180^\circ$ , the dominant contribution to the received field is associated with the edge-diffracted rays "1" and "2", respectively; the field along the direct ray "0" yields the largest contribution in the range  $60^\circ < \varphi_A < 120^\circ$ .

For the calculation of the diffraction loss (at the obstacle edge) of the fields along rays "1" and "2", we need to determine the location of the diffraction points  $P_1$  and  $P_2$  as a function of  $\varphi_A$ . The polar angles  $\varphi_{1,2}$  of  $P_{1,2}$  are obtained as solutions of eq. (7.40) if the obstacle is present, and of eq. (7.43) if the obstacle is absent. The solution of (7.43) is given by

$$\tan \varphi = \sin \varphi_A / (\sin \varphi_E \cos \varphi_A). \quad (8.6)$$

The exact solution of (7.40) is not available, but (7.40) can be approximated by the equation

$$A_1 \cos \varphi + A_2 \sin \varphi = 0, \quad (8.7)$$

where  $A_1$  and  $A_2$  are given by (7.41). This approximation is justified if  $A_3^2 + A_4^2 \ll A_1^2 + A_2^2$ , which is fulfilled if

$$\sin(\varphi_E - \theta_M) \gg D/2r_M. \quad (8.8)$$

This is a condition on the obstacle clearance (cf. (7.10)), which is satisfied in the present example. From (8.7) we obtain an approximate solution of (7.40), viz.

$$\tan \varphi = \sin \varphi_A / (\sin \varphi_E \cos \varphi_A - \tan \theta_M \cos \varphi_E), \quad (8.9)$$

where (7.41) has been used. The solutions (8.6) and (8.9) for the polar angle  $\varphi$  differ only slightly; this difference is neglected in the present example. Thus we take the polar angle  $\varphi_n$  of  $P_n$ ,  $n=1,2$ , to be given by (8.6), with  $0 \leq \varphi_1 \leq \pi$  and  $\pi \leq \varphi_2 \leq 2\pi$ , both in the presence and in the absence of the obstacle.

The Cartesian coordinates  $x_P$  and  $z_P$  of  $P_{1,2}$  are determined from (7.36), viz.

$$x_P = x_M + \frac{1}{2}D \cos \varphi_n \sin \varphi_E \cos \varphi_A + \frac{1}{2}D \sin \varphi_n \sin \varphi_A, \quad (8.10a)$$

$$z_P = z_M + \frac{1}{2}D \cos \varphi_n \cos \varphi_E. \quad (8.10b)$$

Next, we calculate the polar coordinates  $(r_n, \theta_n)$  of  $P_n$  by (6.1), the dimensionless parameter  $v_n$  from (6.21) with  $\psi^i = \theta_n$ , and the knife-edge diffraction loss  $L_n$  by the CCIR formula (6.25).

In the ranges  $0^\circ < \varphi_A < 60^\circ$  and  $120^\circ < \varphi_A < 180^\circ$ , the SSF is now approximated by

$$\begin{aligned} \text{SSF} &= L_1 \quad (\text{dB}), & 0^\circ < \varphi_A < 60^\circ, \\ \text{SSF} &= L_2 \quad (\text{dB}), & 120^\circ < \varphi_A < 180^\circ. \end{aligned} \quad (8.11)$$

Thus, we neglect the second term in (8.5), consistent with our use of the same couple of diffraction points  $P_{1,2}$  in the absence and in the presence of the obstacle. (For a rotationally symmetric feed-radiation pattern  $G_f(\psi)$ , as in (7.6), the second term in (8.5) is even exactly equal to zero.)

In the range  $60^\circ < \varphi_A < 120^\circ$ , the field along the direct ray ( $n=0$ ) towards the feed centre F yields the dominant contribution to the received field. The Cartesian coordinates of F follow from (7.35) as

$$x_F = x_M - \rho_M \cos \varphi_E \cos \varphi_A, \quad (8.12a)$$

$$z_F = z_M + \rho_M \sin \varphi_E, \quad (8.12b)$$

where  $\rho_M$  is given by (7.5a). As before, the polar coordinates  $(r_F, \theta_F)$  of F are calculated from (6.1), and the parameter  $v_F$  is found from (6.21) with  $\psi^i = \theta_F$ . Then the diffraction loss  $L_0$  of the direct ray-optical field towards F is determined by means of the CCIR formula (6.25).

For this range of  $\varphi_A$ , we also evaluate the second term in (8.5). The arrival angle  $\psi$  of the direct ray at F is determined from (7.54) and (7.55a), with the result

$$\cos \psi_a = -\cos \varphi_E \cos \varphi_A, \quad (8.13a)$$

$$\cos \psi_p = -\cos \theta_F \cos \varphi_E \cos \varphi_A - \sin \theta_F \sin \varphi_E, \quad (8.13b)$$

in the absence (subscript a) and presence (subscript p) of the obstacle, respectively.



The correction  $\Delta G_0$  in the SSF due to the change in feed-antenna gain is then calculated from

$$\Delta G_0 = 20 \log [G_f(\psi_p) / G_f(\psi_a)] \quad (\text{dB}), \quad (8.14)$$

where  $G_f(\psi)$  is the feed radiation pattern, given by (7.6). Thus, as in (8.5), the SSF is given by

$$\text{SSF} = L_0 - \Delta G_0 \quad (\text{dB}), \quad 60^\circ < \varphi_A < 120^\circ. \quad (8.15)$$

The formulas (8.11) and (8.15) constitute the present modification of the CCIR model (7.4).

The present engineering model has been used to calculate the SSF for the two parabolic antennas considered in sec. 8.2 (with  $D/\lambda=100$  and  $D/\lambda=400$ , respectively). The results are included in figs. 8.8 and 8.9. Apart from deviations in the ranges  $0^\circ < \varphi_A < 10^\circ$  and  $120^\circ < \varphi_A < 130^\circ$ , where the engineering model clearly fails, useful agreement is observed between the approximate results based on (8.11) and (8.15), and the results of the GTD/UTD analysis.

#### 8.4. The effect of site shielding on coordination areas

In sec. 2.4 we introduced the concept of the coordination area of an earth station, defined as the area around the earth station outside which a terrestrial station neither causes nor is subject to interference greater than a specified permissible level. The application of site shielding may significantly reduce the coordination area of a receiving earth station, as is shown by the following example.

Consider the coordination contour for the Burum-1 receiving earth station of the Netherlands PTT shown in fig. 2.6, and reproduced in fig. 8.11 for convenience. This contour has been calculated by the method of appendix 28 of the Radio Regulations (RR) [9], assuming a constant sidelobe level of the earth-station antenna of -10 dBi in accordance with the CCIR reference radiation pattern (5.2) (although in this assumption the antenna-sidelobe level is generally over-estimated, see figs. 8.2-8.5). The large extent of this contour is mainly due to clear-air transhorizon-propagation phenomena, and less to the hydrometeor-scatter mechanism (see sec. 3.3). In fact, a significant influence of the latter mechanism is confined (according to [9]) to the area bounded by the dotted circle in fig. 8.11. Site shielding cannot be used to protect the earth station against interference by hydrometeor scatter, because this type of interference is received by the antenna main beam, which obviously should remain unobstructed. Thus, the hydrometeor-scatter contour imposes a limit on the reduction of the coordination area obtainable from site shielding.

Referring to fig. 8.11, we observe that the Burum-1 earth station may benefit particularly from site shielding in the two sectors "A" and "B", given by  $20^\circ < \varphi_A < 100^\circ$  and  $140^\circ < \varphi_A < 200^\circ$ , respectively; here,  $\varphi_A$  is the azimuth angle with respect to the azimuthal plane of the antenna (sec. 7.4.2). In these sectors, site shielding reduces possible clear-air interference from terrestrial stations located in the UK and in Scandinavia, respectively. Therefore, we explore the feasibility of shielding the earth station by means of two screens in the form of circular arcs around the station in the sectors A and B, respectively.

The Burum-1 earth station employs a dual-reflector antenna with elevation  $\varphi_E = 23^\circ$  and diameter  $D = 32$  m (thus,  $D/\lambda \approx 425$  at 4 GHz) [10]. These parameters are close to the parameters ( $\varphi_E = 20^\circ$ ,  $D = 400\lambda$ ) of the very large parabolic antenna considered in sec. 8.2. Hence we use the numerical results obtained for the latter

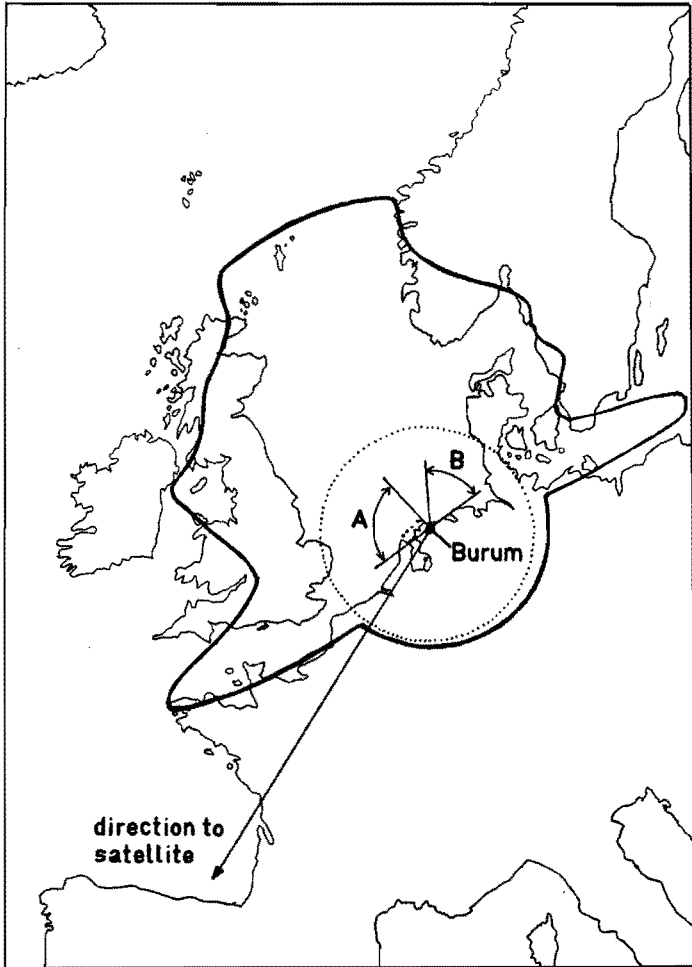


Fig. 8.11. Coordination contours for the Burum-1 receiving earth station, based on appendix 28 of the RR [9]; cf. fig. 2.6.

— Contour for clear-air interference;

..... contour for hydrometeor-scatter interference.

A and B denote the sectors  $20^\circ < \varphi_A < 100^\circ$  and  $140^\circ < \varphi_A < 200^\circ$ , respectively.

antenna, in particular figs. 8.4, 8.5 and 8.9, to determine the parameters of the screens. For the results to be valid for the actual Burum-1 antenna, a more detailed study of this antenna is required.

According to the RR [9], the coordination contour of Burum-1 is reduced to the dotted contour in fig. 8.11, if an extra protection of 50 dB is available. From figs. 8.4 and 8.5 we observe that the sidelobe level of the  $400\lambda$  parabolic antenna in the regions A and B is approximately -30 dBi, instead of the -10 dBi assumed before. Thus, 20 dB of extra protection would seem available from the lower actual sidelobe level of the antenna. From fig. 8.9 we observe that an additional protection of 30 dB in the required sectors A and B can be obtained roughly with screens of relative height  $\Delta z = z_0 - z_M = 300\lambda$  at a distance  $x_M = 1000\lambda$ . Because the antenna is located on the flat ground, we have  $z_M \approx D/2 = 16$  m; thus the obstacle should extend to a height  $z_0 = 38.5$  m above the ground, at a distance  $x_M = 75$  m from the antenna centre.

A screen this large may not always be feasible in practice. If technically feasible, the cost of erection should be compared to the cost of "buying out" the potential interferers located in other countries, e.g. by changing their frequencies or their pointing. This latter possibility will generally not be a viable alternative to protect small, low-cost earth stations. Therefore, we conclude that artificial side shielding is much more attractive for the relatively small earth stations (VSATs), which are being employed more and more in modern satellite communication networks, e.g. for business communication and at CATV head-ends [11].

## 8.5. References

- [1] CCIR, Plenary Assembly, "Earth-station antennas for the fixed-satellite service", *Recommendations and Reports of the CCIR*, vol. IV-1, Rep. 390-5, Geneva, 1986.

- [2] R.G. Kouyoumjian and P.A.J. Ratnasiri, "The calculation of the complete pattern of a reflector antenna", *Proc. Int. Electr. Conf. and Exhibition*, pp. 152-153, Toronto, 1969.
- [3] M.S. Afifi, "Radiation from the paraboloid of revolution", *Electromagnetic wave theory - part 2*, J. Brown, ed., Pergamon, New York, pp. 669-687, 1967.
- [4] S. Silver, ed., "*Microwave antenna theory and design*", Dover, New York, 1965.
- [5] G.L. James and V. Kerdelmelidis, "Reflector antenna radiation pattern analysis by equivalent edge currents", *IEEE Trans. Ant. Prop.*, vol. AP-21, no. 1, pp. 19-24, 1973.
- [6] P.J. Humphrey and D.H. Shinn, "Site shielding for antennas for satellite ground stations", *Marconi Technical Report*, MTR 72/116, 1972.
- [7] M.A. Streete and D.H. Shinn, "Site shielding for earth-station antennas", *Electr. Lett.*, vol. 10, no. 8, pp. 120-121, 1974.
- [8] D.I. Dalgleish, "The influence of interference on the siting of earth stations", *Int. Conf. Sat. Comm. Syst. Techn.*, *IEE Conf. Publ.*, no. 126, pp. 21-27, 1975.
- [9] ITU, "*Radio Regulations*", Geneva, 1982.
- [10] J.Th.R. Schreuder, Netherlands PTT, private communication, 1988.
- [11] D. Chakraborty, "VSAT communication networks - an overview", *IEEE Comm. Magaz.*, vol. 26, no. 5, pp. 10-24, 1988.

## 9. SUMMARY AND CONCLUSIONS

Radio-frequency interference is a major problem in the design of modern radiocommunication systems. The exploration of new (higher) frequency bands cannot keep up with the rapid increase in the demands for telecommunication services. More efficient use of the spectrum, including frequency sharing between different services, is therefore essential.

Mutual interference is the main limitation to the proper operation of frequency-sharing radiocommunication systems. Interference problems pose a variety of new problems of a legal, regulatory and/or technical nature, which are strongly interrelated. The first two categories of problems are dealt with on an international basis by the ITU, and on a national basis by the telecommunication administrations. The technical input for the ITU is continuously provided on an advisory basis by the CCIR; yet many technical problems are still unsolved. This thesis is intended to contribute some possible technical solutions of radio-interference problems.

In chapter 2, we have classified the most important (existing and future) radiocommunication systems for which interference may be a major problem. In particular, we have distinguished between terrestrial systems and satellite systems; many of these systems have to operate in shared frequency bands, especially above 1 GHz. Specific problems arise in frequency sharing between the fixed (terrestrial) service and the fixed-satellite service; in particular, interference from a transmitting terrestrial radio-relay station into a receiving earth station is often of major concern. This problem is illustrated by the large coordination area which is required around an earth station to ensure proper operation even in severe interference conditions. Under certain propagation conditions, the emission of a terrestrial station may reach well beyond the horizon and so prevent the proper operation of a frequency-sharing earth station located hundreds of kilometers away. Considering

the high (and increasing) density of terrestrial radio-relay stations, it is evident that coordination of an earth station with all terrestrial stations within the coordination area can be an immense task. Because of the presently growing number of receiving earth stations, in particular for business systems, point-to-multipoint distribution and broadcast networks, coordination of earth stations is becoming increasingly important.

Transhorizon propagation is the main cause of the large extent of coordination areas, in particular those propagation mechanisms which occasionally yield relatively high field strengths at large distances. We have reviewed the transhorizon-propagation mechanisms in chapter 3, where it is argued that atmospheric superrefraction and ducting are the most important interference mechanisms above the sea and in flat, coastal regions (as in the Netherlands) for frequencies up to about 10 GHz. For higher frequencies, hydrometeor scatter is becoming increasingly important.

A study of prediction models for interference due to ducting (and other "clear-air" mechanisms) is reported in chapter 4. Existing models, including the well-known CCIR model of Rep. 569-3, have been briefly reviewed. Most of these models are of a (semi-)empirical nature and do not yield much insight into the physical mechanisms involved. Measurements are carried out on a European basis by the COST-210 project, to test the validity of these models, and to obtain a better understanding of the physical mechanisms. Typical measured results for the Netherlands have been presented and discussed. These results indicate weaknesses of the current CCIR prediction model, in particular the absence of antenna-height dependence and the unreliability at higher frequencies (above 10 GHz).

Based on the mode theory of tropospheric propagation, a theoretical study of propagation in a typical duct has been carried out (sec. 4.4). This study assumes a number of simplifications, but nevertheless yields important physical insights. It has

been shown that in a duct, the propagation is determined by a set of discrete modes. The number of modes that yield significant contributions to the received field depends greatly on the geometry and the duct parameters. Because of phasing effects between the individual modes, deep fading of the field strength is possible; this fading is also observed in the measurements reported. However, in long-term (time-averaged) measured data, this fading is not observed, owing to the temporal and spatial variability of the duct parameters. It has been argued that the power sum of the modes (instead of their phasor sum) is therefore more realistic for the prediction of time-averaged field strengths. The mode theory turns out to be unsuited for practical interference prediction, because of the large number of input parameters required, and the laborious calculations. For engineering purposes, one has to resort to some (semi-)empirical model.

After having discussed qualitatively and quantitatively the nature of the interference problem and its propagation aspects, we then considered the problem of interference reduction (chapters 5–8).

In chapter 5 we have reviewed interference-reduction techniques from a general point of view. For the specific case of interference from terrestrial stations into satellite earth stations, only a limited number of techniques turns out to be applicable. These techniques have been compared qualitatively. We have argued that interferometric-cancellation techniques are suited for the reduction of a limited number of interference signals, arriving from any direction sufficiently different from the direction of the wanted (satellite) signal. Site shielding is well suited for the reduction of wide-angle interference from an unlimited number of interfering signals, without restrictions on the temporal or spectral characteristics of these signals. An



example of the design approach for an interference canceller in a specific situation is treated in sec. 5.4; the site-shielding technique is the main topic of chapters 6-8.

The site-shielding problem has been formulated as the problem of diffraction at a knife-edge obstacle located in the vicinity of an earth-station antenna. The incident field is modelled as a plane wave with a non-uniform amplitude function. This non-uniformness in the vertical direction is a consequence of the (transhorizon) propagation mechanism by which the incident field reaches the obstacle.

The obstacle-diffraction problem (chapter 6) has been treated in a scalar way. Existing methods for the uniform case have been reviewed and compared, and extended to the non-uniform case. In particular, the well-known CCIR knife-edge diffraction formula from Rep. 715-2 has been extended, by including an additional term in the expression for the site-shielding factor (SSF). This term takes account of the height-gain variability of the incident field. In addition, high-frequency asymptotic methods (GTD/UTD/UAT) have been described and applied to the knife-edge diffraction problem. These methods have an optical character and thus provide direct physical insights into the diffraction problem. With some restrictions, these methods can also be extended to cover more general site-shielding geometries, with more realistic obstacles (obliqueness, thickness, roughness and/or finite conductivity) and with ground-reflection effects.

For the description of the reception of the diffracted field by the (parabolic) earth-station antenna (chapter 7), a three-ray model has been adopted. This model assumes that the wide-angle reception by such an antenna is caused by direct feed spillover (along one ray) and by reflector-edge diffraction (along two rays). The analysis of the associated three-dimensional electromagnetic-field problem has been carried out by GTD/UTD. This method can be applied without restrictions, as long as the antenna-aperture cylinder sufficiently clears the obstacle. The method has

been implemented in a computer programme, which yields accurate numerical results in little processor time.

With this method, the site-shielding factor SSF has been calculated (chapter 8) by comparing the powers received in the absence and in the presence of the shielding obstacle, respectively. Results have been given for a very large parabolic antenna, having its azimuth towards the interference and variable elevation. These results agree well with similar results reported in the literature (but obtained by an aperture-integration method) for a Cassegrain antenna of the same size.

Our method can also be used for the calculation of the SSF as a function of the azimuth angle; this problem was hitherto unsolved. It turns out that for not too small azimuth angles, significant extra protection (in the order of 20-40 dB) can be obtained with realistic site shielding geometries. For small azimuth angles, high values of the SSF are only possible by using very high obstacles at large distances from the earth station.

The effects of the polarizations of the unwanted and wanted fields have also been investigated. The received unwanted power turns out to be more or less polarization-independent; thus, polarization-discrimination at the earth station does not add significant protection against terrestrial interference.

For engineering purposes, a modification of the CCIR site-shielding model has been developed, based on the foregoing GTD/UTD method. This modification has less limitations than the present CCIR model, and yields results which are, in many cases, in good agreement with the results of the GTD/UTD method.

Finally, we have shown that site shielding can be employed to suppress clear-air interference in an earth station to below the level of hydrometeor-scatter interference; this often implies a drastic reduction of the earth-station's coordination area. This may be of most significance for the introduction of new (small) earth stations in densely populated areas (i.e., with heavy interference

potential), for instance for business communications and at cable-TV head ends (VSATs).

In conclusion, we have shown that technical solutions are available to overcome the problem of radio-frequency interference. Yet many questions are still unanswered. Much scientific and technical work will have to be done, to meet the challenges of the expanding radiocommunication services in the future.

## Appendix A. DEFINITIONS OF RELEVANT TERMS BY THE ITU

This appendix summarizes (in alphabetical order) the definitions adopted by the ITU of the terms relevant for the present thesis. These definitions are taken from appendix 1 of the Radio Regulations.

*Accepted interference:* Interference at a higher level than that defined as permissible interference and which has been agreed upon between two or more administrations without prejudice to other administrations.

*Active satellite:* A satellite carrying a station intended to transmit or retransmit radiocommunication signals.

*Administration:* Any governmental department or service responsible for discharging the obligations undertaken in the Convention of the International Telecommunication Union and the Radio Regulations.

*Aeronautical radionavigation service:* A radionavigation service intended for the benefit and for the safe operation of aircraft.

*Allocation (of a frequency band):* Entry in the table of frequency allocations of a given frequency band for the purpose of its use by one or more terrestrial or space radiocommunication services or the radio astronomy service under specified conditions. This term shall also be applied to the frequency band concerned.

*Allotment (of a radio frequency or radio frequency channel):* Entry of a designated frequency channel in an agreed plan, adopted by a competent conference, for use by one or more administrations for a terrestrial or space radiocommunication service in one or more identified countries or geographical areas and under specified conditions.

*Amateur service:* A radiocommunication service for the purpose of self-training, intercommunication and technical investigations carried out by amateurs, that is, by

duly authorized persons interested in radio technique solely with a personal aim and without pecuniary interest.

*Assignment (of a radio frequency or radio frequency channel):* Authorization given by an administration for a radio station to use a radio frequency or radio frequency channel under specified conditions.

*Broadcasting-satellite service:* A radiocommunication service in which signals transmitted or retransmitted by space stations are intended for direct reception by the general public.

*Broadcasting service:* A radiocommunication service in which the transmissions are intended for direct reception by the general public. This service may include sound transmissions, television transmissions or other types of transmission.

*Broadcasting station:* A station in the broadcasting service.

*Coordination area:* The area associated with an earth station outside of which a terrestrial station sharing the same frequency band neither causes nor is subject to interfering emissions greater than a permissible level.

*Coordination contour:* The line enclosing the coordination area.

*Coordination distance:* Distance on a given azimuth from an earth station beyond which a terrestrial station sharing the same frequency band neither causes nor is subject to interfering emissions greater than a permissible level.

*Earth station:* A station located either on the earth's surface or within the major portion of the earth's atmosphere and intended for communication:

- with one or more space stations; or
- with one or more stations of the same kind by means of one or more reflecting satellites or other objects in space.

*Emission:* Radiation produced, or the production of radiation, by a radio transmitting station.

*Fixed-satellite service:* A radiocommunication service between earth stations at specified fixed points when one or more satellites are used; in some cases this service includes satellite-to-satellite links, which may also be effected in the inter-satellite service; the fixed-satellite service may also include feeder links for other space radiocommunication services.

*Fixed service:* A radiocommunication service between specified fixed points.

*Fixed station:* A station in the fixed service.

*Geostationary satellite:* A geosynchronous satellite whose circular and direct orbit lies in the plane of the earth's equator and which thus remains fixed relative to the earth; by extension, a satellite which remains approximately fixed relative to the earth.

*Geostationary-satellite orbit:* The orbit in which a satellite must be placed to be a geostationary satellite.

*Geosynchronous satellite:* An earth satellite whose period of revolution is equal to the period of rotation of the earth about its axis.

*Harmful interference:* Interference which endangers the functioning of a radionavigation service or of other safety services or seriously degrades, obstructs, or repeatedly interrupts a radiocommunication service operating in accordance with the Radio Regulations.

*Interference:* The effect of unwanted energy due to one or a combination of emissions, radiations, or inductions upon reception in a radiocommunication system, manifested by any performance degradation, misinterpretation, or loss of information which could be extracted in the absence of such unwanted energy.

*Land mobile service:* A mobile service between base stations and land mobile stations, or between land mobile stations.

*Mobile-satellite service:* A radiocommunication service:

- between mobile earth stations and one or more space stations, or between space stations used by this service; or
- between mobile earth stations by means of one or more space stations.

This service may also include feeder links necessary for its operation.

*Mobile service:* A radiocommunication service between mobile and land stations, or between mobile stations.

*Mobile station:* A station in the mobile service intended to be used while in motion or during halts at unspecified points.

*Orbit:* The path, relative to a specified frame of reference, described by the centre of mass of a satellite or other object in space subjected primarily to natural forces, mainly the force of gravity.

*Period (of a satellite):* The time elapsing between two consecutive passages of a satellite through a characteristic point on its orbit.

*Permissible interference:* Observed or predicted interference which complies with quantitative interference and sharing criteria contained in the Radio Regulations or in CCIR Recommendations or in special agreements as provided for in the Radio Regulations.

*Radar:* A radiodetermination system based on the comparison of reference signals with radio signals reflected, or retransmitted, from the position to be determined.

*Radiation:* The outward flow of energy from any source in the form of radio waves.

*Radio:* A general term applied to the use of radio waves.

*Radio astronomy:* Astronomy based on the reception of radio waves of cosmic origin.

*Radiocommunication:* Telecommunication by means of radio waves.

*Radiocommunication service:* A service involving the transmission, emission and/or reception of radio waves for specific telecommunication purposes. In the Radio Regulations, unless otherwise stated, any radiocommunication service relates to terrestrial radiocommunication.

*Radiodetermination:* The determination of the position, velocity and/or other characteristics of an object, or the obtaining of information relating to these parameters, by means of propagation properties of radio waves.

*Radiodetermination-satellite service:* A radiocommunication service for the purpose of radiodetermination involving the use of one or more space stations.

*Radiodetermination service:* A radiocommunication service for the purpose of radiodetermination.

*Radiodetermination station:* A station in the radiodetermination service.

*Radionavigation:* Radiodetermination used for the purposes of navigation, including obstruction warning.

*Radionavigation-satellite service:* A radiodetermination-satellite service used for the purpose of radionavigation.

*Radionavigation service:* A radiodetermination service for the purpose of radionavigation.

*Radio waves:* Electromagnetic waves of frequencies arbitrarily lower than 3000 GHz, propagated in space without artificial guide.

*Reflecting satellite:* A satellite intended to reflect radiocommunication signals.

*Satellite:* A body which revolves around another body of preponderant mass and which has a motion primarily and permanently determined by the force of attraction of that other body.

*Satellite link:* A radio link between a transmitting earth station and a receiving earth station through one satellite.



*Satellite network:* A satellite system or a part of a satellite system, consisting of only one satellite and the cooperating earth stations.

*Satellite system:* A space system using one or more artificial earth satellites.

*Spacecraft:* A man-made vehicle which is intended to go beyond the major portion of the earth's atmosphere.

*Space radiocommunication:* Any radiocommunication involving the use of one or more space stations or the use of one or more reflecting satellites or other objects in space.

*Space research service:* A radiocommunication service in which spacecraft or other objects in space are used for scientific or technological research purposes.

*Space station:* A station located on an object which is beyond, is intended to go beyond, or has been beyond, the major portion of the earth's atmosphere.

*Space system:* Any group of cooperating earth stations and/or space stations employing space radiocommunication for specific purposes.

*Station:* One or more transmitters or receivers or a combination of transmitters and receivers, including the accessory equipment, necessary at one location for carrying on a radiocommunication service, or the radio astronomy service. Each station shall be classified by the service in which it operates permanently or temporarily.

*Telecommunication:* Any transmission, emission or reception of signs, signals, writing, images and sounds or intelligence of any nature by wire, radio, optical or other electromagnetic systems.

*Terrestrial radiocommunication:* Any radiocommunication other than space radiocommunication or radio astronomy.

*Terrestrial station:* A station effecting terrestrial radiocommunication.

**Appendix B. NUMERICAL SOLUTION OF THE MODE EQUATION  
ASSOCIATED WITH AN ELEVATED REFRACTIVE-INDEX  
DISCONTINUITY**

**B.1. Introduction**

This appendix deals with the solution of the mode equation (4.32), viz.

$$F(t) = \chi_A(t) - \beta(t)\chi_B(t) = 0, \quad (\text{B.1})$$

where

$$\chi_A(t) = \text{Ai}'(t-\zeta_h)w_1(t+T-\zeta_h) - \text{Ai}(t-\zeta_h)w_1'(t+T-\zeta_h), \quad (\text{B.2a})$$

$$\chi_B(t) = \text{Bi}'(t-\zeta_h)w_1(t+T-\zeta_h) - \text{Bi}(t-\zeta_h)w_1'(t+T-\zeta_h), \quad (\text{B.2b})$$

$$\beta(t) = \text{Ai}(t)/\text{Bi}(t). \quad (\text{B.2c})$$

Here,  $T$  is the (normalized) magnitude of the refractive-index discontinuity at the (normalized) height  $\zeta_h$  above the earth surface, with  $T > 0$  and  $\zeta_h > 0$ ; see (4.22b,e) and fig. 4.7. The roots  $t=t_n$  of (B.1) are complex with  $\text{Im}\{t_n\} < 0$ . The following relations for the Airy functions are quoted here for easy reference (cf. (4.22f) and (4.24)):

$$w_1(\tau) = -j\sqrt{\pi} [\text{Ai}(\tau) + j\text{Bi}(\tau)] = 2\sqrt{\pi} e^{-j\pi/6} \text{Ai}(\tau e^{-2j\pi/3}), \quad (\text{B.3})$$

$$\text{Ai}(\tau)\text{Bi}'(\tau) - \text{Bi}(\tau)\text{Ai}'(\tau) = \pi^{-1}. \quad (\text{B.4})$$

Furthermore, the Airy function  $\text{Ai}(\tau)$  is known to have zeros on the negative real axis only [1, sec. 10.4]. These zeros are denoted by  $\tau = -a_n$ ,  $n=1,2,3,\dots$ , hence

$$\text{Ai}(-a_n) = 0. \quad (\text{B.5})$$

The values of  $a_n$  for  $n = 1, 2, \dots, 10$  are listed in [1, table 10.13]. For large  $n$ , the zero  $a_n$  can be approximated by

$$a_n = \left[ \frac{3\pi}{2} \left( n - \frac{1}{4} \right) \right]^{2/3} + O(n^{-4/3}) \quad (n \rightarrow \infty). \quad (\text{B.6})$$

### B.2. Special cases

The mode equation (B.1) can be solved exactly in two special cases, namely,  $T=0$  or  $\zeta_h=0$ . In both cases, the refractive-index discontinuity disappears and the refractive index increases linearly with height, see fig. 4.7. For  $T=0$ , (B.1) reduces to

$$F(t) = \frac{j}{\sqrt{\pi}} [\beta(t)+j] = -\frac{w_1(t)}{\pi \text{Bi}(t)} = 0, \quad (\text{B.7})$$

which has the solutions

$$t = t_n = a_n \exp(-j\pi/3), \quad n=1,2,3,\dots \quad (\text{B.8})$$

For  $\zeta_h=0$ , (B.1) simplifies to

$$F(t) = -\frac{w_1(t+T)}{\pi \text{Bi}(t)} = 0, \quad (\text{B.9})$$

with the solutions

$$t = t_n = a_n \exp(-j\pi/3) - T, \quad n=1,2,3,\dots \quad (\text{B.10})$$

### B.3. Asymptotic solution for $n \rightarrow \infty$

It is expected that for  $|t| \gg T$  and  $|t| \gg \zeta_h$  (i.e.,  $n \rightarrow \infty$ ), the solution for  $t_n$  approaches the solutions of the two special cases. Therefore, we search for solutions  $t$  of the form

$$t = a \exp(-j\pi/3), \quad (\text{B.11})$$

with  $|\arg(a)| < \pi/3$ ,  $|a| \gg T$  and  $|a| \gg \zeta_h$ . The arguments of the Airy functions in (B.2) are shortly written as

$$t - \zeta_h = [a - \zeta_h \exp(j\pi/3)] \exp(-j\pi/3) = b \exp(-j\pi/3), \quad (\text{B.12a})$$

$$t + T - \zeta_h = [a + (T - \zeta_h) \exp(j\pi/3)] \exp(-j\pi/3) = c \exp(-j\pi/3), \quad (\text{B.12b})$$

with the same restrictions on modulus and argument of  $b$  and  $c$  as were imposed on  $a$ . The following asymptotic expansions can be deduced from [1, sec. 10.4]:

$$\text{Ai}(t) \approx \frac{\exp(j\pi/12)}{2\sqrt{\pi}} a^{-1/4} \exp\left(\frac{2}{3}ja^{3/2}\right), \quad (\text{B.13a})$$

$$\text{Bi}(t) \approx \frac{\exp(j\pi/12)}{2\sqrt{\pi}} a^{-1/4} \left[ -j \exp\left(\frac{2}{3}ja^{3/2}\right) + 2 \exp\left(-\frac{2}{3}ja^{3/2}\right) \right], \quad (\text{B.13b})$$

$$\text{Ai}(t - \zeta_h) \approx \frac{\exp(j\pi/12)}{2\sqrt{\pi}} b^{-1/4} \exp\left(\frac{2}{3}jb^{3/2}\right), \quad (\text{B.13c})$$

$$\text{Ai}'(t - \zeta_h) \approx -\frac{\exp(-j\pi/12)}{2\sqrt{\pi}} b^{1/4} \exp\left(\frac{2}{3}jb^{3/2}\right), \quad (\text{B.13d})$$

$$\text{Bi}(t - \zeta_h) \approx \frac{\exp(j\pi/12)}{2\sqrt{\pi}} b^{-1/4} \left[ -j \exp\left(\frac{2}{3}jb^{3/2}\right) + 2 \exp\left(-\frac{2}{3}jb^{3/2}\right) \right], \quad (\text{B.13e})$$

$$\text{Bi}'(t-\zeta_h) \approx \frac{\exp(-j\pi/12)}{2\sqrt{\pi}} b^{1/4} [j \exp(\frac{2}{3}jb^{3/2}) + 2 \exp(-\frac{2}{3}jb^{3/2})], \quad (\text{B.13f})$$

$$w_1(t+T-\zeta_h) \approx 2 \exp(-j\pi/6) c^{-1/4} \sin(\frac{2}{3}c^{3/2} + \frac{\pi}{4}), \quad (\text{B.13g})$$

$$w_1'(t+T-\zeta_h) \approx 2 \exp(j\pi/6) c^{1/4} \cos(\frac{2}{3}c^{3/2} + \frac{\pi}{4}). \quad (\text{B.13h})$$

Substitution of (B.13) into (B.2), and of (B.2) into (B.1), yields (after some algebra) the approximating mode equation

$$\begin{aligned} F(t) \approx \frac{2\exp(5j\pi/6)}{\pi a^{1/4} \text{Bi}(t)} & \left[ (b/c)^{1/4} \sin(\frac{2}{3}c^{3/2} + \frac{\pi}{4}) \cos(\frac{2}{3}a^{3/2} - \frac{2}{3}b^{3/2}) \right. \\ & \left. + (b/c)^{-1/4} \cos(\frac{2}{3}c^{3/2} + \frac{\pi}{4}) \sin(\frac{2}{3}a^{3/2} - \frac{2}{3}b^{3/2}) \right] = 0. \end{aligned} \quad (\text{B.14})$$

We observe that in the special case  $T=0$ , one has  $b=c$ , and (B.14) reduces to

$$\sin(\frac{2}{3}a^{3/2} + \frac{\pi}{4}) = 0, \quad (\text{B.15})$$

with the solutions

$$a = \left[ \frac{3\pi}{2} (n - \frac{1}{4}) \right]^{2/3} \approx a_n, \quad n=1,2,3,\dots, \quad (\text{B.16})$$

in agreement with the exact solution (B.8). Similarly, in the special case  $\zeta_h=0$ , one has  $a=b$ , and (B.14) simplifies to

$$\sin(\frac{2}{3}c^{3/2} + \frac{\pi}{4}) = 0, \quad (\text{B.17})$$

with the solutions

$$c = \left[ \frac{3\pi}{2} \left( n - \frac{1}{4} \right) \right]^{2/3} \approx a_n, \quad n=1,2,3,\dots \quad (\text{B.18})$$

Accordingly we find

$$a \approx a_n - T \exp(j\pi/3), \quad n=1,2,3,\dots, \quad (\text{B.19})$$

again in agreement with the exact solution (B.10).

For the general case  $T \neq 0$  and  $\zeta_h \neq 0$ , we establish the following asymptotic expansions valid for  $|a| \rightarrow \infty$ :

$$(b/c)^{\pm 1/4} = 1 \mp \frac{1}{4} T e^{j\pi/3} a^{-1} + O(a^{-2}), \quad (\text{B.20a})$$

$$\frac{2}{3} a^{3/2} - \frac{2}{3} b^{3/2} = \zeta_h e^{j\pi/3} a^{1/2} + O(a^{-1/2}). \quad (\text{B.20b})$$

From (B.20b) we observe that  $\text{Im}\{a^{3/2} - b^{3/2}\}$  is positive and increasing as  $|a| \rightarrow \infty$ ,  $|\arg(a)| < \pi/3$ ; hence, we can apply the approximations

$$\cos\left(\frac{2}{3} a^{3/2} - \frac{2}{3} b^{3/2}\right) \approx \frac{1}{2} \exp\left[-\frac{2}{3} j (a^{3/2} - b^{3/2})\right], \quad (\text{B.21a})$$

$$\sin\left(\frac{2}{3} a^{3/2} - \frac{2}{3} b^{3/2}\right) \approx \frac{j}{2} \exp\left[-\frac{2}{3} j (a^{3/2} - b^{3/2})\right]. \quad (\text{B.21b})$$

Substitution of (B.20a) and (B.21) into (B.14) yields for  $c$  the approximating equation

$$\exp\left[-2j \left(\frac{2}{3} c^{3/2} + \frac{\pi}{4}\right)\right] = T e^{-2j\pi/3} / 4a, \quad (\text{B.22})$$

with the solutions

$$c = \left[ \frac{3\pi(n-1/4)}{2} \right]^{2/3} \left[ 1 + \frac{(3j/4) \ln(Te^{-2j\pi/3}/4a)}{(3\pi/2)(n-1/4)} \right]^{2/3}$$

$$\approx a_n + \frac{j}{2} a_n^{-1/2} \ln(Te^{-2j\pi/3}/4a), \quad n=1,2,3,\dots \quad (\text{B.23})$$

Inside the logarithm we can replace  $a$  by its dominant term  $a_n$  to obtain the final asymptotic solution

$$a \approx a_n + (\zeta_h - T)e^{j\pi/3} + \frac{j}{2} a_n^{-1/2} \ln(Te^{-2j\pi/3}/4a_n), \quad (\text{B.24})$$

or

$$t = t_n \approx a_n e^{-j\pi/3} + \zeta_h - T + \frac{1}{2} e^{j\pi/6} a_n^{-1/2} \ln(Te^{-2j\pi/3}/4a_n), \quad (\text{B.25})$$

valid for  $T \neq 0$ ,  $\zeta_h \neq 0$  and  $n \rightarrow \infty$ .

#### B.4. Approximate solution for large $T$ and $\zeta_h$

From a physical consideration, we expect that, for large  $T$  and  $\zeta_h$ , the mode equation has solutions  $t_n$  with  $\text{Im}\{t_n\} \approx 0$ , corresponding to "trapped" modes (see sec. 4.4.4). Therefore, we search for approximate solutions of (B.1) that are real. We start by rewriting (B.1) as

$$\frac{\text{Ai}'(t-\zeta_h) - \beta(t)\text{Bi}'(t-\zeta_h)}{\text{Ai}(t-\zeta_h) - \beta(t)\text{Bi}(t-\zeta_h)} = \frac{w_1'(t+T-\zeta_h)}{w_1(t+T-\zeta_h)} \quad (\text{B.26})$$

For real  $t$  the left-hand side of (B.26) is real, whereas the right-hand side approaches the real value  $(t+T-\zeta_h)^{1/2}$  as  $t+T-\zeta_h \rightarrow \infty$ . Thus for  $t+T-\zeta_h \gg 1$ ,

eq. (B.26) is well approximated by

$$\frac{Ai'(t-\zeta_h) - \beta(t)Bi'(t-\zeta_h)}{Ai(t-\zeta_h) - \beta(t)Bi(t-\zeta_h)} = (t+T-\zeta_h)^{1/2}. \quad (B.27)$$

Approximate solutions of (B.27) can be obtained if  $t \gg 1$ , which implies  $\beta(t) \approx 0$ . We observe that for  $t-\zeta_h > -1$ , the left-hand side of (B.27) is negative (see [1, sec. 10.4]), so no solution is found. For  $t-\zeta_h \ll -1$ , we replace  $Ai(t-\zeta_h)$  and  $Ai'(t-\zeta_h)$  in (B.27) by their asymptotic expansions to obtain the approximating equation

$$\tan\left[\frac{2}{3}(\zeta_h-t)^{3/2} + \frac{\pi}{4}\right] = -(\zeta_h-t)^{1/2}(T-\zeta_h+t)^{-1/2}. \quad (B.28)$$

At the outset we have assumed that  $T \gg \zeta_h - t$ . Hence, the right-hand side of (B.28) is small and (B.28) can be replaced by

$$\tan\left[\frac{2}{3}(\zeta_h-t)^{3/2} + \frac{\pi}{4}\right] = -\tan\left[(\zeta_h-t)^{1/2}(T-\zeta_h+t)^{-1/2}\right], \quad (B.29)$$

which has the solutions

$$\begin{aligned} \zeta_h - t &= \left[\frac{3\pi}{2}\left(n - \frac{1}{4}\right)\right]^{2/3} \left[1 - \frac{(3/2)(\zeta_h-t)^{1/2}(T-\zeta_h+t)^{-1/2}}{(3\pi/2)(n-1/4)}\right]^{2/3} \\ &\approx a_n - a_n^{-1/2}(\zeta_h-t)^{1/2}(T-\zeta_h+t)^{-1/2}, \quad n=1,2,3,\dots \end{aligned} \quad (B.30)$$

In the last term of (B.30), we can replace  $\zeta_h - t$  by its dominant term  $a_n$  to obtain the final solution



$$t = t_n \approx \zeta_h - a_n + (T - a_n)^{-1/2}, \quad n=1,2,3,\dots, \quad (\text{B.31})$$

valid for  $T \gg \zeta_h - t \gg 1$  and  $t \gg 1$ , or equivalently, for  $a_n \ll T$  and  $a_n \ll \zeta_h$ .

### B.5. Numerical procedure

We have solved the mode equation (B.1) numerically by means of a modified Newton iteration procedure, using the exact solutions for  $T=0$  and for  $\zeta_h=0$  and the asymptotic solutions as starting values. The Airy functions have been calculated by means of their power-series expansions [1, eqs. 10.4.2–10.4.5] or (for large arguments) by means of their asymptotic expansions [1, eqs. 10.4.59–10.4.68]. The Airy functions may become very large and rapidly oscillating, hence good initial values are required to ensure convergence of the Newton procedure. In the actual calculation of the solutions  $t_n$ , the parameters  $T$  and  $\zeta_h$  were varied stepwise, whereby the step size sometimes had to be chosen very small to achieve convergence. Proper care should also be taken if two solutions  $t_m$  and  $t_n$  (at the same values of  $T$  and  $\zeta_h$ ) get close to each other. Plots of  $t_n$ ,  $n=1,2,3,\dots$ , in the complex  $t$ -plane are therefore often indispensable for a proper understanding and guidance of the numerical work.

### B.6. Numerical results

We have plotted the loci of  $t_n$  in the complex  $t$ -plane, for several fixed values of  $z_h$  with  $\Delta$  as a parameter. Here,  $z_h$  and  $\Delta$  are related to  $\zeta_h$  and  $T$  by (4.22b,e), which for the selected values of  $\lambda$  and  $a_e$  (see sec. 4.4.4) become

$$\zeta_h = 0.0976 z_h, \quad T = 8.29 \cdot 10^5 \Delta, \quad (\text{B.32})$$

with  $z_h$  in m. Results are shown in figs. B.1–B.4. Here, the solid lines are the loci of  $t_n$  for which  $n$  is constant (with an arrow pointing in the direction of increasing  $\Delta$ ); along the dashed lines,  $\Delta$  is constant; the corresponding roots  $t_n$  are marked by dots at the intersections of these loci.

We observe that the ordering of the modes, which is at customary done by decreasing imaginary part of  $t_n$ , cannot be maintained with increasing  $z_h$  and  $\Delta$  beyond a certain value of  $n$ . For example, for  $z_h=100$  m and  $\Delta=10^{-5}$  (i.e., the example in sec. 4.4.4), mode 6 has the largest value of  $\text{Im}\{t_n\}$ , corresponding to the smallest specific attenuation  $\gamma_n$ . However, it is customary to arrange the modes by increasing  $\gamma_n$ . Therefore, modes 1 to 6 have been rearranged in table 4.2.

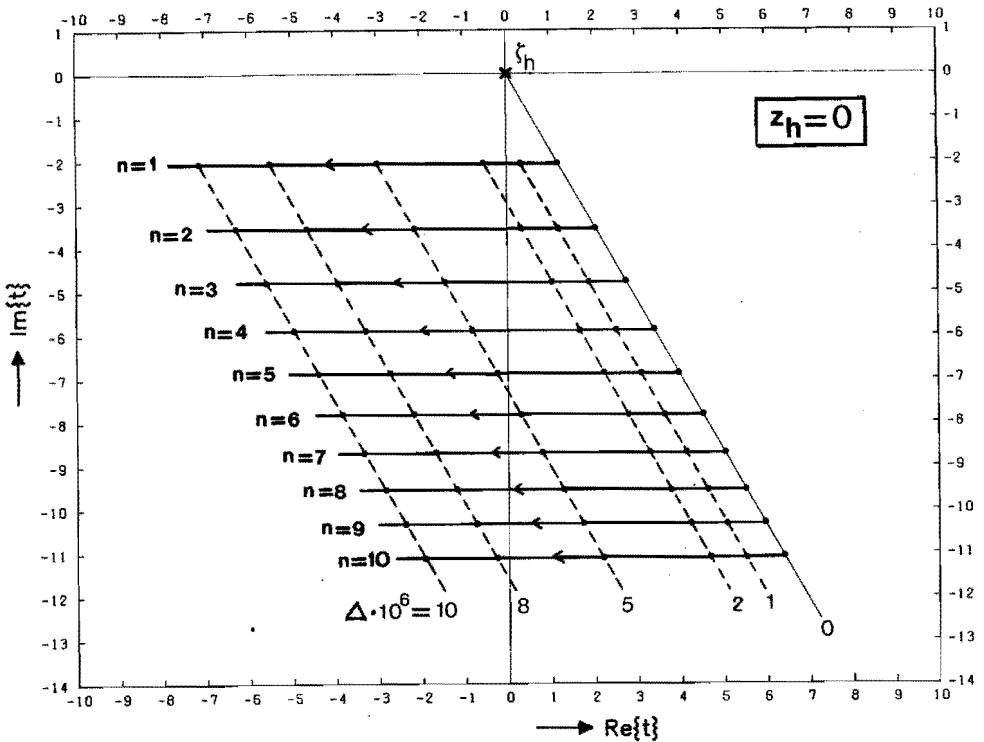


Fig. B.1. The roots  $t_n$  of the mode equation (B.1) for  $z_h=0$ , with  $\Delta$  and  $n$  as parameters.

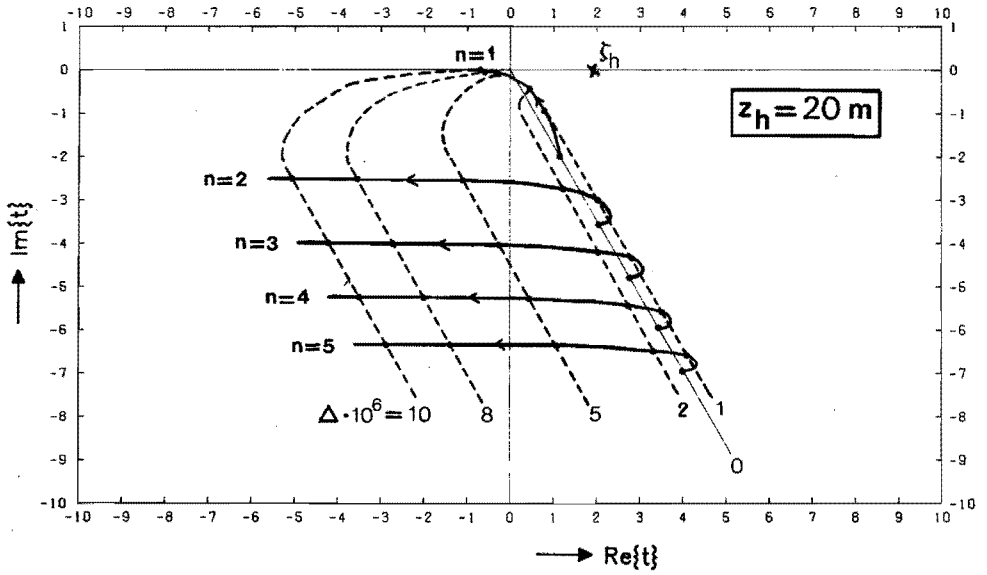


Fig. B.2. The roots  $t_n$  of the mode equation (B.1) for  $z_h=20 \text{ m}$ , with  $\Delta$  and  $n$  as parameters.

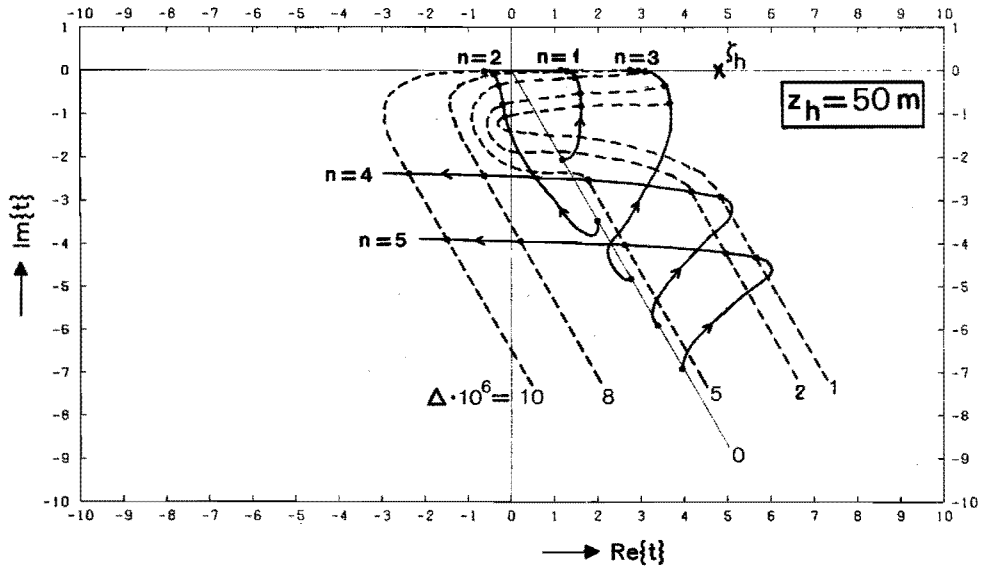


Fig. B.3. The roots  $t_n$  of the mode equation (B.1) for  $z_h=50 \text{ m}$ , with  $\Delta$  and  $n$  as parameters.

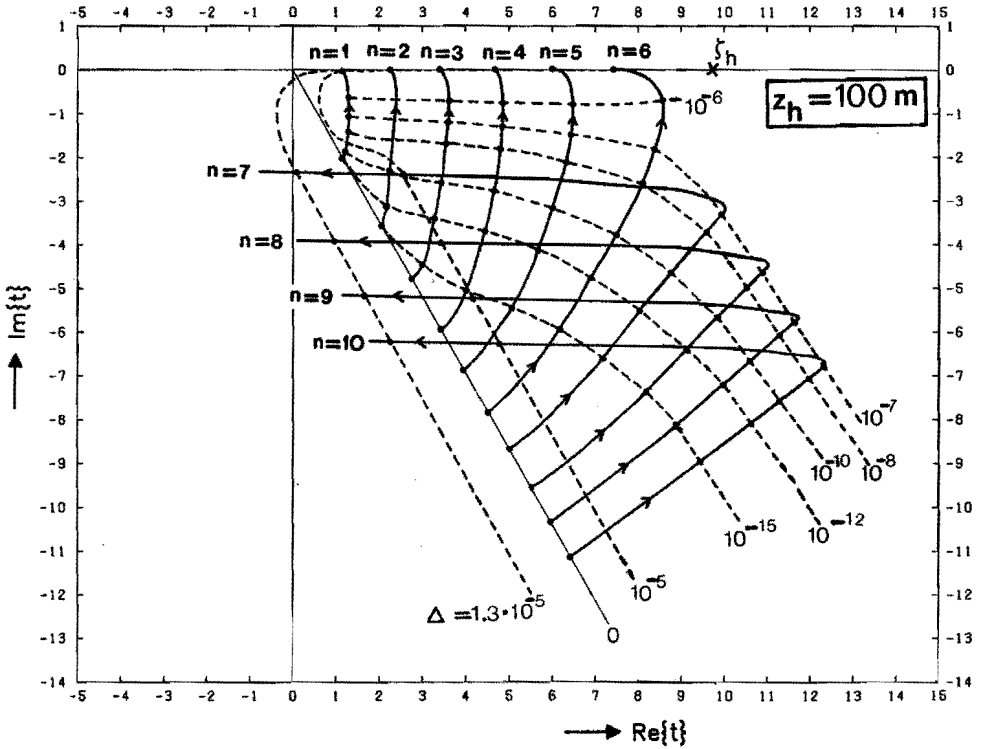


Fig. B.4. The roots  $t_n$  of the mode equation (B.1) for  $z_h=100$  m, with  $\Delta$  and  $n$  as parameters.

**B.7. Reference**

[1] M. Abramowitz and I.A. Stegun, "Handbook of mathematical functions", Dover, New York, 1965.



**Appendix C. GEOMETRICAL PARAMETERS OF THE AXISYMMETRIC PARABOLIC REFLECTOR ANTENNA**

In this appendix we derive expressions for the geometrical parameters of the parabolic antenna. These expressions are needed to determine the GTD/UTD solution to the site-shielding problem of chapter 7.

We employ the spherical  $(\rho, \psi, \varphi)$  coordinate system introduced in sec. 7.4.2, with origin at the paraboloid focus F;  $\psi$  is the angle with the axis of symmetry of the antenna. A cross-section of the reflector surface with the half-plane  $\varphi = \varphi_0$  is shown in fig. C.1. Here we have also indicated the unit vectors  $\hat{e}_0 \times \hat{e}_{\pi/2}$  (along the axis of symmetry) and  $\cos \varphi_0 \hat{e}_0 + \sin \varphi_0 \hat{e}_{\pi/2}$  (perpendicular to the axis of symmetry), where  $\hat{e}_0$  and  $\hat{e}_{\pi/2}$  are defined in (7.34). The centre M of the antenna aperture has

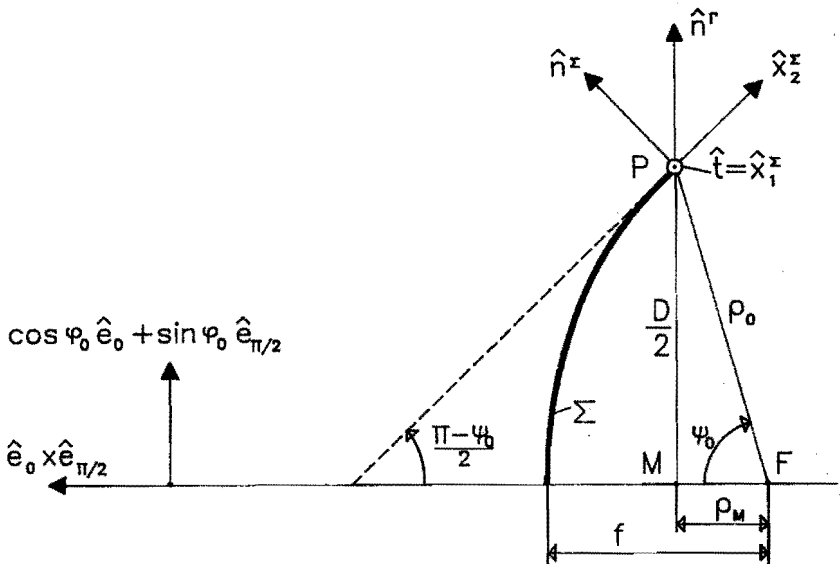


Fig. C.1. Cross-section of the axisymmetric parabolic reflector antenna with the half-plane  $\varphi = \varphi_0$ .

coordinates  $\rho=\rho_M$ ,  $\psi=0$ , while the reflector edge point P has spherical coordinates  $\rho=\rho_0$ ,  $\psi=\psi_0$ ,  $\varphi=\varphi_0$ . At P the reflector surface  $\Sigma$  has the unit normal  $\hat{n}^\Sigma$  and the principal directions  $\hat{x}_1^\Sigma$  and  $\hat{x}_2^\Sigma$ .

The parabolic reflector is completely specified by the focal distance  $f$  and the aperture diameter  $D$ . In spherical coordinates the paraboloid surface  $\Sigma$  is described by

$$\rho = f/\cos^2(\psi/2). \quad (C.1)$$

The subtended angle  $\psi_0$  follows by

$$\rho_0 = \frac{D/2}{\sin\psi_0} = \frac{f}{\cos^2(\psi_0/2)},$$

i.e.,

$$\tan(\psi_0/2) = D/4f. \quad (C.2)$$

The distances  $\rho_0$  and  $\rho_M$  can now be calculated as

$$\rho_0 = f/\cos^2(\psi_0/2) = f + D^2/16f, \quad (C.3a)$$

$$\rho_M = \sqrt{\rho_0^2 - (D/2)^2} = f - D^2/16f, \quad (C.3b)$$

which proves (7.5).

The reflector edge  $\Gamma$  is a circle of radius  $D/2$ . At P we introduce the unit tangent  $\hat{t}$  and the unit normal  $\hat{n}^\Gamma$  to  $\Gamma$ , while the radius of curvature is denoted by  $R^\Gamma$ . These parameters readily follow from fig. 7.9 and fig. C.1, viz.

$$\hat{t} = \sin\varphi_0 \hat{e}_0 - \cos\varphi_0 \hat{e}_{\pi/2}, \quad (C.4a)$$

$$\hat{n}^\Gamma = \cos\varphi_0 \hat{e}_0 + \sin\varphi_0 \hat{e}_{\pi/2}, \quad (\text{C.4b})$$

$$R^\Gamma = D/2. \quad (\text{C.4c})$$

Because of rotational symmetry, the principal directions of the surface  $\Sigma$  at P coincide with  $\hat{t}$  and with the tangent vector to the cross-section parabola at P. The latter tangent is known to make an angle  $(\pi-\psi_0)/2$  with the axis of symmetry (fig. C.1). Thus, the principal directions are found to be

$$\hat{x}_1^\Sigma = \hat{t} = \sin\varphi_0 \hat{e}_0 - \cos\varphi_0 \hat{e}_{\pi/2}, \quad (\text{C.5a})$$

$$\hat{x}_2^\Sigma = \cos(\psi_0/2)(\cos\varphi_0 \hat{e}_0 + \sin\varphi_0 \hat{e}_{\pi/2}) - \sin(\psi_0/2)(\hat{e}_0 \times \hat{e}_{\pi/2}). \quad (\text{C.5b})$$

The normal  $\hat{n}^\Sigma$  to  $\Sigma$  at P coincides with the normal vector to the cross-section parabola at P. From fig. C.1 it is readily seen that

$$\hat{n}^\Sigma = \sin(\psi_0/2)(\cos\varphi_0 \hat{e}_0 + \sin\varphi_0 \hat{e}_{\pi/2}) + \cos(\psi_0/2)(\hat{e}_0 \times \hat{e}_{\pi/2}). \quad (\text{C.5c})$$

Finally, we determine the principal radii of curvature  $R_{1,2}^\Sigma$  of  $\Sigma$  at P. To that end, we consider the normal sections of  $\Sigma$  with the planes  $V_1$  and  $V_2$  through P parallel to  $\hat{n}^\Sigma$  and  $\hat{x}_1^\Sigma$ , and to  $\hat{n}^\Sigma$  and  $\hat{x}_2^\Sigma$ , respectively. The radii of curvature at P of these normal sections are equal to  $R_1^\Sigma$  and  $R_2^\Sigma$ . As a preliminary, the equation (C.1) of the paraboloid surface is rewritten as

$$\rho = 2f - \rho \cos\psi. \quad (\text{C.6})$$

Here,  $\rho = |\vec{x} - \vec{x}_F|$  measures the distance to F and  $\psi$  is the angle between  $\vec{x} - \vec{x}_F$  and  $\hat{e}_0 \times \hat{e}_{\pi/2}$ . Thus, (C.6) can be reduced to the equivalent form



$$(\vec{x}-\vec{x}_P) \cdot (\vec{x}-\vec{x}_P) = \left[ 2f - (\vec{x}-\vec{x}_P) \cdot (\hat{e}_0 \times \hat{e}_{\pi/2}) \right]^2 \quad (C.7)$$

The plane  $V_1$  is described by the parametric representation

$$\vec{x} = \vec{x}_P + \xi_1 \hat{x}_1^\Sigma - \eta_1 \hat{n}^\Sigma, \quad (C.8)$$

where  $\xi_1, \eta_1$  are rectangular coordinates in  $V_1$  with origin at P. By inserting (C.8) into (C.7) and by use of the relation

$$\vec{x}_P - \vec{x}_F = \frac{1}{2}D (\cos \varphi_0 \hat{e}_0 + \sin \varphi_0 \hat{e}_{\pi/2}) + \rho_M (\hat{e}_0 \times \hat{e}_{\pi/2}), \quad (C.9)$$

it is found that the normal section of  $\Sigma$  with  $V_1$  is described by

$$\xi_1^2 + \sin^2(\psi_0/2) \left[ \eta_1 - \frac{D/2}{\sin^3(\psi_0/2)} \right]^2 = \frac{(D/2)^2}{\sin^4(\psi_0/2)}, \quad (C.10)$$

which is the equation of an ellipse. Its radius of curvature  $R_1^\Sigma$  at P (where  $\xi_1=0, \eta_1=0$ ) is calculated from

$$R_1^\Sigma = \left\{ \left[ 1 + (d\eta_1/d\xi_1)^2 \right]^{3/2} \left| d^2\eta_1/d\xi_1^2 \right|^{-1} \right\} \Big|_{\xi_1=0, \eta_1=0}, \quad (C.11)$$

which yields

$$R_1^\Sigma = 2f/\cos(\psi_0/2). \quad (C.12)$$

The plane  $V_2$  coincides with the plane of the cross-section in fig. C.1, and is described by the parametric representation

$$\vec{x} = \vec{x}_F + \xi_2(\hat{e}_0 \times \hat{e}_{\pi/2}) + \eta_2(\cos\varphi_0 \hat{e}_0 + \sin\varphi_0 \hat{e}_{\pi/2}), \quad (\text{C.13})$$

where  $\xi_2, \eta_2$  are rectangular coordinates in  $V_2$  with origin at F. By inserting (C.13) into (C.7), it is found that the normal section of  $\Sigma$  with  $V_2$  is described by

$$\eta_2^2 = 4f(f - \xi_2), \quad (\text{C.14})$$

which is the equation of the cross-section parabola shown in fig. C.1. The radius of curvature  $R_2^\Sigma$  at P (where  $\xi_2 = \rho_M = f - D^2/16f$ ,  $\eta_2 = D/2$ ) is calculated from a formula similar to (C.11), with the result

$$R_2^\Sigma = 2f/\cos^3(\psi_0/2). \quad (\text{C.15})$$

This completes the determination of the antenna parameters in (7.45).



## ACKNOWLEDGEMENTS

The completion of this thesis has only been possible thanks to various contributions from others.

The cooperation with the colleagues of the COST-210 project has been pleasant and fruitful. I am particularly grateful to Martin Hall from the Rutherford Appleton Laboratory, chairman of COST 210, for his guidance and support of my unexperienced chairmanship of Working Group 3 of the project. I am also indebted to Tim Hewitt (British Telecom Research Laboratories) for his useful comments on sec. 4.3 of this thesis.

The hospitality received during my educational stay at the Electromagnetics Institute, Technical University of Denmark, is greatly acknowledged. I especially thank Henning Bach and Kim Brown for instructive discussions on the geometrical theory of diffraction.

I have also had much benefit from the contacts and the cooperation with various colleagues from the Dr. Neher Laboratories of the Netherlands PTT. I like to thank them all for their numerous contributions to the completion of this thesis.

The work described in this thesis has been performed mainly during my stay at the Telecommunications Group of the Eindhoven University of Technology. I am grateful to all members of this group, including the students involved, for their cooperation and their contributions.

Last, but certainly not least I am very grateful to Marian Stada for pointing out a number of grammatical and typographical errors, and to Doret Pellegrino and Jeanne van Alebeek for devotedly typing the manuscript.



## SAMENVATTING

Vanwege de toenemende vraag naar telecommunicatiediensten is toekenning van hetzelfde radiocommunicatiekanaal aan verschillende diensten onvermijdelijk. Inherent aan dit meervoudig gebruik van frekwentiebanden ("frequency sharing") is het optreden van systeemstoringen door radio-interferentie. Een belangrijke oorzaak van interferentie is ongewenste over-de-horizon-propagatie van microgolven afkomstig van straalzenders. Deze propagatie kan een ernstige belemmering vormen voor storingsvrije ontvangst van (relatief zwakke) satelliet signalen in grondstations. Beschermende maatregelen zijn veelal noodzakelijk om aan de operationele eisen (storingsvrije ontvangst gedurende bijvoorbeeld 99% van de tijd) te kunnen voldoen.

Dit proefschrift geeft een overzicht van de mechanismen die verantwoordelijk kunnen zijn voor over-de-horizon-propagatie. Het belangrijkste mechanisme — troposferische "ducting" — is nader onderzocht. Als experimentele ondersteuning van dit onderzoek is een aantal metingen uitgevoerd, in het kader van het Europese COST-210 samenwerkingsproject. Aan de hand van deze metingen worden mogelijke tekortkomingen van de bestaande (semi-)empirische predictiemodellen gesignaleerd. Een theoretisch model van het ducting-mechanisme wordt beschreven en uitgewerkt voor een specifiek voorbeeld.

Een literatuurstudie is verricht naar methoden ter bestrijding van radio-interferentie. Eén van deze methoden, welke gebruik maakt van een adaptief onderdrukkingssysteem, is nader uitgewerkt voor de toepassing in kabel distributiesystemen, ter bestrijding van storingen ten gevolge van omroepiraterij. Voor de bescherming van satelliet-grondstations tegen radio-interferentie ten gevolge van over-de-horizon-propagatie blijkt afscherming van het grondstation een geschikt middel te zijn.

Het nuttig effect van een dergelijke afscherming vindt een natuurlijke beperking door het optreden van diffractie aan de rand van het afschermende obstakel. Bestaande modellen voor de berekening van het afschermende effect van een obstakel zijn slechts beperkt toepasbaar. Met behulp van een model gebaseerd op de geometrische diffractietheorie (GTD) is het afschermingsprobleem diepgaand onderzocht. De numerieke resultaten van dit model komen goed overeen met de vergelijkbare resultaten uit de literatuur. Aan de hand van dit GTD-model is een eenvoudiger, praktisch-toepasbaar model opgesteld, waarvan de resultaten goed overeenkomen met die van het GTD-model.

De praktische betekenis van afscherming in het kader van "frequency sharing" wordt geïllustreerd aan de hand van een voorbeeld. De resultaten suggereren dat afscherming vooral voor relatief kleine grondstations aantrekkelijk kan zijn.



## VERANTWOORDING

In dit proefschrift zijn resultaten beschreven die ten dele behaald zijn door bijdragen van anderen. Deze bijdragen worden hieronder nader omschreven.

— *Interference from digital radio-relay stations into satellite TV receivers (par. 2.2.5).*

Ir. J.P.N. Haagh verrichte, in het kader van zijn afstudeerwerk in de vakgroep Telecommunicatie van de Technische Universiteit Eindhoven, theoretisch en experimenteel onderzoek naar de betreffende interferentiesituatie. De experimentele resultaten in par. 2.2.5 van dit proefschrift zijn aan dit afstudeerwerk ontleend. Ir. C.A.M. Geus (PTT) en de auteur van dit proefschrift hebben ir. Haagh bij zijn afstudeerwerk begeleid.

— *Transhorizon-propagation experiments (par. 4.3).*

De propagatie-experimenten beschreven in par. 4.3 zijn financieel mogelijk gemaakt door steun van de Nederlandse PTT (DNL). Technisch zijn deze experimenten mogelijk geweest door de samenwerking met British Telecom (BTRL), de Deutsche Bundespost (FI/DBP) en de Nederlandse PTT (DNL), in het kader van het Europese COST-210 project.

— *Application of interference cancellation for the protection of cable networks against radio pirates (par. 5.4).*

Deze paragraaf bevat een overdruk van het artikel "Interference protection of cable networks against radio pirates". Het onderzoek beschreven in dit artikel is mede uitgevoerd door afstudeerders en stagiairs in de vakgroep Telecommunicatie (TUE), onder begeleiding van prof. dr. J.C. Arnbak en de auteur van dit proefschrift. Prof. Arnbak is de schrijver van het inleidende gedeelte (pags. 7-9) van dat artikel.





## CURRICULUM VITAE

De auteur van dit proefschrift werd op 30 juli 1955 geboren te Heerlen. Van 1967 tot 1973 volgde hij de middelbare—schoolopleiding (VWO) aan het Bernardinus-college te Heerlen.

In 1973 begon hij met de studie Elektrotechniek aan de Technische Hogeschool Eindhoven (thans TUE). Zijn afstudeerwerk verrichtte hij in de vakgroep Telecommunicatie, en betrof onderzoek naar de defocuseereigenschappen van het Schwarzschild—antennesysteem. In 1981 behaalde hij zijn ingenieursdiploma en tevens zijn leraarsbevoegdheid Natuur— en Wiskunde.

Gedurende en na zijn studie nam hij deel aan een aantal nationale en internationale schaaktoernooien, hetgeen in 1982 resulteerde in de titel Internationaal Meester.

Van 1982 tot 1983 doceerde hij Natuurkunde aan het Peellandcollege te Deurne.

Van 1984 tot 1988 was hij werkzaam als wetenschappelijk assistent in de vakgroep Telecommunicatie van de TUE. Tevens was hij een groot deel van deze periode één van de Nederlandse vertegenwoordigers in het Europese COST—210 project, als voorzitter van Werkgroep 3 van dit project. Zijn onderzoeken in die periode hebben geleid tot het ontstaan van dit proefschrift.



**STELLINGEN**

**behorende bij het proefschrift van**

**P. M. J. SCHEEREN**

1. De CCIR-formule voor meskantdiffractie van een uniforme vlakke invallende golf kan op eenvoudige wijze uitgebreid worden tot het geval van een niet-uniforme vlakke golf. De uitbreiding bestaat uit het toevoegen van een extra term die de hoogteafhankelijkheid van het invallende veld in rekening brengt.
  - *CCIR, Plenary Assembly, "Propagation by diffraction", Recommendations and Reports of the CCIR, vol. V, Rep. 715-2, Geneva, 1986.*
  - *Dit proefschrift, par. 6.5.4.*
  
2. De bruikbaarheid van de CCIR-formule voor de berekening van het afschermende effect van een obstakel in de nabijheid van een grondstationantenne kan aanzienlijk worden vergroot door de formule niet te baseren op het diffractieveld in het antennemiddelpunt, maar op het diffractieveld dat daadwerkelijk de belangrijkste bijdrage tot het ontvangen veld levert.
  - *CCIR, Plenary Assembly, "Earth-station antennas for the fixed-satellite service", Recommendations and Reports of the CCIR, vol. IV-1, Rep. 390-5, Geneva, 1986.*
  - *Dit proefschrift, par. 8.3.1.*
  
3. De grafische resultaten van Streete en Shinn suggereren dat het afschermende effect van een obstakel sterker wordt bij toenemende afstand tussen het obstakel en de af te schermen grondstationantenne. Deze suggestie is misleidend, aangezien de hoogte van het obstakel in deze resultaten niet constant wordt gehouden. Bij vaste obstakelhoogte wordt de afschermende werking doorgaans juist zwakker als de afstand tussen antenne en obstakel toeneemt.
  - *M.A. Streete and D.H. Shinn, "Site shielding for earth-station antennas", Electr. Lett., vol. 10, no. 8, pp. 120-121, 1974.*
  - *Dit proefschrift, par. 8.2.5.*

4. De uitbreiding voor negatief argument van de in de UTD gebruikte overgangsfunctie  $F$ , zoals die voorgesteld is door Kouyoumjian en Pathak, garandeert niet in alle gevallen continuïteit van het totale elektrische veld en is daarom niet uniform bruikbaar.
  - *R.G. Kouyoumjian and P.H. Pathak, "Authors' reply" to J.D. Cashman, Comments on "A uniform geometrical theory of diffraction for an edge in a perfectly conducting surface", IEEE Trans. Ant. Prop., vol. AP-25, no. 5, pp. 447-451, 1977.*
  - *Dit proefschrift, par. 7.5.7.*
  
5. Luebbbers beschrijft een op GTD/UTD gebaseerde methode voor de berekening van transmissieverliezen ten gevolge van diffractie aan terrein op over-de-horizon-paden. Deze methode geeft alleen dan betere resultaten (ten opzichte van metingen) in vergelijking met andere methoden indien zeer gedetailleerde informatie van het terrein op het pad beschikbaar is.
  - *R.J. Luebbbers, "Finite-conductivity uniform GTD versus knife-edge diffraction in prediction of propagation path loss", IEEE Trans. Ant. Prop., vol. AP-32, no. 1, pp. 70-76, 1984.*
  - *G.H. Schut, "Toepassing van de Geometrische Theorie van Diffractie voor diffractieberekeningen", Stageverslag, vakgroep Telecommunicatie, TU Eindhoven, 1988.*
  
6. Bij het ontwerp van gedefocusseerde reflectorantennesystemen voor multiple-beam of contoured-beam toepassingen dient men zowel met de faseverdeling als met de amplitudeverdeling van het veld in de antenneapertuur rekening te houden. Systemen gebaseerd enkel op een fasebeschouwing hebben niet de verre-veldeigenschappen die men op grond van die beschouwing zou verwachten.
  - *P.M.J. Scheeren, M.H.A.J. Herben and E.J. Maanders, "Scan properties of the Schwarzschild antenna", Proc. 11th European Microwave Conf., pp. 561-566, Amsterdam, 1981.*

7. Een deterministisch model van een mobiele-radiokanaal, gebaseerd op de geometrische optica, kan een goede beschrijving geven van de overdracht van het kanaal, mits in dit model rekening wordt gehouden met de incoherente verstrooiing van het electromagnetische veld door ruwe oppervlakken.  
  
— *R. v.d. Hulst, "Determination of the impulse response of a mobile channel by simulation. A deterministic approach."*, *Afstudeerverslag, vakgroep Telecommunicatie, TU Eindhoven, 1987.*
8. Het plaatsen van antennes voor het ontvangen van satelliet signalen op het dak van een gebouw geschiedt veelal uit statusoverwegingen of uit gewoonte. Technisch gezien verdient een plaatsing op de grond in vele gevallen de voorkeur.
9. Door de beknoptheid van technisch-wetenschappelijke artikelen in de vakliteratuur is het narekenen van de gebruikte berekeningen vaak zeer moeilijk, hetgeen twijfel over de juistheid van de resultaten in de hand werkt.
10. Het succes van het huidige systematische onderzoek van eindspelstellingen uit het schaakspel met behulp van computers doet vermoeden dat vele klassieke nagslagwerken op eindspelgebied binnen een tiental jaren achterhaald zullen zijn.  
  
— *E. Mednis, "Endgames with minor pieces"*, *New In Chess Magaz.*, no. 87/8, pp. 86–97, 1987 and no. 88/2, pp. 56–59, 1988.
11. Het probleem dat tegenwoordig een groot deel van de leerkrachten in het voortgezet onderwijs na het vijftigste levensjaar het werk niet meer aankan, is niet zo zeer een gevolg van de 50-jarige leeftijd van leerkrachten, maar vooral van de 100-jarige leeftijd van het huidige onderwijssysteem.